MAGNETIC AND OTHER PROPERTIES OF DETRITAL ILMENITE AND PSEUDORUTILE

by

Michael John Wort

Thesis submitted for the degree of

Doctor of Philosophy

Department of Mineral Resources Engineering
Imperial College of Science and Technology
London SW7 2BP

January 1980

M.J. WORT

MAGNETIC AND OTHER PROPERTIES OF DETRITAL ILMENITE AND PSEUDORUTILE

ABSTRACT

"Ilmenite" from two Western Australian deposits and an Indonesian pseudorutile sample have been examined by X-ray diffraction, magnetic susceptibility determination, Mössbauer spectroscopy, neutron diffraction, ore microscopy, electron probe microanalysis and chemical analysis.

Magnetic fractions were produced using a Cook isodynamic separator, and detailed susceptibility measurements were obtained using the Faraday method; the Gouy method; an a.c. mutual inductance bridge; and a vibrating-sample magnetometer.

The chemical composition and the mineralogical content of magnetic fractions of naturally altered detrital "ilmenite" particles have been used to explain their measured magnetic susceptibilities.

Anomalies in the published magnetic data for ilmenite were partially resolved. In addition new data have been gained for the poorly-characterised, non-stoichiometric mineral pseudorutile, which has been shown to be a magnetic spinglass.

Magnetocrystalline anisotropy in ferrianilmenite has been found to be sufficiently strong to rotate and orient partly-rounded grains placed in a 0·2T magnetic field. X-ray diffraction on magnetically-oriented grains of ferrianilmenite has confirmed that the magnetic spin axes are aligned perpendicular to the crystallographic 'c' axis, and gives supporting evidence for the epitaxial orientations assumed by the secondary rutile and pseudorutile which form on the ilmenite substrate.

Free chromite has been found in the West Australian detrital ilmenite deposits and its influence on the Cr_2O_3 content of the commercial ilmenite concentrates produced has been briefly discussed.

ACKNOWLEDGEMENTS

I wish to thank my supervisor, Mr. M.P. Jones, for his technical and tactical advice, constructive criticism and constant encouragement during the course of this project.

My thanks are also due to Professor U. Ts. Andres, Mr. C.H.J. Beaven, Mrs. E. Lewis, Mr. M. Clements and the other staff of the Mineral Technology Department, Imperial College, for their help and advice.

I am grateful to Professor B.R. Coles of the Solid State Physics Department, Imperial College, and to his staff and research workers for access to magnetic equipment and for help with experimentation and magnetic theory.

I also wish to thank other Imperial College staff including Professor D. Rogers, Dr. D. Williams, Dr. R.S. Osborn, Mr. F. Huggins and Mr. R. Curtis for help with X-ray diffraction; Dr. B. Dalgleish, Mr. L. Dutton and Mr. H. Haddow for help with ilmenite synthesis; and Mr. P. Suddaby and Mr. N. Wilkinson for electron probe point analyses.

I am indebted to Dr. B.W. Fitzsimmons and particularly Mr. I. Sayer at Birkbeck College, London, for the Mössbauer spectra and for technical advice.

The neutron diffraction spectra were produced through the cooperation of Dr. D.H.C. Harris and Mr. G. Proudfoot of the Materials Physics Division, A.E.R.E. Harwell, to whom I tender my thanks.

For provision of heavy mineral samples, my thanks are due to Mr. J.M. Davey, Manager of the Capel, W.A. operations of Associated Minerals Consolidated Ltd., and to Dr. K.J. Henley of Amdel, South Australia for a sample of Indonesian pseudorutile.

I am especially grateful to my friend and research colleague Dr. E. Greaves for valuable technical discussions on many respects of this work and for introducing me to computer fitting of Mössbauer data and the interpretation of Mössbauer spectra.

The chemical analyses for this project were carried out by courtesy of Tioxide International Limited at their Central Laboratories, Stockton-on-Tees, and I am particularly grateful to Mr. J. Whitehead, Mr. J. Marshall and Mr. D. Holden for their help and advice.

To my wife Raelene and son Alexander, who have patiently and cheerfully endured three years of neglect, and who have totally supported my endeavours, I am deeply indebted. Equally I am indebted to my late father and my mother for the sacrifices they made to secure me a tertiary education.

Finally, this work could not have been accomplished without financial support and the help provided by Professor E. Cohen. Fellowships were obtained initially from the André Dorfman Trust, administered by Imperial College, and latterly from the Stanley Elmore Trust Fund administered by The Institution of Mining and Metallurgy, London, whose support is gratefully acknowledged.

CONTENTS

		Page
Title		
Abstract		i
Acknowledgements		ii
Table of Contents		iv
List of Figures		ix
List of Tables		xvi
List of Appendices		xviii
Chapter 1	INTRODUCTION	
Section 1.1	Background to the investigation	1
1.2	Scope of investigation	3
1.3	Aims	3
1.4	Objectives	4
1.5	Presentation	4
Chapter 2	MATERIALS INVESTIGATED	
Section 2.1	Source of materials	6
2.2	Preparation of detrital heavy mineral samples and treatment programme	6
Chapter 3	ILMENITE ALTERATION	
Section 3.1	Review of literature on ilmenite alteration and properties of altered ilmenite	10
	Conclusions	23
3.2	Alteration textures	24
3.3	Models of ilmenite alteration	25
Chapter 4	MAGNETIC THEORY	
Section 4.1	Introduction	31
4.2	Discussion of basic concepts in magnetism	31
	General	31
	Spin arrangements	32
	Magnetic domains	37

	Spinglasses	38
	Superparamagnetism	38
	Magnetic ions	42
	Information sources	42
4.3	Measurement units	42
4.4	Some useful equations	44
Chapter 5	MAGNETIC PROPERTIES OF MINERALS	
Section 5.1	Paramagnetic minerals	46
5.2	Ferro-, ferri- and antiferromagnetic minerals	46
5.3	Minerals considered	47
5.4	Hematite	47
5.5	Ilmenite	51
	Anisotropy measurements	54
5.6	Effect of composition on the magnetic properties of ilmenite	56
5.7	Hematite-ilmenite solid solution $xFeTiO_3.(1-x)Fe_2O_3$	59
5.8	Magnetite and chromite	65
	General	65
	Magnetite	65
	Chromite	66
Chapter 6	MEASUREMENT OF MAGNETIC SUSCEPTIBILITY	
Section 6.1	Introduction	68
6.2	Magnetic balances	68
6.3	The Gouy method	69
	Theory	69
	Apparatus	71
	Experimental procedure	71
6.4	The Faraday method	72
	Theory	72
	Apparatus	75
	Experimental procedure	75
6.5	Electronic a.c. mutual inductance bridge	77

6.6	Vibrating sample magnetometer	78
6.7	Frantz-type magnetic separators	80
	Introduction	80
	Theory	80
	Apparatus	84
	Experimental procedure	84
	Calibration	86
Chapter 7	METHODS FOR MEASURING MAGNETIC TRANSITION TEMPERATURES	
Section 7.1	Ferromagnetic Curie point	91
7.2	Ferrimagnetic Curie point	96
7.3	Antiferromagnetic Néel point	96
Chapter 8	X-RAY DIFFRACTION	
Section 8.1	Introduction	98
8.2	Theory	98
8.3	The Chung matrix-flushing method for quantitative XRD	98
8.4	Procedure for Chung Method	101
8.5	Mineral spectra	102
	Ilmenite ($FeTiO_3$)	102
	Rutile (TiO_2)	102
	Pseudorutile ($Fe_2Ti_3O_9$)	103
	Arizonite ($Fe_2Ti_3O_9$)	103
Chapter 9	NEUTRON DIFFRACTION AND MÖSSBAUER SPECTROSCOPY	
Section 9.1	Neutron diffraction	109
	General	109
	Neutron diffraction of ilmenite	110
9.2	Mössbauer spectroscopy	114
	General	114
	Sample preparation	118
	Ilmenite	118

Chapter 10	RESULTS FOR ILMENITE-RICH CONCENTRATE FROM THE SOUTH CAPEL DEPOSIT, W.A.	
Section 10.1	Introduction	122
10.2	Material studied	124
10.3	Initial magnetic fractionation	124
10.4	Handpicking of minerals	126
10.5	Chemical analyses	126
	Interpretation of Fig. 10.2	128
10.6	Density determinations	129
10.7	Detailed susceptibility determinations	132
	Cook separator fractions	132
	High-χ ferrimagnetic sub-fractions	136
10.8	Qualitative X-ray diffraction	136
	Search for ferromagnetics	136
	Progressive changes in spectra	138
	Special features	140
	Solid solution in high-χ fractions	140
	Magnetic orientation effects	142
10.9	Quantitative X-ray diffraction	149
	General	149
	Results	149
	Low susceptibility fractions	152
10.10	Mössbauer investigations	153
10.11	Microscopic observations (reflected light)	159
10.12	EPMA investigations	161
10.13	Alteration model	162
Chapter 11	RESULTS FOR ENEABBA ALTERED ILMENITE	
Section 11.1	Introduction	170
11.2	Material studied	170
11.3	Magnetic fractionation and susceptibility determination	174
11.4	Qualitative X-ray diffraction	174
11.5	Quantitative X-ray diffraction	176

11.6	Microscopic observations (reflected light)	178
11.7	EPMA investigations	183
Chapter 12	RESULTS FOR PSEUDORUTILE	
Section 12.1	Introduction	186
12.2	Composition of pseudorutile	188
12.3	Stoichiometry of South Australian pseudorutile	189
12.4	Indonesian pseudorutile	189
	Origin of sample	189
	Sample description	189
	X-ray diffraction	194
	Stoichiometry	197
	Magnetic properties	197
Chapter 13	CONCLUSIONS	206
BIBLIOGRAPHY		210
ADDITIONAL REFERENCES		217

LIST OF FIGURES

		Page
2.1	Preparation sequence and treatment programme for heavy mineral samples	7
3.1	Early model of ilmenite alteration, based on observations of leucoxene pseudomorphous after ilmenite (Edwards, 1942)	26
3.2	Model of ilmenite alteration, derived from Bailey et al (1956)	26
3.3	Model of ilmenite alteration derived from Grey and Reid (1975)	26
3.4	Relationship of the intersecting plane to idealised alteration zoning	29
3.5	Average chemical composition of altered ilmenite and other samples	29
4.1	The main types of magnetic behaviour	33
4.2	Relation of magnetic properties to temperature for the main types of magnetic material	34
4.3	Various possible arrangements of magnetic spin moments (modified after Scheiber, 1967)	36
4.4	The superexchange mechanism	38
4.5	Spin rotation across a domain wall	41
4.6	Effect of particle size on properties of ferromagnetic materials	41
4.7	Orbital diagram for Fe^{3+} showing unpaired electrons	43
5.1	The system $FeO-Fe_2O_3-TiO_2$ showing the compositions of the major phases	48
5.2	The spin-canting of hematite	48
5.3	Curves of weak magnetisation and specific susceptibility for hematite	50

FIGURES - Cont'd.

5.4	The antiferromagnetic structure of hematite, compared with that of ilmenite	50
5.5	Susceptibility of MnO powder, showing field dependence below T_N	53
5.6	The anisotropic magnetic susceptibility of ilmenite (Bizette and Tsai)	53
5.7	The temperature dependence of the specific susceptibility for an ideal, antiferromagnetic material	55
5.8	Laue back-reflection pattern for a single crystal of ilmenite from Kenya	55
5.9	The anisotropic susceptibility of a single crystal fragment of ilmenite from Kenya	57
5.10	Lattice parameters of the ilmenite-hematite solid solution series	57
5.11	Spontaneous magnetisation (I_s) and Curie point (θ_c) variations for the ilmenite-hematite solid solution series	61
5.12	The ilmenite-hematite solvus (Elsdon)	61
5.13	The ilmenite-hematite solvus (Lindsley)	63
5.14	Magnetic phase diagram for the ilmenite-hematite system	63
6.1	Arrangement of the magnetic balance	70
6.2	The Gouy method of susceptibility determination	70
6.3	Major and minor hysteresis loops of an electromagnet.	73
6.4	Magnetisation curve for a paramagnetic containing a small amount of ferromagnetic impurity	73
6.5	The Faraday Method	76
6.6	Some pole-piece designs which may be used with the Faraday Method	76
6.7	Simplified form of vibrating sample magnetometer (VSM)	79

FIGURES - Cont'd.

6.8	Calibration curve obtained for the Cook separator	82
6.9	Relationship of particle susceptibility (χ) to the separation current at a given track side-slope for a Frantz isodynamic separator	83
6.10	Schematic cross-section through the pole pieces of a Cook isodynamic magnetic separator	83
6.11	Cook isodynamic magnetic separator fitted with a vibrating spiral feeder	85
6.12	Sketch of the separation track for a Cook isodynamic magnetic separator	85
6.13	Technique for the determination of critical current	88
7.1	Saturation magnetisation and Curie points (T_c) of Fe, Co and Ni	92
7.2	Temperature dependence of ferromagnetic behaviour in zero applied field	92
7.3	Variation of magnetisation for a hematite sample during heating and subsequent cooling	94
7.4	Thermomagnetic separator used by Japanese workers for determining Curie points	95
7.5	Lack of sharpness in determinations of ferromagnetic Curie point	97
7.6	Paramagnetic susceptibility in the region of the ferrimagnetic Curie point	97
7.7	Susceptibility of an ideal antiferromagnetic above and below T_N	97
8.1	XRD spectra of Indonesian and South Australian pseudorutile	107
9.1	X-ray and neutron scattering amplitudes for a potassium ion	111
9.2	Arrangement of a neutron diffractometer	111

FIGURES - Cont'd.

9.3	Neutron diffraction spectra of ilmenite	112
9.4	XRD spectrum of synthetic ilmenite	112
9.5	Mössbauer calibration spectrum of iron at 293°K	116
9.6	Mössbauer spectrum of synthetic ilmenite at 293°K	117
9.7	Mössbauer spectrum of ilmenite at 5°K (Grant et al, 1972)	119
9.8	Mössbauer spectrum of synthetic ilmenite at 59.5°K	120
9.9	Mössbauer spectrum of synthetic ilmenite at 22°K	120
10.1	Geological setting of the Capel heavy mineral field	123
10.2	Chemical variation of magnetic fractions of altered ilmenite from the South Capel deposit	123
10.3	Chemical variation of magnetic fractions of detrital ilmenite from Quilon	130
10.4	Relative degree of alteration of magnetic fractions of altered ilmenite from the South Capel deposit	131
10.5	XRD spectrum of Capel 0.30A magnetics plus 20% Fe	139
10.6	Variation of peak position for the 70.24° ($CuK\alpha$) line of ilmenite with changing Fe_2O_3 content	143
10.7	XRD spectrum of Capel 0.05A magnetics with 0.2T field perpendicular to the mount	145
10.8	XRD spectrum of Capel 0.05A magnetics with 0.2T field parallel to the mount	146
10.9	XRD spectrum of Capel 0.05A magnetics with no magnetic field	147
10.10	Relative orientations of ilmenite and overlying secondary pseudorutile and rutile	148
10.11	Mössbauer spectrum of 0.05A, $-15°+10°$ magnetics at 293°K	155
10.12	Mössbauer spectrum of 0.05A, $-15°+10°$ magnetics at 80°K	156

FIGURES - Cont'd.

10.13 Mössbauer spectrum of cleaned, black 0.30A magnetics at 293°K 157

10.14 Mössbauer spectrum of cleaned, black 0.30A magnetics at 80°K 158

10.15 Typical textures - 0.05A magnetics - South Capel deposit 164

10.16 Isotropic altered phases and secondary rutile. 0.05A magnetics - South Capel deposit 164

10.17 Three-zoned grain with isotropic core. 0.05A magnetics - South Capel deposit 164

10.18 Leached grain with pits and relict exsolved blebs. 0.05A magnetics - South Capel deposit 165

10.19 Efflorescent alteration spots attacking the rim and core. 0.05A magnetics - South Capel deposit 165

10.20 Alteration of the rim and also penetrating the core. 0.05A magnetics—South Capel deposit 165

10.21 Advanced alteration centred upon cracked areas - 0.05A magnetics - South Capel deposit 166

10.22 Hemo-ilmenite with leached, pitted rim - 0.35A magnetics - South Capel deposit 166

10.23 Efflorescent spots of alteration in diffuse bands - 0.35A magnetics - South Capel deposit 166

10.24 Banded alteration - 0.35A magnetics - South Capel deposit 167

10.25 Relict isotropic streaks in finely pitted grain - 0.35A magnetics - South Capel deposit 167

10.26 EPMA slow scans for Ti, Mn and Fe across grain shown in Fig. 10.17 167

10.27 Two-phase grain from 0.45A magnetics, South Capel deposit 168

10.28 Veins of secondary rutile cut across anisotropic altered ilmenite. 0.30A magnetics, South Capel deposit 168

FIGURES - Cont'd.

10.29	Chromite grains in east coast ilmenite concentrate	168
10.30	Idealised model of ilmenite alteration	169
11.1	Location of the Eneabba heavy mineral deposit	171
11.2	XRD spectrum of Eneabba 0.05A magnetics with 0.2T field acting perpendicular to the mount	177
11.3	Heavily pitted grain after original hemo-ilmenite. Eneabba altered ilmenite concentrate	181
11.4	Two-phase altered grain. Eneabba altered ilmenite concentrate	181
11.5	Two-phase altered grain with weakly anisotropic core. Eneabba altered ilmenite concentrate	181
11.6	Three-phase grain. 0.05A magnetics, Eneabba altered ilmenite	182
11.7	Three-phase grain with impure secondary rutile in intermediate zone. Eneabba altered ilmenite concentrate	182
11.8	EPMA slow scans for Ti, Mn and Fe across grain shown in Fig. 11.6	184
11.9	EPMA slow scans for Ti and Fe across 3-zoned grain shown in Fig. 11.7	184
12.1	Some occurrences of pseudorutile	187
12.2	Grains of Indonesian pseudorutile, pseudomorphous after 'hexagonal' ilmenite crystals	191
12.3	Indonesian pseudorutile with overgrowth of marcasite-pyrite and cemented quartz grain	191
12.4	Indonesian pseudorutile grain with relict ilmenite and a zircon inclusion	192
12.5	Indonesian pseudorutile with grooved surface	192
12.6	XRD spectrum of Indonesian pseudorutile	195
12.7	Comparison of XRD spectra for hematite, ilmenite, pseudorutile and rutile	196

FIGURES - Cont'd.

12.8	Low-temperature susceptibility of Indonesian pseudorutile	198
12.9	Neutron diffraction spectrum of pseudorutile at $4^{\circ}K$	198
12.10	Mössbauer spectrum of Indonesian pseudorutile at $293^{\circ}K$	202
12.11	Mössbauer spectrum of Indonesian pseudorutile at $80^{\circ}K$	203
12.12	Mössbauer spectrum of Indonesian pseudorutile at $4.2^{\circ}K$	204

XRD SPECTRA

South Capel Deposit

F1	0.05A magnetics + 20% Fe	225
F2	0.10A magnetics + 20% Fe	226
F3	0.15A magnetics + 20% Fe	227
F4	0.20A magnetics + 10% Fe	228
F5	0.25A magnetics + 20% Fe	229
F6	0.30A magnetics + 20% Fe	230
F7	0.35A magnetics + 20% Fe	231
F8	0.40A magnetics + 20% Fe	232
F9	0.45A magnetics + 20% Fe	233

Eneabba Altered Ilmenite

G1	0.05A magnetics + 10% Fe	235
G2	0.15A magnetics + 10% Fe	235
G3	0.25A magnetics + 10% Fe	236
G4	0.35A magnetics + 10% Fe	236
G5	0.45A magnetics + 20% Fe	237
G6	0.50A magnetics + 10% Fe	237
G7	0.60A magnetics + 10% Fe	238

LIST OF TABLES

		Page
Table 4.1	Comparison of the characteristics of the main types of magnetic material	35
Table 4.2	Spin-only moments of some ions of the First Transition Series	43
Table 5.1	Cell parameters for ilmenite, $FeTiO_3$	52
Table 5.2	Elemental composition of Capel Bulk Ilmenite by XRF	59
Table 5.3	Magnetic behaviour of Ilmenite-Hematite solid solutions	64
Table 6.1	Comparison of Gouy and Faraday methods of susceptibility measurement	74
Table 6.2	Magnetic susceptibility standards	87
Table 8.1	XRD spectra for ilmenite ($FeTiO_3$)	104
Table 8.2	XRD spectra for rutile (TiO_2)	105
Table 8.3	XRD spectra for pseudorutile ($Fe_2Ti_3O_9$)	106
Table 8.4	XRD spectrum for arizonite after Overholt et al	108
Table 9.1	Analysis of neutron diffraction lines in the ilmenite spectrum by Shirane et al (1959)	113
Table 10.1	Size distribution of Capel crude gravity concentrate	125
Table 10.2	Magnetic fractionation of Capel crude gravity concentrate	125
Table 10.3	Analyses of magnetic fractions of altered ilmenite from Capel	127
Table 10.4	Density of magnetic fractions	132
Table 10.5	Susceptibilities of magnetic fractions of Capel ilmenite by Faraday method	133
Table 10.6	High-field susceptibility of weakly magnetic fractions by Faraday method	133

Table 10.7	Calculated and measured susceptibilities for fractions of altered ilmenite from Capel	135
Table 10.8	High- χ ferrimagnetic sub-fractions	137
Table 10.9	Curie point and susceptibility of ferrimagnetic fractions	137
Table 10.10	Comparison of equivalent lines in hematite and ilmenite XRD spectra	141
Table 10.11	Comparison of apparent mineral compositions for magnetic fractions of altered Capel ilmenite	150
Table 10.12	Mineral contents of low-susceptibility fractions as indicated by quantitative XRD	150
Table 10.13	Measured parameters in Fe^{57} Mössbauer effect spectra	154
Table 11.1	Compositions of heavy mineral fractions from strand lines in the Adamson deposit	172
Table 11.2	Size distribution of Eneabba altered ilmenite	172
Table 11.3	Composition of Eneabba altered ilmenite	173
Table 11.4	Magnetic separation of Eneabba altered ilmenite	175
Table 11.5	Susceptibility measurements on Eneabba altered ilmenite by the Faraday method	175
Table 11.6	Mineral contents of magnetic fractions of Eneabba altered ilmenite	179
Table 11.7	EPMA results for two 3-zoned grains of Eneabba altered ilmenite	185
Table 12.1	Composition of pseudorutile	188
Table 12.2	EPMA results for Indonesian pseudorutile	193
Table 12.3	Neutron diffraction spectrum of pseudorutile	200
Table 12.4	Measured parameters in Fe^{57} Mössbauer effect spectra for pseudorutile	200
Table 12.5	Magnetic hyperfine fields (H) of iron-bearing oxide minerals	205
Table B1	Calibration of Magnetic Field (Gouy method)	220

APPENDICES

		Page
Appendix A	Synthesis of ilmenite	218
Appendix B	Magnetic field calibration for the Gouy method	219
Appendix C	Calculation of specific susceptibility for the Gouy method	221
Appendix D	Calculation of specific susceptibility for the Faraday method	222
Appendix E	Calculation of calibration constants for the Cook magnetic separator	223
Appendix F	Quantitative XRD spectra for magnetic fractions from the South Capel deposit	224
Appendix G	Quantitative XRD spectra for magnetic fractions of Eneabba altered ilmenite	234
Appendix H	List of symbols	239

CHAPTER 1

INTRODUCTION

1.1 Background to the investigation

Australia's beach sand mining companies currently provide some 30% of the total world ilmenite production of 4×10^6 tonne/a, which comes from both beach-sand and hard-rock deposits. Most of the Australian ilmenite is used for titania pigment manufacture by the sulphate route. Over 90% of Australia's production comes from the rich Western Australian deposits, which unlike some ilmenite deposits on the east coast are not contaminated by excessive amounts of chromite. The largest ilmenite reserves in Western Australia occur in the Capel and recently discovered Eneabba districts, and are fossilised beach strands in which the ilmenite has been considerably altered since deposition.

When this work started only very rough correlations were available between the mineralogical, chemical and magnetic properties of the grains in any commercial concentrates of detrital ilmenite. Good correlations would permit the production of improved mineral concentrates and allow greater efficiency in mineral treatment operations. Even in ilmenite concentrates which are of saleable grade, the distribution of contaminants between the various minerals present is not adequately known. Thus the chromium in W. Australian ilmenite is wrongly thought to occur mainly in solid solution in ilmenite (Welch et al, 1975, p1073), and highly magnetic grains with strongly ferromagnetic properties are popularly but wrongly considered to be "magnetite".

The mineral pseudorutile,which was found in Western Australian ilmenite in 1966 (Temple), is not generally recognised within the industry as a major component of the commercial ilmenite concentrates. In 1975, Lissiman and Oxenford expressed the view that pseudorutile is a component of a mixture of alteration phases corresponding to the (previously discredited) mineral "arizonite", although Welch et al (1975) included pseudorutile in the X-ray diffraction spectra of ilmenite sands worked by Westralian Sands Ltd. This uncertainty about the status of pseudorutile is understandable, since it is only in recent years that the structure and some of the properties of pseudorutile have been described, and the magnetic nature of this mineral has not been known.

Although a vast body of research data is available in the literature for pure synthetic compounds and for metallic alloys, the magnetic properties of minerals in general have been a neglected field of study. The magnetic oxides used by the tape recording industry, ferrites employed as commercial magnets and as electronic components, and materials suitable for magnetic 'bubble' memories in computers, are just a few topics which are considered in the available literature. In view of the great volume of current magnetic research, the relative disregard for natural minerals is surprising. Fortunately, a good deal of information is already known about some of the minerals studied in this investigation (i.e. ilmenite, hematite and magnetite), but some of the observed magnetic features of ilmenite and hematite have still not been adequately explained, however.

1.2 Scope of investigation

The investigation was mainly concerned with the study of detrital altered ilmenite, pseudorutile and secondary rutile. Other detrital and secondary oxide minerals were also considered when they occurred in the same samples. Most of the samples were obtained from Western Australia, but samples from other areas were also studied briefly. The properties of pure ilmenite were also examined in order to form a starting point for the investigation of ilmenite alteration effects.

1.3 Aims

A general aim of the present work has been to investigate the inter-relationships between the magnetic properties of mineral particles and their mineralogical compositions, chemical analyses and X-ray diffraction spectra, for fractions of different average magnetic susceptibility. These fractions have been prepared from heavy mineral concentrates rich in ilmenite that shows various degrees of alteration through pseudorutile to secondary rutile (commercial leucoxene). The results of the investigation will be of value to the companies producing concentrates, and also to the TiO_2 pigment industry which consumes these concentrates.

Another general aim has been to establish a test programme which can be used to study material from any detrital ilmenite deposit, to derive the parameters required for efficient mineral separation and to ensure that the necessary chemical quality of the concentrates can be reliably obtained.

1.4 Objectives

A specific objective has been to establish whether the magnetic susceptibility of altered ilmenite particles can be correlated directly with their mineralogical composition.

Another objective has been to elucidate the magnetic nature of pseudorutile.

1.5 Presentation

The findings of this investigation have been presented as follows.

In Chapter 2, the materials investigated are briefly listed and the sequence of preparation and testing is outlined.

In Chapter 3, the available literature on various aspects of ilmenite alteration is reviewed in historical sequence. This chapter forms a useful background to the terminology and the concepts which are selectively examined in greater detail in later chapters. Alteration textures and alteration models are also discussed.

Chapter 4 covers the basic theories of magnetism which underly the descriptions of mineral magnetic properties as summarised in Chapter 5. Chapter 6 describes methods used for measuring magnetic susceptibility while in Chapter 7, techniques for measuring magnetic transition temperatures are discussed.

In Chapter 8, the X-ray diffraction procedures employed are presented, whilst Mössbauer spectroscopy and neutron diffraction methods are considered in Chapter 9.

Results of investigations on material from the South Capel deposit, near Bunbury, W.A. are presented and discussed in Chapter 10, and for material from the Eneabba deposit north of Perth, W.A. in Chapter 11. Work on Indonesian pseudorutile is presented in Chapter 12.

Finally, in Chapter 13, the conclusions of the investigation are presented.

CHAPTER 2

MATERIALS INVESTIGATED

2.1 Source of materials

The majority of this work has been conducted on a sample of crude gravity concentrate from the Capel operations of Associated Minerals Consolidated, formerly Western Titanium Ltd., near Bunbury, Western Australia.

Products from the other beach sand mining companies having operations in the Capel area have not been examined.

Less detailed work has also been conducted on a badly-altered ilmenite, rich in pseudorutile, from the Eneabba operations of Associated Minerals Consolidated.

A sample of Indonesian pseudorutile from the island of Singkep, supplied by Dr. K.J. Henley of Australian Mineral Development Laboratories (Amdel) of Adelaide, South Australia, has also been studied.

Other samples examined briefly for purpose of comparison with West Australian material include heavy mineral concentrates from Pulmoddai, Sri Lanka, supplied by Ceylon Mineral Sands Corporation. Various samples of hemo-ilmenite from Norway were also examined in the course of the X-ray diffraction studies.

The nominally pure ilmenite used for reference measurements (Section 5.5) was synthesised by the author.

2.2 Preparation of detrital heavy mineral samples and treatment programme

The general preparation sequence and the treatment schedule adopted are given in the flowsheet, Fig. 2.1.

Fig. 2.1 Preparation sequence and treatment programme for heavy mineral samples

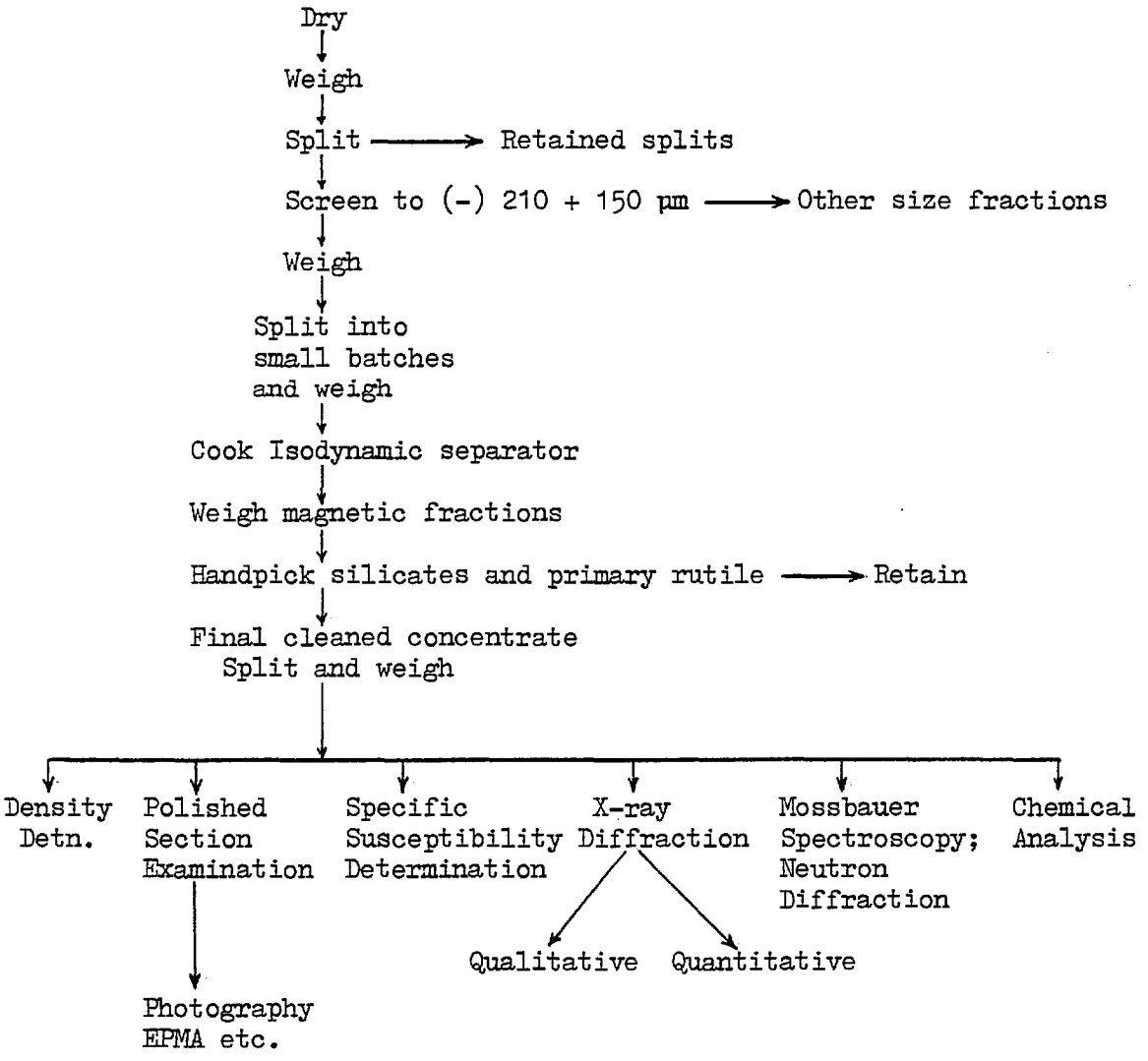

Heavy liquid separation was not used to remove the light minerals. Since many of the altered ilmenite grains are known to be porous it was important not to contaminate these grains with heavy liquids. The last traces of these liquids are very difficult to remove, and could affect density determinations and hence the apparent values of mass magnetic susceptibility obtained by the Gouy method (Section 6.3).

Several steps in the preparation sequence are extremely slow and had to be conducted with great care in order to secure reproducibility of recovery values and product quality. The magnetic fractionation by a Cook isodynamic separator according to the specific susceptibility of the grains (Section 6.7), was done in small batches of 20-40 g, permitting comparison of the results obtained with each batch, and assessment of the repeatability achieved. The yield of most of the more weakly susceptible fractions was so low that large quantities of material had to be magnetically separated to produce small amounts of the desired products. (These same low susceptibility fractions contained the most silicate minerals, and required the longest time to clean).

An exceedingly tedious step requiring great care was the handpicking of silicates and primary rutile grains by an electrostatically charged needle. The method was the surest and safest way of handling the small weights of fine-grained particles.

A close size range of feed to a magnetic separator results in improved efficiency of separation and greater repeatability, due to a decreased incidence of entrained or misplaced particles. The size range selected for magnetic separation, (-210 +150 μm), was the coarsest fraction that was present in sufficient quantity in the

natural size distribution of the material, and this was chosen to improve the speed of the handpicking step.

In many cases there was insufficient final cleaned sample to permit all the various determinative tests to be applied. The tests therefore had to be done in sequence - susceptibility determination, photography, and density determination on the natural grain size, with material used for different magnetic tests kept separate to avoid the effects of any weak remanent magnetism modifying the results of subsequent tests. X-ray diffraction and/or Mössbauer spectroscopy or neutron diffraction tests were conducted after grinding the fractions to a fine powder. The quantitative X-ray diffraction tests 'consumed' some of this powder by mixing it with various standards. Any remaining unused powder was available for chemical analysis. Insufficient material was obtained at currents higher than 0.45A to provide a chemical analysis. This was a consequence of the natural distribution of the mineral grains, and the paucity of grains with specific susceptibilities between 60 and 2.5×10^{-2} JT^{-2} kg^{-1}.

CHAPTER 3

ILMENITE ALTERATION

3.1 Review of literature on ilmenite alteration and properties of altered ilmenite

In the study of ilmenite alteration, the relevant literature goes back over 70 years, and it is only comparatively recently that the complexities of the phenomenon show signs of being satisfactorily resolved.

In the progressive development of the subject, a variety of spurious mineral names have been proposed along the way, resulting in considerable controversy and confusion.

Leucoxene (i.e. impure secondary TiO_2) was apparently named by Gumbel (1874) but its mineral composition had remained in doubt until Tyler and Marsden's work (1938). They used X-ray diffraction to examine leucoxene samples and deduced that "leucoxene is a microcrystalline form of rutile, anatase or perhaps brookite, and that the material develops from surface weathering or hydrothermal alteration of sphene or ilmenite".

Arizonite was a name proposed by Palmer in 1909 (Overholt et al, 1950) for a material with the composition $Fe_2O_3.3TiO_2$. "Arizonite" was studied by Overholt, Vaux and Rodda, (1950). From X-ray diffraction studies, they concluded that arizonite was an impure mixture of hematite (Fe_2O_3), ilmenite ($FeTiO_3$), anatase (TiO_2) and rutile (TiO_2), derived from the weathering of ilmenite. Their X-ray studies were made using films and it is doubtful that the same precision and accuracy could have been obtained in 1950 as with modern cameras and diffraction technique.

Curnow and Parry (1954) reported on impure ilmenites from eastern Australian beach sands, and commented on the oxidation of ferrous ions to the ferric state during oxidation between 600° and 800°C, which gave an apparent increase in magnetic susceptibility. The high temperature products showed rutile and an unknown but apparently tetragonal mineral.

The first detailed study of the chemical and mineralogical composition of detrital ilmenite specimens was carried out by Lynd et al (1954). They reviewed the available literature and concluded that there was "no reason to postulate the existence of a hypothetical compound, arizonite, to account for the composition of titaniferous beach sand concentrates", and that the concentrates they studied were "examples of the different products that can result from various degrees of alteration of primary ilmenite". They clearly recognised the possibility of progressive alteration and of products of differing composition. They also provided detailed chemical analyses for magnetic fractions collected at progressively increasing separation currents, and high quality photomicrographs of ilmenite showing different stages of alteration. They noted that the more altered fractions appeared to contain more rutile and hematite, with only negligible amounts of ilmenite.

Although Lynd et al concluded that "the ratios of Fe_2O_3 to total iron in the different ores indicate that oxidation has accompanied alteration" and that "the higher TiO_2 to Fe ratio in the altered ores is good evidence that leaching of iron has occurred", they failed to explain why their curves for the Quilon and Brazilian ilmenites showed an apparent <u>decrease</u> in oxidation (for less magnetic fractions collected at higher currents) until a certain separation current was reached, beyond which the expected progressive

increases in oxidation with decreasing magnetic susceptibility then became evident. However Lynd et al's data can be explained by the present investigations (Section 10.5). They unwittingly provided sufficient evidence to indicate the presence of a new mineral phase (pseudorutile) of which they quoted the main X-ray diffraction peak, but which evaded precise definition until 1966.

At this stage, the feeling of various researchers that another phase existed besides ilmenite, hematite and the TiO_2 polymorphs, is evident from the persistence of the controversy over arizonite.

The next stage in the development of ilmenite alteration theory came in 1956 in work published by Bailey, Cameron et al.

This was the first detailed work specifically to examine ilmenite alteration as such, and like Lynd et al, provided abundant supporting data. In their attempt at quantitative documentation, they did not wholly succeed, due partly to the unavoidably subjective nature of their mineralogical descriptions, partly due to the fact that they failed to report the side slope of the Frantz isodynamic magnetic separator which they used to separate their mineral fractions, and also as a result of using separation current increments which (for the more highly magnetic fractions) were so large as to mask the slight changes in mineralogy taking place. However, they qualitatively defined three sequential stages of ilmenite alteration: (1) patchy ilmenite, (2) amorphous iron titanium oxide and (3) end-product leucoxene. Criteria for optical recognition of these stages were given, together with the valuable observations that "in the materials studied, alteration of part of a grain to leucoxene is always preceded by alteration of that part

to amorphous iron-titanium oxide" (referring to the spatial distribution of the relict and secondary phases) and that stages 1 and 3 could overlap so that "many grains are composites of unaltered ilmenite, amorphous material and leucoxene". Their photomicrographs showed a range of typical textures, which they explained as the result of penetration of alteration both along crystallographic planes of weakness and fractures in the grains.

They correctly noted that leucoxene showing brown internal reflections is more magnetic than that showing white internal reflections, and that "separation of.... altered ilmenite into clean subfractions of sharply distinct mineralogical composition is not likely to be achieved by physical means". Their contention that "no marked change in magnetic susceptibility takes place during the alteration of ilmenite to amorphous iron-titanium oxide", is in conflict with their generalisation that "alteration is accompanied by progressive decrease in magnetic susceptibility", and data which contradict the first statement will be presented in this work (Chapter 10).

Bailey et al (1956) failed to detect any evidence of the "hypothetical mineral arizonite". They stressed the presence of amorphous iron titanium oxides and used single-crystal methods to document the collapse and broadening of ilmenite peaks as alteration proceeded; the progressively weaker and more diffuse nature of the X-ray patterns from more highly altered ilmenites; and the re-appearance of distinct, well-discernible spectra in the better-crystallised leucoxene end-products.

The data presented by Bailey, Cameron et al support their finding that no simple relation exists

between stage of alteration, chemistry of alteration and magnetic susceptibility. However, the present author considers that this is mainly a consequence of the finely intergrown nature of the primary and secondary phases.

Allen (1956), used electron micrographs to claim that leucoxene is not always a secondary rutile, but is commonly an amorphous titanium oxide containing one percent or less of well crystallised grains of anatase which contribute to observed X-ray patterns. He also mentioned yet another dubious mineral (hydrotitanite), and drew attention to variations in the amount of absorbed water. Bailey and Cameron (1957) then drew attention to the problem of usage of the term leucoxene, which is now retained as a name for impure high-titania secondary rutile by the titania pigment industry but which is of course not a bona-fide mineral species.

Flinter (1959) in his study of Malayan ilmenite grains developed the approach of Bailey, Cameron et al by systematically attempting to correlate progressive changes in density, powder colour, low power microscope appearance and Vickers microhardness. He also presented results of ore microscopy on magnetic fractions, their chemical analyses and their X-ray diffraction powder patterns. He reported attempts to recrystallise altered ilmenite by heating - which resulted in the formation of rutile and pseudobrookite, and "established that normal ilmenite can alter, in the solid state, to a material that resembles rutile with iron oxide present in a colloidal state, and which retains the rhombohedral form of the ilmenite".

The ilmenites examined by Flinter may have included grains free from solid solution of hematite since the highest susceptibility he quotes of 93.92 x 10^{-6} erg. $Oe^{-2}g^{-1}$ (CGS) is very close to the 96 x 10^{-6} value for pure synthetic ilmenite. In quoting the side slope employed on his Frantz isodynamic magnetic separator, and in calculating the magnetic susceptibility of his fractions, Flinter gives magnetic data which are more useful than those of Bailey, Cameron et al., and the data are detailed enough to allow the calibration constant of his machine to be calculated (Section 6.7). Like earlier workers using the magnetic separation technique, Flinter used increments of separation current which were bigger than ideal.

Flinter's data in part contradicted the findings of Bailey and Cameron, in that he regarded the second, amorphous stage of alteration as showing a marked decrease in magnetic susceptibility, having a susceptibility less than 40 x 10^{-6}erg $Oe^{-2}g^{-1}$ (CGS). His findings that a few percent of water was present led him to re-introduce yet another discredited mineral name - 'hydroilmenite' - that was not subsequently accepted by other workers. He also greatly oversimplified the magnetic changes occurring during alteration by stating that "the decrease in mass magnetic susceptibility is directly related to the oxidation of the Fe^{2+} to Fe^{3+} and to no other factor".

In a study of leucoxene from Quilon, India, Karkhanavala, Momin and Rege (1959) carried out X-ray diffraction tests on 3 groups of handpicked grains of different colours. Rutile, anatase, pseudobrookite and hematite were detected, and it was shown that black grains thought to be ilmenite did not in fact consist of this mineral. No residual ilmenite could be detected in the dark leucoxenes even in grains that were thought to constitute the first stage of alteration. This evidence is consistent with the X-ray diffraction behaviour of other commercial high-titania leucoxene concentrates - e.g. from Western Australia.

Most of the X-ray data were presented qualitatively and no tables of d-spacings or intensities were given. They took the absence of ilmenite to indicate that this mineral had been completely altered since the sharp X-ray patterns they obtained did not give them cause to believe that any "amorphous or cryptocrystalline phase" was present.

A subsequent paper by Karkhanavala and Momin (1959) on the alteration of ilmenite was in fact a study of the effects of controlled artificial oxidation at 650°C and 850°C, using commercial grade Quilon ilmenite concentrate as the starting material. They presented tables of their X-ray diffraction spacings and intensities, and measured the magnetic susceptibility of their products by the Gouy method (Section 6.3). Unlike Curnow and Parry (1954), they found that the susceptibility decreased with increasing temperature of oxidation, and this may be simply ascribed to the fact that Curnow and Parry were using an impure ilmenite concentrate from the east coast of Australia which is notorious for its unacceptably high content of free chromite. (Oxidation of impure chromites might well be expected to form more highly magnetic spinels if ferrous ions were present in the original grains). It was also found that ilmenite oxidised at 850°C for 6 or more hours gave a mixture of hematite, pseudo-brookite and rutile that was almost indistinguishable from a natural "brown" leucoxene. It is likely however that this result is a fortuitous consequence of the composition of their starting materials, and should not be regarded as applicable to material from any deposit.

Karkhanavala contributed still further with a paper on the nature of arizonite (1959). The earlier findings of Overholt et al (1950) were criticised, and it was argued that there was no evidence for the existence of ilmenite and very little for the existence of hematite, because of incorrect

intensities, and that doubt existed about the presence of rutile. Karkhanavala therefore deduced that there is no real justification for regarding the X-ray pattern of natural "arizonite" as being composed of a mixture of hematite, anatase, rutile and ilmenite. He agreed that arizonite cannot be synthesised under dry conditions, but claimed to have successfully synthesised* a small quantity of arizonite by hydrothermal means. He concludes that arizonite is a genuine mineral which forms by the hydrothermal alteration of ilmenite. No subsequent workers have confirmed this hydrothermal synthesis, and arizonite has remained a discredited mineral (Fleischer, 1967).

The reaction of ilmenite with hydrogen sulphide to form pyrite and rutile is discussed briefly by Gruner (1959). The alteration of ilmenite under reducing conditions in unconsolidated sediments was further examined by Carrol (1960), who mentions the encrustation of ilmenite by pyrite, suggesting it has formed from the ferrous ion of the ilmenite. Such alteration of ilmenite by sulphidization was re-examined by Dimanche and Bartholomé (1976) (see below).

Lynd (1960) attempted to assess the mechanism and rate of ilmenite weathering from results of leaching and etching tests using weak acid solutions. He concluded that ilmenite is most readily attacked by acid solutions along twin lamelle if present, but that the basal planes are otherwise the most rapidly etched. Humic acid and sulphuric acid were the most effective leaching agents of those likely to be in ground water. Subsequently Lynd (1960b) discussed the terminology

*A monoclinic, metastable form of $Fe_2Ti_3O_9$ has been synthesized at 770°C by Grey and Reid (1972) and corresponds to n = 5 in the homologous series $(Cr,Fe)_2\ Ti_{n-2}\ O_{2n-1}$. However, the XRD spectrum of this mineral is very different from those of arizonite and pseudorutile.

of various workers and their comments on his own paper of 1954, and also attacked Karkhanavala's claim to have formed arizonite, and made suggestions for making the meaning of certain terms (e.g. leucoxene) used in papers on ilmenite alteration very much more precise. Lynd himself was then criticised in a further contribution from Golding (1961), who took the classification of various types of leucoxene very much further and also discussed the effect of variations in the primary mineralogy and of included minerals on the characteristics of the final alteration products. Golding concluded that apart from ilmenite, sphene and ferroan rutile were the minerals most likely to alter to leucoxene.

Fleischer (1964), commenting on a proposed new ilmenite-alteration mineral called proarizonite, rejected the new phase and likened it to arizonite, which he recalled had been rejected earlier by Overholt et al (1950).

A break-through occurred when Teufer and Temple (1966) treated small grains of altered ilmenite as if they were single crystals, and recorded the diffraction patterns from different grain orientations using rotating crystal, equi-inclination Weissenberg and precession camera techniques. From these patterns they deduced that a major portion of the grains consisted of a hexagonal mineral with a disordered structure and the theoretical composition $Fe_2Ti_3O_9$ for which they proposed the name pseudorutile. They considered that the nearly perfect hexagonal close packing of oxygen atoms present in ilmenite is only slightly affected during the transformation ilmenite-to-pseudorutile-to-rutile. The oxidation of ilmenite to pseudorutile was illustrated by an equation, but no details of the mechanism were given.

No claim was made by Teufer and Temple that their new mineral solved the problems raised by the previously suggested minerals arizonite and proarizonite which had the same nominal composition. They merely pointed out that their table of interplanar spacings and intensities for pseudorutile was distinctly different from those published for arizonite and proarizonite, and stressed that superposition of most of the powder lines might result in pseudorutile being mistaken for rutile.

Temple (1966b) went further and incorporated the discovery of pseudorutile into a re-assessment of ilmenite alteration. His study incorporated descriptive reflection microscopy, qualitative and quantitative analysis by electron probe microanalyser, and also correlation of wet chemical analyses with specific gravity, specific surface and qualitative magnetic behaviour. Unlike earlier workers, he did not analyse fractions of differing susceptibility produced by magnetic separation from a given detrital ilmenite concentrate. He was able to show by X-ray diffraction that pseudorutile was a major component in the Trail Ridge and Quilon concentrates, and he showed that the powder patterns of altered ilmenites from three continents could be indexed in terms of the three minerals ilmenite, pseudorutile and rutile alone, with all the diffraction lines accounted for.

Oxidation and reduction experiments were also reported by Temple, and the products were examined by electron micrography and electron-probe microanalysis. Note was made that the alteration of ilmenite in nature is in some respects analogous to high temperature oxidation as claimed by earlier workers.

An analysis of drill hole samples from progressively increasing depth in the Trail Ridge, Florida deposit pointed clearly to enrichment in TiO_2 in the near surface layers corresponding to peak development of leucoxene, and confirmed that alteration takes place in situ. The ilmenite alteration profile was found to be accompanied by the etching and corrosion of epidote and garnet grains, which was negligible at the base of the deposit but very advanced near the surface.

Although pseudorutile remained at this stage an incompletely characterised mineral, the evidence for its existence was considerable. This evidence failed to convince Fleischer (1967), who considered that the papers presented by Teufer and Temple (1966) and by Temple (1966) only added more confusion, and that their data failed to establish pseudorutile as a species. Other workers however were already accepting the evidence for pseudorutile, and in 1971, Larrett and Spencer described an apparently pure pseudorutile from a South Australian locality. The composition obtained by electron probe microanalysis was shown to be very uniform. The X-ray diffraction film gave lines agreeing closely with those of Teufer and Temple but many of the weaker lines were not detected. Properties determined included specific gravity, magnetic susceptibility and the mean optical reflectance in air at four wavelengths. The description of optical properties included the apparent isotropic nature of the grains but the inconsistency with a non-isometric structure was not discussed.

Jones (1974) during an optical microscopy examination and electron-probe microanalyser study of the industrial reduction of Australian ilmenite, briefly discussed the morphology of detrital ilmenites and specifically looked for pseudorutile by electron probe microanalysis. It was confirmed by slow scanning across individual grains that in general,

regions enriched in titanium are relatively depleted in iron. The general finding however was that the various phases occurring in weathered ilmenite are so finely intergrown that they cannot be resolved by EPMA. That this is so for the vast majority of altered grains has also been the author's experience (Chapter 10).

Grey and Reid (1974) discussed the close coincidence of all the main diffraction lines of pseudorutile with those of rutile, and were able to determine its approximate amount by a quantitative XRD technique (Section 10.9). By this technique they were able to demonstrate the increased amounts of pseudorutile and rutile in an 'altered ilmenite' concentrate from Capel, Western Australia, when compared with a less altered ilmenite concentrate from the same deposit.

In 1975 Grey and Reid re-examined the South Australian pseudorutile together with a slightly impure Indonesian specimen which gave sharper reflections for some of the lines. A single grain of the Indonesian material was used to carry out a complete structural analysis which permitted the hexagonal space group to be identified, ($P6_322$). Their structural model was an averaged representation and indicated that pseudorutile was not a wholly disordered mineral but in fact possessed a one-dimensional periodic structure parallel to the c-axis consisting of well-ordered chains with imperfect lateral ordering. This partial order would contribute to the observed mineral stability, for Teufer and Temple's work had failed to explain why pseudorutile was such a persistent phase, and Grey and Reid further pointed out that the pseudorutile composition corresponds to the maximum removal of iron from the ilmenite stucture without concurrent removal of oxygen. The formation of secondary rutile from pseudorutile requires not only the leaching out of the iron, but also removal of oxygen and thus the breakdown of the close-packed oxygen

lattice. The first stage of ilmenite alteration (to pseudorutile) was postulated by Grey and Reid to take place chiefly below the water table, while the second stage of alteration (pseudorutile to rutile) was considered to take place mainly above the water table. The consequences of this model are complicated by the fact that even the surface layers can become saturated when the water table rises in the wet season (as for example in the Capel deposits in Western Australia). It is unlikely, however, that this question can be ever entirely removed from the field of speculation, since a full record of palaeoclimate, ground water chemistry and water table depths would be required to settle the matter.

Dimanche and Bartholomé (1976) reviewed the alteration of ilmenite in sediments. On South African detrital ilmenite they distinguished 4 optically different stages of ilmenite alteration which they correlated with reflectivity (which increases as the alteration proceeds from about 18% to 21.22%) and TiO_2 content, ranging from 50% to over 90%. It was not made clear whether or not the quoted TiO_2 analyses refer to homogeneous areas of individual grains or to the bulk composition of a fraction specially prepared, and consisting predominantly of grains showing the particular stage of alteration. The optical properties of pseudorutile were dismissed as "not well known... this prevents a precise correlation between microscopic observation and X-ray crystallography".

Grey and Reid's equations for the two stage alteration of ilmenite to pseudorutile, and pseudorutile to rutile, were expanded to show the influence of hydrogen ions.

The oxidation of ilmenite to distinctive intergrowths of hematite and leucoxene in red beds is also discussed by Dimanche

and Bartholomé, and in a section on laterites and bauxites, it is claimed that ilmenite in bauxites can alter directly to leucoxene or anatase, as well as to a 'patchy ilmenite' as described by Bailey et al. The original source of these observations (Hartman, 1959) is before the discovery of pseudorutile and the conclusions are therefore suspect.

Dimanche and Bartholomé also review data on the sulphuration of ilmenite in stratiform copper deposits. An important observation is that the amount of a sulphide growing around an altered detrital grain of ilmenite is not necessarily related to the amount of leucoxene formed. Thus an iron sulphide crystal which started growing at the expense of iron contained in the ilmenite, could subsequently grow at the expense of other sources in the immediate environment. The overall impact of their review is to highlight the importance of post-depositional processes for alteration of ilmenite.

Conclusions:

Despite the extensive discussion which has been presented in the literature over various possible definitions of the term 'leucoxene', there has been general agreement that it consists mainly of secondary titanium oxide, formed by alteration of pre-existing titaniferous minerals. In this investigation on West Australian detrital ilmenite, the secondary titanium oxides have been shown to consist almost entirely of rutile, and the author in consequence refers mainly in the subsequent text to 'secondary rutile'.

Probably the major step forward in the understanding of ilmenite alteration came in 1966 with the recognition and initial description of pseudorutile. Data gathered in this investigation (Chapter 10) support published evidence that pseudorutile is a bona-fide mineral species.

3.2 Alteration textures

Characteristic textures of progressively altered ilmenite have been illustrated by Lynd et al (1954), Bailey et al (1956), Temple (1966) and Dimanche and Bartholomé (1976).

In addition to the development of an outer zone of secondary rutile displaying internal reflections under crossed polarisers, the inner parts of the altered grains show a variety of textural features. These may be developed singly to the exclusion of others, or they may be jointly developed and occupy different areas of the same grain. The irregular penetration of the external environment along sub-microscopic cracks and planes of weakness, and through porous zones, results in a multi-front attack on the original ilmenite. 'Efflorescent' spots of alteration may appear apparently at random, or along the walls of cracks, and these spots grow in size as the alteration proceeds. This leads to patchy and mottled areas, which are often centred on crack systems. Alternatively the spots may lie along parallel crystallographic planes, resulting eventually in internal bands of secondary rutile. Light to intense pitting may also develop, and it has here been shown that the pits often have a common alignment with exsolved titanhematite blebs which remain in the less-altered core (Section 10.11). Such a texture has been recorded by Dimanche and Bartholomé (1975, p193).

Although secondary rutile can develop well into the core of the original ilmenite grain, the bulk of the secondary rutile development appears to be in the outer zone. This effect has been demonstrated by comparing the XRD spectra from handpicked material carrying visible secondary rutile with the XRD spectra of the 'black' material remaining after handpicking. This 'black' material had less rutile than the visibly rutile-bearing material, although significant rutile was still present.

Photomicrographs of textures observed in this study are given in Sections 10.11 and 11.6. Textures resulting from the natural alteration of triangular lamellar intergrowths of ilmenite and magnetite (ilmeno-magnetite) were not observed in this study, but have been illustrated by Dimanche and Bartholomé (1975).

3.3 Models of ilmenite alteration

Factors which are considered to influence the progress of ilmenite alteration are as follows:

1. The initial composition and texture of the grains at the time of burial
2. The presence or absence of cracks and other flaws
3. The ambient chemical environment
4. The duration of burial

There is general agreement that ilmenite alteration occurs in situ, after deposition. Since all grains in a given heavy mineral strand are considered to have been buried for the same length of time, it is clear that the net reaction rates of some grains are very much faster than others. This is especially true in those deposits where grains occur ranging from almost pure ilmenite right through to almost iron-free secondary rutile. In part these differences can be ascribed to the depth of the grains in the deposit, particularly with reference to the fluctuations of the water table, which can be considered as a feature of the chemical environment. While the first 2 factors above are obviously important, they may be over-ridden by the third, as for example when highly fractured grains are protected from chemical attack by being cemented into goethite masses ("coffee-rock".)

Probably the earliest concept of ilmenite alteration is modelled in Fig. 3.1. The first advance came when Bailey et al (1956), provided a 3-stage hypothesis of alteration which may be summarised schematically by a core of relict ilmenite surrounded by successive concentric rings of patchy ilmenite, amorphous Fe-Ti oxide and leucoxene (secondary rutile), Fig. 3.2.

The discovery of pseudorutile by Teufer and Temple (1966) permits an alternative model (Fig. 3.3), which is also incomplete since it does not account for optical or X-ray amorphism.

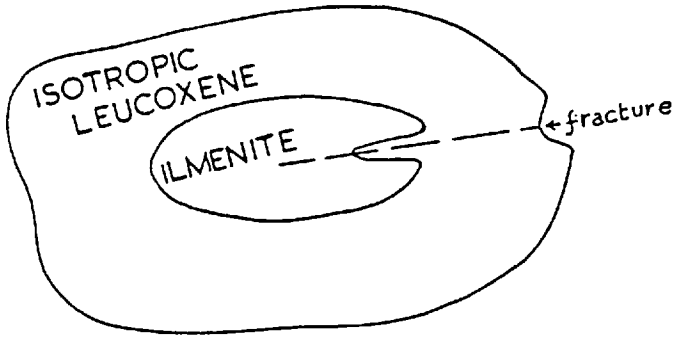

Fig. 3.1 Early model of ilmenite alteration, based on observations of leucoxene pseudomorphous after ilmenite (Edwards, 1942)

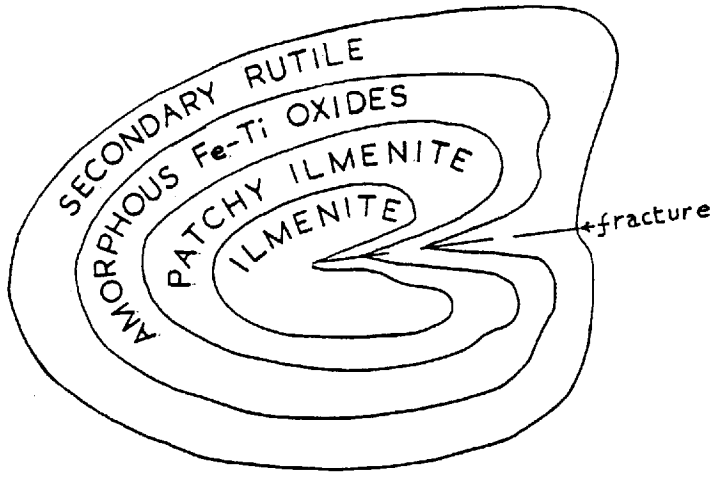

Fig. 3.2 Model of ilmenite alteration, derived from Bailey et al(1956).

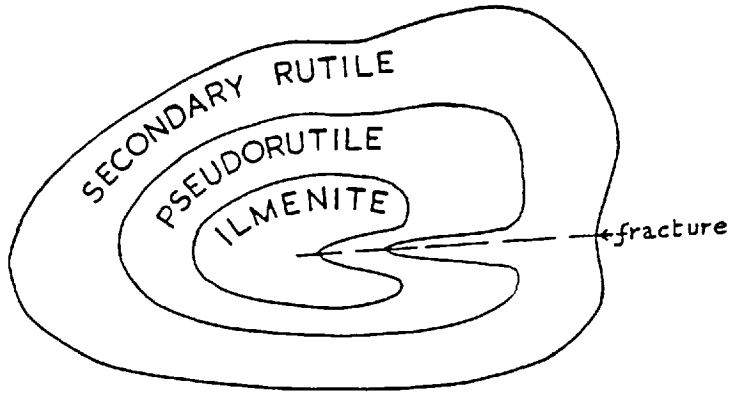

Fig. 3.3 Model of ilmenite alteration derived from Grey and Reid(1975).

Teufer and Temple (1966) suggested that the alteration of ilmenite to pseudorutile followed the equation:

$$\underset{\text{ilmenite}}{Fe_3^{2+}\,Ti_3O_9} \xrightarrow{\text{oxidation}} \underset{\text{pseudorutile}}{Fe_2^{3+}\,Ti_3O_9} + \tfrac{1}{2}\,\underset{\text{hematite}}{Fe_2^{3+}O_3}$$

They could only explain the further alteration of pseudorutile to rutile by reference to the changes that occur when pseudorutile is heated above 800°C

$$\underset{\text{pseudorutile}}{Fe_2^{3+}\,Ti_3O_9} \xrightarrow{>800^\circ C} \underset{\substack{\text{(ferric)}\\ \text{pseudobrookite}}}{Fe_2^{3+}\,TiO_5} + \underset{\text{rutile}}{2TiO_2}$$

Grey and Reid (1975) used a 2-stage chemical model:

1) $$\underset{\text{ilmenite}}{3Fe^{2+}\,TiO_3} \longrightarrow \underset{\text{pseudorutile}}{Fe_2^{3+}\,Ti_3O_9} + \underset{\text{leached out}}{Fe}$$

This equation indicates the loss of one third of the iron and the oxidation of remaining iron to the ferric state.

2) $$\underset{\text{pseudorutile}}{Fe_2\,Ti_3O_9} \longrightarrow \underset{2^\circ\text{ rutile}}{3TiO_2} + \underset{\text{leached out}}{2Fe^{3+} + 3O^{2-}}$$

The rutile is considered to be titanium oxide which goes "into solution" when the pseudorutile lattice breaks up, but which immediately reprecipitates epitaxially on to the relict pseudorutile substrate. This theory is supported by Golding's (1961) concept of a "transitory colloidal suspension of titania in situ" to explain colloidal features. In Stage 1 the pseudorutile would form topotaxially by the diffusion of iron outwards through the essentially unchanged oxygen lattice: in Stage 2 the oxygen lattice is broken up since both oxygen and iron are removed.

Grey and Reid's (1975) equations were further modified by Dimanche and Bartholomé (1976), to show the influence of hydrogen ions and oxygen:

3) $3Fe^{2+}\ TiO_3 + 2H^+ + \frac{1}{2}\ O_2$

$\longrightarrow\ Fe_2^{3+}\ Ti_3O_9 + Fe^{2+} + H_2O$

4) $Fe_2\ Ti_3O_9 + 4H^+ \longrightarrow\ 3TiO_2 + 2Fe^{2+} + 2H_2O + \frac{1}{2}\ O_2$

Grey and Reid (1975) suggested that reaction (1) occurs below the water table, while reaction (2) commences above the water table, and cited Temple's (1966) observation that it only proceeds to any extent in the topmost few metres of the Florida deposit. It is clear however that the two formulae are a gross simplification of a very slow process that is controlled by the diffusion rate of iron through ilmenite and by complex variations in the ambient chemical environment which affect the leaching rate of the iron. Many of the West Australian ilmenite deposits contain zones of 'coffee-rock' consisting of ilmenite and other heavy minerals cemented by goethite and silica, and it is strongly suggested that the goethite represents a reprecipitation of iron leached from adjacent ilmenite-bearing sands.

The key question of why in certain deposits the alteration should proceed to essentially complete conversion of ilmenite to pseudorutile, with minimal or no development of secondary rutile, has not yet been satisfactorily explained.

Altered grains commonly show an outer zone of secondary rutile, but very fine grained 'isotropic' altered ilmenite and secondary pseudorutile cannot normally be optically distinguished. Bailey et al (1956) claimed that in their materials, leucoxene (secondary rutile) was never in direct contact with ilmenite but that 'amorphous iron-titanium oxide' could always be seen to intervene. Despite this claim, concentric three zoned grains which might be expected to be fairly common are in fact very rare, even allowing for the fact that the surface of the polished section will not intersect all grains along their maximum diameter, Fig. 3.4. Three-zoned grains have been examined in this work however, and photomicrographs are reproduced in Chapter 10.

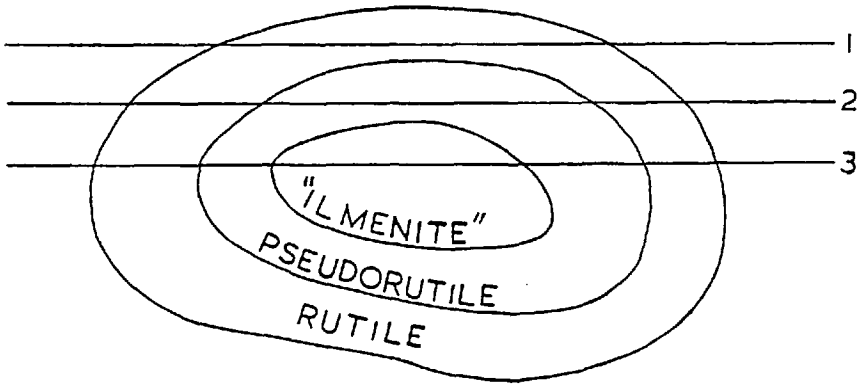

Fig. 3.4 Relationship of the intersecting plane to idealised alteration zoning

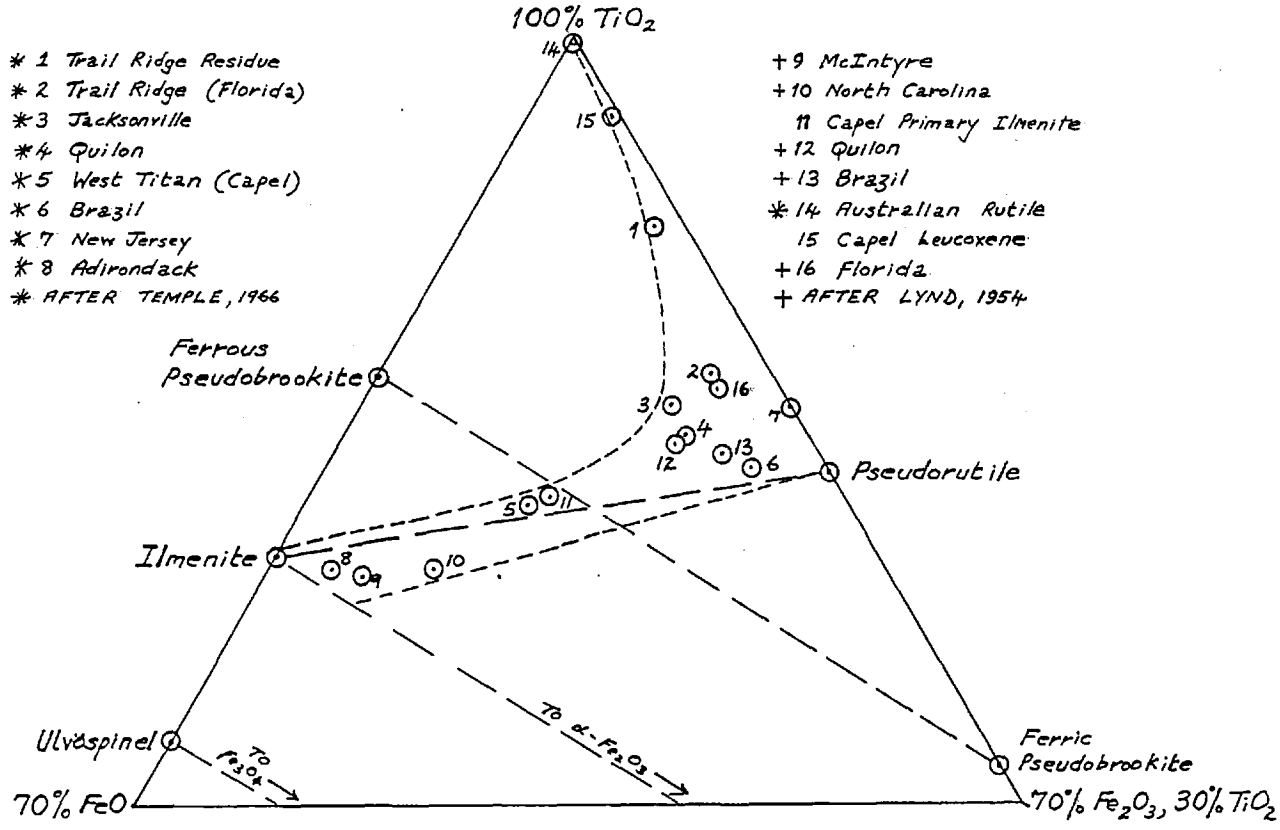

Fig. 3.5 Average chemical composition of altered ilmenite concentrates and other samples (redrawn after Temple, 1966).

The chemical trend of ilmenite alteration can be visualised from Fig. 3.5, and it is interesting to note that the alteration band crosses the line of the pseudobrookite solid-solution series.At normal temperatures only (ferric) pseudobrookite is stable and ferrous pseudobrookite is only known from high temperature materials: this accounts for the absence of members of the pseudobrookite series from the natural ilmenite alteration sequence. (Ferric pseudobrookite and rutile are formed however when ilmenite is oxidised at temperatures above 800°C (Jones, 1973)).

The spread of the composition band in Fig. 3.5 can be interpreted in terms of the onset of formation of secondary rutile from pseudorutile. Because secondary rutile develops before conversion of ilmenite to pseudorutile is complete, observed compositions tend to be richer in TiO_2 and lower in Fe_2O_3 than would otherwise occur. It is not known whether the concentrates whose normalised average compositions are given in Fig. 3.5 have been previously cleaned of primary rutile. Small amounts of this mineral would slightly affect the analyses. It must also be pointed out that the concentrates probably contain particles displaying a wide range of alteration states and magnetic susceptibilities.

CHAPTER 4

MAGNETIC THEORY

4.1 Introduction

Magnetic properties of matter were first studied in detail by Bacon in the 16th Century, but it was not until the experiments of Oersted in 1820 and Faraday in 1831 that the relationship between magnetic fields and electric currents became established.

Classical theories of diamagnetism, paramagnetism, and ferromagnetism which were developed from the work of Ampère, Weber, Langevin, Curie and Weiss, have since been replaced by the explanations of modern quantum mechanics which account for much finer details of magnetic phenomena and are widely employed in current research in solid state physics.

4.2 Discussion of basic concepts in magnetism

General:

The magnetic properties of matter are a function of the properties of the constituent atoms, which contain electrons each of which may be considered to be spinning on its own axis and circulating in its own orbit. Magnetic moments are associated both with the orbital motion and with the spin. The magnetic moments due to motion and due to spin in the first Bohr orbit (as for instance in hydrogen) are equal in strength and represent a fundamental unit of magnetic moment known as the Bohr magneton, $\mu_B = 9.2732 \times 10^{-24}\ JT^{-1}$.

The spin and orbital magnetic moments are vectors, parallel to the spin axis and perpendicular to the plane of the orbit, respectively. The overall moment of the whole atom is the vector sum of the electron magnetic moments.

If two electrons are within a given energy level (orbital) they rotate in opposite directions and their magnetic moments exactly cancel. Such "pairing" of all the electrons in the atom leads to absence of a magnetic moment, corresponding to net diamagnetic behaviour as shown by many ionic and molecular solids, and closed-shell atoms such as Ne, A. A diamagnetic substance is one which is repelled from a region of increasing magnetic field. All matter is diamagnetic in the sense that so long as a magnetic field is applied the electron orbits will move in such a way as to oppose the field, in accordance with Lenz's law of electromagnetic induction. The induced diamagnetic magnetisation is negative. The diamagnetic susceptibility, which is the magnetisation divided by the free space induction, is thus also negative and it is generally one or two orders of magnitude smaller than paramagnetic susceptibilities.

Paramagnetic susceptibilities are positive, and result if some electrons within the atom are left unpaired, leaving the atom as a whole with a net magnetic moment. Paramagnetic substances are attracted into regions of increasing magnetic field, and they form a very broad group which can be split into distinct major sub-groups as shown in Fig. 4.1. The empirical behaviour of the main types of magnetic material is illustrated in Fig. 4.2, and the characteristics of the various types are compared in Table 4.1.

Spin arrangements:

Various possible arrangements of magnetic spin moments are possible within the broad paramagnetic group, as shown in Fig. 4.3. Ordered arrangements of magnetic spins result from exchange interactions which may be positive or negative, and which lead to an apparent cooperative effect. This latter concept makes possible a classification of magnetic behaviour into two broad categories:

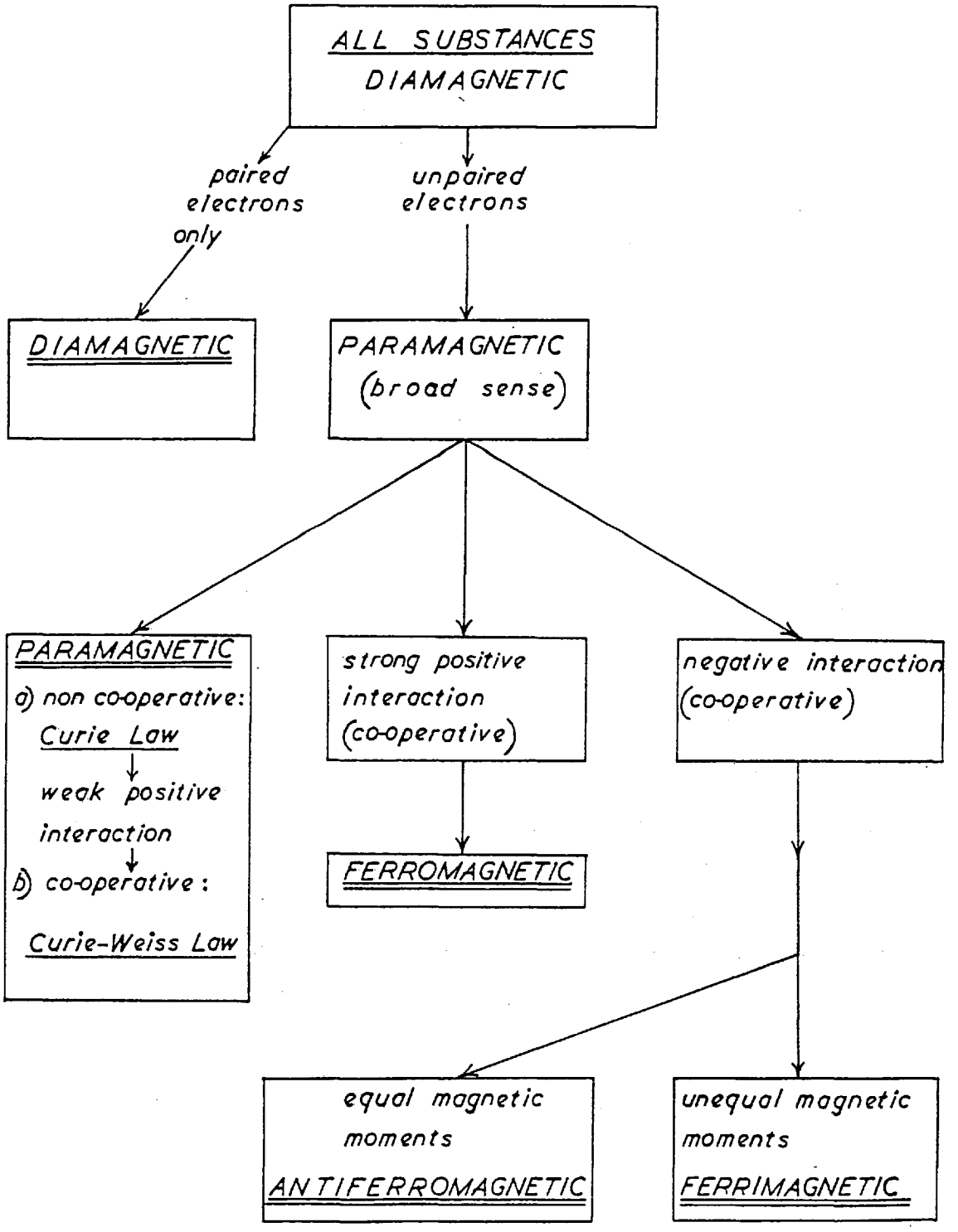

Fig. 4.1 The main types of magnetic behaviour (after Lee, 1963)

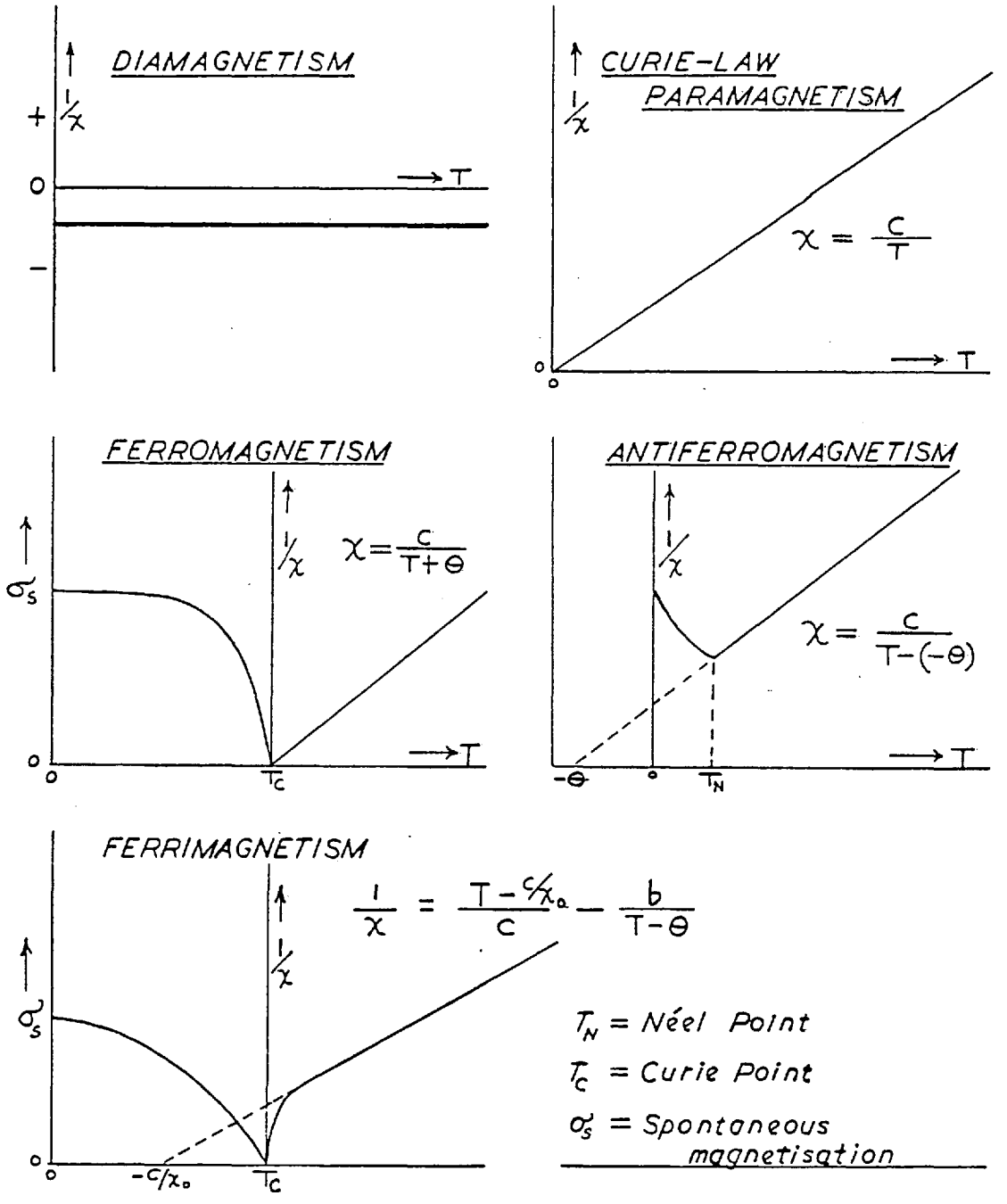

Fig. 4.2 Relation of magnetic properties to temperature for the main types of magnetic material.

Table 4.1

Comparison of the characteristics of the main types of magnetic material

Effect of external field on material	Diamagnetism $M < H$	Paramagnetism $M > H$	Ferromagnetism $M \gg H$	Ferrimagnetism $M > H$	Antiferromagnetism $M > H$
Examples	Most inorganic compounds, except those containing transition element ions; atoms with closed shells.	Salts and certain complexes of transition elements	Metals such as Fe, Co, Ni and their alloys	Fe_3O_4, $FeCr_2O_3$, γ-Fe_2O_3	Ti_2O_3, $Fe\,TiO_3$
Origin	Caused by orbital motion of electrons; a universal property. Most noticeable when all electrons are 'paired'.	Caused by spin and (usually) orbital momentum of unpaired electrons. Orbital component may be partially or completely quenched. In ideal paramagnetism there is no interaction of the magnetic moments. Effective moments are not generally calculable from first principles.	Magnetic spin moments lie parallel within individual domains. Positive interaction occurs between the magnetic moments	Each domain consists of two sublattices (A,B) of antiparallel spins. The moment of one sublattice is stronger than the other. Negative exchange interaction between A and B sites	Ideally each domain consists of two antiparallel sub-lattices of equal magnetic moments. However, spins may not be perfectly antiparallel. Negative exchange interaction between A and B sites
Magnitude of specific susceptibility (χ) at 293°K	Negative and very small ~1 x $10^{-2}JT^{-2}kg^{-1}$	Positive and small 1-100 x $10^{-2}JT^{-2}kg^{-1}$ Underlying diamagnetism is masked	Positive and very large. >10,000x10^{-2} $JT^{-2}kg^{-1}$	Positive; small to large. 1- ~10,000 x$10^{-2}JT^{-2}kg^{-1}$	Positive; small 1- ~100 x $10^{-2}JT^{-2}kg^{-1}$
Dependence of χ on					
a) Temperature	Theoretically none	$\chi \propto I/T$ Curie Law for ideal paramagnetics. $\chi \propto 1/(T+\theta)$ Curie-Weiss Law (non-ideal paramagnetics)	Complex	Not linear for $T \gtrsim T_c$	Linear above T_N
b) Field	None	None	Described by hysteresis curves below T_c	Described by hysteresis curves below T_c	Dependent below T_N

Modified after Mulay, 1963

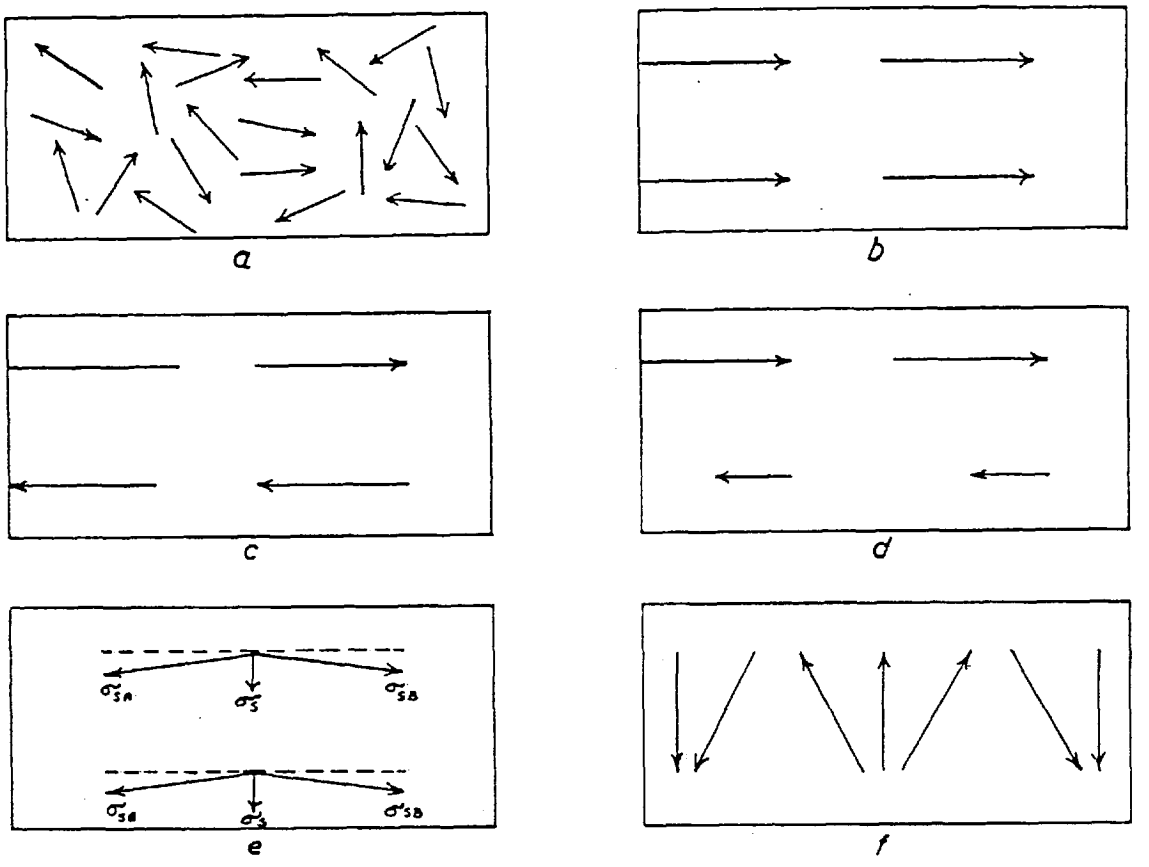

(a) disordered paramagnetic state
(b) parallel spins: ferromagnetism
(c) antiparallel spins: Néel type antiferromagnetism
(d) uncompensated antiparallel spins: Néel type ferrimagnetism
(e) canted spin Dzialoshinskii type weak ferromagnets
(f) helical spiral structures: compensated antiferromagnetic or uncompensated ferrimagnetic

Fig. 4.3 Various possible arrangements of magnetic spin moments (modified after Schieber, 1967)

1) Non-cooperative (statistical) behaviour of individual magnetic moments as found in diamagnetism and ideal (Curie Law) paramagnetism.

2) Cooperative behaviour of the magnetic moments leading to non-ideal (Curie-Weiss Law) paramagnetism, and ferromagnetic, ferrimagnetic and antiferromagnetic spin structures.

Ferro-, ferri- and antiferromagnetism share the feature that above a critical temperature which is characteristic of a given material, the cooperative behaviour collapses and the susceptibility, which was previously field dependent, gives way to the much weaker susceptibility of the paramagnetic regime which normally is only temperature dependent. Below the critical temperature, the magnetic spins within individual small regions known as domains are all mutually parallel, and the susceptibilities of the materials are field dependent.

Magnetic domains: The concept of domains was postulated by Weiss in 1907 (Stacey & Banerjee, 1974). He described a ferromagnetic as being divided into numerous small domains, each of which were spontaneously magnetised to saturation. By this theory, the process of magnetization then becomes one of converting the specimen from a state in which there are numerous domains magnetized in random directions, to the state where a suitably oriented domain grows under the influence of the field at the expense of the others. Eventually only one domain is left, and when (in a sufficiently high field) this rotates into alignment with the applied field, the magnetization has reached saturation.

Within an individual domain the magnetic spins take up a parallel orientation, due to an aligning force which opposes thermal agitations. This aligning force is an exchange interaction whereby the mutual electrostatic energy of two atoms is minimized if the unpaired magnetic spins of the electrons in the

3d shells are parallel to one another. The atomic magnetic moments thus collectively cooperate with one another, producing an alignment force which is proportional to the alignment itself (Stacey & Banerjee, 1974). Exchange interactions are strongest between nearest neighbour atoms. In oxide structures, the nearest neighbours are oxygen ions, and direct exchange interactions are not possible. Instead, a superexchange mechanism operates (Fig. 4.4) in which the moments of two magnetic ions coupled through an oxygen are antiparallel and thus effectively self-cancelling (Lindsley, 1976). The superexchange interactions are negative, and can lead to development of two magnetically opposing sub-lattices. In crystals where the opposing magnetic moments of the sublattices are equal, the net magnetism is zero and the crystal is antiferromagnetic. If one sublattice is stronger than the other, a net magnetic moment occurs and the crystal is ferrimagnetic.

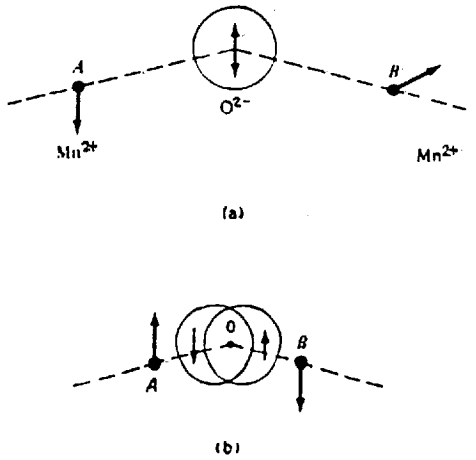

a) Consider two Mn^{2+} ions approaching an O^{2-} ion. Imagine the outer electrons of the oxygen to constitute two superimposed orbits, one spin up, the other spin down.

b) When the Mn^{2+} ions closely approach the O^{2-} ion, the spins of the oxygen set themselves antiparallel to the Mn^{2+} ion spins.

Fig. 4.4 The superexchange mechanism (taken from Cullity, 1972)

Domains in minerals can sometimes be observed by using the Faraday effect or the Bitter technique (Cullity, 1972).

Spinglasses: A newly discovered type of magnetic material which does not fit neatly into earlier classifications is the spinglass. Spinglasses (Sherrington, 1975) or mictomagnets as they are also known (Beck, 1978) were first named in 1970. They display features analogous to certain

apsects of both ferromagnetism and antiferromagnetism - hence the term micto - (i.e. mixed) magnetism.

There are certain orientations of the magnetic spins which can give a minimum potential energy state. The system is neither antiferromagnetic nor ferromagnetic on any scale, nor need it be unique. Nevertheless as the temperature drops there comes a critical temperature T_f, at which the spins notice the existence of this minimum potential energy state, and settle into it as T tends to zero (Edwards and Anderson, 1975). Above the freezing temperature T_f, spinglass materials behave paramagnetically. Even below T_f, they display no long-range ordering of the spins: in this they are distinguishable from true antiferromagnetics, which show long range order below T_N.

In synthetic alloys showing spinglass behaviour, the properties have been considered to be due to the freezing of superparamagnetic clusters (see below) into random spin orientations (Canella and Mydosh, 1972). Other authors consider spinglass behaviour to be due to random competition between ferromagnetic (positive) or antiferromagnetic (negative) exchange interactions. Many systems can provide such conditions, including amorphous materials, in some of which relaxation effects are evident (Sherrington, 1975). Because of the random spin orientations, spinglasses do not have a magnetic cell.

Until recently, virtually all known spinglasses were synthetic alloys. Behaviour qualitatively similar to that of a spinglass has been described for certain compositions of hematite-ilmenite solid solution (Section 5.7). In this investigation it was demonstrated that pseudorutile is a spinglass (Wort and Jones, in press) and synthetic pseudobrookite has also recently been identified as a spinglass (Atzmony et al, 1979).

Superparamagnetism: Ferromagnetic particles when not magnetised to saturation generally display many domains. Boundaries between any two domains are called Bloch or domain walls, over the width of

which the spins rotate progressively from the direction taken by the spins in the first domain, till they take up a direction the same as the spins in the second domain (Fig. 4.5). Commonly domain walls are several tens of nanometers thick, depending on competition between the crystal anisotropy energy and the magnetic exchange energy (Cullity, 1972 p288). For very small particles, it is no longer energetically possible for domain walls to form, and below a critical diameter D_s, which is poorly defined, the particles will be single domains. If still finer particles are present, then for a critical diameter D_p (Fig. 4.6), magnetic coercivity becomes zero. For such particles the thermal fluctuations are now of sufficient magnitude to overcome anisotropy forces and spontaneously reverse the magnetisation of a particle from one easy direction to another, even in the absence of an applied field. If a field is applied the magnetic moments of the particles will align, but thermal energy will tend to disalign them and they behave in a manner analogous to normal paramagnetics. Whereas the normal magnetic moment of an atom or ion is only a few Bohr magnetons, a 5 nm particle of (for example) iron, containing 5560 atoms, will also have a huge moment of 5560 x 2.2 μ_B. The behaviour of such fine ferromagnetic particles led to the coining of the term 'superparamagnetism'. Superparamagnetic materials display other special features such as reversible magnetisation to saturation without hysteresis, and once these materials are magnetised they can never be demagnetised (Cullity, 1972). Constraints on superparamagnetic behaviour occur with increase above a critical volume V_B, called the blocking volume, or below a critical temperature, T_B, called the blocking temperature. An increase of volume or a decrease in temperature will increase the very short magnetic relaxation times above those which are required for superparamagnetic behaviour (Tarling, 1971).

Superparamagnetic behaviour can be shown by fine grained magnetite and hematite (Sections 5.4, 5.5). It is possible that secondary hematite formed by alteration processes, and dispersed

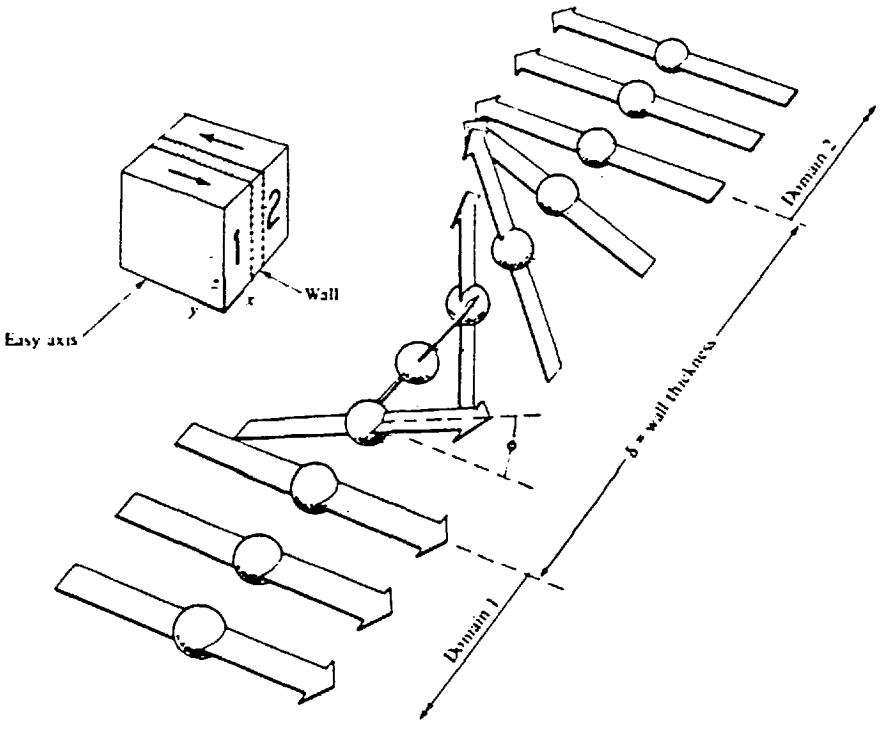

Fig. 4.5 Spin rotation across a domain wall (taken from Cullity,1972)

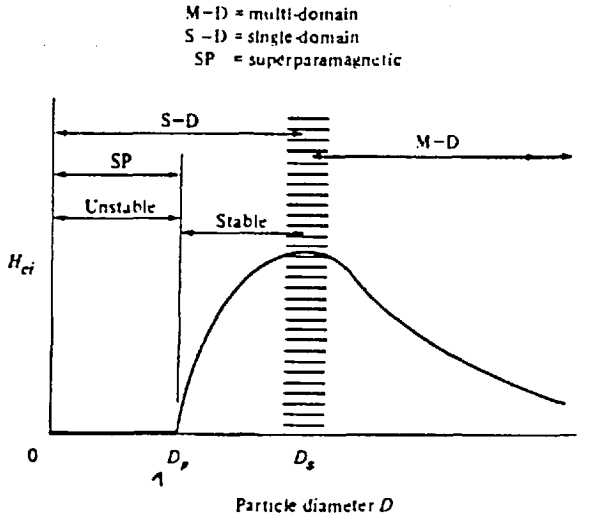

Fig. 4.6 Effect of particle size on properties of ferromagnetic materials (taken from Cullity, 1972)

in secondary pseudorutile and/or in secondary rutile, could produce a superparamagnetic response. Such fine grained hematite would be invisible optically and, having a grain size of only 50 nm or less, would only be seen with difficulty by an electron microscope. However, such small grains will still diffract X-rays (Cullity, 1956).

Fine grained ferrimagnetics can also behave superparamagnetically, and a superparamagnetic region has been defined for ilmenite with low-levels of hematite in solid solution (Section 5.7).

Magnetic ions: The metallic ions which can contribute to the observed magnetic properties of the minerals studied in this investigation are chiefly Fe^{2+}, Fe^{3+}, Mn^{2+}, Mn^{3+} and Cr^{3+}. The Ti^{4+} ion which is also present does not have a magnetic moment and so does not contribute. The relative magnetic moments of ions in the first transition series are given in Table 4.2, and an explanation in terms of the pairing of electrons is given in Fig. 4.7 for the Fe^{3+} ion.

Information sources: Further details of the main types of magnetism discussed above are adequately presented in many available textbooks. The treatment given by Cullity (1972) is especially lucid and informative.

4.3 Measurement units

The practical theory of magnetism developed around a magnetic pole concept that was validated by inverse square law experiments that were reported using the CGS (centimetre-gramme-second) system of units. Physics, and science in general, subsequently adopted the MKSA (metre-kilogramme-second-ampere) system, and this became widely used in electrical engineering but only to a small extent in magnetism. The more recently introduced S.I. system, which developed from the rationalised MKSA system, has not been generally adopted as yet for published magnetic research. The reasons for this are

Table 4.2

Spin-only Moments of some Ions of the First Transition Series

	Number of 3d electrons	Spin-only moment in β
Ti^{4+} V^{5+}	0	0
Ti^{3+} V^{4+}	1	1
V^{3+}	2	2
V^{2+} Cr^{3+} Mn^{4+}	3	3
Cr^{2+} Mn^{3+}	4	4
Mn^{2+} Fe^{3+}	5	5
Fe^{2+}	6	4

(After Cullity, 1972 p183)

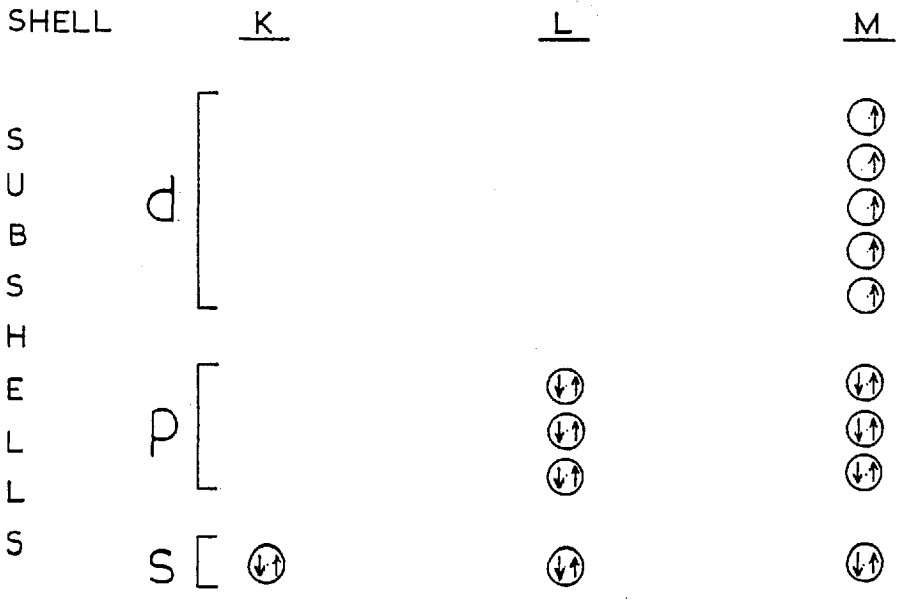

Fig. 4.7 Orbital diagram for Fe^{3+} showing unpaired electrons (after Andrews & Kokes, 1965 p624)

that the CGS units lend themselves readily to the scale of effects observed in magnetic experiments, and that disagreement occurred among various exponents of MKSA theory as to how the basic equations of magnetisation should be written (Cullity, 1972 p22). A great deal of confusion over magnetic units exists in the literature, and it was not until recently that textbooks attempting to give units for magnetic susceptibility in the S.I. system became available. In this investigation the author follows the Sommerfeld definition of susceptibility ($k = M/Bo$) (Crangle, 1977 p15). The advantage of this system is that it converts easily to the CGS system. The S.I. units for individual magnetic parameters are given in the equations presented in the following section.

4.4 Some useful equations

The relationships between magnetization and applied field, magnetic permeability and magnetic susceptibility, are expressed in the S.I. system in a different way from the C.G.S. system.

Thus, in the S.I. system, we have the relationship that

$$B_o = \mu_o H \quad \ldots\ldots \quad (1)$$

Where B_o is the free space induction (Tesla), H is the field ($A\ m^{-1}$), and μ_o is the magnetic permeability of free space. ($\mu_o = 4\pi \times 10^{-7}\ H\ m^{-1}$). It follows that H cannot be measured directly, and we can only measure B_o.

The magnetic induction B in a medium placed in the field is the sum of the free space induction plus the product of the induced magnetisation of the sample with the permeability of free space, thus

$$B = B_o + M\mu_o = \mu_o H + \mu_o M = \mu_o (H + M) \ldots\ldots \quad (2)$$

where M = magnetisation per unit volume in $JT^{-1}\ m^{-3}$ or Am^{-1}

The magnetic susceptibility per unit volume is k, defined as $k = \frac{M}{B_o}$ $JT^{-2}\,m^{-3}$ ..... (3)

But χ , the susceptibility per unit mass, (or specific susceptibility) $= k/\rho$ $JT^{-2}\,kg^{-1}$ ..... (4)

where ρ is the density of the material in $kg\,m^{-3}$.

Also the relative permeability of the material, μ_r is given by $\mu_r = B/B_o = 1 + \mu_o k$ ..... (5)

Most magnetic measurements reported in the literature are not in SI units. It is therefore important to know that the equivalent equations in the C.G.S. system to equations (1) to (5) are respectively

$B = H$ (in free space) ..... (6)

$B = H + 4\pi I$ where I = magnetic moment per unit volume ..... (7)

$k = I/H$ and $\chi = k/\rho$ ..... (8),(9)

$\mu = B/H = 1 + 4\pi k$ ..... (10)

A consequence of the C.G.S. system is that k, the volume susceptibility, is a dimensionless number, with no units.

Specific susceptibility values are readily changed from S.I. to C.G.S. units, by multiplying the S.I. value by 10^{-4}. Thus for ilmenite at room temperature, $\chi = 96 \times 10^{-2}\ JT^{-2}\ kg^{-1}$(S.I) $= 96 \times 10^{-6}\ erg\ Oe^{-2}\ g^{-1}$. (C.G.S.) In general, papers on magnetism do not use the full C.G.S. units shown, but simply state e.m.u./g i.e.electromagnetic units per gram.

B, H and M are magnetic vectors. In magnetically anisotropic materials, the susceptibility is also a vector - more specifically a second-rank polar tensor (Newnham, 1974). The full 6 parameters then needed to describe the magnetic properties can be reduced for anisotropic crystals, depending on their symmetry. Thus only two values of susceptibility are required to describe the magnetic properties of graphite (Parasnis, 1961). In the present investigations on ilmenite, only the two parameters $\chi_{||}$ and $\chi_{\perp}$, the susceptibilities respectively parallel to and perpendicular to the magnetic spin axis, are considered.

CHAPTER 5

MAGNETIC PROPERTIES OF MINERALS

5.1 Paramagnetic minerals: The magnetic properties of minerals are closely dependent on the concentration of the contained magnetic ions. The measured susceptibilities of paramagnetic silicates such as olivines, garnets, pyroxenes, amphiboles and biotites for example, agree quite well with calculated values. Such calculated susceptibilities are determined from the known concentration of magnetic ions, using the effective Bohr magneton numbers for the particular ions concerned (Nagata et al, 1957; Syono 1960; Vernon, 1961). Variations in the effective magnetic moment of Fe^{2+} were investigated by Parks and Akhtar, (1968).

5.2 Ferro-, ferri- and antiferromagnetic minerals: These minerals possess domains within which the magnetic spin moments are ordered to lie in particular directions. Normally, the domain spin axes will lie along magnetically 'easy' directions in the crystal e.g. along the cube diagonals [III] for magnetite. The effect of the spin directions on the magnetic symmetry is to increase the number of possible point groups, from 32 in magnetically un-ordered crystals to 90 in ordered crystals, with a corresponding increase in the number of possible space groups from 230 to 1421 (Birss, 1964).

As a consequence of these symmetry considerations, the symmetry point group of the magnetic unit cell will be different from that of the chemical unit cell. Also the magnetic unit cell may be larger than the chemical unit cell, due commonly to a doubling of the repeat distance along one axis. The possibility also arises of a single crystal having a different magnetic symmetry when unmagnetized, from when it is magnetised in a particular direction (Bloss, 1971).

5.3 Minerals considered

In this investigation, the minerals to be discussed are ilmenite, hematite, ilmenite-hematite solid solution, magnetite, chromite, pseudorutile, pseudobrookite and rutile. The complex properties of the first 4 minerals have been extensively studied and reported upon, and a brief summary of their properties is given below. Very little has been published about pseudorutile since its discovery reported in 1966, and its magnetic nature has not been studied (see Chapter 12). Pseudobrookite was known to be paramagnetic at temperatures above $90^{o}K$ (Nagata, 1961 p113): recent work has shown that pure synthetic ferric pseudobrookite (Fe_2TiO_5) is an anisotropic spinglass with $T_f \simeq 55^{o}K$ (Atzmony et al, 1979). Pure rutile is paramagnetic but the magnetic properties of natural ferriferous rutiles have not been reported in detail.

A general diagram of the system $FeO-Fe_2O_3-TiO_2$ shows the relative composition of all the above phases with the exception of chromite (Fig. 5.1).

5.4 Hematite

Hematite, $Fe_2^{+3}O_3$, has been detected as a minor phase in the X-ray diffraction spectra of some fractions of altered ilmenite (Chapter 10) and its magnetic structure and properties have a major influence on the properties of hematite-ilmenite solid solutions (see below). The details of the crystal and magnetic structures have been reviewed by Nagata (1961), Stacey & Banerjee (1974), and Lindsley (1976).

The crystal structure is rhombohedral, conforming to space group $R\bar{3}C$. The oxygen ions occur in triplets forming a 'pseudo-molecule' of $Fe-O_3-Fe$, (Lindsley, 1976) and lie in the (0001) plane to form a slightly distorted close-packed hexagonal structure with the iron cations occupying 2/3 of the available octahedral interstitial sites. Published lattice parameters vary slightly. Lindsley (1976) quotes $a_H = 5.0343 \pm 0.0005\text{Å}$, $c_H = 13.742 \pm 0.0005\text{Å}$ for pure synthetic material. Hematite is antiferromagnetic with a weak parasitic ferromagnetism due to a slight

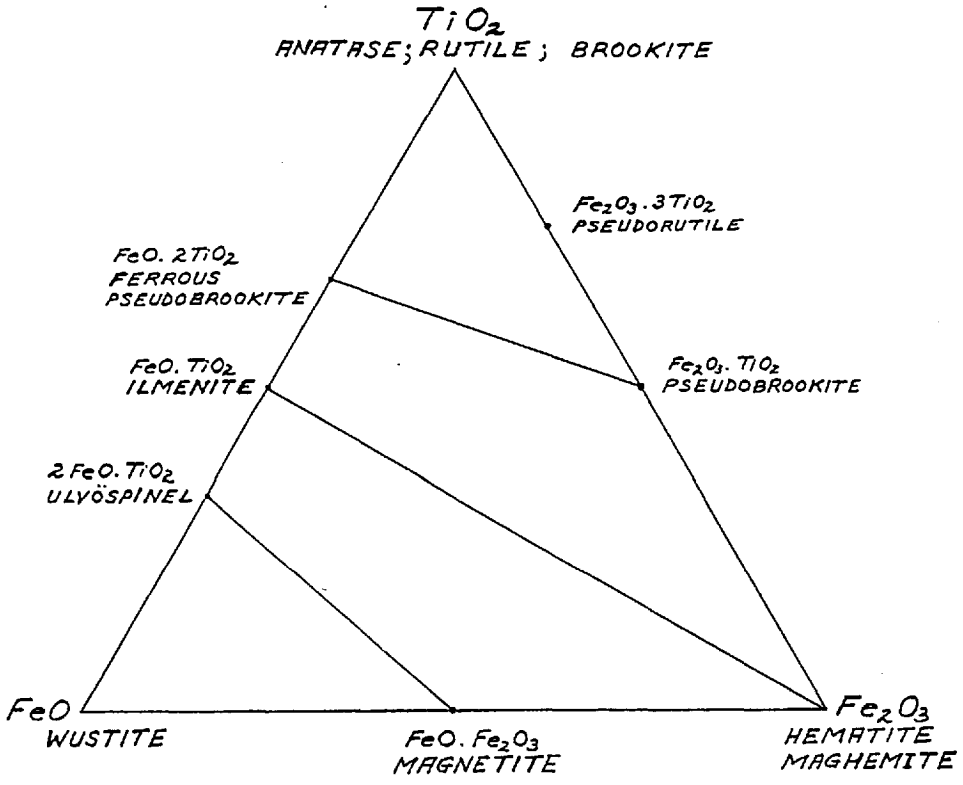

Fig. 5.1 The system FeO - Fe_2O_3 - TiO_2 showing the compositions of the major phases.

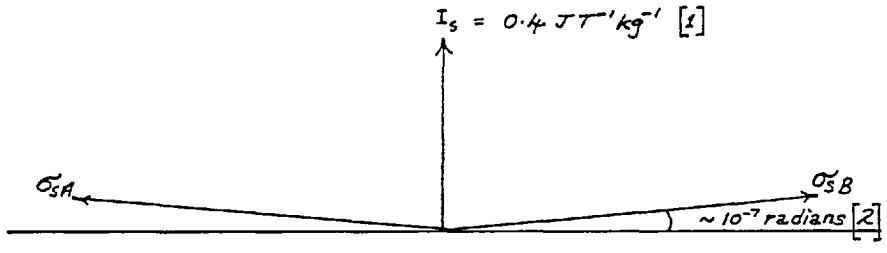

Fig. 5.2 The spin-canting of hematite.
(Data from [1] Stacey and Banerjee, 1967 and [2] Flanders, 1971).

angular deviation (canting) from perfect parallelism in the spins of opposing magnetic sub-lattices (Fig. 5.2). The critical temperature for this weak ferromagnetism is taken generally to be the same as the antiferromagnetic Néel point, 953°K. A further magnetic (spin-flop) transition in hematite occurs at 250°K, (the Morin transition). Above 250°K the magnetic spins lie in the basal plane (0001). Below 250°K the spins lie along the c-axis, and the spin-canting disappears (Stacey & Banerjee, 1974). The antiferromagnetic structure of hematite is not readily apparent from the shape of the specific susceptibility curves.

The specific susceptibility, χ, is anisotropic and temperature dependent below the Morin transition, since it has a lower value parallel to the c-axis than the value in the basal plane. Above the transiton, χ is relatively constant, and Néel and Pauthenet (1952) show a value close to 20 $\times 10^{-2} JT^{-2} kg^{-1}$ for a natural crystal of Elba hematite of high but unstated purity, measured in a field in excess of 1T. (Fig. 5.3). Pastrana and Hopstock (1977) show a range of 23-39 x $10^{-2} JT^{-2} kg^{-1}$ for natural hematites at 293°K with χ_∞, (the magnetic susceptibility extrapolated to infinite field strength) being approximately 25 x $10^{-2} JT^{-2} kg^{-1}$ for reagent grade synthetic hematite.

The antiferromagnetic structure of hematite was elucidated by neutron diffraction (Shull et al, 1951) and at room temperature the spin moments of all Fe^{3+} ions lying between adjacent (0001) layers of oxygen are parallel. Alternate iron layers have their spins oppositely directed however (Fig. 5.4). The magnetic unit cell has the same dimensions as the crystallographic cell. The symmetry of the magnetic cell is different, however. Thus at room temperature the chemical unit cell belongs to point group $\bar{3}m$, but the magnetic point group is $2/m$, changing to $\bar{3}m$ below the Morin transition (Newnham, 1974).

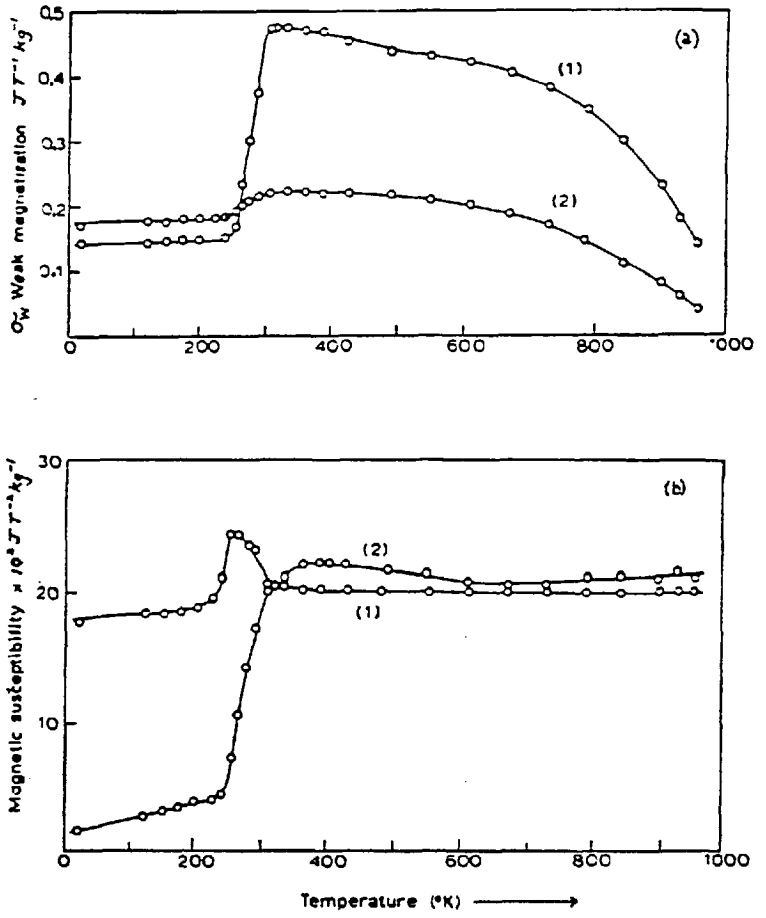

Fig. 5.3 Curves of weak magnetisation σ_w (where $\sigma = \sigma_w + \chi H$) and specific susceptibility χ for hematite (1) in a direction $\perp c$; (2) $\| c$. (Taken from Scheiber, 1967, after Néel and Pauthenet, 1952).

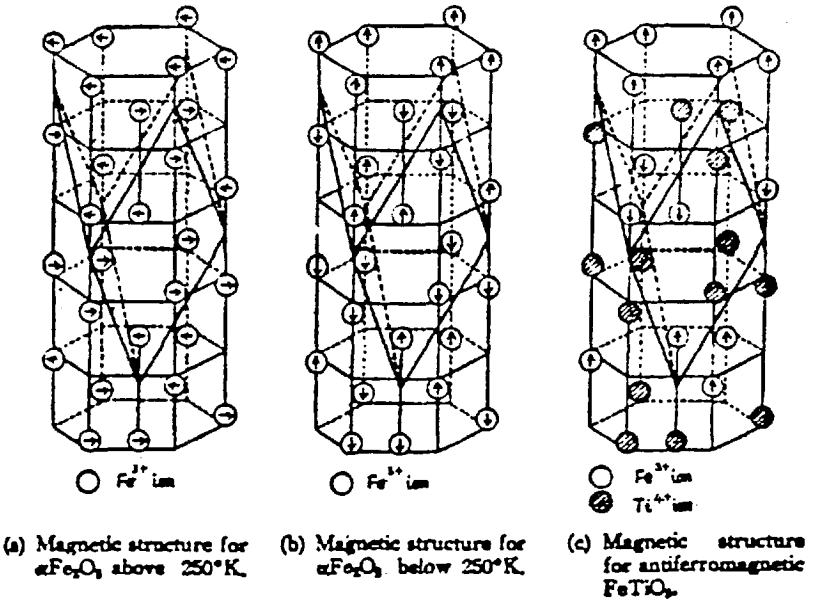

Fig. 5.4 The antiferromagnetic structure of hematite, compared with that of ilmenite. (Taken from Nagata, 1961).

5.5 Ilmenite

Ilmenite, $Fe^{2+}TiO_3$, is a major constituent of commercial ilmenite concentrates of detrital origin: for the more altered concentrates it may not be the main phase present. The crystal and magnetic structures of ilmenite have been summarised by Nagata (1961), and Stacey and Banerjee (1974). The crystal structure (Barth and Posnjak, 1934) has been refined by Raymond and Wenk (1971). Like hematite, ilmenite has a rhombohedral crystal structure. Unlike hematite however, in which all occupied metal sites are similar, ilmenite displays ordering along the c-axis, with (0001) layers of Ti^{4+} alternating with layers of Fe^{2+} ions. This produces a slightly lower symmetry corresponding to $R\bar{3}$. Every $Fe\text{-}O_3\text{-}Fe$ unit of hematite is here represented by an $Fe\text{-}O_3\text{-}Ti$ unit. Viewed along the c-axis direction, the sequence of ions is Fe-O-Ti-O-□-O-Ti-O-Fe-O-□-O-Fe...., where □ represents an unfilled octahedral metal site. Published and determined cell parameters are given in Table 5.1. The magnetic unit cell has a C_h value twice that of the chemical cell. The magnetic structure is shown in Fig. 5.4.

The magnetic spin axis of ilmenite was shown by Bizette and Tsai (1956) to be along the c-axis for a single natural crystal with mean specific susceptibility of 92 x $10^{-2}JT^{-2}kg^{-1}$ and which had a Néel point (T_N) of 68°K. Synthetic ilmenite has yielded T_N values of 55°K (Ishikawa and Akimoto, 1957), and 56°K (Stickler et al, 1956). Mössbauer measurements made by the Birkbeck College group on a synthetic powder prepared by the author (Appendix A) indicated T_N = 59.5°K, which is reasonably close to the 55°K Mössbauer value found by Syono and Ito in 1972 (Senftle et al, 1975).

At room temperature, pure synthetic ilmenite has a paramagnetic specific susceptibility of 96 x $10^{-2}JT^{-2}kg^{-1}$ (author's sample) confirming the determination of Chevallier (1953). Senftle et al (1975) found a peak susceptibility (χ) of about 770 x $10^{-2}JT^{-2}kg^{-1}$ for a synthetic sample at its Néel point of 57.0°K. This compares well with

$\chi \sim 700 \times 10^{-2}$ found at $T_N = 56^\circ K$ by Stickler et al (1967), and $\chi = 729$ at $56^\circ K$ by Heller (1964).

Unfortunately, Bizette and Tsai (1956), did not state the chemical or mineralogical purity of their sample, nor the exact strength of the field used to determine χ. (The field strength could affect the observed χ values at temperatures below T_N, Fig. 5.5). Although their study is widely quoted, other workers have not commented directly on the anomalous features of their curve for susceptibility versus temperature (Fig. 5.6).

Table 5.1
Cell parameters for Ilmenite, $FeTiO_3$

Source	a_{rh}	α_{rh}	a_h	c_h	Material
ASTM 3-781	5.523Å	54°51'	5.079Å	14.135Å	Natural
Shirane et al (1962)	5.538Å	54°41'	5.087	14.085	Synthetic
Raymond & Wenk 1971			5.085	14.088	Moon
			5.091	14.056	Earth
Lindsley 1976			5.088	14.080	Synthetic
Author's sample			5.087	14.010	Synthetic

These anomalous features, considered in relation to the curve for an ideal simple antiferromagnet (Fig. 5.7) are as follows:

1) The Néel points for $\chi_{\parallel}$ and $\chi_{\perp}$ occur at <u>different</u> temperatures.

2) The peak (Néel Point) values of $\chi_{\parallel}$ and $\chi_{\perp}$ do <u>not</u> coincide.

3) $\chi_{\parallel}$ and $\chi_{\perp}$ have distinctly different values above the Néel point - i.e. their ilmenite is apparently magnetically anisotropic while in the paramagnetic regime.

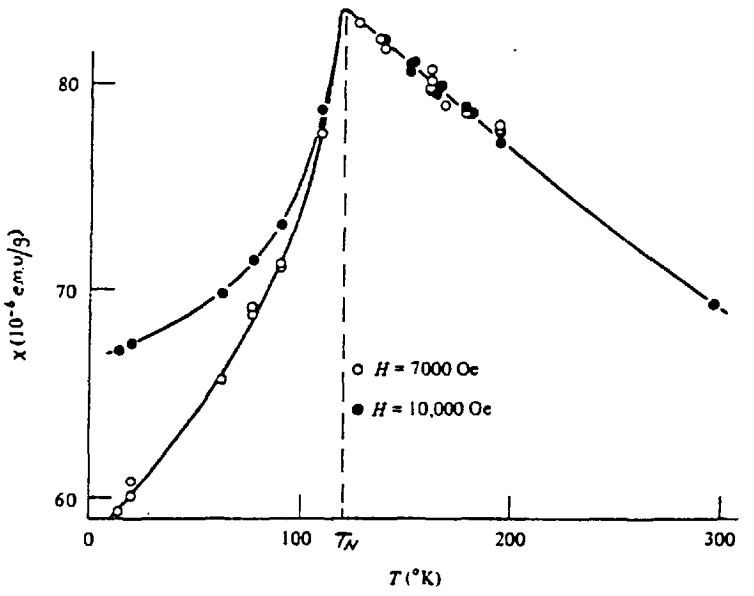

Fig. 5.5 Susceptibility of MnO powder, showing field dependence below T_N (Taken from Cullity, 1972, p167).

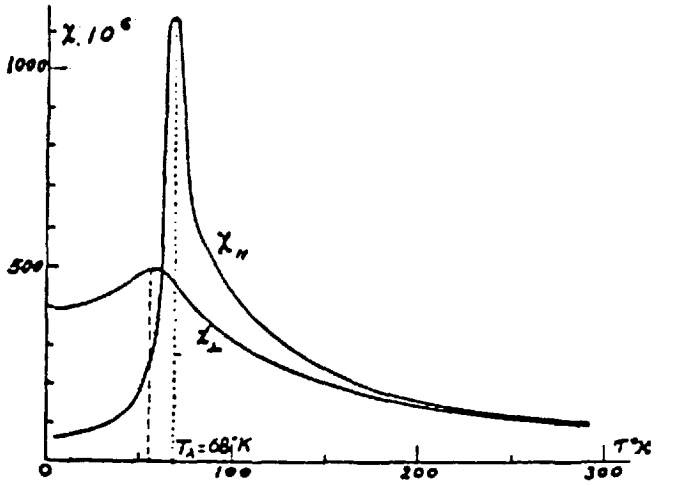

Fig. 5.6 The anisotropic magnetic susceptibility of ilmenite. (Taken from Bizette and Tsai, 1956).

While several workers have since published curves for the temperature dependence of ilmenite susceptibility, they have only reported the mean χ value of powdered samples (Heller,1964; Stickler et al,1967). Susceptibility curves were also presented by Senftle et al(1975). They discussed various susceptibility equations, and suggested that Bizette and Tsai's anisotropy measurements should be repeated on a lunar ilmenite (free of Fe^{3+}) when a single crystal of sufficient size becomes available.

Anisotropy measurements: Since it was not clear whether the anomalies in Bizette and Tsai's curves were due to impurities in their specimen or to experimental difficulties, an attempt was made to obtain some pure single crystals of natural ilmenite in order to repeat the study. Crystal fragments were obtained from three likely specimens by courtesy of Dr. A.M. Clark and Mr. P. Tandy of the Mineralogy Section of the British Museum of Natural History, London, S.W.7. X-ray diffraction patterns obtained on film using an 114.83 mm diameter camera were scanned for obvious lines of impurities, including exsolved hematite. Due to the great similarity in the X-ray diffraction powder patterns of these two minerals, detection of a small amount of exsolved hematite is very difficult, and of a small amount of dissolved hematite equally so. Unfortunately insufficient material was available to be able to take advantage of the better angular resolution given by a diffractometer (Zussman, 1977).

A flat-faced chip of the apparently purest specimen* was then examined by the Laue back-reflection technique, yielding a pattern (Fig. 5.8) that indicated the c-axis was almost perfectly perpendicular to the chip face. This chip was then used to investigate the temperature dependence of the specific susceptibility using a Foner vibration magnetometer equipped with a cryostat and temperature control, by courtesy of Dr. C. Guy and Mr. P. Mitchell of Imperial College.

* Ilmenite from Kenya (B.M. Nat. Hist., 112, 1944)

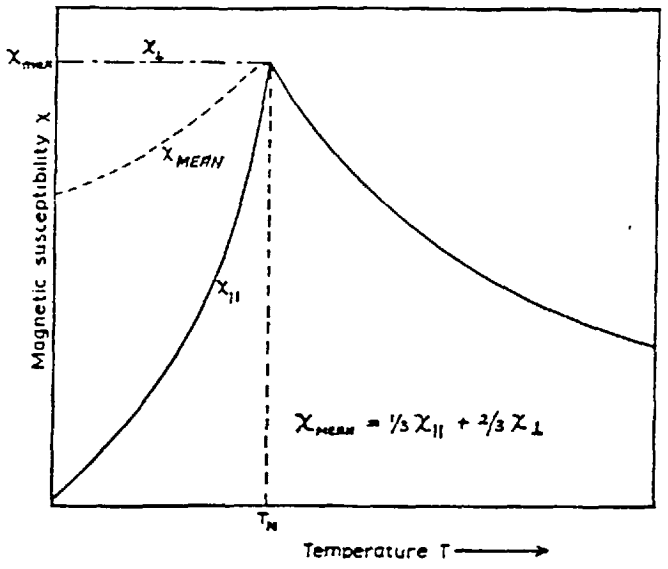

Fig. 5.7 The temperature dependence of specific susceptibility for an ideal, antiferromagnetic material. (Taken from Scheiber, 1967).

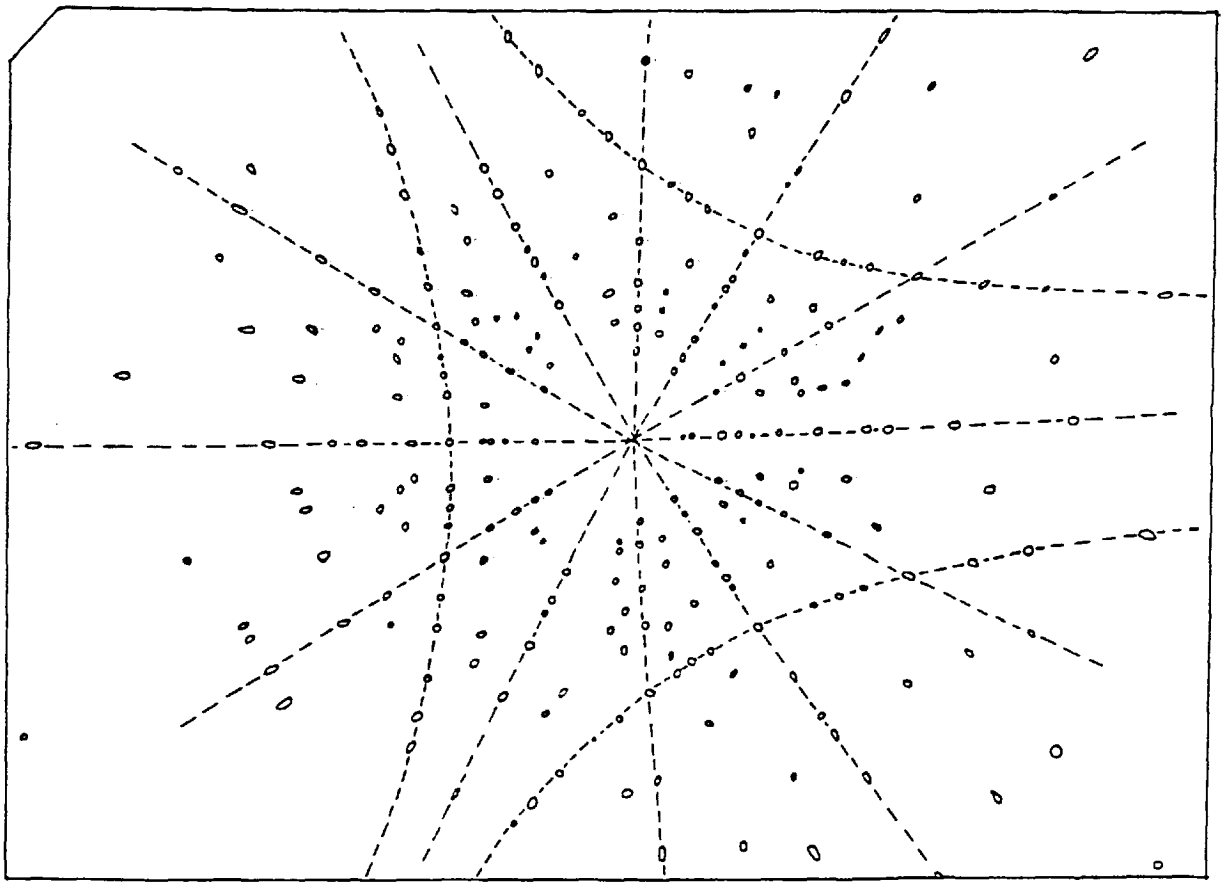

Fig. 5.8 Laue back-reflection pattern for a single-crystal fragment of ilmenite from Kenya.

The curves obtained for $\chi_{\parallel}$ and $\chi_{\perp}$ are given in Fig. 5.9. The shape of the curve for $\chi_{\parallel}$ is similar to that given by Bizette and Tsai(1956). However the curve for $\chi_{\perp}$ is very different from that of Bizette and Tsai, for it does not show a peak at T_N but only a shoulder, and below T_N the value of $\chi_{\perp}$ continues to rise to a peak value at approximately $8^{\circ}K$. The curve for $\chi_{\parallel}$ also shows a shoulder, at about $10^{\circ}K$. An explanation for these features will require further study but it is clear that because of compositional differences or other factors, the susceptibility curves of natural ilmenite can be variable. Most importantly, the anisotropy of susceptibility above T_N has been confirmed, in agreement with the results of Bizette and Tsai(1956). The results obtained are also in agreement with the theoretical calculations of Goodenough and Stickler (1967), who showed that the negative trigonal field of ilmenite is enhanced by spin-orbit coupling and by a large magnetic anisotropy, orienting spins along the c-axis even in the paramagnetic region.

The composition, determined by EPMA using a Cambridge Microscan 5 equipped with a Link system energy dispersive spectrometer with computerised calculation of composition, was FeO 47.1%, TiO_2 52.9%. No Mn or areas of chemical inhomogeneity were detected. An almost perfect line match was obtained when the sample was compared with pure synthetic ilmenite using a Guinier de Wolff XRD camera (Dr. R. Osborn of the Crystallography Department, Imperial College).

5.6 Effect of composition on the magnetic properties of ilmenite

The Fe^{2+} ion in ilmenite may be substituted by other divalent ions, and various workers have investigated some of the magnetic properties of synthetic ilmenites, $Me^{2+}TiO_3$, where Me = Fe, Ni, Co and Mn (Ishikawa and Sawada, 1956; Ishikawa and Akimoto, 1958; and Goodenough and Stickler, 1967).

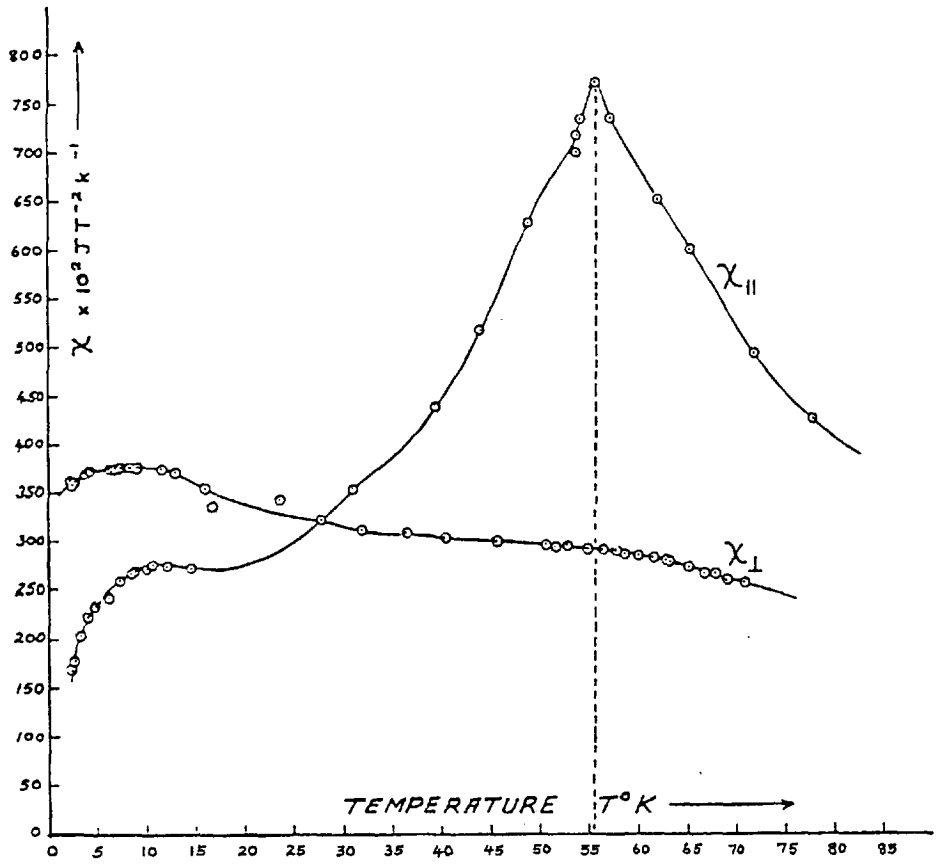

Fig. 5.9 The anisotropic susceptibility of a single-crystal fragment of ilmenite from Kenya.

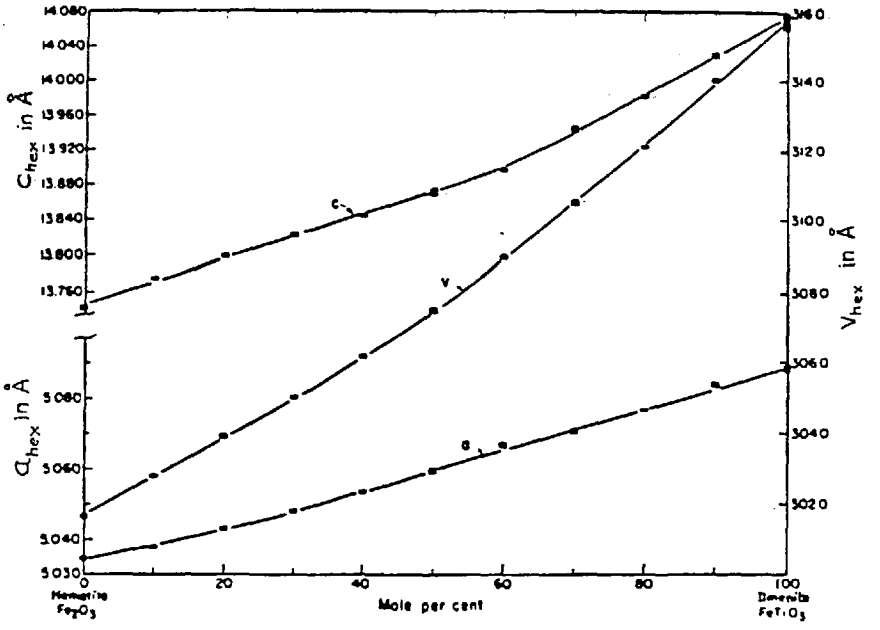

Fig. 5.10 Lattice parameters of the ilmenite-hematite solid solution series. (Taken from Lindsley, 1976).

While the $MeTiO_3$ solid solutions with α-Fe_2O_3 (which can all display ferrimagnetism with the exception of $MgTiO_3$) have been intensively studied by Japanese researchers, the solid solutions $MeTiO_3$ with $FeTiO_3$ have not been reported at all.

Natural ilmenites are probably always chemically impure, and they commonly contain some substituted Mn (Snetsinger, 1969), and/or some Mg: Ca and Si have also been noted by the author. Baker (1962) lists V, Nb, Cr, Cu, Al and U as "detected"; Zn up to 3000* p.p.m.; Ge up to 10 p.p.m.; and Sn up to 8 p.p.m. Cr and V are routinely determined in commercial ilmenite analyses to permit calculation of a corrected TiO_2 value, (Section 10.5) and both these elements have ions which, in certain valence states, could contribute to the magnetic properties, (Table 4.2). The possibility of the Cr and V being largely present in spinel grains rather than in the ilmenite lattice must be held in mind. The major and minor elements present in Capel ilmenite concentrate after handpicking to remove mineral impurities are given in Table 5.2.

Pure $MgTiO_3$ is not known in nature but geikielite (Mg, Fe)TiO_3 is known from the gem gravels of Sri Lanka. Compositions in the range (Fe,Mg)TiO_3 are known as picro-ilmenite and are characteristically found in kimberlite, (Elsdon, 1975). Since Mg^{2+} has no magnetic moment, it is expected that high Mg varieties of geikielite will have a markedly lower susceptibility than pure ilmenite. Cell parameters for $MgTiO_3$ are $a_H = 5.054A^o$ and $C_H = 13.898A^o$. (Lindsley, 1976).

Pyrophanite, $MnTiO_3$, has been recorded from Sweden and Brazil (Ford, 1966), and Neumann(1974) reports ilmenite specimens from Norway with up to 30% MnO.

Both Mn and Mg occur in West Australian ilmenite in small quantity, at approximate levels of 1.3-1.7% MnO, 0.12-0.18% MgO. The Mn^{2+} ion has a magnetic moment of 5 μ_B while Fe^{2+} has only 4 μ_B. The presence of Mn^{2+} thus causes a slight increase in the magnetic susceptibility. Cell parameters for pyrophanite are $a_H = 5.137A^o$, $C_H = 14.29A^o$ (Lindsley, 1976).

* A zinc-bearing ilmenite containing up to 37% Zn with the postulated formula (Zn, Mn, Fe) TiO_3 has been reported by Brown et al (1970).

It is of interest that the commercial production of synthetic rutile from ilmenite concentrated by the Western Titanium process is affected by the presence of small amounts of both manganese and magnesium (Grey and Reid, 1974; Jones, 1974).

Table 5.2
Elemental composition of Capel Bulk Ilmenite by XRF*

MAJOR	INTER	MINOR	TRACE
Ti	Mn	Nb	S
Fe			Cl
			K
		(Mg)+	Ca
			Zn
			Zr
> 5%	5-0.5%	0.5-0.05%	<0.05%

* By Analytical Services, Imperial College

\+ Known to be present, but below XRF detection limit

5.7 Hematite-ilmenite solid solution. $xFeTiO_3.(1-x)Fe_2O_3$.

The substitutional solid-solution and subsequent unmixing of hematite and ilmenite have been studied by ore-microscopists since at least 1926 (Edwards, 1960).

It was established by Japanese workers, who studied a full range of homogeneous synthetic, chilled compositions, that a gradational change occurred in lattice parameters (Fig. 5.10, (Nagata and Akimoto, 1956; Ishikawa and Akimoto, 1957 and 1958; Ishikawa, 1958). By thermo-magnetic separation, Nagata and Akimoto (1956) determined the variation of Curie point with the chemical composition of hematite-ilmenite solid solutions, and they were able to show that an essentially straight-line change occurred between the Néel point of ilmenite at 55°K and the Curie point of hematite at 953°K.

The strength of the saturation magnetisation was also investigated as a function of composition (Fig. 5.11), and the peak value indicated of ~100 e.m.u/g(C.G.S.) exceeds that of magnetite (90 e.m.u/g). It was clear that natural homogeneous solid solutions in the relevant composition range could make a major contribution to the magnetic properties of rocks and this discovery was a significant contribution to the development of palaeomagnetic studies. However, slow-cooled natural homogeneous compositions are mainly restricted to a narrow region close to pure hematite and pure ilmenite. The stability of solid solutions is indicated by the solvus, the curved line of which separates a field of homogeneous stable solid solution from a field of two or more solid phases which may often form by exsolving (i.e. unmixing) from the homogeneous composition. The solvus in Fig. 5.12 by Carmichael (1961) on the basis of observed exsolution after 100 days, has been contested by Lindh in 1972 (Elsdon,1975) and more recently by Lindsley(1976). Despite this disagreement it is clear that at temperatures between 1070-1300°K a complete solid solution with $R\bar{3}C$ structure exists between hematite and ilmenite. If Lindsley is correct - the peak lies closer to 1070°K and, in addition, the solvus is asymmetric (Fig. 5.13).

Nagata(1961) plots the Curie points of natural grains with compositions in the range 50-70 mol.% ilmenite. These presumably came from rapidly chilled lavas so that exsolution did not occur. Many examples of natural ilmenite with exsolved hematite occur, for example, from the large Tellnes deposit in Norway. When exsolution takes place during slow cooling, the two phases that are formed, although individually closer in composition to the hematite and ilmenite end-members, are still not pure. Successive cycles of exsolution have been known to occur with progressive cooling, and the last phases to form are the purest present. The terminology adopted for these phases generally follows that of Buddington et al(1963), and is followed in this investigation:

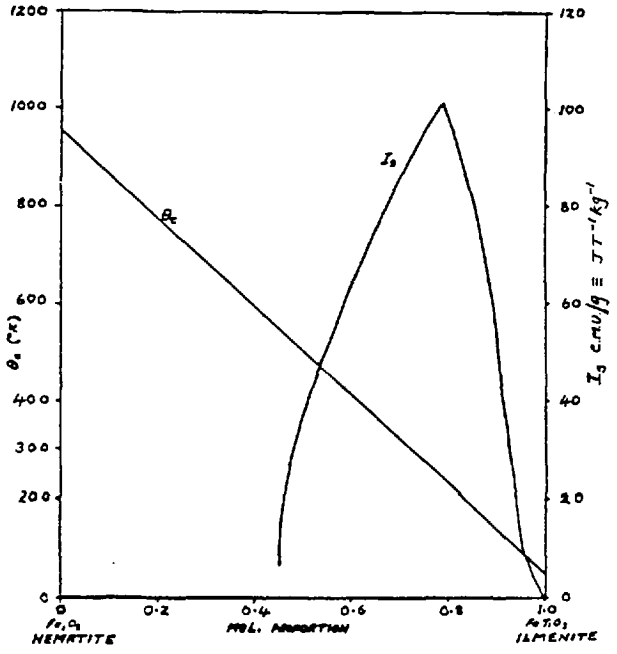

Fig. 5.11 Spontaneous magnetisation (I_s) and Curie point (θ_c) variations for the ilmenite-hematite solid solution series. (Based on Ishikawa and Akimoto, 1958; Nagata and Akimoto, 1956: taken from Stacey and Banerjee, 1974).

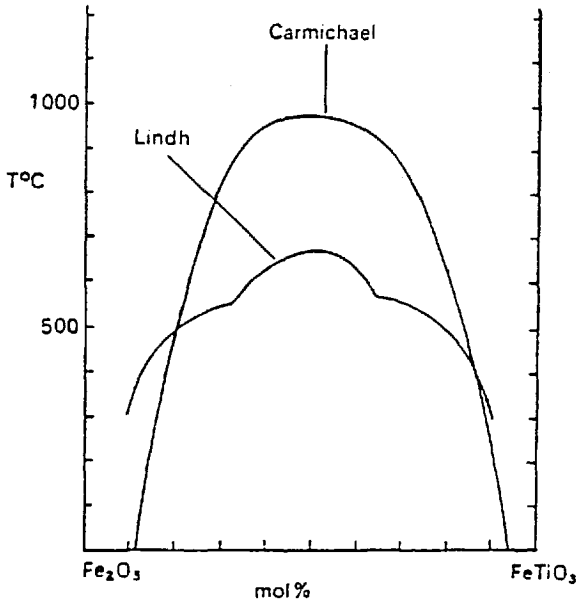

Fig. 5.12 The ilmenite-hematite solvus. (Taken from Elsdon, 1975).

Ferrianilmenite: homogeneous solid solution close in composition to the ilmenite end-member.
Titanhematite: homogeneous solid solution close to the hematite end member in composition.
Hemo-ilmenite: A two phase system of exsolved titan-hematite in a ferrianilmenite host.
Ilmeno-hematite: A two phase system of exsolved ferrian-ilmenite in a titanhematite host.

Grains of both the last two types have been identified by the author (Chapters 10,11).

The ilmenite-hematite solid solution series is important in this investigation because of its effect on the magnetic properties of the detrital grains. These properties depend critically on the chemical composition of the grains and also (for compositions close to 50% ilmenite, 50% hematite) on their thermal history. The original intensive studies of the system were due to the discovery that certain compositions were ferrimagnetic, and also that compositions containing nearly equal proportions of the hematite and ilmenite molecules showed self-reversal of their magnetisation direction, with serious implications for palaeomagnetic investigations.

The present state of knowledge has been summarised by Nagata (1961) and Stacey and Banerjee(1974), and is illustrated by Fig. 5.14 and Table 5.3. From the continuous solid solution which occurs for ilmenite-hematite mixtures at high temperatures, it appears that at such temperatures all compositions have the $R\bar{3}C$ hematite structure. Compositions which acquire the ordered $R\bar{3}$ structure after cooling below Tc, give ferrimagnetic behaviour with the magnetic spin axes lying in the (0001) plane. Pure ilmenite has the $R\bar{3}$ structure with the magnetic spin axes directed parallel to the c-axis (Bizette and Tsai, 1956), so that at some exceedingly small hematite concentration, the magnetic spins must flip from the basal plane into parallelism with the c-axis.

A superparamagnetic region has been defined in which short-range ferrimagnetic clusters persist (Hoffman,1975). In previous work on the composition $x = 0.12$, neutron diffraction showed no long-range magnetic

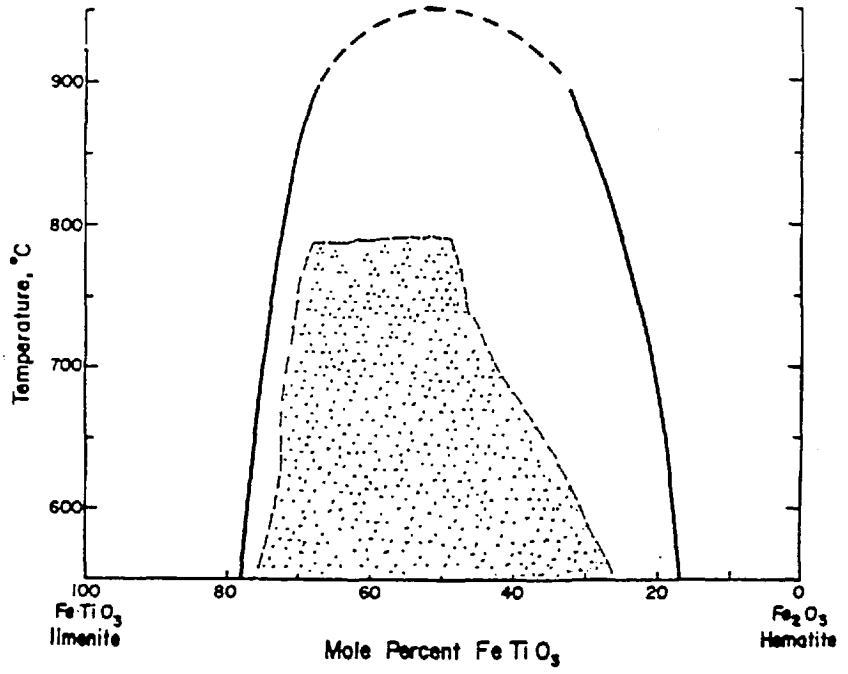

The join Fe_2O_3-$FeTiO_3$ showing the Hem-Ilm miscibility gap of Carmichael (1961) (hoop-shaped curve) and Lindsley's estimate of the region (stippled area) within which the miscibility gap must lie.

Fig. 5.13 The ilmenite-hematite solvus.(Taken from Lindsley, 1976b).

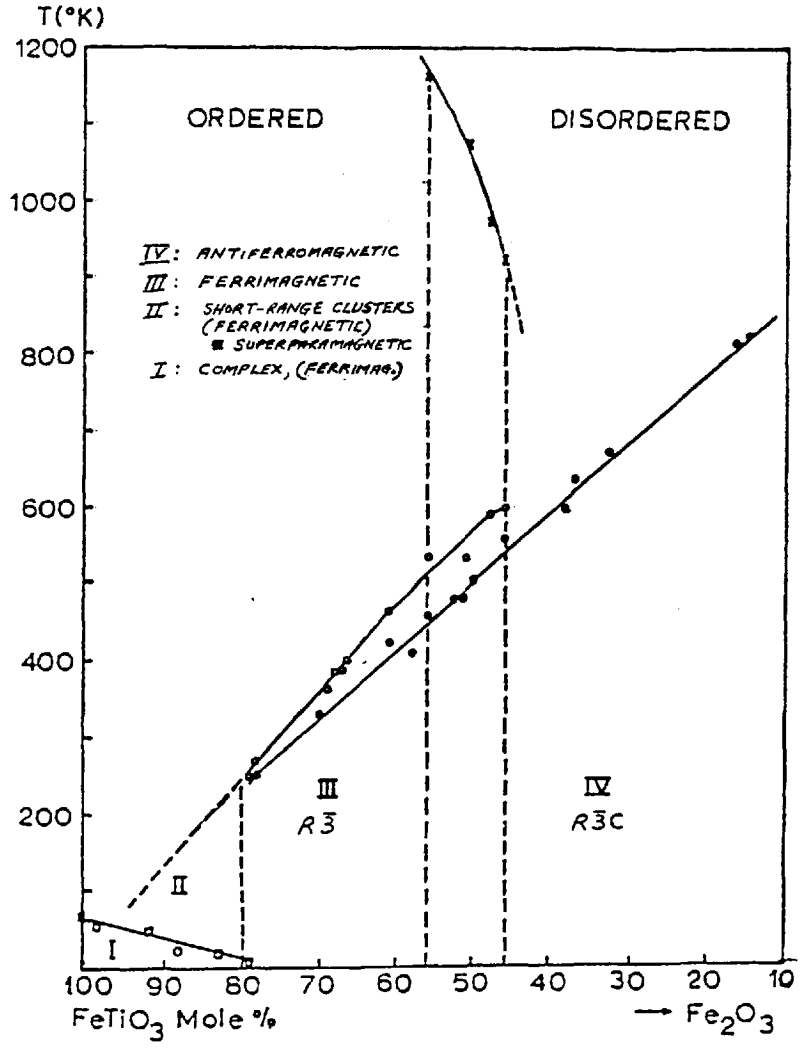

Fig. 5.14 Magnetic phase diagram for the ilmenite-hematite system. (Based on Ishikawa; taken from Hoffman, 1975).

ordering down to 4.2°K (Shirane et al,1962) despite an apparent Néel temperature of 170°K. Mössbauer spectroscopy at 80°K, which would be expected to yield a ferromagnetic spectrum, gave a typical paramagnetic spectrum. The neutron diffraction result is qualitatively similar to spinglass behaviour, while the paramagnetic Mössbauer spectrum indicates superparamagnetism (Greaves,1979). These features are explainable by a very fine grain size of the ferrimagnetic clusters in Shirane et al's sample.

Table 5.3

Magnetic behaviour of Ilmenite-Hematite solid solutions $xFeTiO_3.(1-x)Fe_2O_3$

Composition	Magnetic Behaviour	Crystal Structure	Magnetic Spin Direction
x = 1.0	Antiferromagnetic	$R\bar{3}$	$\parallel c$
1 > x > 0.45	Ferrimagnetic	$R\bar{3}$	$\perp c$
x = 0.5	Self-reversing remanence can occur	$R\bar{3}$ or $R\bar{3}C$ depending on cooling history	$\perp c$
0.5 > x > 0	Antiferromagnetic + parasitic ferromagnetic, with large coercive force	$R\bar{3}C$	$\perp c$

Evidence for hematite-ilmenite solid solution in studied grains are presented in Section 10.7, and the results of some experiments to monitor the rotation of grains so that the spin axes align with a magnetic field (as can occur in a commercial magnetic separator) are presented in Section 10.8.

The magnetic properties of hemo-ilmenite differ from pure ilmenite in that firstly the ilmenite groundmass commonly contains enough ferric ion to produce a ferrimagnetic structure, and secondly the exsolved titanhematite itself displays a weak ferromagnetism.

Thus for certain hemo-ilmenites from the Norwegian Tellnes deposit in which the ilmenite ground-mass is almost pure ilmenite (Norton, 1976), the presence of the exsolved hematite can readily be demonstrated as shown by the author's measurement of a field-dependent susceptibility component using Norton's material.

Some detailed studies of the remanent magnetism of hemo-ilmenite from Allard Lake, Quebec, have been reported by Carmichael (1959,1961). This (hard) remanent magnetism is due to the exsolved titanhematite phase which contains 13% ilmenite, while the ferrian-ilmenite groundmass contains 90% ilmenite.

5.8 Magnetite and chromite

General: Magnetite (Fe_3O_4) and chromite ($FeCr_2O_4$) are only considered briefly since they form a very minor part of the present investigations.

Magnetite is commonly considered to be the most magnetic mineral, although as noted above, certain compositions of hematite-ilmenite solid solution actually have a higher value of spontaneous magnetisation.

Magnetite: The magnetic structure is ferrimagnetic, and consists of two sub-lattices (A,B) of opposing parallel spins which have unequal strength. This is due to the character of the ions which form each sublattice - the magnetically stronger B sub-lattice is built of ions with a stronger magnetic moment. The magnetic properties are reviewed in detail by Stacey and Banerjee(1974).

Despite the high spontaneous magnetisation (90 e.m.u/g(C.G.S.) $\equiv$ 90 $JT^{-1}kg^{-1}$(SI)) magnetite is a magnetically soft material in that the net remanent magnetisation becomes very low when an applied field is removed. This is relevant to the commercial separation of magnetite by repeated passes through low-intensively magnetic separators.

Geologically, the most abundant 'magnetites' are in fact oxidised titanmagnetites, i.e. members of the magnetite-ulvöspinel (Fe_2TiO_4) solid solution series, which have suffered some degree of high temperature oxidation. This high-temperature subsolidus oxidation

causes "exsolution" of lamellar or granular ilmenite, and the oxidation mechanism has been indicated by both experimental and textural evidence. Haggerty (1976) reviews the characteristic textures that result from progressive oxidation.

No credence is given currently to earlier theories of a solid solution series of magnetite with "cubic" or γ-ilmenite, the latter having a 'defect' structure which would result in magnetic properties in a way analogous to the well-known but imperfectly-defined properties of γ-hematite which is magnetically similar to magnetite. A literature review on the γ-ilmenite question and an attempted synthesis have been reported by Banerjee (1963).

No magnetite or titan-magnetite have been found in West Australian commercial ilmenite concentrates during the present investigation, although they were expected and sought for in fractions with obviously ferromagnetic behaviour. Several West Australian beach-sand concentrators have low intensity magnetic "scalpers" to remove small amounts of supposed magnetite from the main feed to the separators. The properties of these grains can be explained as being due to hematite-ilmenite solid solution.

Chromite: This mineral is an undesirable impurity in ilmenite concentrates intended for TiO_2 pigment manufacture by the sulphate route, since Cr ions give a yellow undertone effect to the otherwise white pigment. A maximum of 0.05% Cr_2O_3 is permitted in commercial concentrates, and most actual analyses are about 0.03%. Chromite-bearing east Australian ilmenite concentrates are therefore stock-piled in large quantities although there is the future possibility that they could be synthetically upgraded and made suitable for the chloride route process of TiO_2 manufacture.

Like magnetite, chromite has a spinel structure and is magnetically a ferrite, but it has a much weaker magnetic susceptibility than magnetite. The large number of cations

that can be accommodated by the spinel structure lead to great variations in the chemical composition and in the properties of chromite. Typical variations have been reported by Rao(1978), and by Schwerer and Gundaker(1975).

Chromium as chromite is less deleterious than Cr in solid solution in the lattice of ilmenite, with regard to TiO_2 pigment manufacture by the sulphate route. This is because chromite has a lower solubility than ilmenite, and so is more likely to be retained in the insoluble residue and rejected.

CHAPTER 6

MEASUREMENT OF MAGNETIC SUSCEPTIBILITY

6.1 Introduction

There are many methods described in the literature for the measurement of magnetic susceptibility, including magnetic balances, vibration magnetometers and a.c. induction bridges. The detailed theory is covered in many texts including Selwood (1956), Mulay(1963), and Cullity(1972).

6.2 Magnetic balances: Susceptibility determination by so-called force methods, which are based on measurements of the force acting on a body when placed in a non-uniform magnetic field, requires the use of a magnetic balance.

The basic components of this equipment are a d.c. electromagnet, calibrated for field intensity with respect to the current flowing; a balance; and a sample container and suspension system. The balance should ideally be of the electronically controlled force compensation type, so that the sample cannot move up and down in the field during measurement. This is especially important for measurement of ferromagnetic samples.

Most magnetic balances are custom designed and built, although some automatically recording balances of the Faraday and Gouy type have been commercially available in recent years.

Some magnetic balances operate in a vacuum with elaborate temperature controls; others are fully automated and linked to recording devices. Unfortunately, many such balances have maximum load limitations and can only handle minute quantities of sample. Weights are recorded to the nearest microgram, and for accuracy the balance has to be supported on special vibration-free mountings.

For this investigation a d.c. electromagnet was constructed in the Mineral Technology Section of the Royal School of Mines, to a design by Prof. U. Ts. Andres.

The d.c. electromagnet was set up on a mobile platform beneath a stout table, on which was set an electronic Mettler PT320 balance having a continuous digital read-out to the nearest milligram. The sample suspension system was hung by a thin pyrex glass rod from the lower weighing pan hook. This passed through a hole in the table so that the sample occupied a suitable position in the field of the electromagnet. Current to the electromagnet was monitored by ammeter and controlled by rheostat. The equipment as a whole is illustrated in Fig. 6.1.

The design of the sample container varied with the actual measurement system employed. Initial field calibration was carried out using the Gouy method; most other measurements were conducted using the Faraday method.

6.3 The Gouy method

Theory: For a long straight uniform rod of material suspended with one end in the middle of a region of high uniform field, and the other end in a region of weak field, it can be shown that the magnetic force (F) acting on the sample at a particular value of the high field is given by:

$$F = \tfrac{1}{2} (k_s - k_a) A(B_{OM}^2 - B_{OL}^2)$$

where B_{OM} is the high value of free space induction (field)
B_{OL} is the weak free space induction, which in most cases can be ignored
k_s is the volume susceptibility (k) of the sample
k_a " " " " " of the ambient atmosphere
A is the cross-sectional area of the sample rod.

The field gradient is taken to be directed downwards, i.e. perpendicular to the field.

For a particulate solid packed into a cylindrical container, it is necessary to calculate the effective cross-sectional area from a knowledge of the sample weight, its mean specific gravity, and the height of the sample column (Andres, pers. comm.). Ferromagnetic impurities are readily detected by the Gouy method, but it

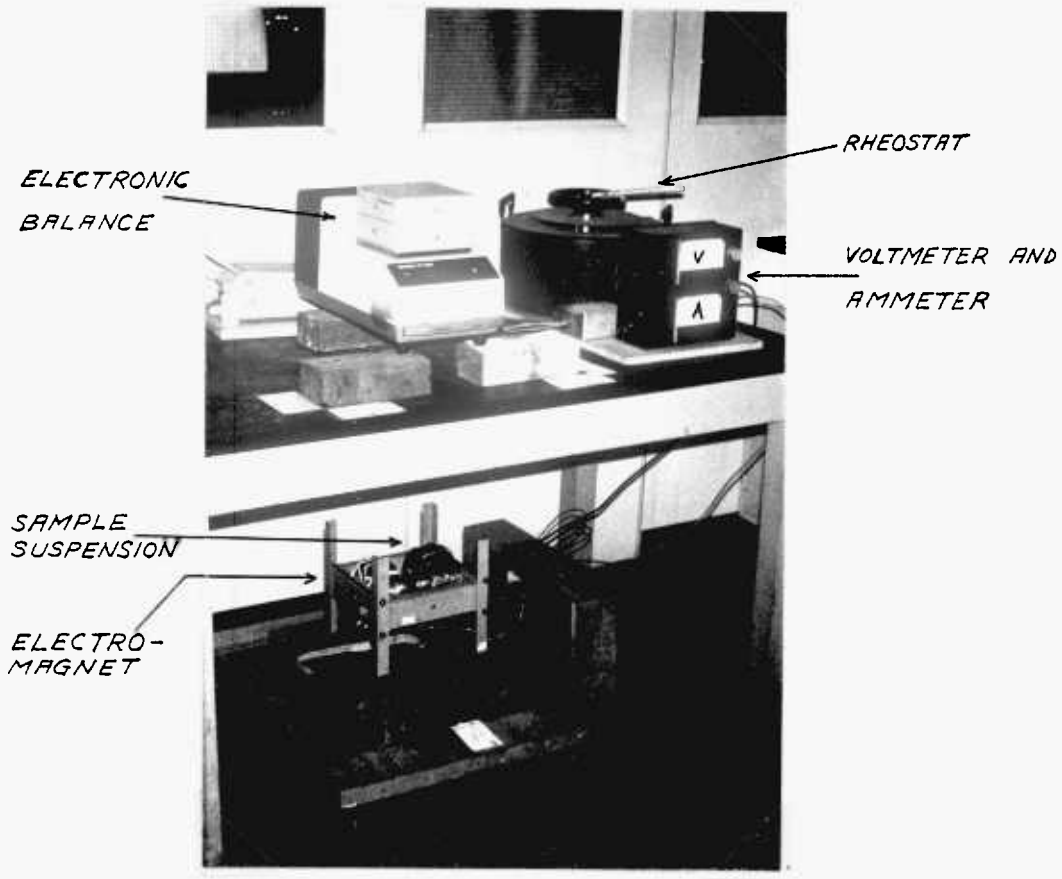

Fig. 6.1 Arrangement of the magnetic balance.

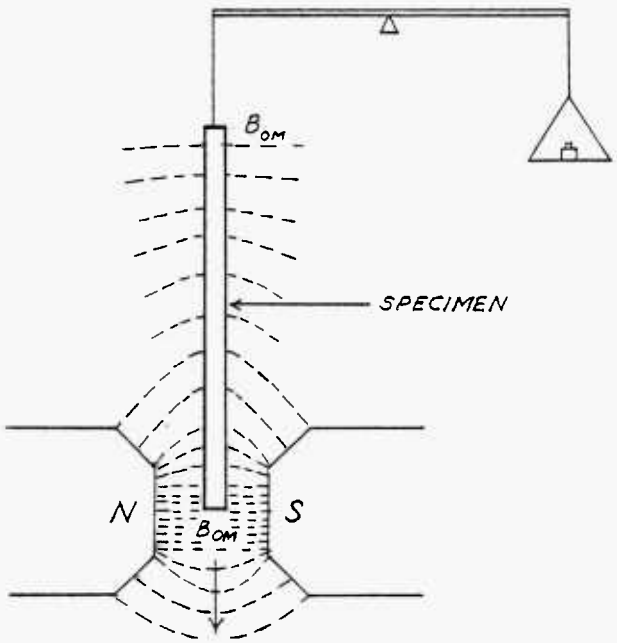

Fig. 6.2 The Gouy method of susceptibility determination.

cannot yield an accurate susceptibility value if they are present.

Apparatus: A schematic diagram of the Gouy apparatus is shown in Fig. 6.2. The pole piece configuration is normally as shown, i.e. conical poles with flat terminal faces to produce a region of uniform field. The sample tube was constructed of precision-bore silica tubing, fitted with suspension lugs, and a hook at the base for suspending a stabilising weight. Sample tubes of various diameters were constructed (1.8 mm, 4 mm, 6 mm) to accommodate various amounts of sample. The largest available sample weight was tested in order to maximise the observed forces.

Experimental procedure: The weight of the entire suspension was measured with the sample container empty. The magnet current was then set successively at 5, 10, 15 and 20A, and at each current the weight of the system was noted. The apparent decrease in weight as the current was increased, was due to the diamagnetic repulsion of the silica sample-tube from the high-field region.

The sample-tube was next removed from the system and by a combination of tapping and tamping was carefully packed with the mineral grains or powder. Generally, uncrushed mineral grains were employed from the size range -210 μm +150 μm. Failure to obtain firm packing of the grains is considered by the author to be the biggest single source of error for Gouy determinations. Poorly packed magnetically anisotropic grains will be free to rotate and to orientate themselves selectively in the applied field so that their main susceptibility axis or 'easy' direction is parallel to the field. A lower susceptibility will then be presented in the direction of the gradient. Elongated particles will also align with their major dimension parallel to the field because of their magnetic shape anisotropy. The susceptibility values determined from anisotropic samples with such preferred orientations are not the same as the values obtained from samples having a random distribution of the magnetic spin axes.

After the height of the sample in the loaded tube was noted, the sample was hung from the balance, and the total weight of the suspended system was noted. The magnet was switched on and readings of the apparent weight were taken at 5, 10, 15 and 20A. After the 20A reading, the current was reduced to zero and the weight of the system was noted to check for drift. The cycle of readings was then repeated as a check. Readings were always made on a rising current loop, since this procedure effectively eliminated field variations at a given current due to the hysteresis cycle of the magnet, Fig. 6.3. The incremental magnetic force, corrected for the diamagnetic force on the sample-tube, was now tabulated against the magnetic field for each current value. A summary of the field calibration procedure is given in Appendix B, and an example of the Gouy susceptibility calculation in Appendix C.

6.4 The Faraday method

Theory: For a small sample placed where $B_o \cdot \frac{dB_o}{dx}$ is approximately constant over the sample length, (Fig. 6.6) the magnetic force acting on the sample can be shown to be

$F_X = V (k_s - k_a) B_o \frac{dB_o}{dx}$, where V is the volume of the sample, k_s and k_a are as defined for the Gouy method, and B_o is the free space induction.

For an apparent change in weight ∂_w at a given field,

$F_X = g \partial_w$, where g is the acceleration due to gravity (Cullity, 1972).

Should $B_o \frac{dB_o}{dx}$ not be constant, for example when conical pole pieces are employed, then values of B_o and $\frac{dB_o}{dx}$ intermediate between those occurring at the top and bottom of the specimen will apply. In such a situation it is not generally possible to measure accurately the field values with a Hall-effect gaussmeter, although approximate values can be obtained and the mean gradient calculated. A better solution is to use a fairly rigid suspension (e.g. of silica rod) which is not susceptible to a significant

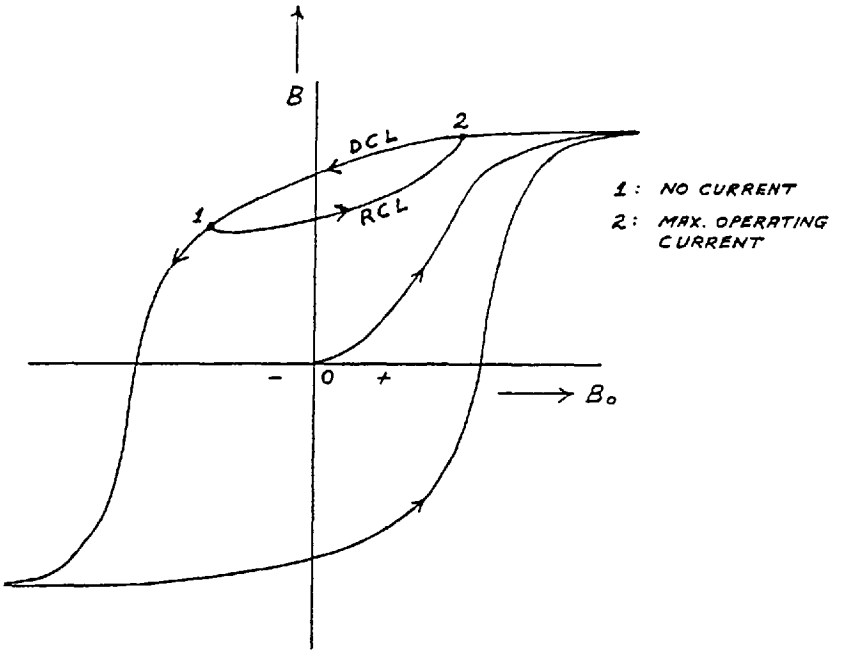

Fig. 6.3 Major and minor hysteresis loops of an electromagnet. (RCL = Rising current loop, as used for experiments). (DCL = Descending current loop).

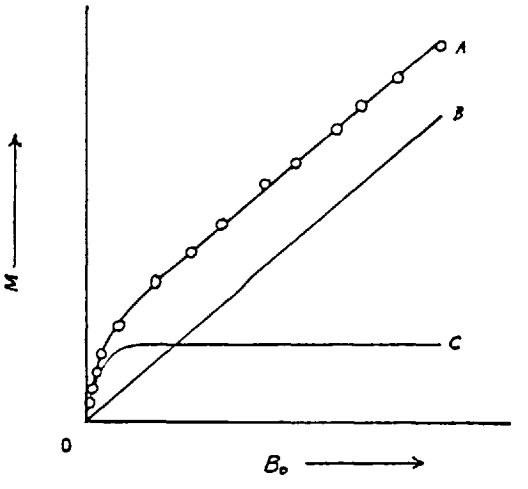

Fig. 6.4 Magnetisation curve A for a paramagnetic B containing a small amount of ferromagnetic impurity C. (After Cullity, 1972).

degree of stretching, and to calibrate the sample position using a known susceptibility standard. The specific magnetization σ of the sample can be determined from the relation $\sigma = \chi B_o$. The mean value of B_o must then be determined by use of a calibrated gaussmeter, but it is unlikely however that high fields can be determined with an accuracy better than $\pm$ 10 Oe (C.G.S).

Since the sample is small and the difference in field between the top and bottom of the sample is thus also small, it is easy to magnetically saturate a ferromagnetic sample by employing a sufficiently high field, and the effects of the field-dependent susceptibility are thus minimised. This is the big advantage of the Faraday method over the Gouy method, Table 6.1, since the latter does not provide a correct susceptibility value for a sample containing a field-dependent component. Such components in the low-field part of the Gouy rod will exhibit a much higher susceptibility than those components down in the high-field region. A further advantage of the Faraday method is that it permits estimation of the paramagnetic susceptibility for a paramagnetic sample containing minor amounts of saturatable ferromagnetic impurity (Fig. 6.4).

Table 6.1

Comparison of Gouy and Faraday Methods of Susceptibility Measurement.

Method	Advantages	Limitations
Gouy	.An absolute method .Can be calibrated by a standard substance and used as a relative method .A very sensitive detector of field-dependent behaviour (ferromagnetic impurities)	.Only accurate for paramagnetics .Requires accurate knowledge of H_{max} if used as an absolute method .Requires a relatively large sample .Requires accurate knowledge of density for χ to be calculated.
Faraday	.Can give high accuracy when calibrated by standards .Suitable for both paramagnetics and ferromagnetics .Requires very little sample .Can operate with conical or Faraday-type pole pieces	.A relative method .Requires very accurate and repeatable positioning of sample .Weighing errors tend to be relatively larger than with Gouy method

During the course of this investigation, the Faraday method has proved to be more suitable than the Gouy since recalibration is quick, and sample weights around 0.1 g are sufficient instead of around 1 g or more being required.

Apparatus: A diagram illustrating the sample presentation system - also called the Curie method by some authors - is given in Fig. 6.5. The pole pieces may have various profiles (Fig. 6.6), and ideally the design should give a small region of the field space such that $B_o \frac{dB_o}{dx}$ is approximately constant, or failing this that $\frac{dB_o}{dx}$ is at least constant.

A sample placed in such a field space can be slightly misplaced during repeat readings, and yet yield a closely similar result. An alternative method when conical pole pieces are employed is to place the sample at the point where $Bo\frac{dB_o}{dx}$ is a maximum, thus maximizing the observed magnetic force. The exact position yielding maximum force is readily determined by measuring the force on a highly susceptible standard sample mounted on an extensible calibrated suspension. Conical pole pieces have the advantage that they do not have to be changed for carrying out Gouy determinations. (This is important because whenever a magnetic circuit is dismantled the magnetic characteristics change, even if the same pole pieces are replaced). Also the shape of the field is laterally symmetrical and tends to pull the sample into a central position every time.

Experimental procedure: This is very similar to that used for a Gouy measurement, but it is not necessary to correct for the diamagnetic behaviour of the silica sample container. The reference material of standard susceptibility is packed into the same container to the same height as the unknown, and is suspended in the field at exactly the same point. The assumption is made that the field strength, field gradient, diamagnetic effect of the container, and effect of the displaced ambient atmosphere, are exactly the same providing that the ambient temperature is the same, for a given magnet current.

Fig. 6.5

The Faraday Method

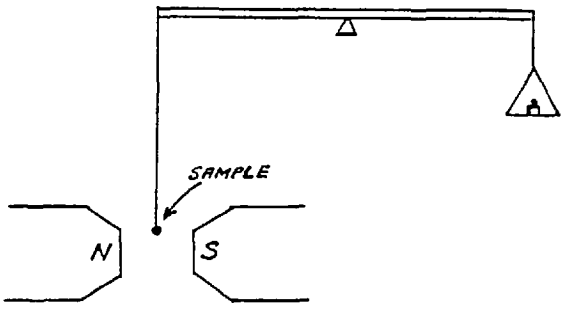

Fig. 6.6

Some pole-piece designs which may be used with the Faraday method. (After Mulay, 1963).

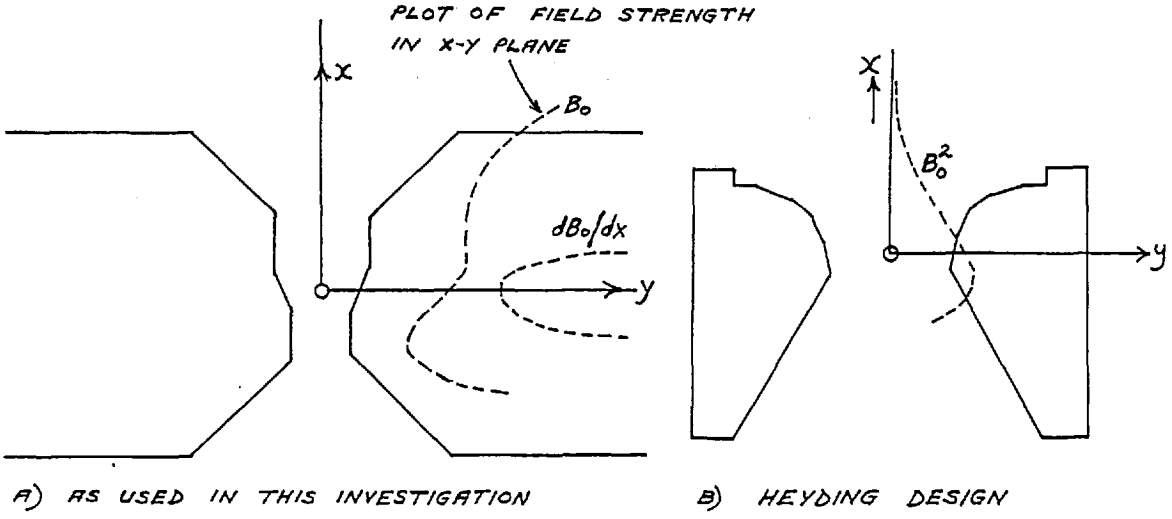

An example of susceptibility calculation for the Faraday method is given in Appendix D. The characteristic feature of a sample containing a ferromagnetic component is that the apparent susceptibility is highest in the lowest field employed, and decreases as the current is increased. It is clear that the value reported for such a sample must be normalised in some way, and the general practice is to extrapolate the susceptibility to infinite field by plotting susceptibility against the reciprocal field or against reciprocal magnet current. With a truly paramagnetic specimen, any variations in the susceptibility value at different fields reflects the accuracy and repeatability of the determination. Since the magnetic forces are highest at high fields, the high field determinations have lower relative weighing errors than the low-field determinations.

6.5 Electronic a.c. mutual inductance bridge

Measurement of the low-temperature susceptibility of Indonesian pseudorutile was conducted by courtesy of Prof. B.R. Coles and his staff on the a.c.inductance bridge maintained by the Solid State Physics Department of Imperial College.

The principles of the a.c. inductance bridge method have been discussed by Pillinger et al (1958). In the particular balance employed a cylindrical sample is placed on the end of a long rod and lowered inside a cryostat until the sample sits inside a primary coil. The a.c. signal in this primary coil induces an alternating magnetism in the sample, the flux of which cuts a secondary coil. The in-phase component of the voltage induced in the secondary coil is balanced by the bridge operator to a null point by means of an adjustable ratio transformer, the reading of which is noted at each temperature with the sample (a) in the coil and (b) raised out of the coil. The difference in the two readings is directly proportional to the susceptibility of the sample. Thus from an accurate knowledge of the susceptibility of the sample at a particular temperature included in the measurement range, the value of the susceptibility corresponding to a reading at

any other temperature can be determined. If such a known susceptibility is not available, only the shape of the susceptibility v. temperature curve can be obtained.

The cryostat is of a standard type, and temperatures close to the sample position are monitored by means of a calibrated resistance thermometer with a digital read-out.

For the Indonesian pseudorutile sample (Section 12.4), and also for Curie point determinations on highly magnetic fractions of Capel ilmenite containing grains with hematite-ilmenite solid solution (Section 10.7), the samples were prepared by mixing a small portion of the sample with Durofix glue, and rolling the mixture into a cylinder not more than 2 mm in diameter and up to 1 cm long. The samples consisted of natural grains in the size range -600 +200 μm for the pseudorutile, and -210 +150 μm for the hematite-ilmenite solid solutions.

6.6 Vibrating sample magnetometer

Foner (1959) described a vibrating sample magnetometer (VSM) in which the magnetic moment is measured for a sample vibrated perpendicularly to a uniform magnetic field, (Fig. 6.7). This method, which has been briefly summarised by Cullity (1972, p67), eliminates or minimises some of the errors associated with other methods. A VSM of modified Foner type, in which the sample vibrates parallel to the applied field, was employed for measuring the magnetic susceptibility anisotropy of a relatively pure sample of natural ilmenite,(Section 5.5).

The sample is inserted into the measuring zone on the end of a rod which is electromechanically reciprocated at a precise frequency. The oscillating magnetic field of the sample induces an alternating sample signal in the detection coils. The current to a reference electromagnet is controlled by a servosystem which balances the sample signal with a reference signal. This reference signal is modified by the variations in the current supplied to the reference magnet. The reference-magnet current is a

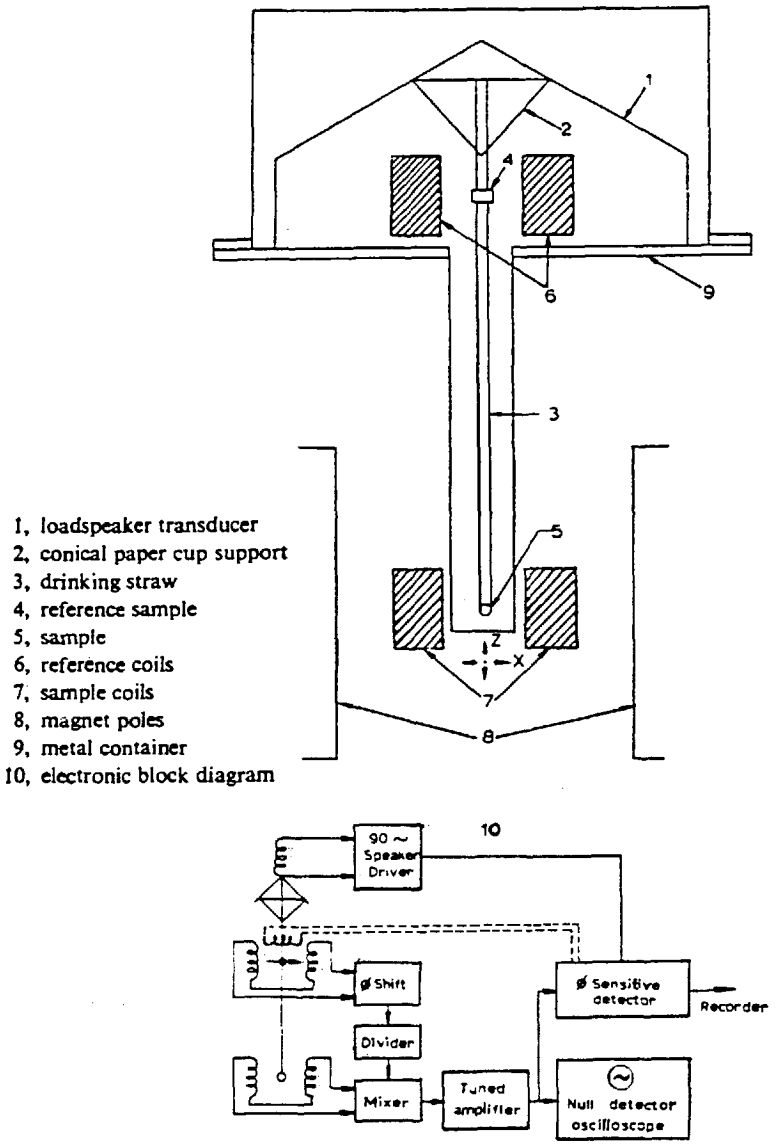

Fig. 6.7 Simplified form of vibrating sample magnetometer (VSM). (Taken from Foner, 1959).

direct measure of the magnetic moment, and hence of the susceptibility of a paramagnetic sample.

As with the a.c. induction bridge, the apparatus is enclosed by a cryostat. Temperatures are monitored by means of a carbon resistance thermometer, and the changes with field of the magnetic moment of the sample are displayed by an X-Y chart recorder.

6.7 Frantz-type isodynamic magnetic separators

Introduction: The Frantz isodynamic separator was used for separating sulphide minerals in 1943 by Gaudin and Spedden (Hess,1959). The latest version incorporates a current-reversal facility for neutralising remanent magnetism of the pole pieces, to permit separation of high-susceptibility ferromagnetics at very low coil currents.

An instrument manufactured by Cook, which is similar to an early model of the Frantz, has been used in this investigation for preparing magnetic fractions.

Theory: The theory of Frantz-type magnetic separators has been discussed by McAndrew(1957), whose treatment can be summarised as follows:

$$\sin \theta / \chi = K i^n$$

where θ is the side-slope angle measured from the horizontal
χ is the specific susceptibility
i is the separator current
n is a constant index close to 2, determined by calibration
K is a constant for an individual machine, " "

This equation suggests that the separation achieved is affected only by the variables θ, χ and i. The separation is nominally independent of the size, mass and density of the grains being separated, and variations in the longitudinal slope angle ϕ should not affect the separation. The angle ϕ does however affect the feed rate, and also begins to affect the separation adversely

when the particles move down the track rapidly. This is because of the presence of a product-splitting riffle which extends half way up the centre of the track from the discharge end. Any particles which fail to move into the upper, 'magnetic' stream before encountering the central splitter inevitably remain in the lower, 'non-magnetic' stream.

The equation should be regarded as an empirical relationship only, since $K\, i^n$ is McAndrew's approximation for $\frac{1}{g} \cdot \frac{dH^2}{dx}$. In a solenoid the field produced depends upon i and not upon i^n. The term $\frac{dH^2}{dx}$ is equivalent to $2H \frac{dH}{dx}$, and, while the field is related to the current in the coils, both it and especially the gradient $\frac{dH}{dx}$ depend also upon the pole piece geometry. There is therefore no fundamental reason why n should have the value 2 as McAndrew suggests.

The McAndrew empirical equation does bring out the importance of the side-track angle, θ. Many published accounts fail to quote the value of θ employed, and few give values for n and K. These omissions do not allow the results of different investigators to be meaningfully compared.

The equation holds up to a certain maximum current - the limit of linearity on a calibration graph of $\log(\sin\theta/\chi)$ as ordinate plotted against log i on the abscissa, Fig. 6.8.

Using his equation, McAndrew produced calibration curves for his particular separator showing the relationship between collection current and susceptibility for magnetic products. It follows from these curves (Fig. 6.9) that for highly susceptible materials a small difference in current can make a great difference to the susceptibility of the particles separated, whilst for low susceptibility materials relatively large changes in current make little difference to the susceptibility.

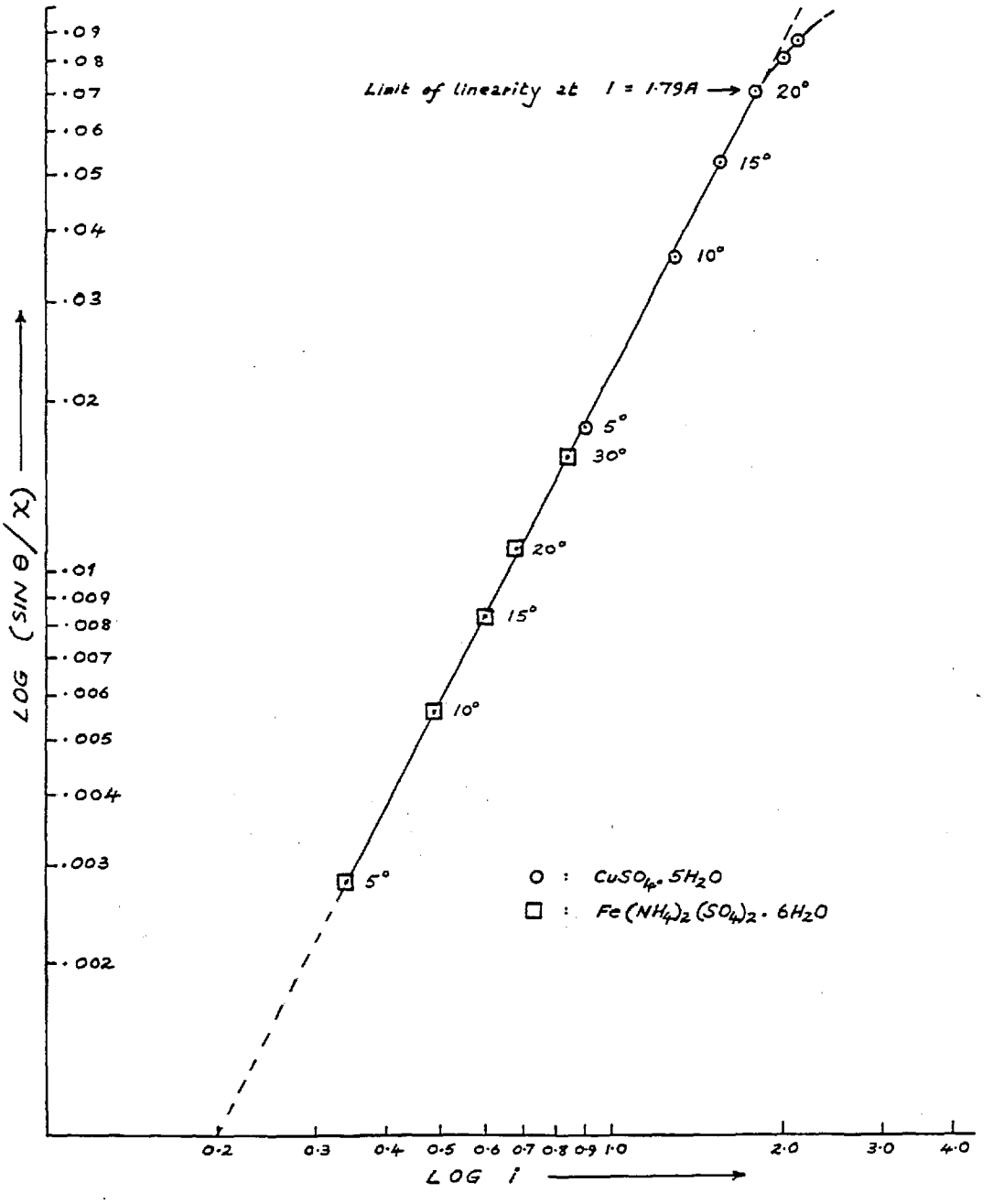

Fig. 6.8 Calibration curve obtained for the Cook separator.

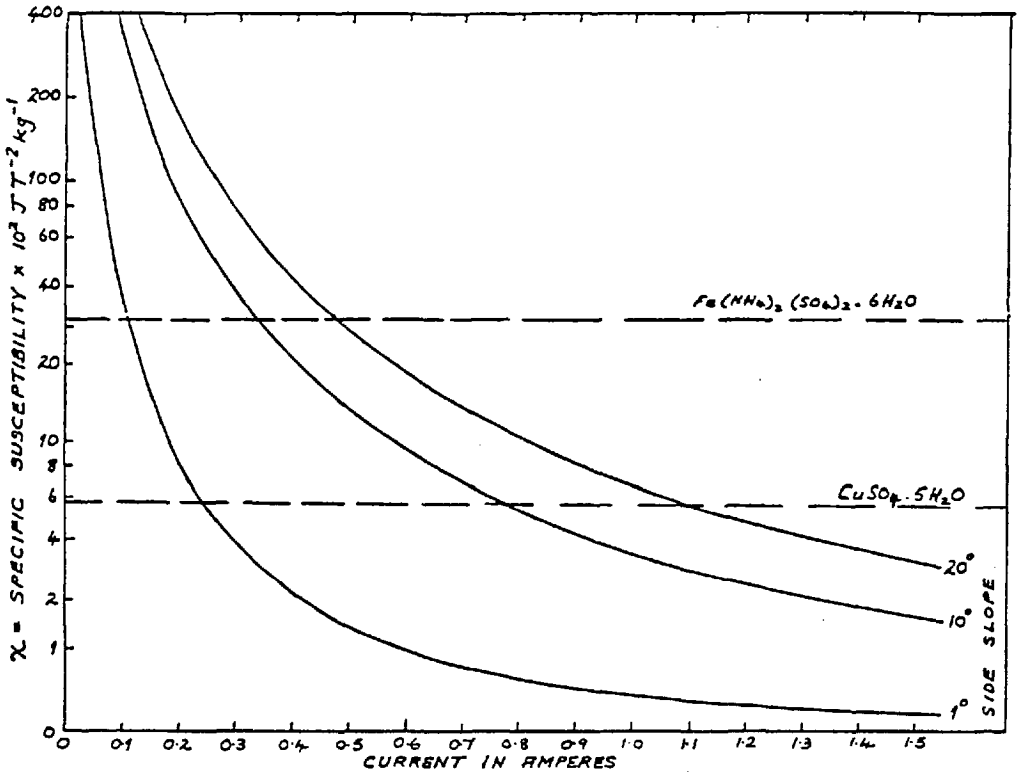

Fig. 6.9 Relationship of particle susceptibility(χ)to the separation current at a given track side slope for a Frantz isodynamic separator. (McAndrew, 1957).

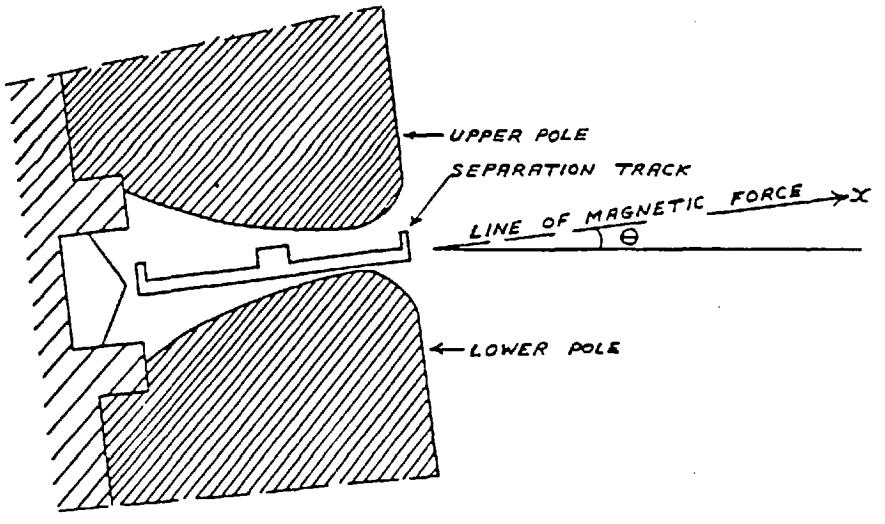

Fig. 6.10 Schematic cross - section through the pole pieces of a Cook isodynamic magnetic separator.

The ideal pole piece geometry (Fig. 6.10) is such that for any position across the track, the product $B_o \frac{dB_o}{dx}$ is constant, and the force experienced by a particle is thus independent of its position in the x direction. Whether this is true for the Cook machine is not known. If the design is not perfect, then the force experienced by a particle will depend on its position across the track, and therefore all particles should have the same initial starting position. This has been achieved by limiting the feed stream to a narrow band immediately adjacent to the lower track lip. This corresponds to a feed rate of approximately 0.3 - 0.4 g/min at a side slope of 10°, and to lower feed rates for steeper side-slopes. This procedure, though slow and tedious, gave closely repeatable product analyses.

Any magnetic particle moving along the lower edge of the separation track has to "shoulder" its way through the rest of the particle stream to reach the upper part of the track. A wide belt of particles reduces the chances of doing this before the track splitter position is passed. If the belt of particles is so wide that it occupies more than half the track width, then the splitter directs all particles higher than the track mid-line into the magnetic product, regardless of their susceptibility. Surges in the feed rate leading to such conditions often happen when the standard feed cones are used alone.

Apparatus: The Cook machine is shown in Figs. 6.11 and 6.12. Failure to achieve a suitably slow and steady feed rate results in a lack of repeatability in the amount and quality of the products obtained. Consequently, this machine was fitted with a special feeder.

The machine had an ammeter divided into 0.1A intervals which could be confidently interpolated to 0.05A. The track vibrator was not adjustable and vibration intensity was, therefore, eliminated as an adjustable separation variable.

Experimental procedure: The base of the instrument was levelled. The side track angle was then set at 10° for all routine separations, and the longitudinal slope was $22\frac{1}{2}^{\circ}$. The side track angle was checked by using an inclinometer against the plane face of the pole pieces, but no adjustments were found in practice to be necessary. The magnet

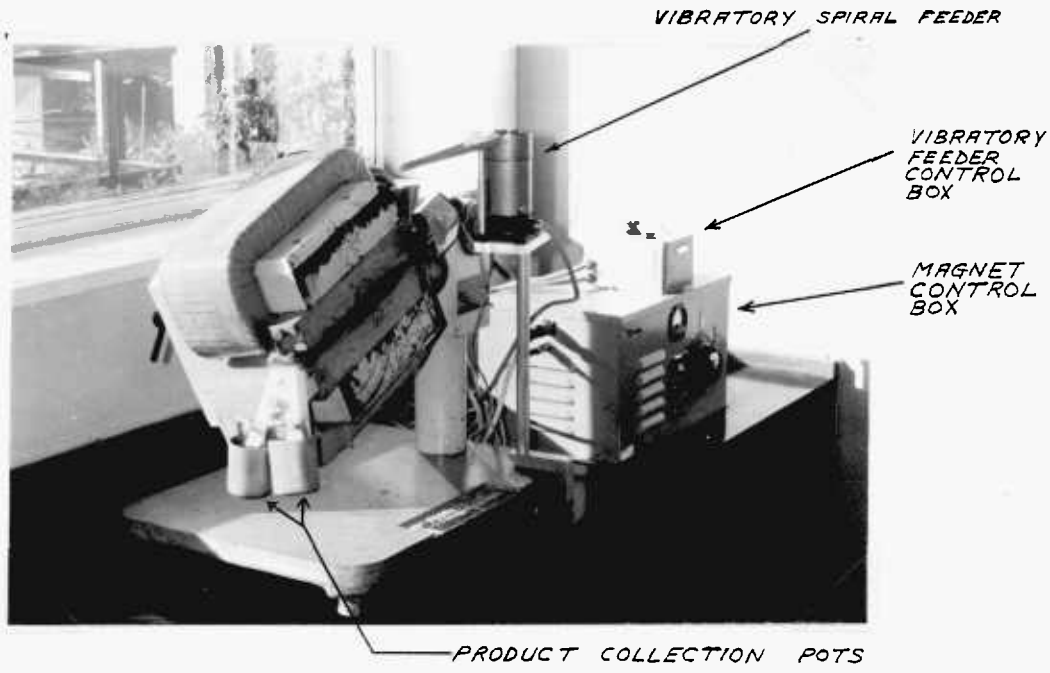

Fig. 6.11 Cook isodynamic magnetic separator fitted with a vibrating spiral feeder.

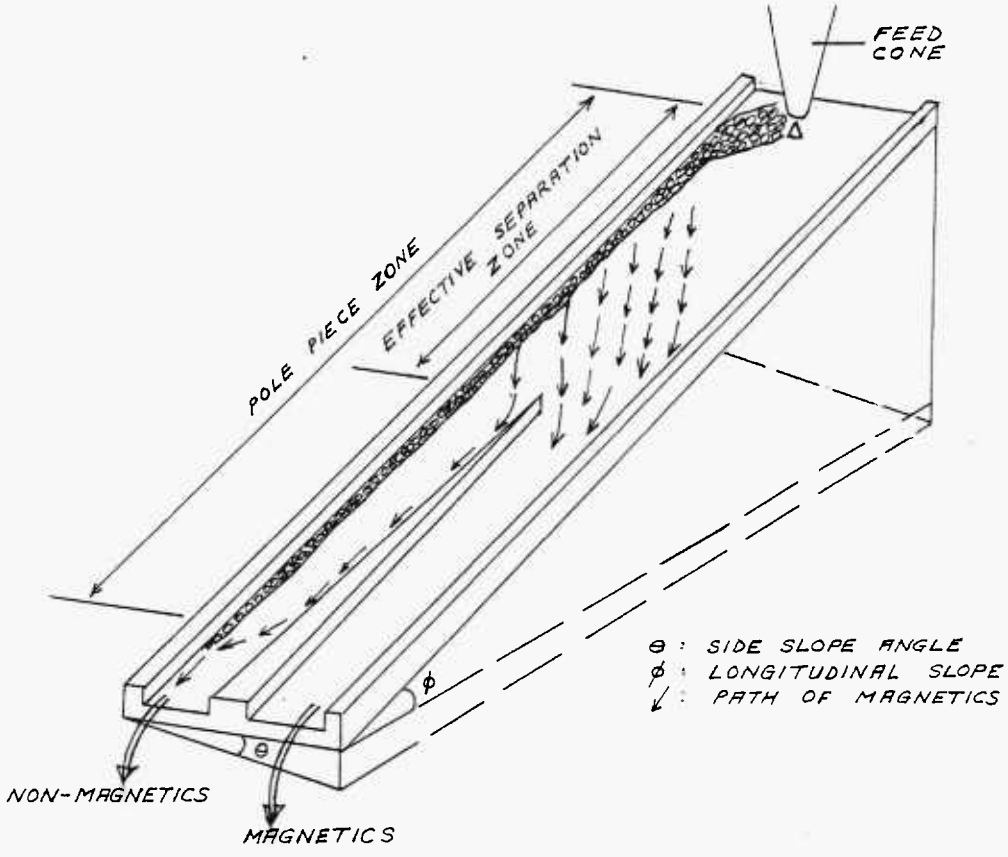

Fig. 6.12 Sketch of the separation track for a Cook isodynamic magnetic separator.

current was then cycled 3 or 4 times up to a maximum of 2.25A, to settle the magnet into the hysteresis loop which would be used.

The track vibrator was switched on and the current raised to 0.05A - a value sufficiently low to pull off the ferromagnetics without causing excessive bridging of particles and blocking of the track. The sample to be separated was then placed in the well of the vibratory feeder, and the feed rate adjusted to the desired range of 0.3 - 0.4 g/min. During the separation the current was maintained at 0.05A. After the separation, the current was cycled up to 2.25A, then back to zero, then up to the next separation current e.g. 0.10A. Separation cycles continued as before, using the non-magnetics from a preceding pass as feed, up to the desired maximum separation current. The magnetics at each current and the final non-magnetics were retained and weighed, to calculate the recovery distribution.

Special care was taken when setting the current for each pass, to ensure that the current set-point was approached from a lower current value. Thus, all settings were part of the lower, current-increasing part of the hysteresis loop, which yields significantly different field values from those obtained when the current is decreasing.

Calibration: In this investigation the calibration constants were determined using the same method as McAndrew, by noting the critical current for a given side slope at which 50% of the material reports to the magnetics.

Three standard substances were used, for which the paramagnetic susceptibility was determined by the Gouy method: copper sulphate, $CuSO_4.5H_2O$; manganese sulphate $MnSO_4.4H_2O$, and ferrous ammonium sulphate $Fe(NH_4)_2(SO_4)_2.6H_2O$. The susceptibilities of these standards were cross-checked between themselves by the Faraday method.

Published and measured susceptibilities of these compounds are compared in Table 6.2.

Table 6.2

Magnetic susceptibility standards

Compound	SPECIFIC SUSCEPTIBILITIES at 293°K ($\times 10^2 JT^{-2}kg^{-1}$) Published	Gouy	Faraday	Cook
$CuSO_4.5H_2O$ (1)	(5.85a, 5.69e (5.88b	5.63d	5.86h 4.9g	4.84*
$Fe(NH_4)_2.(SO_4)_2.6H_2O$ (2)	(32.45b (32.49c (31.26f	31.08	31.28	(31.08 assd.)
$MnSO_4.4H_2O$ (3)	65.46a	65.41	65.41n	65.41n

a CRC Handbook of Chemistry & Physics (1966) — calc. from χ_m

b McAndrew (1957)

c Angus & Hill, (1943)

d finely ground crystals

e Krishnan & Mookherji, (1938b)

f Candela & Mundy, (1961)

g L.F. Gate, English Clays Lovering Pochin & Co. Ltd. - (pers. comm.) - using gelatin capsule container in which grains were probably free to rotate

h $MnSO_4.4H_2O$ used as a calibration standard ($\chi = 65.41$)

n assumed value

(1) mol. wt. = 249.71 S.G. = 2.284 $T_N = 0.03°K$ (Schieber, 1967)

(2) mol. wt. = 392.16 S.G. = 1.864

(3) mol. wt. = 223.06 S.G. = 2.107

*due to anisotropy

During a calibration test on the Cook separator with a given compound, weights of the magnetic and non-magnetic products were collected and recorded at a range of currents for side slopes of 5°, 10°, 15° and 20°. A perfect 50% split was never achieved, and the critical currents determined for a given side-slope were those which gave a repeatable approximate 50% split, Fig. 6.13.

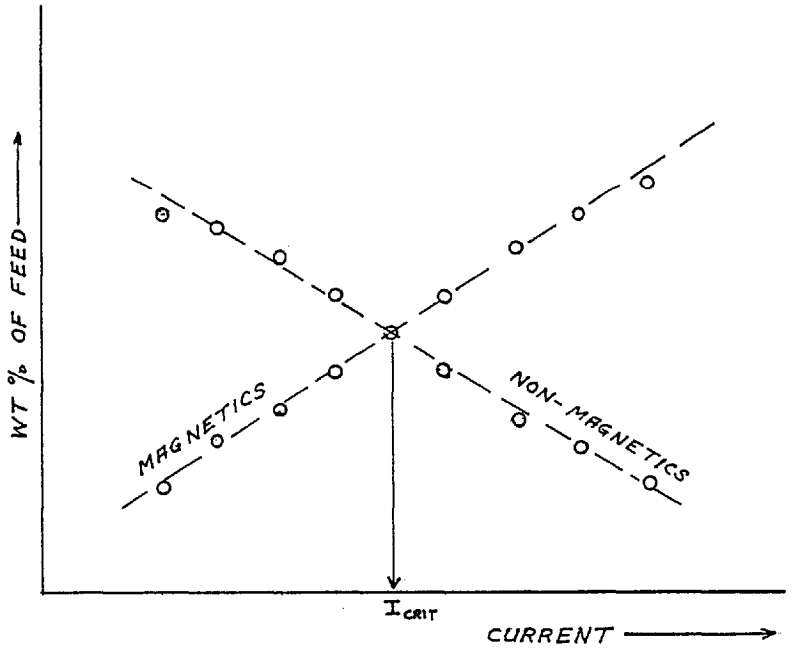

Fig. 6.13 Technique for determination of critical current (diagrammatic).

The size fraction chosen for calibration tests was -850 μm +425 μm. Fresh Analar grade materials were used as standards in all cases. (It was found that a dehydration effect occurred with $MnSO_4.4H_2O$ left for some months in a plastic bag). With $MnSO_4.nH_2O$ the specific susceptibility decreases as the water of crystallisation increases.

Optical examination of the standards employed showed that the copper sulphate was mostly single crystal; the ferrous ammonium sulphate largely twinned crystals and aggregates; and the manganese sulphate consisted of microcrystalline aggregates.

It was not found possible to obtain a susceptibility equal to the published value for $CuSO_4.5H_2O$. On the Cook Separator, a value of $\chi = 4.84$ was found to be consistent with critical current data plotted for $MnSO_4.5H_2O$ and Fe Amm.sulphate. It was shown optically that the $CuSO_4.5H_2O$ employed consisted largely but not entirely of anisotropic single crystal grains. The marked magnetic anisotropy of single crystal $CuSO_4.5H_2O$ at room temperature has been known for some time (Krishnan and Mookherji,1936, 1938), the susceptibility axes forming an approximately uniaxial spheroid: an approximately 30% difference in susceptibility was reported between the major and minor values. Since grains are free to rotate on the track of the separator, they therefore selectively orientate themselves so that their major susceptibility axis is parallel to the applied field, i.e. approximately perpendicular to the separation track. Grains which are not single crystal will take up an orientation dependent on that of the component grains.

McAndrew(1957) did not report on this anisotropy, or on whether his Gouy check determinations were done on single crystals, aggregates, or on a powder of crushed material. A possible explanation of his results is that the particles he separated were finely polycrystalline, so that the anisotropy typical of single crystals did not become apparent.

The calibration curve obtained for the Cook separator was shown in Fig. 6.8. Values of $K = 2{\cdot}265$ and $n = 1.96213$ were obtained by solving simultaneously the calibration equation $\log(\sin\theta/\chi) = \log K + n \log i$ for two points on the line, (see Appendix E). Values employed in Fig. 6.8 for the susceptibilities of the three standards $CuSO_4.5H_2O$, $MnSO_4.4H_2O$, and $Fe(NH_4)_2(SO_4)_2.6H_2O$ were respectively 4.84, 65.4 and 31.08 x 10^{-2} $JT^{-2}kg^{-1}$.
It will be seen that linearity ceases at a maximum current of 1.79A. The implications of the calibration current, being defined as that for a 50% yield of the standard substance, are that around 50% of grains corresponding exactly in susceptibility to the current used in a particular separation pass, will remain in the non-magnetics.

It is believed however that the actual number of such 'misplaced' grains in a sample which shows a wide range of susceptibility will be very small, so that no significant error is introduced. No two mineral particles probably have exactly the same specific susceptibility, in contrast to a pure crystalline standard in which all the grains are nominally identical.

CHAPTER 7

METHODS FOR MEASURING MAGNETIC TRANSITION TEMPERATURES

7.1 Ferromagnetic Curie point

The Curie point is strictly defined as the temperature at which the spontaneous magnetization (Section 4. 2) becomes zero (Crangle,1977).

Most of the problems related to Curie point determination result from the fact that there are many different experimental methods for its determination. Each of these methods carries its own implicit definition of Curie point, and it is not easy to prove that these definitions are totally equivalent.

Magnetic equipment which can be employed includes magnetic balances (Doell and Cox, 1967; Schwartz, 1968); torsion balances (Larochelle, 1961; Clark, 1967) and also fluxgate magnetometers (Weigts et al, 1967). Equipment used for revealing non-magnetic properties such as the specific heat anomaly; specific resistivity anomaly; irregularities in the DTA curve; disappearance of magnetic superlattice lines during neutron diffraction, and disappearance of a 6-line spectrum during Mössbauer spectroscopy, can also be employed to indicate the Curie point (Schieber, 1967).

The spontaneous magnetization has its highest value, σ_s, at absolute zero. In ferromagnetic substances it is rather insensitive to temperature except near the Curie point (Fig. 7.1), and it is virtually unaffected by an external magnetic field (Lee, 1963). At the Curie point, thermal agitations overcome the interactions which produce mutual alignment of the atomic magnetic moments, and the material behaves paramagnetically at all higher temperatures (Fig. 7.2).

When magnetization curves for true ferromagnetics intersect the temperature axis almost perpendicularly as in Fig. 7.1, the experimental (as opposed to calculated) Curie point is readily defined. Other substances however, including ferrimagnetics

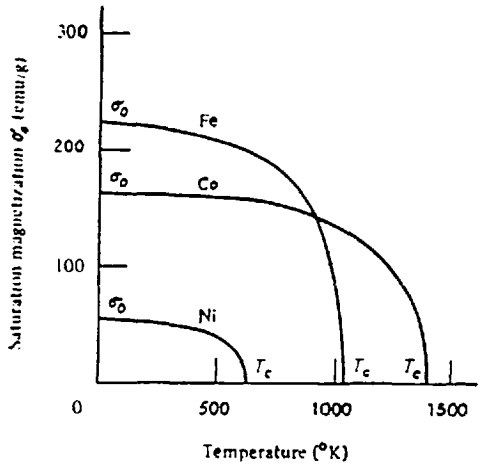

Fig. 7.1 Saturation magnetisation and Curie points (T_c) of Fe, Co and Ni. (Taken from Cullity, 1972, p122).

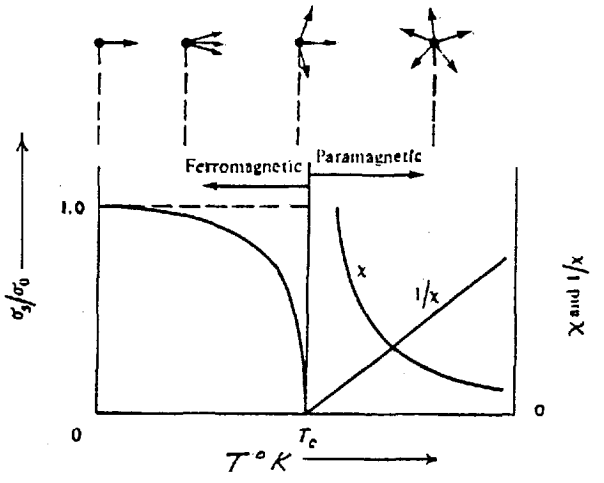

Fig. 7.2 Temperature dependence of ferromagnetic behaviour in zero applied field. Upper sketch shows the qualitative distribution of spin directions in a single domain ($T<T_c$) and in a group of atoms ($T>T_c$).
(Taken from Cullity, 1972, p127).

and substances with a weak ferromagnetic component, do not show such sharp intersections e.g. hematite, Fig. 7.3.

Additional methods for determining the Curie point of a ferromagnetic include using a hysteresigraph, and raising the temperature until the hysteresis curve shrinks and disappears, or measuring the coercive force and noting the temperature at which this disappears. Nagata, Akimoto and Uyeda(1953) describe a thermomagnetic separator (Fig. 7.4) in which the temperature at which cooling particles become attracted to an overhead magnet is noted. Small grains of sample are laid on a platform inside a tube. Heat is supplied by an external furnace and it is thus very difficult to ensure uniform heating of the support platform. Due to the flowing N_2 gas there is also a problem with temperature gradients and with thermal shielding of the thermocouple contact. A particle is lifted when $m.\chi.\frac{H dH}{dx} > mg$. Thus lifting can occur even at temperatures well below the Curie point if $\frac{H dH}{dx}$ is big enough. Such an apparatus was briefly experimented with in this investigation before being abandoned as impractical. Nagata and Akimoto (1956) used such an apparatus to establish the linear variation of Curie point between the end-members of a synthetic hematite-ilmenite solid solution series. In view of their own assessment of the actual Curie points being up to $10^{\circ}C$ higher than their determined values, this linearity must be regarded as approximate only.

For this investigation, the Curie points of ferrimagnetic fractions were deduced from curves of susceptibility versus temperature by determining the temperature corresponding to the peak χ value, using an a.c. induction bridge, (Section 6.5) made available in the Solid State Physics Department of Imperial College.

T_N itself is most easily determined by investigating the value of χ over a suitable temperature range. Many apparently paramagnetic substances have been shown by susceptibility determinations at very low temperatures to be antiferromagnetic - e.g. $CuSO_4.5H_2O$. Since other, non-antiferromagnetic materials may also show a susceptibility peak, the only conclusive evidence for antiferromagnetism is provided by neutron diffraction (Section 9.1).

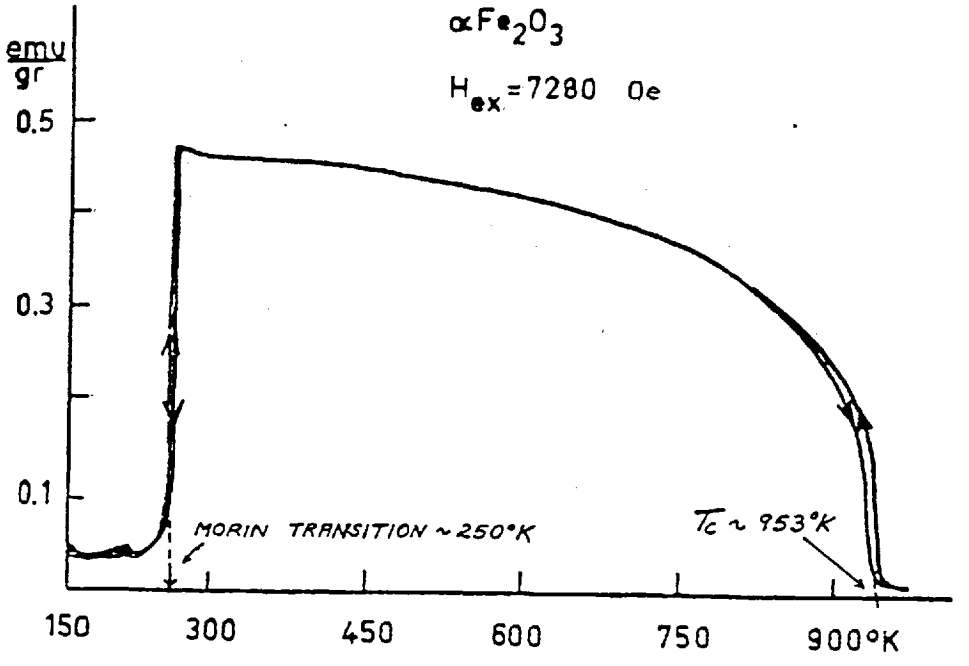

Fig. 7.3 Variation of magnetisation for a hematite sample during heating and subsequent cooling. (Taken from Schwarz, 1968).

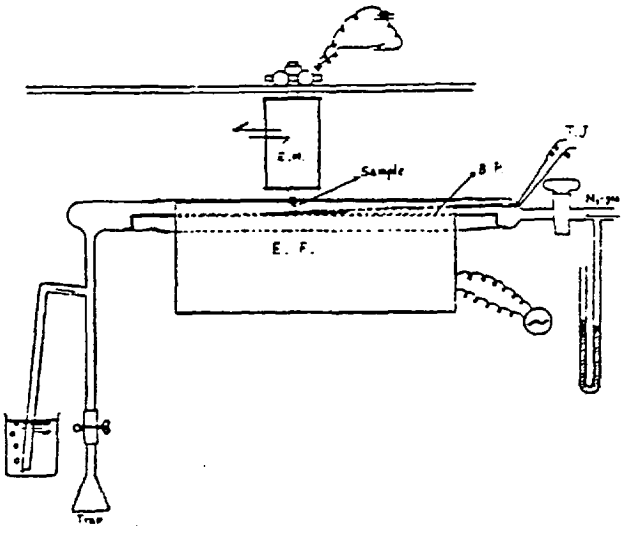

B.P..... brass plate
E.M.....electro-magnet
E.F..... electric furnace
T.J..... thermo-junction

Fig. 7.4 Thermomagnetic separator used by Japanese workers for determining Curie points. (Taken from Nagata, Akimoto and Uyeda, 1953).

The Curie point Θ_p determined by measurements in the paramagnetic regime is not always the same as that obtained from measurements in the ferromagnetic regime which yield Θ_f, (Fig. 7.5). The reason for the lack of sharpness is thought to be due to the persistence of some small magnetically ordered clusters at temperatures above the Curie point.

In the Curie-Weiss law equation for ferromagnetics $\chi = C/T-\Theta$, where C is the Curie constant, Θ is approximately equal to the Curie point temperature, and hence is large and positive.

7.2 Ferrimagnetic Curie point

For ferrimagnetics (e.g. magnetite and other magnetic spinels) a paramagnetic Curie point Θ_p may also be determined, (Fig. 7.6). In this case the susceptibility has a complex relationship which at high temperature reduces to $\chi = \frac{C}{T+C/\chi_o}$. The temperature T_c is called the ferrimagnetic Curie point; at T_c the susceptibility becomes infinite and spontaneous magnetization re-appears. Discrepancy between Θ_p and T_c is thought to be due to short-range spin clusters, as in the case of ferromagnetism (Cullity,1972).

7.3 Antiferromagnetic Néel point

For antiferromagnetics (Fig. 7.7), susceptibility in the paramagnetic regime is given by:

$\chi = \frac{C}{T-(-\Theta)} = \frac{C}{T+\Theta}$. At a critical temperature called the Néel point (T_N), the susceptibility is a maximum. Below T_N the behaviour is antiferromagnetic and above T_N, paramagnetic. The value of Θ is theoretically negative, since Θ is proportional to the molecular field coefficient. This is another way of saying that the exchange force is negative (Table 4.1). In practice, however, determined values of Θ may be large and negative, or small and positive, and have no obvious relation to T_N.

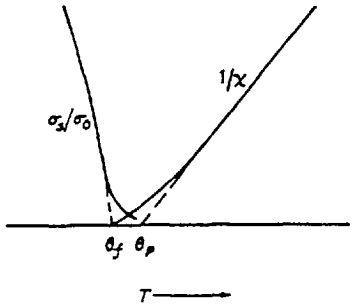

Fig. 7.5 Lack of sharpness in determinations of ferromagnetic Curie point. (Taken from Cullity, 1972, p128).

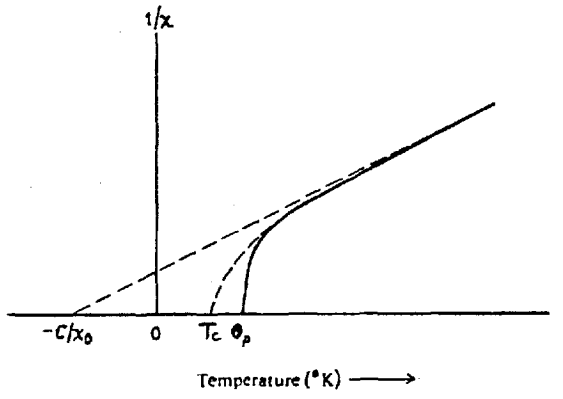

Fig. 7.6 Paramagnetic susceptibility in the region of the ferrimagnetic Curie point. (Taken from Cullity, 1972, p193).

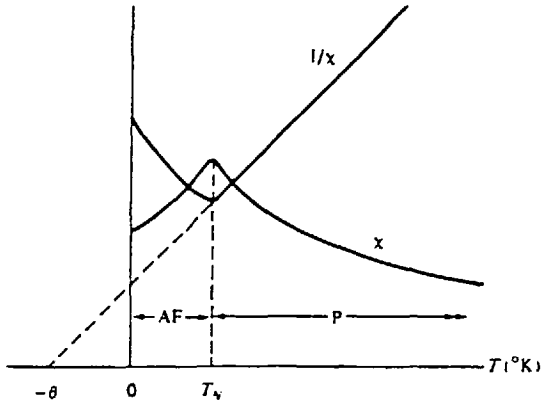

Fig. 7.7 Susceptibility of an ideal antiferromagnetic above and below T_N. (Taken from Cullity, 1972, p156).

CHAPTER 8

X-RAY DIFFRACTION

8.1 Introduction

The bulk of the XRD work in this investigation has been carried out on a Philips diffractometer using Cu Kα radiation and a graphite crystal monochromator. A small amount of powder camera work has been carried out and some Laue back-reflection photographs have been taken. In the diffractometer work, care has been taken to use a consistent, standardised technique, to minimise orientation effects and to obtain reproducible results. With the diffractometer, it has been possible to demonstrate progressive changes in the alteration of ilmenite in much finer detail than with the ore microscope.

8.2 Theory

The basic theory and techniques of both powder camera and powder diffractometer investigations are well known, (Cullity, 1956; Lipson and Steeple, 1970; Klug and Alexander, 1974; and Zussman, 1977). A suitable reference for quantitative diffraction of mineral mixtures containing X-ray amorphous phases was recommended by Mr. D. Holden of Tioxide International Ltd., in which Chung(1974a) gives a "Matrix flushing" technique for quantitative XRD which permits determination of the amount present not only of each crystalline phase but also of any amorphous matter.

8.3 The Chung matrix-flushing method for quantitative XRD

This technique is claimed by Chung (1974a) to be faster than, yet as reliable as, the conventional internal-standard method. The working equation provides a direct relationship between peak intensity and concentration of each crystalline phase, free from mass absorption coefficients since these have been cancelled out.

The method assumes that the identities but not the quantities of the crystalline phases in a mineral mixture are already known. Reference mixtures are made up from a pure specimen of each known phase mixed in equal proportions by weight with a suitable internal standard. These reference mixtures are then used to prepare X-ray diffractograms in which the intensities corresponding to a selected line of the mineral phase and of the standard are noted, and the intensity ratio of mineral phase to standard is calculated. It is normally assumed that the degree of crystallinity of the mineral phases used to prepare the reference mixtures matches the crystallinities of the mineral phases in the natural mixtures. However, when the method is used specifically to determine the amorphous content of a specimen, the minerals used to prepare the reference mixtures must be of known crystallinity - preferably highly crystalline, and ideally 100% X-ray diffracting.

A diffractogram is prepared from the natural mixture into which a known weight of the internal standard has been blended. The intensities of selected peaks for each phase are noted together with the intensity for the internal standard. The data so obtained are substituted in the Chung working equation, which is calculated for each component in turn.

$$X_i = \frac{X_c}{I_c} \cdot \frac{I_i}{K_i}$$

where X_i = Wt. fraction of phase i

I_i = Intensity of X-rays diffracted by a selected plane (hkl) of phase i in the mixture.

I_c = Intensity for a selected plane (hkl) of the internal standard.

K_i = Ratio of the intensities of the selected peak of component i to the selected peak of the internal standard, as measured from the 50/50 reference mixture. (Hereafter termed the 'reference intensity ratio').

X_c = Wt. proportion of the internal standard added to the mixture being analysed.

Even if all the standards are highly crystalline, the sum of the X_i terms will not equal 100% when X-ray amorphous matter is present in the unknown specimen. Consequently the amount of amorphous material can be determined by difference. Unfortunately, this calculated figure also becomes a repository for errors in the individual X_i terms.

Chung recommended the use of corundum as the internal standard, and this has previously been used for indicating relative intensities by the "I/I_{cor}" figures quoted for some crystalline substances (1977 Powder Diffraction File, JCPDS).

However, the d = 2.552 Å line of corundum is close to the d = 2.54 Å line of ilmenite; and the d = 2.165 Å corundum line is close to the d = 2.188 Å line of rutile and the d = 2.187 Å line of pseudorutile.

These similar peak positions would not prevent the use of corundum as an internal standard but they could cause difficulties if relative intensity data were estimated from a sample to which corundum had been added.

In this work, the practice of Grey and Reid(1974) has been followed and high purity iron (produced from iron carbonyl) of high crystallinity was used as the internal standard: its lines do not interfere with those of ilmenite, rutile or pseudorutile. The iron was added to the diffraction samples in the ratio 1:5 respectively by weight. The other standard materials used were synthetic ilmenite, synthetic rutile and carefully cleaned Indonesian pseudorutile.

In the absence of amorphous phases (in both standards and unknowns) and where all phases are approximately stoichiometric, then the proportion of a mineral calculated by this method will match that obtained from a normative chemical calculation. In practice this applies only if the number of phases is small and no confusion can arise from the same element being partitioned between many minerals.

Chung's method was tested by making up a synthetic test mixture of 25% each of natural rutile; fine grained iron; hematite; and synthetic ilmenite. Reference spectra of hematite, ilmenite and rutile in a 50% mix by weight with iron were produced and measured. Reference ratios K_i from these reference spectra were applied in the Chung matrix flushing formula, using measurements from the spectrum of the synthetic test mixture. The results obtained were as follows: hematite 25.5%, rutile 22.3%, iron 24.6% and ilmenite 27.6%. The level of accuracy obtained in this test is not as good as that obtained by Chung with his test mixtures (Chung,1974a). However, unlike Chung the author did not use constant-time counting over each peak but instead used peak height measurements made from the recorded diffractogram. However, the accuracy obtained would readily show the trend of mineralogical changes in progressively altered ilmenite, provided there was not a large amount of amorphous material present.

8.4 Procedure for Chung Method

Cleaned portions of each fraction were cut out from the available material by coning and quartering. These portions were hand ground by agate mortar and pestle. A 114.83 mm X-ray powder camera was used to check for spotty lines and this established that a minimum grinding time of 20 minutes was required.

The powders were then lightly mixed with an additional 20% by weight of -37 μm metallic iron powder using the mortar and pestle. The doped mixtures were then placed in glass-backed aluminium cavity slides approximately 1 mm thick. The powder was lightly tamped with the edge of a glass slide and finally scraped smooth with a sharp edge.

The Philips diffractometer standard settings employed for all Chung tests were: scanning rate 1° 2θ/min, time constant 2, diverging slit 2°, receiving slit 1° and chart speed 1 cm/min. On the pulse height analyser the settings were 'attenuation' 4, 'lower level' 350 (equivalent to 1.75 volts), and the window was set in threshold mode.

8.5 Mineral spectra

Ilmenite ($FeTiO_3$): During examination of the XRD spectrum of the author's synthetic ilmenite, reference was initially made to the data for ilmenite given on the ASTM 3-0781. However, as is so often the case, (due to slight variations in powder composition, preparation technique, particle orientation effects and XRD instrumental conditions), the synthetic ilmenite spectrum did not closely match the ASTM data. The main discrepancy was in line intensity. A line observed at d = 1.37 Å, unlisted in ASTM 3-0781, was found in an ilmenite spectrum given by Brown (1961). In addition, hkl values 102, 204, 108 and some other reflections listed in ASTM 3-0781 were found to be incompatible with trigonal symmetry, since the requirement is that $-h + k + l = 3n$ where $n = 0, 1, 2 \ldots$. Correct indices for the above reflections are 012, 024 and 018. The synthetic ilmenite intensities were much closer to those listed by Brown. Additional weak lines, noted and indexed for the synthetic ilmenite, have also been observed in the XRD spectrum of Norwegian ilmenite from the Tellnes deposit.

The most ilmenite-rich fraction of the Capel material (0.30 A magnetics) also had relative intensities closer to Brown's(1961) data than to ASTM 3-0781. An indication of the weathered state of the Capel ilmenite was given by the broader peaks and much lower intensities obtained when the sample was run under the same instrumental conditions as the synthetic ilmenite.

Ilmenite spectra are compared in Table 8.1. The similarity of the spectrum of hematite to that of ilmenite is discussed in Section 10.8.

Rutile (TiO_2): The spectrum obtained from handpicked non-magnetic ($\chi < 1 \times 10^{-2} JT^{-2} kg^{-1}$) Capel rutile is given in Table 8.2, and the intensities listed were used for peak height corrections during quantitative XRD. Concentrates of high-grade secondary rutile from Capel have been found to give spectra indicating that secondary rutile is not as crystalline as primary rutile with respect to peak width, and the spectra also display the presence of minor anatase (TiO_2).

Pseudorutile ($Fe_2Ti_3O_9$): The spectrum of Indonesian pseudorutile from which all visible impurities and grains coated with secondary rutile had been removed is given in Table 8.3. An indexable but unlisted line, noted in the spectra of certain weakly magnetic fractions of altered ilmenite, is included for completeness.

The spectra obtained by Grey and Reid(1975) for pseudorutile specimens from South Australia and Indonesia are reproduced in Fig. 8.1. The presence of ilmenite and rutile in small amount in the Indonesian sample are clearly indicated.

Arizonite: The interplanar spacings and intensities of arizonite (Overholt et al,1950), also reported to have the composition $Fe_2Ti_3O_9$, are given in Table 8.4 for comparison. Some of the spacings are very close to those of rutile and pseudorutile. Overholt et al(1950) claimed that arizonite was simply a mixture of hematite, ilmenite, anatase and rutile. However, pseudorutile may also be a component of this mixture.

Table 8.1

XRD spectra for ilmenite, ($FeTiO_3$)

	ASTM 3-0781			SYNTH ILM		ALTD.ILM FROM CAPEL(4) 0.30A MAGS (BLACK)		BROWN*	
hkl[1]	dÅ	I/I_1	$2\theta_2$	dÅ	I/I_1	dÅ	I/I_1	dÅ	I/I_1
012	3.73	50	23.85	3.74	28	3.72	19	3.73	45
104	2.74	100	32.68	2.75	100	2.74	100	2.75	100
110	2.54	85	35.34	2.55	70	2.54	81	2.546	70
113	2.23	70	40.45	2.24	30	2.23	25	2.240	30
-	-	-		2.18	2	n.v.	-	-	-
(202)[3]	-	-	(42.98)	2.10	2	n.v.	-	-	-
024	1.86	85	48.97	1.87	35	1.87	27	1.867	35
116	1.72	100	53.25	1.725	60	1.72	34	1.726	60
018	1.63	50	56.45	1.62	10	1.63	13	1.633	10
214	1.50	85	61.85	1.505	31	1.50	32	1.506	20
300	1.47	85	63.26	1.47	30	1.47	22	1.469	25
(208*	-	-	68.20)	1.37	3	1.37	2	1.375	3
1,0,10	1.34	70	70.24	1.34	19	1.34	14	1.340	15
220	1.27	60	74.75	1.27	5	n.d.	-	1.272	10
036[3]	-	-		1.23	1	"	-	1.226	3
312	1.20	30	79.94	1.21	3	"	-	1.211	3
0,2,10	1.18	60	81.58	1.19	7	"	-	1.187	6
134	1.15	70	84.19	1.15	8	"	-		
226	1.12	70	86.99	1.12	9	"	-		
2,1,10) 309)	1.07	70	92.18	1.08	8	"	-		

n.v. not visible
n.d. not determined

1) indices corrected where necessary

2) Calc. for CuKα (Average) = 1.54178 Å

3) Author's indexing

4) Discrete lines of other phases (i.e. rutile, pseudorutile), are not here included.

*Brown, (1961).

Table 8.2

XRD spectra for rutile, (TiO_2)

ASTM 4-0551				CAPEL RUTILE	
hkl	dÅ	I/I_1	2θ*	dÅ	I/I_1
110	3.245	100	27.49	3.24	100
101	2.489	41	36.08	2.48	49
200	2.297	7	39.22	2.29	6
111	2.188	22	41.26	2.18	20
210	2.054	9	44.09	2.05	10.5
211	1.687	50	54.38	1.69	65
220	1.624	16	56.68	1.62	19
002	1.480	8	62.78	1.48	6
310	1.453	6	64.09	1.45	10.5
301	1.360	16	69.06	1.36	19
112	1.347	7	69.82	1.35	10

*Calc. for CuKα (Average) = 1.54178Å

Table 8.3

XRD spectra for pseudorutile $(Fe_2Ti_3O_9)$

	ASTM 19-635[1]			INDONESIAN[2]		
hkl	d Å	I/I_1	2θ*	d Å	I/I_1[3]	2θ
111^+	3.85	40d	23.10	3.88	20	22.94 b
$(230^{++}$	2.86	36	31.22)	-	-	-
$140^+, 131^+$	2.77	40d	32.32	2.79	32	32.10c,b
100	2.489	60	36.08	2.49	79	36.02 a
002	2.297	4	39.22	2.31	17	39.0 a
101	2.187	50	41.28	2.19	66	41.18 a
102	1.688	100	54.35	1.69	100	54.18 a
261^+	1.630	40d	56.45	1.63	12	56.30 b
$081^+, 123^+$	1.470	40d	63.26	1.47	7	63.26 c,b
110	1.436	30	64.94	1.44	14	64.70 b
181^+	1.380	20d	67.92		Higher angle	
103	1.304	4	72.48		lines insufficiently	
200	1.244	2	76.59		resolved by	
201	1.200	2	79.94		diffractometer	
004	1.149	6	84.28			
202	1.094	12	89.60			
104	1.043	8	95.31			
114	0.897	8	118.50			
212	0.870	6	124.77			

1 Teufer and Temple Nature 211 179-181, 1966.

* Calc. for CuK α = 1.54178 Å

++ Author's indexing for previously unlisted line showing maximum development in Capel 0.55A magnetics

\+ Author's indexing indicating possible contributory reflections

2 Discrete lines of ilmenite and rutile not here listed

3 Contribution of superposed lines subtracted using intensities of Capel rutile (Table 8.2) and 0.30A mags (Table 8.1).

b broad, low-intensity hump

a superposition of rutile line

c " " ilmenite line

d diffuse

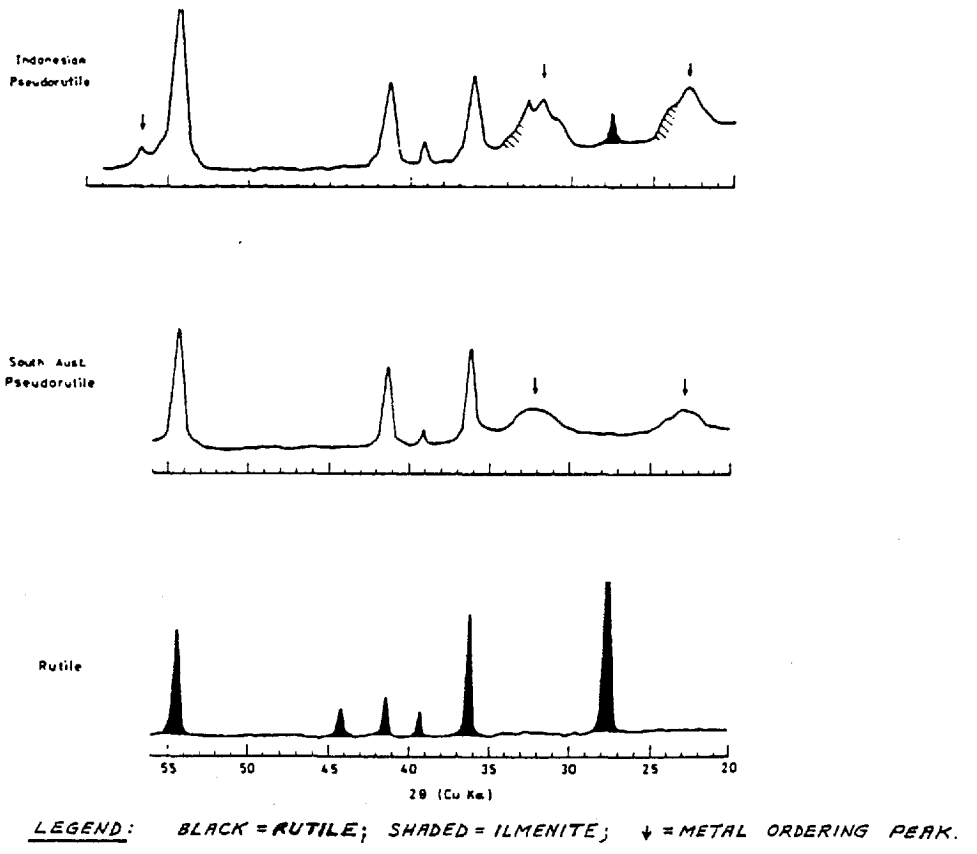

Fig. 8.1 XRD spectra of Indonesian and South Australian pseudorutile compared with the spectrum of rutile. (Taken from Grey & Reid, 1975).

Table 8.4

XRD spectrum for arizonite after Overholt et al, 1950.

d Å	I/I_1	2θ*	Comments**
3.87	30	22.98	Pseudorutile 23.10/diffuse
3.67	40	24.25	Hematite 24.32/25
3.50	100	25.45	Anatase 25.30/100
3.23	30	27.62	Rutile 27.49°/100
2.96	10	30.19	
2.66	90	33.69	Hematite 33.30/100
2.51	80	35.77	Hematite 35.78/50
2.48	Tr	36.22	Rutile 36.09/41, pseudorutile 36.08/60
2.419	5	37.17	Anatase 36.98/10
2.370	10	37.96	Anatase 37.83/20
2.196	20	41.10	Hematite 41.01/30
2.180	Tr	41.42	Rutile 41.26/22; pseudorutile 41.28/50
2.080	Tr	43.51	
1.885	10	48.28	Anatase 48.09/35
1.863	Tr	48.89	Ilmenite 48.97/85
1.833	20	49.74	Hematite 49.59/40
1.687	70	54.38	Rutile 54.38/50 pseudorutile 54.35/100
1.660	30	55.34	Anatase 55.11/20
1.624	5	56.68	Pseudorutile 56.45/40d
1.595	10	57.80	Hematite 57.76/16
1.478	30	62.88	Hematite 62.59/35; anatase 62.74/14
1.449	20	64.28	Hematite 64.13/35
1.359	10	69.12	Anatase 68.82/6
1.334	10	70.60	Anatase 70.37/6
1.308	Tr	72.22	Hematite 72.10/20
1.261	20	75.37	Anatase 75.10/10
1.162	5	83.12	Hematite 83.12/10
1.137	10	85.38	
1.101	5	88.88	Hematite 88.78/14
1.088	5	90.23	Pseudorutile 98.60/12
1.052	5	94.24	Hematite 93.89/18; anatase 94.28/4
1.042	5	95.43	Anatase 95.24/4; pseudorutile 95.31/8

* Calculated for Cu Kα (Average) = 1.54178Å

** Nominal positions and relative intensities of reflections for anatase, hematite, ilmenite, rutile and pseudorutile taken from ASTM cards 21-1272; 13-534; 3-0781; 4-0551 and 19-635 respectively. Not all the lines expected for these minerals are present, however.

CHAPTER 9

NEUTRON DIFFRACTION AND MÖSSBAUER SPECTROSCOPY

9.1 Neutron diffraction

General: Neutron diffraction is a spectroscopic method suitable for the study of powdered or single crystal samples of crystalline materials.

The wavelength of a neutron beam is given by $\lambda = h/mV$ where h is Planck's constant, V is the neutron velocity, and m is the neutron mass. For diffraction purposes, neutron beams are usually obtained from nuclear fission reactors. The experimental arrangement is similar to that in an X-ray diffractometer, using a collimated monochromatic beam directed on to the specimen. However, because of its poor resolution and low intensity, ND spectroscopy is not a substitute for XRD.

The theory of neutron diffraction was reported by Bacon(1955), and its application to the analysis of magnetic crystals is briefly discussed by Cullity(1972) and Crangle(1977). Only a brief description of the ND method is included here.

The ND method is a unique and powerful tool for elucidating the nature of any magnetic order which may exist in a crystalline substance because neutron scattering is sensitive to differing directions of magnetic spin moments on adjacent crystal planes. The neutron diffraction itself follows a Bragg Law relation ($n\lambda = 2d \sin\theta$), as with XRD. However, the ND relative peak intensities obtained are different from XRD intensities because of the different atomic scattering factors that are applicable. X-rays "see" only the electrons surrounding the nucleus, while neutrons "see" only the nucleus and the magnetic spin moments. The X-ray scattering amplitudes are proportional to the atomic number of the elements concerned, and fall off as the angle between the incident and scattered directions increases, at a rate dependent on $\sin\theta/\lambda$.

The neutron scattering amplitudes, however, are independent of atomic number and do not vary with Θ, (Fig. 9.1).

Neutron diffraction on a pseudorutile-rich sample (Section 12.4) was carried out at A.E.R.E. Harwell by courtesy of Dr. H.C. Harris and with the help of Mr. G. Proudfoot. The experiments were carried out in the Dido reactor using the Badger 2 diffractometer. The powdered sample was placed in a vanadium sample tube and positioned in the neutron beam by marking the tube with cadmium foil and photographing the transmitted beam.

The sample tube was sealed against liquid helium by use of an indium wire washer, and was mounted inside a metal cryostat. The principles of the neutron diffractometer arrangement are shown in Fig. 9.2. The BF_3 counter was moved through 0.1° increments with a 100 second count-time at each position. Counts were output by teletype and plotted by hand.

Neutron diffraction of ilmenite: Examination of the ND spectrum of ilmenite (Fig. 9.3, after Shirane et al, 1959) shows that it is very different from the XRD spectrum of the same mineral (Fig. 9.4). Not only are the peaks shifted in position due to the shorter wavelength (approx. 1×10^{-1} nm) of the thermal neutrons, but the relative peak intensities are also completely different. By picking off the 2Θ positions from Shirane et al's spectrum (no tabulated data were presented) it was possible to calculate the approximate d-spacings and to correlate these with the d-spacings listed on the ASTM 3-0781 XRD data card. In this way 5 "extra" lines which do not appear in XRD spectrum were identified (Table 9.1). These "extra" lines are the result of structure factor (F) effects, and this was proved by running a computer program to calculate the structure factors (F) for the extra lines. Under neutron diffraction conditions, it was found that the F value for the two low angle peaks (111) and(100) were a substantial fraction of the F value for the main peak (210), but a very low fraction under XRD conditions (Table 9.1). The F-calculation program was used by courtesy of Dr. D. Williams of

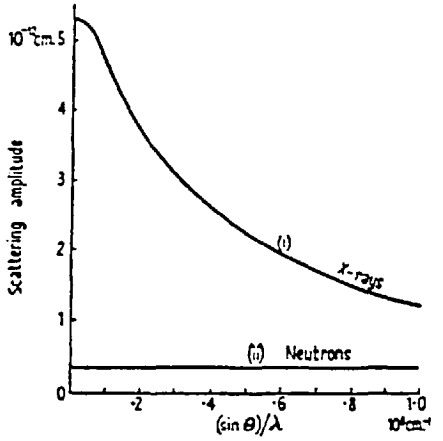

Fig. 9.1 X-ray and neutron scattering amplitudes for a potassium ion (taken from Bacon, 1955).

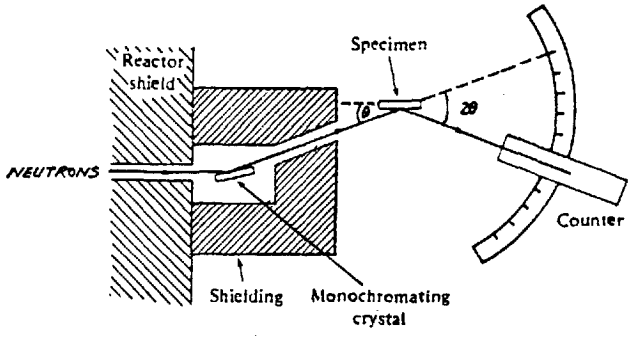

Fig. 9.2 Arrangement of a neutron diffractometer (taken from Cullity, 1972).

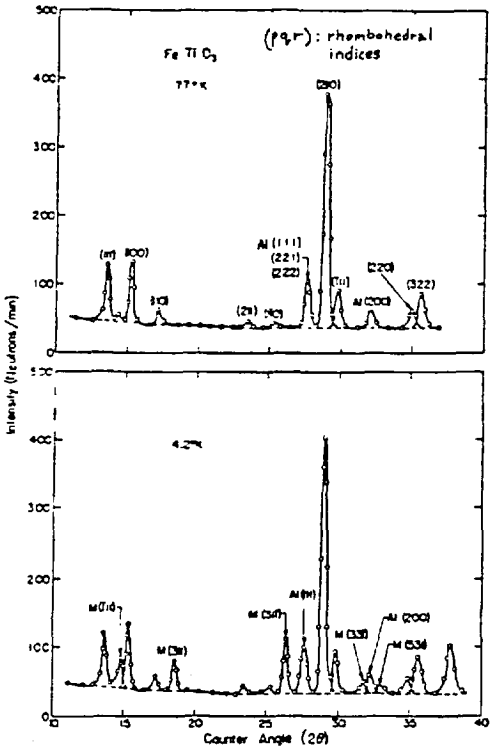

Fig. 9.3 Neutron diffraction spectra of ilmenite (taken from Shirane et al, 1959).

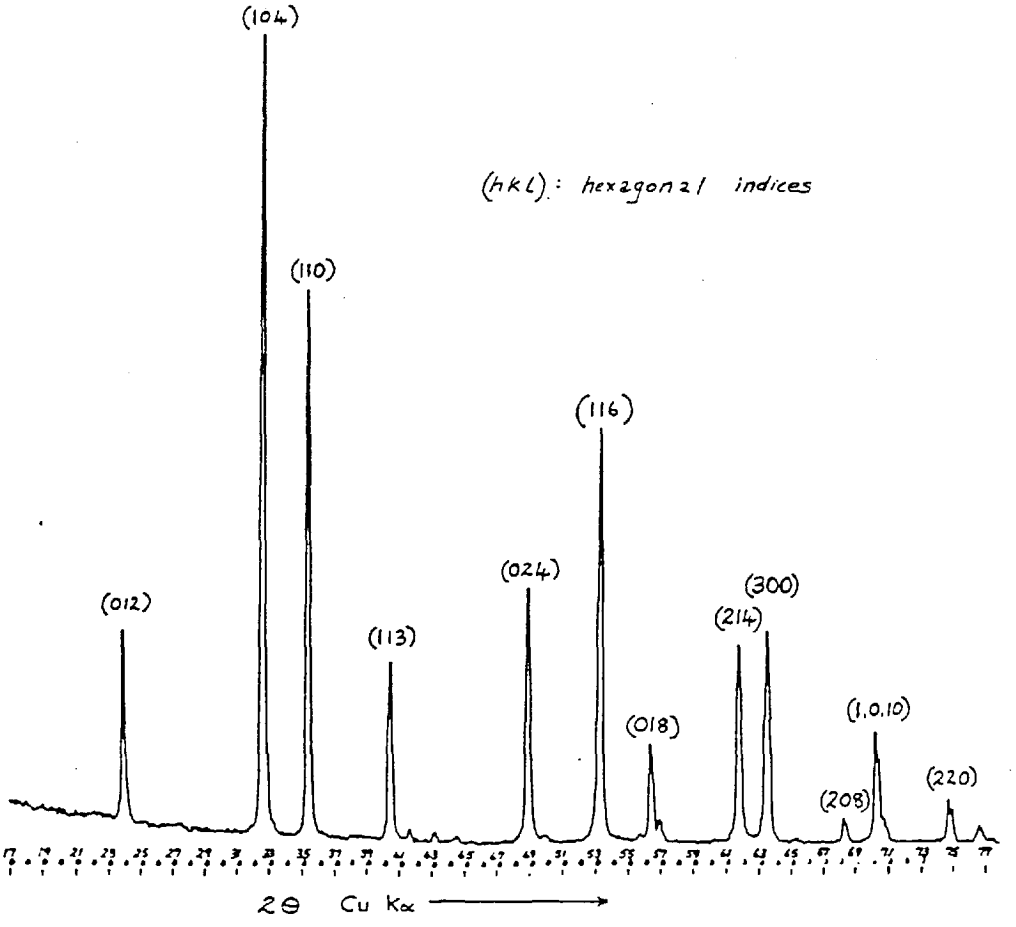

Fig. 9.4 XRD spectrum of synthetic ilmenite.

TABLE 9.1

Analysis of neutron diffraction lines in the ilmenite spectrum given by Shirane et al. (1959).

INDEX pqr	EQUIV. hkl	APPROX. 2θ	d CALC.FROM θ	d CALC.FROM Index[1]	d ASTM 3-0781	Calc.F FOR ND	Calc.F FOR XRD
111	003	13.6	4.73	4.69	-	70	*11
100	101	15.4	4.18	4.20	-	49	* 8
110	$\bar{1}02$	17.2	3.74	3.73	3.73	12	28
211	104	23.5	2.75	2.75	2.74	31	100
$1\bar{1}0$	$2\bar{1}0$	25.3	2.56	2.54	2.54		
221	015	27.6	2.34	2.37	-		*
222	006	27.6	2.34	2.35	-		
210	113	29.0	2.23	2.24	2.23	100	42.85
$\bar{1}11$	$\bar{2}01$	29.9	2.17	2.18	-		*
220	024	35.0	1.91	1.87	1.86	40	87
322	107	35.7	1.83	1.83	-	78	*10

*Lines not appearing on XRD spectrum.

[1]Using a_{hex} = 5.0881Å, C_{hex} = 14.080Å, from Lindsley, (1976).

the Crystallography Department at Imperial College.

This principle of 'extra' indexable lines in the ND system of a mineral being due to structure factor effects has been used to explain similar "extra" lines in the ND spectrum of pseudorutile (Section 12.4).

Shirane et al's ND spectrum for ilmenite at 4.2°K shows additional magnetic superlattice lines. These superlattice lines do not appear in the spectrum at 77°K, since this temperature is well above the Néel point (55°K). These magnetic superlattice lines were indexed in terms of the larger magnetic cell.

9.2 Mössbauer spectroscopy

General: The theory, practice and interpretation of data obtained by the Mössbauer technique have been described by Greenwood and Gibb(1971). The aim in this investigation was to use Mössbauer spectroscopy as a tool to provide information on the following:

1) The valence states of the iron present and their approximate proportions

2) The number of different coordination sites occupied

3) The presence or absence of magnetic ordering at a given temperature.

The Fe^{57} 14.41-KeV Mössbauer spectra obtained from the author's samples were prepared by the Mössbauer group at Birkbeck College, London, by courtesy of Dr. B.W. Fitzsimmons and Mr. I. Sayer. Data in the form of punched tapes were processed and fitted by the author using a Mössbauer fitting program made available by Dr. I.R. Fitch and Dr. I. Morrison of the Chemistry Department, Imperial College.

The Birkbeck College equipment employed Co^{57} in a rhodium matrix as the γ-ray source. The detector used was a methane-argon proportional counter, and the spectrometer was based on

an Elscint Ltd. "MEDA" multichannel analyser (MCA) connected to purpose built Elscint modules (amplifier, transducer, drive system etc.). Calibration for each set of experiments conducted at a particular attenuation setting of the drive was carried out using thin iron foil enriched in Fe^{57}, and a typical calibration spectrum is given in Fig. 9.5.

Features of a paramagnetic Mössbauer absorption spectrum are illustrated by that for synthetic ilmenite (Fig. 9.6) and the parameters which may be obtained from it are as follows:

1. The isomer shift (I.S.): This indicates the valence state of the Fe ions. Typical values of I.S. relative to iron metal are
   (small) 0.2 - 0.6 mm/sec for Fe^{3+}
   (large) 0.8 - 1.5 mm/sec for Fe^{2+} (from Greenwood and Gibb 1971)

2. The quadrupolar split (Q.S.): This is a measure of the electric field gradient at the Fe^{57} nucleus. A large Q.S. is associated with an octahedral site, while small Q.S. values are more typical of tetrahedral sites. Each site produces its own doublet, or double peak. A single peak (singlet) is due to a vanishingly small Q.S., which is equivalent to a zero electric field gradient, and indicative of a highly symmetric environment.

   The Q.S. of Fe^{3+} is dependent on temperature, in contrast to that of Fe^{2+}, which is little affected.

The presence of an infinite repeating lattice is not necessary in order for observation of Mössbauer resonance, and good spectra may be obtained from glassy or amorphous materials.

A ferromagnetic (such as metallic iron) below its Curie point generally gives a 6-peaked spectrum(Fig. 9.5) in those cases where the crystal magnetic field (hyperfine field) is high compared to the electric field gradient. (These conditions are assumed in the standard computer fitting program employed.) However, when the electric field gradient (mm/s) is comparable with or higher than the hyperfine field (mm/s), the normal symmetrical 6-peaked

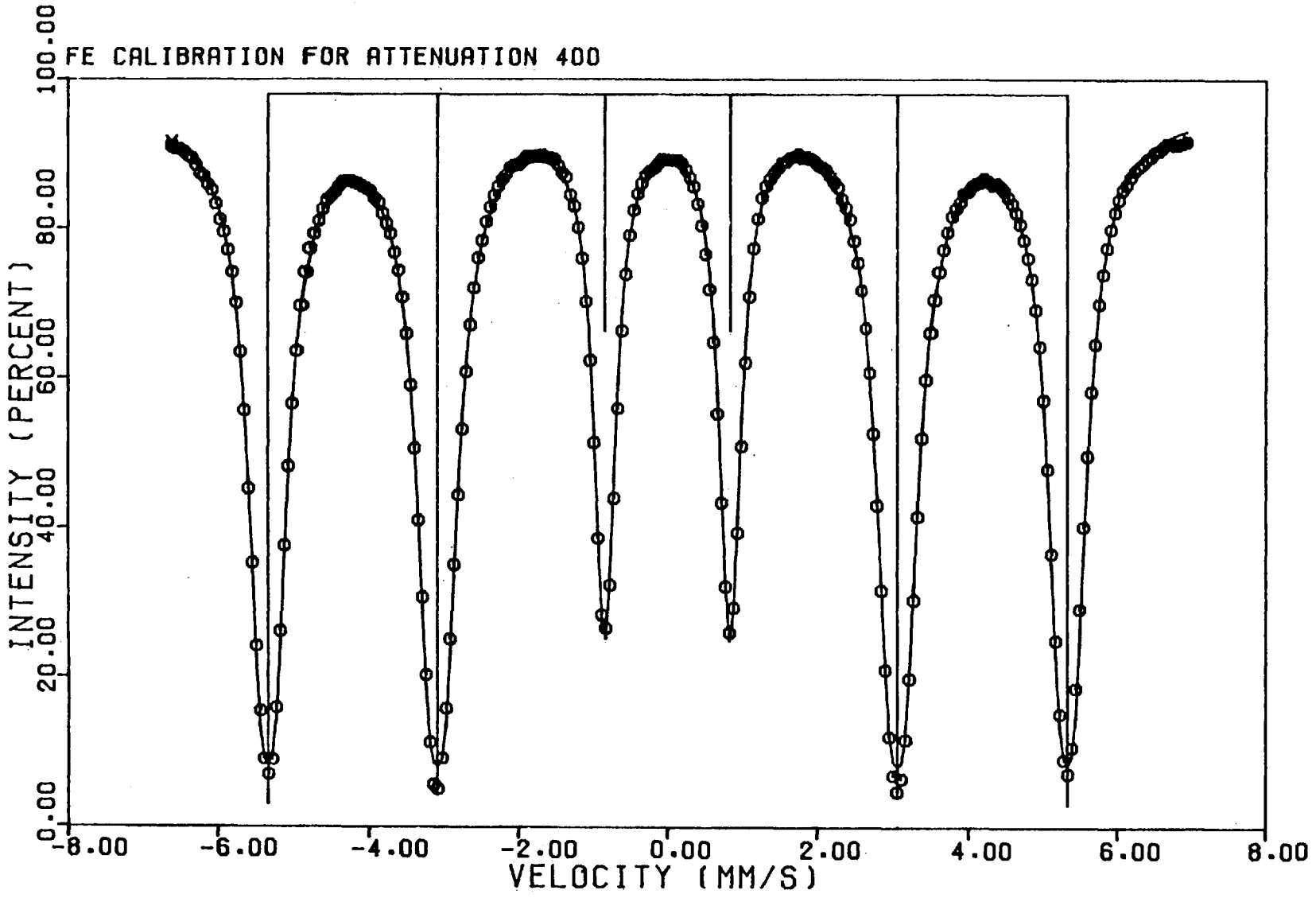

Fig. 9.5 Mössbauer calibration spectrum for iron at 293°K

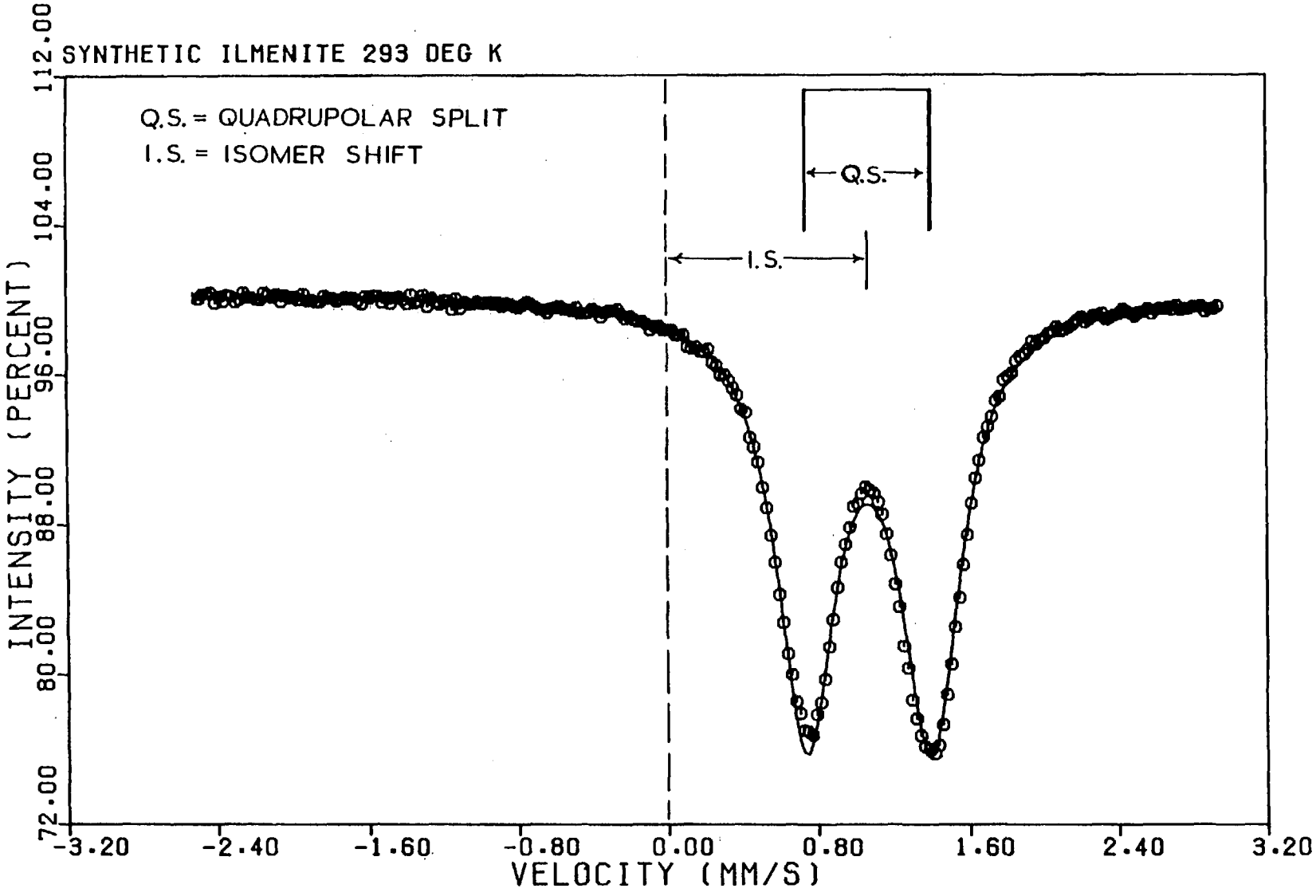

Fig. 9.6 Mössbauer spectrum of synthetic ilmenite at 293°K

spectrum is not observed. This is the explanation of the Mössbauer spectra obtained for ilmenite at low temperatures (see below).

Sample preparation: Using chemical analyses for total iron as a guide, mounts were prepared in which the iron contents were between 5-8 mg/cm^2. Since the powdered samples themselves were much richer in iron than this, they were diluted with a requisite amount of iron-free graphite powder, and after blending were placed as a thin layer inside plastic disc mounts.

Ilmenite: The Mössbauer spectrum of ilmenite has been discussed by Ruby and Shirane (1961), Shirane et al(1962) and Shirane and Ruby(1962) in studies of the ilmenite-hematite solid solution series using synthetic oxides.

Below its Néel point (T_N = 55°K), ilmenite does not yield a symmetrical, 6-peaked Mössbauer spectrum. Thus a spectrum for 20°K (Shirane et al,1962) shows a 3-peaked spectrum, while Ito and Morimoto(1973) present a spectrum for 4.2°K which shows 6 peaks, 5 of which have partly coalesced. These features indicate that the electric field gradient is comparable with the magnetic hyperfine field. Grant et al(1972) obtained a similar but better resolved spectrum (Fig. 9.7) for synthetic ilmenite at 5°K, produced using a narrow line source (Co^{57} in Cu).

Using an advanced 'second-order' fitting program, they obtained a good fit for the 5°K spectrum and found that $H_{INT} = (-)43 \pm 3$KOe.

As a check on its properties, the author's synthetic ilmenite was subjected to Mössbauer spectroscopy. The spectrum for 293°K gave a good fit, and yielded parameters (I.S. = 1.07 mm/sec; Q.S. = 0.66 mm/sec) agreeing closely with the data of Ito and Morimoto(1973). At 59.5°K, reported by I. Sayer (Birkbeck College Mössbauer Group - pers. comm.) to be the effective magnetic transition point, the ferrous doublet was noticeably asymmetric (Fig. 9.8). At 22°K a third peak, partly

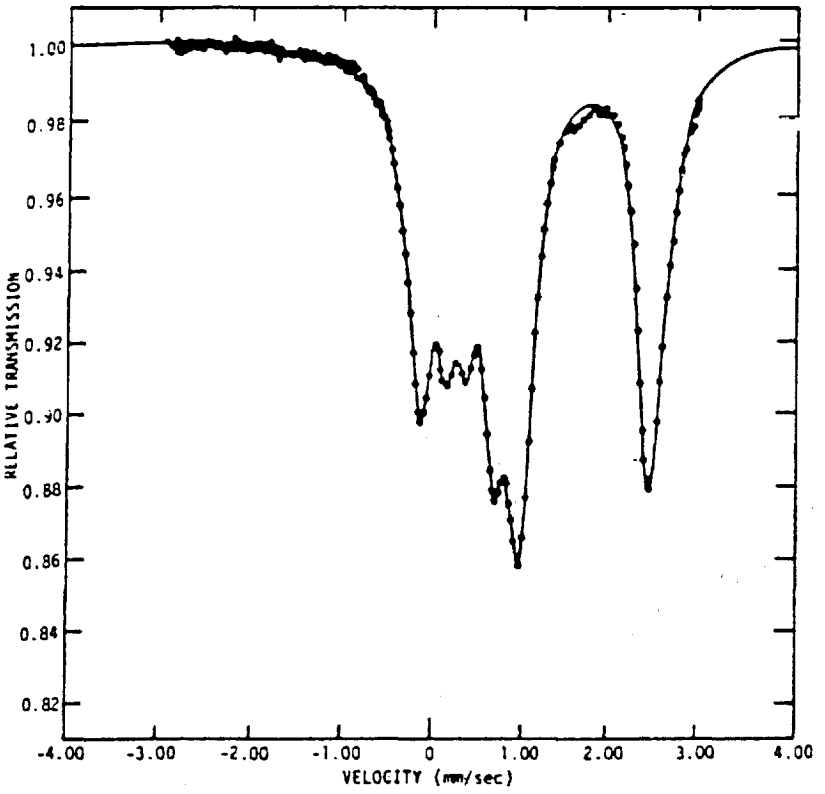

Fig. 9.7 Mössbauer spectrum of synthetic polycrystalline ilmenite at 5°K (taken from Grant et al, 1972)

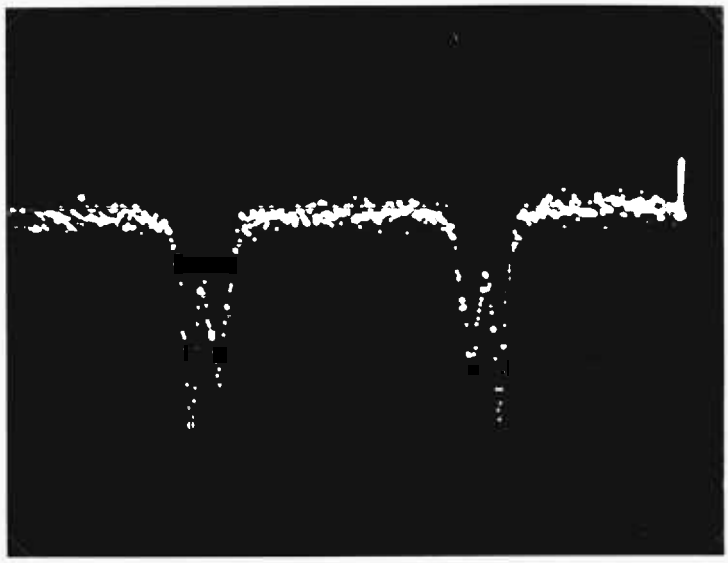

Fig. 9.8 Mössbauer spectrum of synthetic ilmenite at 59.5°K.



Fig. 9.9 Mössbauer spectrum of synthetic ilmenite at 22°K.

superimposed on the main peak of the doublet, became apparent (Fig. 9.9). Unfortunately, neither the 59.5°K nor the 22°K spectrum could be resolved by the standard fitting program. However the parameters obtained from the 293°K spectrum were considered to be a sufficient indication of the high purity of the sample.

The room-temperature Mössbauer spectra of naturally occurring ilmenites have been reported by Gibb et al(1969), and by Abras and Mansur(1975). In both these papers the presence of Fe^{3+} is reported. Gibb et al claimed that the apparent proportions of Fe^{2+} to total iron could be used as an index of the degree of alteration which had taken place. No mention was made of pseudorutile, although the major problem was identified as being the characterisation of the ferric-bearing phase. No ferric-bearing phase was identified in XRD spectra of the same samples, but Gibb et al did note that for one sample "The pattern does bear some resemblance to that of an iron titanate given as $Fe_2O_3.3TiO_2$" and went on to mention Teufer and Temple's study(1966) which they were cautious about accepting. Examination of the XRD spectra given by Gibb et al strongly suggest that pseudorutile was indeed present in their Harvey sample, and this would largely explain its $Fe_2^{3+}O_3$ analysis (27.19%).

Mössbauer investigation of ilmenite fractions containing hematite in solid solution, and of Indonesian pseudorutile, are reported in Sections 10.10 and 12.4 respectively.

CHAPTER 10

RESULTS FOR ILMENITE-RICH CONCENTRATE FROM THE SOUTH CAPEL DEPOSIT, W.A.

10.1 Introduction

The geology and mineralogy of the ilmenite deposits in the Capel field have been described by Welch(1964) and Welch et al(1975). Flowsheets of the recovery processes used in Western Australia were reviewed by Nairn(1965), and they remain essentially the same today although Reichert cones have since been increasingly employed for the initial gravity separation instead of spirals.

There are two main fossil heavy mineral strand lines in the Capel field (Fig. 10.1) and the individual deposits have been worked by four mining companies. The South Capel deposits worked by Associated Minerals Consolidated (formerly Western Titanium Limited) lie between the Capel and Abba rivers, and contain approximately 10.88×10^6t of heavy minerals. Between 1956 and 1972, 2.85×10^6t were mined out (Welch et al,1975). The approximate mineralogical content of the heavy mineral assemblage is as follows:

Ilmenite (54% TiO_2)	75
Altered Ilmenite (60% TiO_2)	8
Zircon	9
Rutile	1
Secondary rutile (leucoxene)	4
Monazite and xenotime	0.5
Garnet, staurolite, kyanite tourmaline, epidote, spinels and traces of pyrite	2.5
	100.0

The interdependent nature of the mineralogical, chemical and magnetic properties of detrital ilmenites has made it necessary at several points in this Chapter to refer the reader from one section of the text to another during the interpretation of the results obtained.

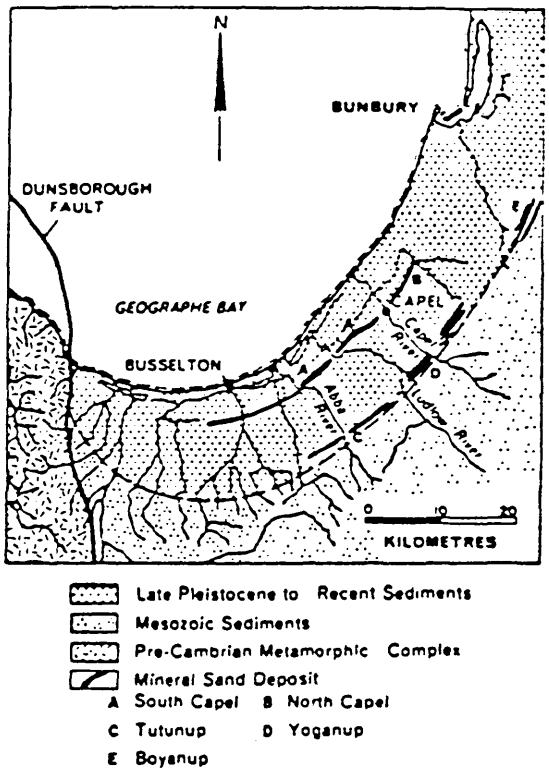

Fig. 10.1 Geological setting of the Capel heavy mineral field. (Taken from Lissiman and Oxenford, 1975)

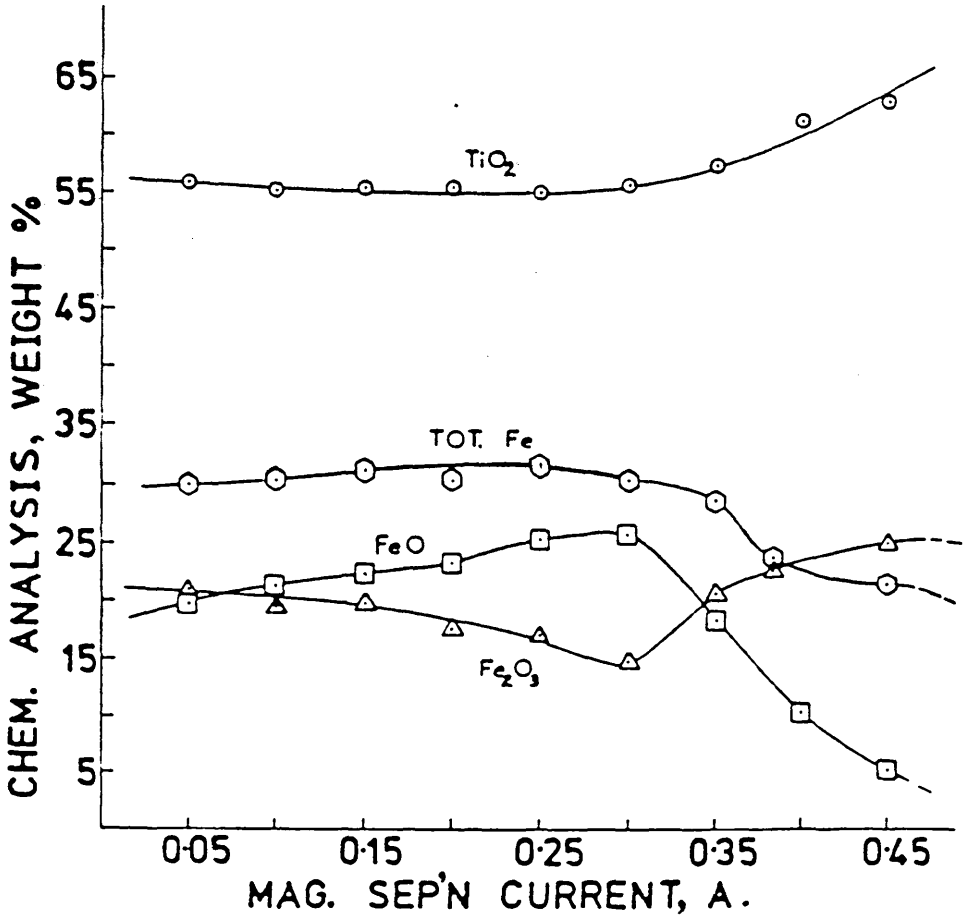

Fig. 10.2 Chemical variation of magnetic fractions of altered ilmenite from the South Capel deposit, Western Australia

10.2 Material studied

The bulk of the material studied in this investigation consists of a crude gravity concentrate that had not been magnetically separated. This material had therefore not been subjected to any magnetic effects other than the earth's field. The preparation procedure adopted for the gravity concentrate is shown in the flowsheet, Section 2.2, Fig. 2.1. The natural size distribution of the concentrate is given in Table 10.1. The heavy mineral content (S.G.> 2.89) is 96.3%.

10.3 Initial magnetic fractionation

The magnetic fractionation of the heavy mineral concentrate was conducted on a Cook isodynamic separator, calibrated by the procedure outlined in Section 6.7.

Each magnetic fraction contains grains ranging in colour from black through brown to pale fawn, and the proportion of pale coloured grains increases progressively for fractions collected at currents greater than 0.30A. This general progressive lightening of the average surface colour of the grains can be even more readily seen when powdered samples are compared.

Although within each fraction there are grains which clearly differ in their degree of alteration, the fractionation method applied indicates that the mean specific susceptibility of each grain is appropriate to the fraction to which it reports.

The most highly magnetic fraction was collected at a current of 0.05A, and included particles that tended to stick to the upper pole of the magnet and which in the field of a small hand magnet formed linear chains or "stringers" which would turn end-over-end when the direction of the magnetic field was reversed. The presence of magnetite either as discrete grains or as inclusions within ilmenite grains was initially suspected.

Separation of fractions having progressively weaker susceptibilities was continued using separation currents up to and including 0.8A. By this point the yield of magnetic product was so small that the next current employed was 2.25A. The results of this separation are given in Table 10.2.

Table 10.1.

Size distribution of Capel crude gravity concentrate

Size, μm	Wt. %	Cum. Wt. % finer
+425	0.10	99.90
+300	1.14	98.76
+210	10.12	88.64
+150	38.22	50.42
+105	43.49	6.93
-105	6.93	
	100.00	

Table 10.2.

Magnetic fractionation of Capel crude gravity concentrate.

(-210 +150 μm fraction)

Cook Sep'n. Current, A.	Lr. $\chi \times 10^2$	Wt. %	Comments
0.05	2737	11.73	Black grains predominate, but some grains present with secondary rutile coatings
0.10	703	11.06	"
0.15	317	12.54	"
0.20	180	13.65	"
0.25	116	15.67	Garnet common
0.30	81	13.79	Pure synth.ilm.(χ=96x10^{-2}JT^{-2}kg^{-1}) would report here
0.35	60	4.24	Garnet common
0.40	46	2.24	"
0.45	37	1.19	"
0.50	30	0.54	Secondary-rutile-coated brown grains ~50%
0.55	25	0.40	Epidote, staurolite appear
0.60	21	0.22	
0.65	18	0.22	Mainly secondary rutile
0.70	15	0.26	Staurolite v.common
0.75	13.5	0.17	"
0.80	11.9	0.15	
2.25	n.d	1.22	Mainly buff and fawn secondary rutile
Non-mags	1 > χ	10.71	Mostly qtz. kyanite, zircon, rutile and secondary rutile
		100.00	

n.d: not determinable - in non-linear part of calibration range.

10.4 Handpicking of minerals

All minerals other than titanium bearing species were removed by handpicking. The benefits of this tedious procedure were that the cleaned products were essentially composed only of ilmenite, pseudorutile and rutile, and the XRD spectra subsequently obtained were free of absorption effects from other species.

The more weakly magnetic fractions collected at currents of 0.40A or greater, showed increasing amounts of black primary rutile and it was not always possible to distinguish these grains confidently from black-skinned secondary rutile. The latter was shown to exist in small amount by examination of black grains of very low susceptibility in polished section. All detectable primary rutile was removed so that it could not contribute to the apparent rutile content shown by the XRD spectrograms. Where doubt existed, grain counts for primary rutile were made on briquetted sub-fractions so that any unpicked primary rutile could be subtracted from the rutile content determined by XRD.

10.5 Chemical analyses

Cleaned sub-splits of the magnetic fractions collected at currents between 0.05A and 0.45A were analysed by courtesy of Tioxide International Ltd. at their Central Laboratories in Stockton-on-Tees. Insufficient material was available to permit chemical analysis of magnetic fractions collected at currents greater than 0.45A. The results of the analyses are given in Table 10.3, and the major oxides are displayed graphically in Fig. 10.2. The high Cr_2O_3 content of the 0.45A magnetics was accounted for by free chromite.

Table 10.3

Analyses of magnetic fractions of altered ilmenite from Capel, W. Australia.

Sepn. Current A	Cook calc. Lr. χ $\times 10^2$ $JT^{-2}kg^{-1}$	Analyses, Wt. %							
		TiO_2	Tot.Fe	FeO	Fe_2O_3	Cr_2O_3	V_2O_5	MnO	MgO
0.05	2737	55.8	30.0	19.7	20.9	0.04	0.13	1.33	0.18
0.10	703	55.1	30.3	21.4	19.5	0.04	0.15	1.47	0.16
0.15	317	55.4	31.1	22.3	19.7	0.04	0.14	1.49	0.18
0.20	180	55.4	30.3	23.2	17.6	0.04	0.13	1.47	—
0.25	116	55.0	31.5	25.2	17.0	0.04	0.15	1.52	0.13
0.30	81	55.7	30.3	25.7	14.8	0.04	0.13	1.68	—
0.35	60	57.4	28.6	18.3	20.6	0.05	0.13	1.66	0.17
0.40	46	61.5	23.7	10.2	22.6	0.07	0.17	1.48	—
0.45	37	63.2	21.5	5.2	25.0	0.29	0.16	1.28	—

Analyses by Tioxide International Limited

Interpretation of Fig. 10.2: It had initially been expected that the most highly magnetic fraction would contain the freshest , least altered ilmenite. Despite the presence of grains with apparently ferromagnetic behaviour noted during preparation of the 0.05A magnetic fraction, no magnetite was found during microscopic examinations in reflected light. Very small numbers of grains showing fine exsolved titan-hematite were detected however. The presence of hematite would not in itself explain the high magnetic susceptibilities. However it is known that the host phase for exsolved hematite is itself a ferrianilmenite (Edwards,1960 p70).

Ferrianilmenites have well documented ferrimagnetic properties (Stacey and Banerjee,1974, p37) and their presence explains the high susceptibilities and apparently ferromagnetic behaviour of some of the grains in the 0.05A magnetic fraction. Further studies on sub-fractions of this highly magnetic material are reported in Section 10.7.

Reflected light microscopy revealed that the fraction containing the pinkest, freshest ilmenite was the 0.30A magnetics. This was supported by the ilmenite line intensities from the XRD spectra. More highly magnetic fractions however were visibly more altered, and the 0.05A magnetics contained particles with pronounced rims of secondary rutile. This high degree of alteration suggests that ferrianilmenite weathers and alters more rapdily than purer ilmenite. A tendency for ferrianilmenite to be strongly affected by supergene alteration has been noted by Rumble,(1976), who records the alteration products as being fine grained intergrowths of rutile and hematite or of rutile alone.

This discovery that the highly magnetic ferrianilmenites are more altered yet remain more highly magnetic than the purer ilmenite correlates with the apparent decrease in Fe_2O_3 noted for fractions between 0.05A and 0.30A in Fig. 10.2. Curves of

essentially the same shape were produced by Lynd et al(1954) for samples of natural ilmenite from Quilon, India. When Lynd's curves are redrawn from his detailed assay data so that the different analyses are all displayed on the same graph (Fig. 10.3), they provide an essentially similar pattern to Fig. 10.2.

For fractions collected at currents greater than 0.30A, (Fig. 10.2) the decrease in FeO and expected increase in Fe_2O_3 and TiO_2 follow the pattern expected for progressive alteration of ilmenite to pseudorutile. The final trends of the curves for currents greater than 0.45A are a) TiO_2 rising towards 100% b) Fe_2O_3 decreasing to zero. Unfortunately the yield of magnetic products at currents greater than 0.45A was insufficient to permit chemical analysis. However, the trend of the alteration was followed mineralogically by the XRD spectra of samples in this weakly magnetic region (Section 10.9).

Because there are essentially only three minerals present, the proportions of ilmenite, pseudorutile and rutile in each fraction may be estimated by normative calculation, as demonstrated by Grey and Reid(1974). All the FeO, MgO and MnO have been allocated to ilmenite; the Fe_2O_3 to pseudorutile, and any remaining 'unconsumed' TiO_2 to rutile. (The results are given in Table 10.7).

The trend of the alteration for the magnetic fractions whose analyses are given in Table 10.3 is shown in Fig. 10.4. For this figure, MgO and MnO analyses were used to calculate 'equivalent FeO' values which were added to the actual FeO analyses. The sum of FeO, Fe_2O_3 and TiO_2 was then normalised to 100%.

10.6 Density determinations

Density determinations were conducted using a standard pycnometer bottle. Distilled water was employed as the fluid and its density at a given measured temperature was taken from standard tables. Measurements with a fluid filled bottle were

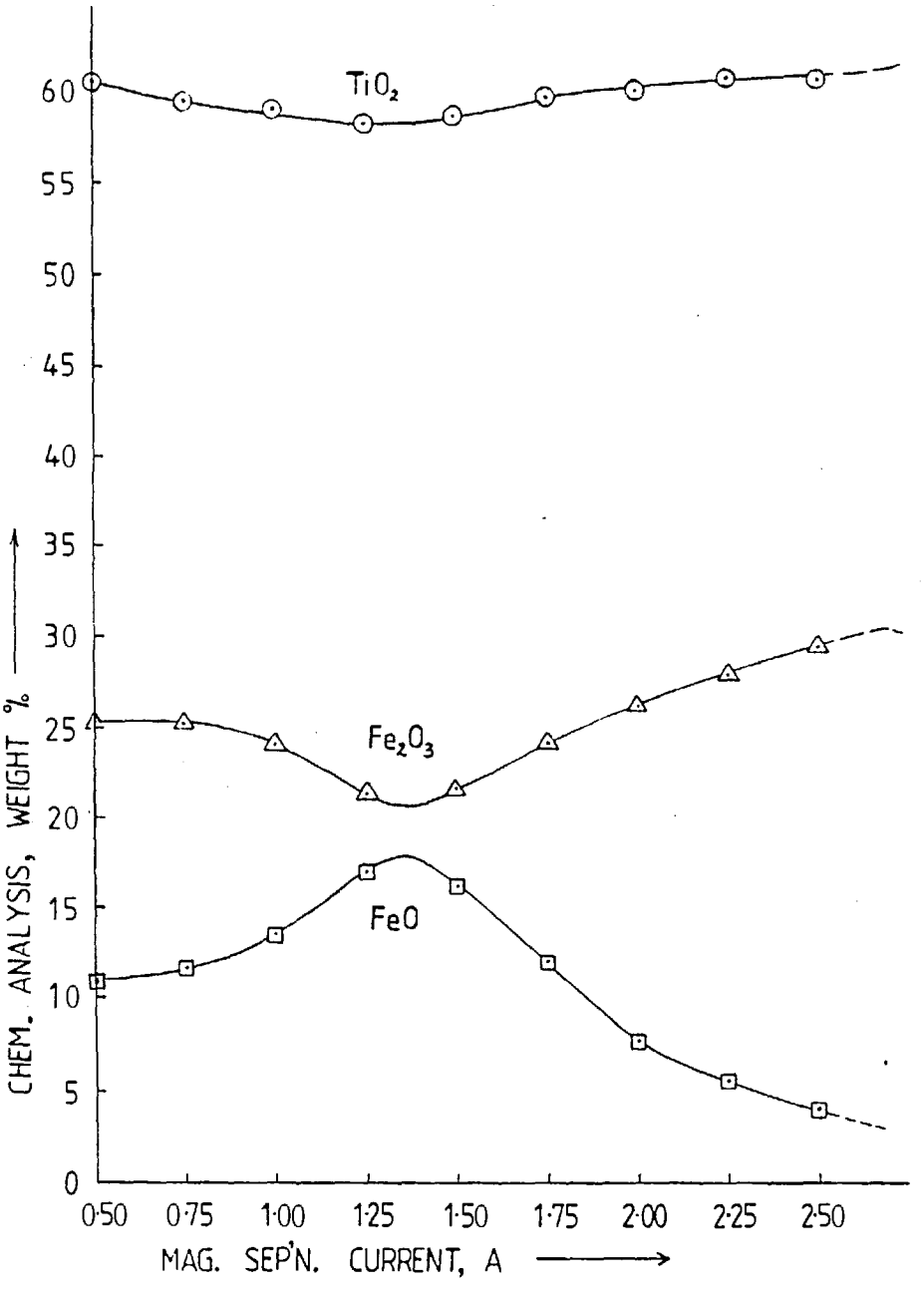

Fig. 10.3 Chemical variation of magnetic fractions of detrital ilmenite from Quilon, India (data from Lynd et al, 1954)

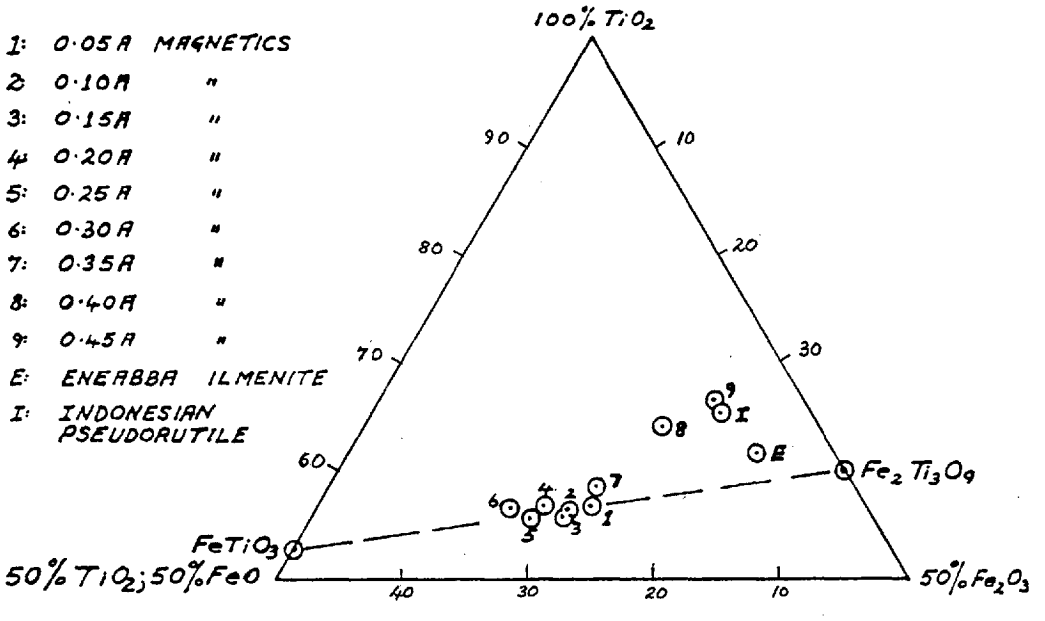

Fig. 10.4 Relative degree of alteration of magnetic fractions of altered ilmenite from the South Capel deposit, compared with two highly altered materials (E,I).

made after extracting dissolved gases under vacuum.

The measurements (Table 10.4) show an overall decrease in density from the highly magnetic to the weakly magnetic fractions as expected from the mineralogical compositions. Reference densities relevant in this context are pure synthetic ilmenite 4.78; pseudorutile 4.18; rutile, 4.2. An apparent density value below 4.2 (Table 10.4) is interpreted as a porosity effect in the secondary rutile. Determinations were repeatable to within $\pm$0.01 g/cc. Insufficient material was available in the weakly magnetic fractions collected at currents above 0.40A.

Table 10.4

Density of magnetic fractions

Magnetic fraction	Density g/cc	Density kg/m^3
0.05A	4.58	4580
0.15A	4.49	4490
0.25A	4.50	4500
0.35A	4.39	4390
0.40A	4.02	4020

10.7 Detailed susceptibility determinations

Cook separator fractions: Ferrimagnetic minerals display field-dependent susceptibilities which are highest in very low fields. For this reason the calculated susceptibilities of ferrimagnetic fractions collected at low currents on the Cook isodynamic separator are very high. The Faraday method of susceptibility determination permits the determination of susceptibility in high fields that are not practical on the Cook owing to the inevitable choking of the track.

Table 10.5 gives the results of specific susceptibility (χ) determinations by the Faraday method at 4 magnet currents. Values of susceptibility extrapolated to infinite field for the ferrimagnetic fractions (F) were determined graphically. For weakly magnetic fractions the low current determinations (at 5A) lose accuracy due to the relative errors in measuring the weak magnetic force.

Table 10.5

Susceptibilities of magnetic fractions of Capel ilmenite by Faraday method

Cook Mags(A)	Faraday* χ Values x 10^2 JT^{-2} kg^{-1} 5A	10A	15A	20A	$H\infty$	
0.05	361	284	231	213	170	F
0.10	186	165	138	130	115	F
0.15	129	118	104	104	100	F
0.20	95	95	87	86	84	F
0.25	90	88	84	84	82	F
0.30	72	74	77	75	-	P
0.35	55	57	57	57	-	P
0.40	41	41	41	41	-	P
0.45	33	33	31	31	-	P
$10^{-3} \times H\frac{dH}{dx}$	5052	16878	35309	50806		

F: Ferrimagnetic phases present
P: Paramagnetic

* Determined with conical pole pieces and 0.045g capacity container

Table 10.6

High-field susceptibility+ of weakly magnetic fractions by Faraday method

Cook Mags.	Calc. Cook Lr. χ	Faraday* $\chi \pm 0.30$
0.50A	30	31.7
0.55A	25	26.2
0.60A	21	22.0
0.65A	18	18.8
0.70A	15	17.4
0.75A	13.5	14.1
0.80A	11.9	12.7
2.25A	(Range 11.9 → 1.0)	n.d.
Non-Mags	<1	n.d.

*Determined with Faraday pole pieces and a 0.12g-capacity container.

+: x $10^2 JT^{-2} kg^{-1}$

The mass magnetic susceptibilities of the fractions collected at room temperature at low separation currents are much higher than the susceptibility of pure synthetic ilmenite ($\chi_{il} = 96 \times 10^{-2}$ JT^{-2} kg^{-1}). As noted in Section 10.3, the qualitative behaviour of grains in these fractions is ferromagnetic, which is explained by the fact that the high Fe_2O_3 contents observed include solid solution of hematite in ilmenite. Such solid solution is known to produce a highly magnetic, ferrimagnetic structure (Nagata,1961; Stacey & Banerjee,1974) for compositions in the range 45% to almost 100 molar % ilmenite.

For paramagnetic fractions (P) it is clear that the Cook isodynamic separator (and Frantz-type separators in general) whencalibrated with care can yield χ determinations that are sufficiently accurate for many requirements.

In Table 10.6 high-field specific susceptibilities of weakly magnetic paramagnetic fractions,which were not chemically analysed due to lack of sufficient sample, are compared with their nominal Cook susceptibility. Small amounts of possible hematite and goethite were not detected by their ferromagnetic response.

Using normative, calculated mineral compositions, the expected susceptibility of certain fractions has been calculated (Table 10.7). For the paramagnetic fractions, the expected and actual susceptibilities are similar. The correlation thus demonstrated between susceptibility and the mineralogical (and hence chemical) composition for paramagnetic grains is valuable for product quality control. If for example it was desired to keep rutiliferous material (Table 10.7) out of the concentrate, the magnetic separators could be 'tuned' to reject grains with a susceptibility less than $57 \times 10^{-2} JT^{-2} kg^{-1}$.

Table 10.7

Calculated and measured mass magnetic susceptibilities for magnetic fractions of altered ilmenite from Capel, W. Australia.

Sep'n Current A	Cook calc. $Lr\chi \times 10^2$	Normative Compn. % ILM	% PSR	% RUT‡	Calc. $\chi \times 10^2$ $JT^{-2}kg^{-1}$	Actual $\chi \times 10^2$
0.05	2737	45	52	3	61	170 F
0.10	703	49	49	2	64	115 F
0.15	317	50	49	1	65	100 F
0.20	180	52	44	3	65	84 F
0.25	116	57	43	-	70	82 F
0.30	81	58	37	3	69	75 P
0.35	60	43	52	4	59	57 P
0.40	46	25	57	14	43	41 P
0.45	37	14	63	23	35	31 P

F = Ferromagnetic P = Paramagnetic

‡ = These figures are used to normalise the chemically calculated composition to 100% minerals. This procedure brings the rutile contents closer to the XRD determinations.

Note (1) Susceptibility values used to calculate χ were ilmenite 96, rutile 1.2 and pseudorutile 34.5 x 10^{-2} J T^{-2} kg^{-1} respectively.

(2) Apparent susceptibilities as determined in low fields by a Cook isodynamic separator for ferromagnetic fractions are higher than other determinations on account of the field-dependence of the susceptibility of ferromagnetic materials.

High-χ ferrimagnetic sub-fractions: The highly magnetic 0.05A fraction from the Cook separator was further fractionated at 0.05A by varying the side-slope angle. Separations were made sequentially with 25°, 15° and 10° side-slope settings. The sub-fractions obtained were analysed chemically after being used for XRD analysis (Section 10.8). Results of the separation and chemical analysis are given in Table 10.8. The Fe_2O_3 contents show a sympathetic variation with the susceptibility. This suggests that the most highly magnetic fraction derives its properties from a higher level of hematite (Fe_2O_3) in solid solution in the ilmenite. This indicates that the three sub-fractions correspond to points on the ilmenite-rich side of the magnetization curve (Fig. 5.11, Section 5.7).

Curie point determinations (Section 7.1) were conducted on two sub-fractions using an a.c. inductance bridge (Section 6.5). The critical temperatures for magnetic ordering were found to lie below $70^{o}K$ (Table 10.9). This result points to a very low concentration of hematite dissolved in the ilmenite, between zero and 3% molar. According to Hoffman(1975), compositions close to pure ilmenite with low critical temperatures correspond to a region with short-range ferrimagnetic clusters (Fig. 5.14), which result in properties similar to superparamagnetism (Section 4.2) if the clusters are small enough in size. However, XRD on magnetically-oriented samples (Section 10.8) shows that the spin-directions are firmly locked parallel to the crystal c-axis, and no superparamagnetism has therefore developed.

10.8 Qualitative X-ray diffraction

Search for ferromagnetics: Because of the apparently ferromagnetic behaviour of some of the grains in the 0.05A magnetic fraction, discrete magnetite and hematite were sought for in the XRD spectrum of this fraction. No peaks of these minerals were detectable. To determine the detection limits, calibration mixtures were prepared

Table 10.8

High-χ ferrimagnetic sub-fractions

	Cook side-slope angle		
	25°	15°	10°
% TiO_2 (corr'd)	55.7	56.3	55.6
% Fe_2O_3	21.5	21.0	20.3
% FeO	19.6	19.4	20.8
% Tot. Fe	(30.3)	(29.8)	(30.4)
% Cr_2O_3	0.03	0.03	0.03
% V_2O_5	0.10	0.11	0.12
% MnO	1.20	1.35	1.42
% MgO	0.20	0.18	0.17
% SiO_2	i.s.	i.s.	0.20
	98.33	98.37	98.64
wt % of feed	2.98	3.02	5.07

Chemical analyses by Tioxide International Ltd.

i.s. = insufficient sample

Table 10.9

Curie point and susceptibility of ferrimagnetic fractions

	Cook calc. Lr.$\chi \times 10^2$	Faraday $\chi(H\infty)\times 10^2$	Curie Point °K
0.05A/25°	6663 ± 1530*	380	68
0.05A/-25°+15°	4081 ± 937	220	n.d.
0.05A/-15°+10°	2738 ± 629	160	50*

*This value is less than the Néel point of pure ilmenite (55°K). Reasons for this are not clear, but it might be due to the effects of natural impurities e.g. Mn. $MnTiO_3$ has a Néel point of 41°K (Ishikawa and Akimoto, 1958, II).

* Indicated errors are for ± 0.005A current variation

using additions of highly crystalline hematite and magnetite. It was found possible to detect additions of only 1% by weight of each of these minerals. For hematite, the most readily detectable peak occurred at 62.59° between ilmenite peaks at 61.85° and 63.26° 2θ (CuKα). The main magnetite line at 35.48° is shared by the 35.34° ilmenite line. For magnetite the 62.64° peak was still discernible at 2% by weight but only the 30.13° peak could be detected at the 1% level. The presence of small amounts of X-ray amorphous hematite and magnetite in the 0.05A magnetics cannot be totally excluded, however.

Progressive changes in spectra: The spectra for the first 6 fractions for separation currents between 0.05A and 0.30A differed slightly in their peak heights and in the height ratios of the peaks of different minerals. The addition of pure iron powder (-37 μm) as an internal standard showed that relative to the iron, the ilmenite peak heights (Fig. 10.5) increased gradually reaching a maximum in the 0.30A fraction. Qualitatively it was noted that the net height of the 54.35° peak (pseudorutile plus rutile) was slightly greater than for the 27.49° main rutile peak. This became more marked for fractions collected at currents above 0.30A and reached a max. difference in the 0.45A fraction. At currents higher than 0.45A the 27.49° rutile peak grows significantly and is higher than the 54.35° peak in the 0.65A and all higher-current fractions. These qualitative observations can be summarised by saying that initially pseudorutile can be seen to increase at the expense of the ilmenite but that in more weakly magnetic fractions the rutile increases at the expense of the pseudorutile. The main ilmenite line at 32.68° is the last to disappear but is still distinct in the 0.65A magnetic fraction.

X-ray diffraction of hand-picked pale buff secondary rutile from the Cook non-magnetics at 2.25A showed that in this fraction pseudorutile has already disappeared from the XRD spectrum. Such high-TiO_2, pale coloured secondary rutile forms a significant proportion of the Capel commercial rutile concentrates. A small amount of anatase (TiO_2) occurs but it has not been possible to

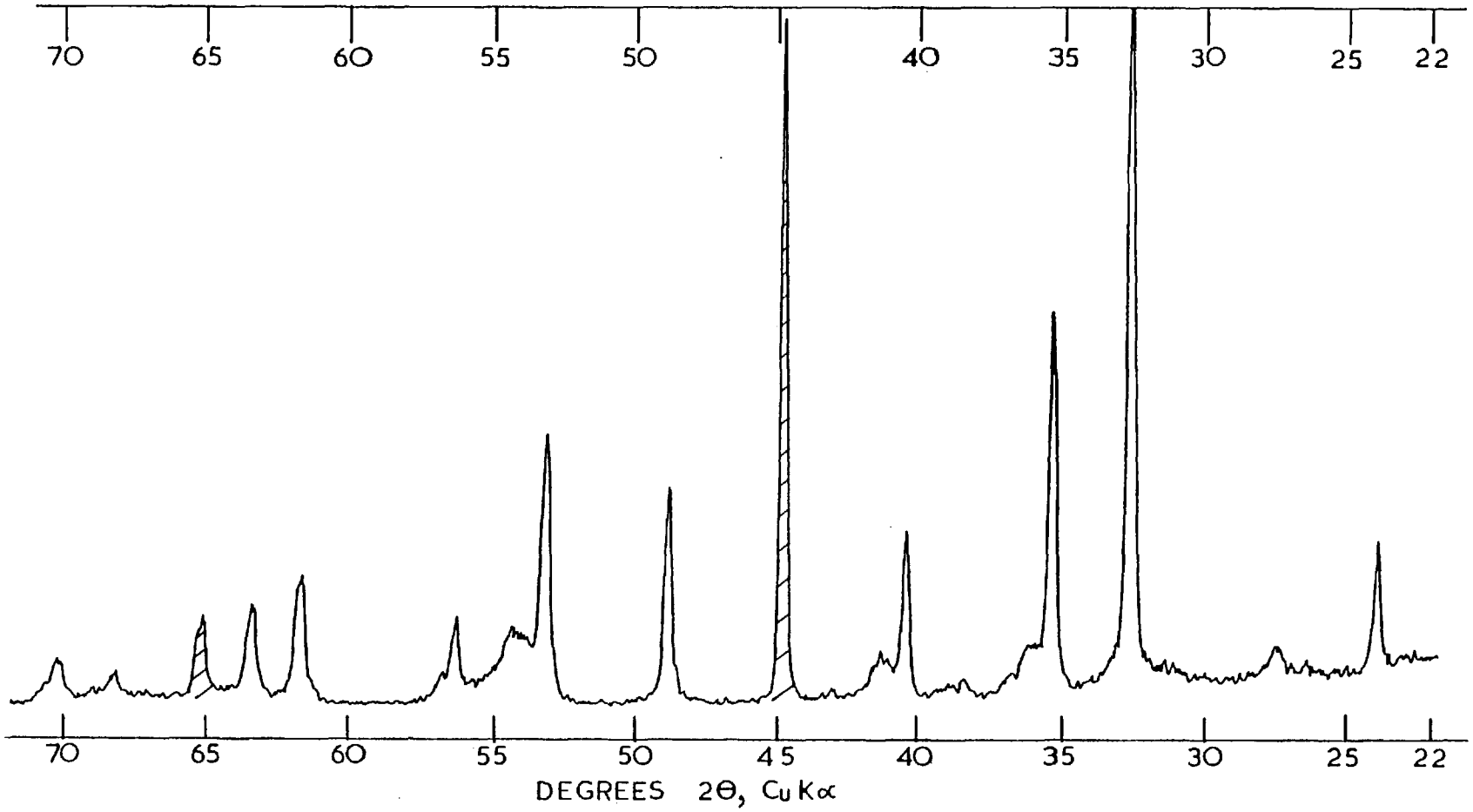

Fig. 10.5 XRD spectrum of Capel 0.30A magnetics plus 20% Fe (Iron peaks are shaded).

optically distinguish any discrete anatase under the binocular microscope. Most probably the anatase is mainly of secondary origin and is intergrown with the secondary rutile.

Special features: XRD spectra of magnetic fractions in the range 0.55A - 0.80A show the presence, in addition to anatase, of very small and variable amounts of secondary hematite, ferric pseudobrookite, brookite (TiO_2) and goethite (FeO.OH).

An isolated XRD line at 31.22°(2θ) first appears in the 0.40A fraction, reaches a peak in the 0.55A fraction and is still weakly present in the 0.80A fraction. The observed peak position corresponds closely to that expected for a pseudorutile (230) reflection using the unit cell parameters determined by Grey and Reid(1975).

Grain-counting of chromite in the 0.45A fraction indicated approximately 0.5% chromite by volume. This is by far the highest concentration of chromite in the magnetic fractions and correlates with the 0.29% Cr_2O_3 analysis. Only weak traces of possible chromite lines were detectable in the XRD spectrum however.

Solid-solution in high-χ fractions: The XRD spectrum of hematite resembles an ilmenite spectrum with peaks shifted to slightly higher 2θ angles, (Table 10.10). Solid solutions of the two minerals give spectra with peaks having intermediate positions and intermediate intensities. Peak positions of members of the solid solution series can be used to give only a rough (and not an exact) indication of the composition, since it is not known whether the changes in 2θ are linear with composition, and the effects of small amounts of manganese on the peak positions are not known.

High-χ sub-fractions of the 0.05A magnetics (Section 10.7) were subjected to XRD scanning at a slow ($\frac{1}{2}$° 2θ/min) rate. The peak position differences are at a maximum for the equivalent peaks 70.24° (ilmenite) - 72.10° (hematite). Scans of this portion of the spectrum revealed a correlation between the peak

Table 10.10

Comparison of equivalent lines in hematite and ilmenite XRD spectra for Cu Kα radiation

ILMENITE*		HEMATITE**		
2θ	Rel. I	2θ	Rel. I	Δ 2θ
23.85	50	24.32	25	0.47
32.68	100	33.30	100	0.62
35.34	85	35.78	50	0.44
40.45	70	41.01	30	0.56
48.97	85	49.59	40	0.62
53.25	100	54.38	60	1.13
56.45	50	57.76	16	1.31
61.85	. 85	62.59	35	0.74
63.26	85	64.13	35	0.87
70.24	70	72.10	20	1.86

*ASTM 3-0781 **ASTM 13-534

position and Fe_2O_3 content (Fig. 10.6), which is in sympathy with the observed mean susceptibilities. Only a small amount of Fe_2O_3 is considered to be in solid solution however, the balance being attributable to pseudorutile.

The 0.05A magnetic subfractions together form only 11.7% of the crude gravity concentrate, and only 14.2% of the grains reporting to a bulk Capel ilmenite concentrate. This is why the XRD spectrum of bulk ilmenite concentrate gives line spacings close to those of stoichiometric ilmenite (Jones,1973), although peak intensities obtained are significantly lower than those for unaltered ilmenite.

Magnetic orientation effects: Any grain with an elongate shape and a positive magnetic susceptibility will align its long axis parallel with an applied field, provided the grain is free to rotate. In grains which are well rounded this shape anisotropy effect becomes weaker, and disappears for a spherical specimen (Cullity, 1972 p243).

In single-crystal mineral grains which are markedly elongate, the shape anisotropy competes with any crystal anisotropy present, in a manner dependent upon the relative orientation and relative strengths of the anisotropy energies. Optical examination has shown no twinned crystals in the altered ilmenite fractions, and the grains were considered by the author to be mainly single crystals. The majority of the grains are approximately equant, but individual grains in polished section have length-to-breadth ratios up to 3. It was therefore conceivable that crystal anisotropy effects would predominate and to test this hypothesis some XRD mounts were made of the 0.05A magnetics. The uncrushed grains were mixed with Durofix glue fluidized with acetone, which was left to set in the 0.2T field of a permanent magnet. Two orientations were prepared a) with the field parallel to the face of the mount, b) with the field perpendicular to the mount. XRD spectra were then obtained and compared with that from a mount left to set with no applied field.

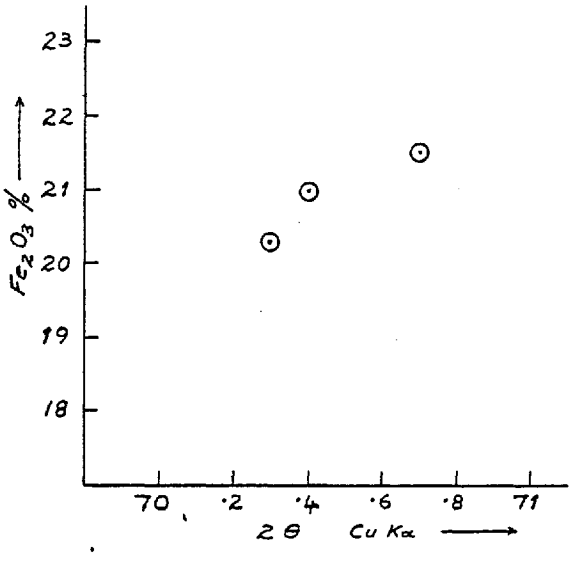

Fig. 10.6 Variation of peak position for the 70.24° (CuK_α) line of ilmenite with changing Fe_2O_3 content of the magnetic fraction.

The only planes which can contribute to an XRD reflection are those which happen to be oriented parallel with the plane of the mount. With the field perpendicular, the prism planes (110), (300) and (220) were strongly enhanced, while non-prism planes(214), (116), (204), (113) and also the main ilmenite peak (104) were totally missing (Fig. 10.7). With the field parallel, the prism reflections were either totally absent or weakened (Fig. 10.8). The control sample, set out of the field, showed all the faces (Fig. 10.9). It is clear that with the field perpendicular, much stronger prism reflections are obtained due to rotation of the grains so that prism planes, and hence the c-axes, are parallel to the face of the mount. This indicates that the magnetic spin axis is perpendicular to the c-axis, in agreement with the known orientation of the spins in ferrimagnetic hematite-ilmenite solid solutions. This result therefore supports other evidence for the presence of hematite-ilmenite solid solutions in this fraction. Evidence is also afforded for the relative orientation of the secondary minerals which develop on the ilmenite substrate. Several rutile prism reflections are weak or absent with the field perpendicular, but are enhanced with the field parallel, suggesting that the rutile c-axis may grow perpendicular to the ilmenite c-axis. The pseudorutile intensities are quite weak in the 0.05A magnetics but there is a suggestion that the pseudorutile c-axis may be parallel to the ilmenite c-axis. A diagram presented by Grey and Reid(1975) supports this tentative conclusion (Fig. 10.10).

Similar magnetic orientation tests were attempted with the 0.30A magnetics which form the fraction richest in ilmenite. No clear-cut evidence was obtainable however, due to the low peak intensities. Certainly no major orientation effects were apparent and this is in keeping with the paramagnetic behaviour found in other tests. Further work on this sample would require the use of a much higher magnetic field.

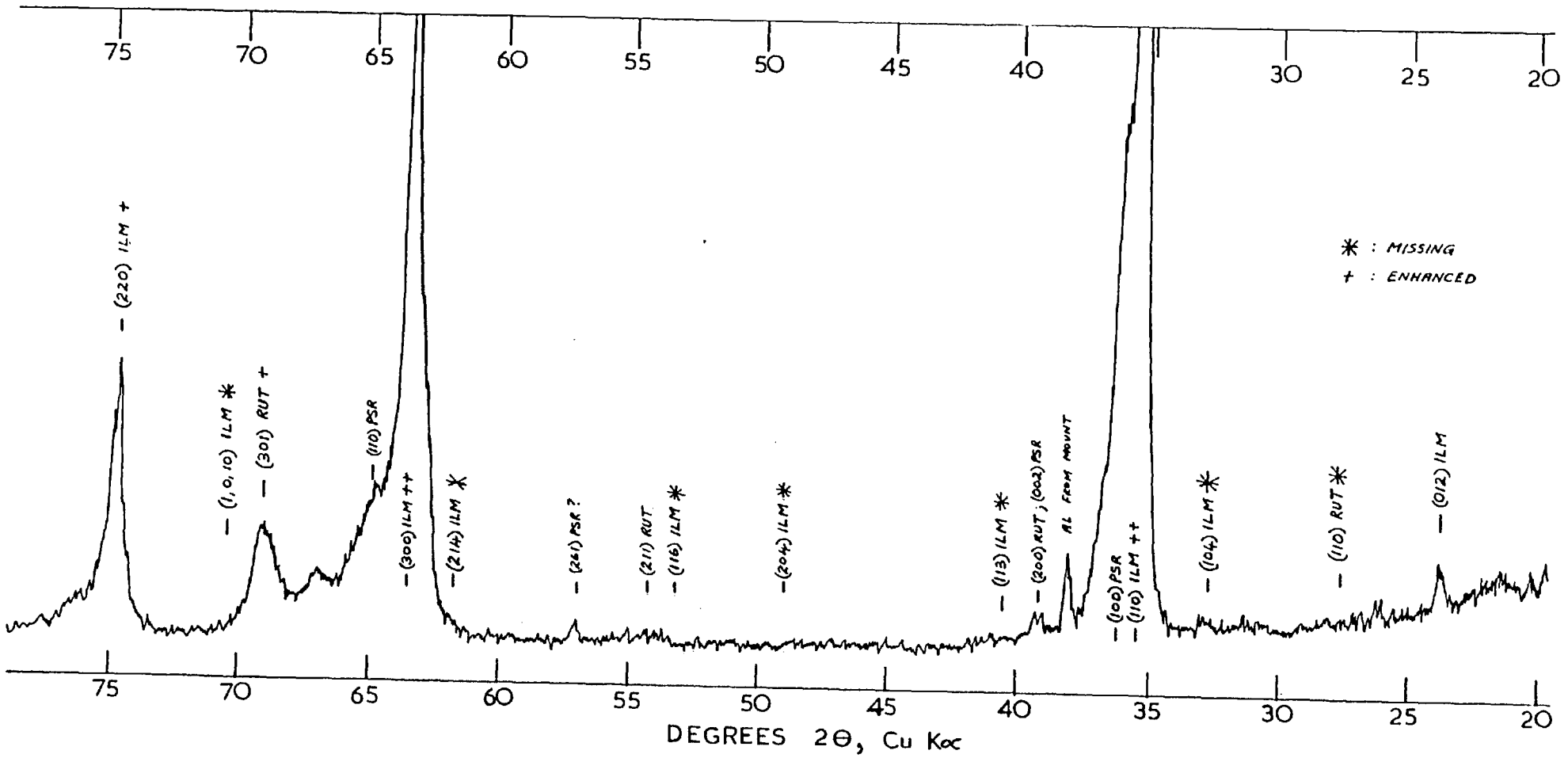

Fig. 10.7 XRD spectrum of Capel 0.05A magnetics set in Durofix with 0.2T field perpendicular to the mount. (Particle grain size -210 +150 um; aluminium cavity-slide).

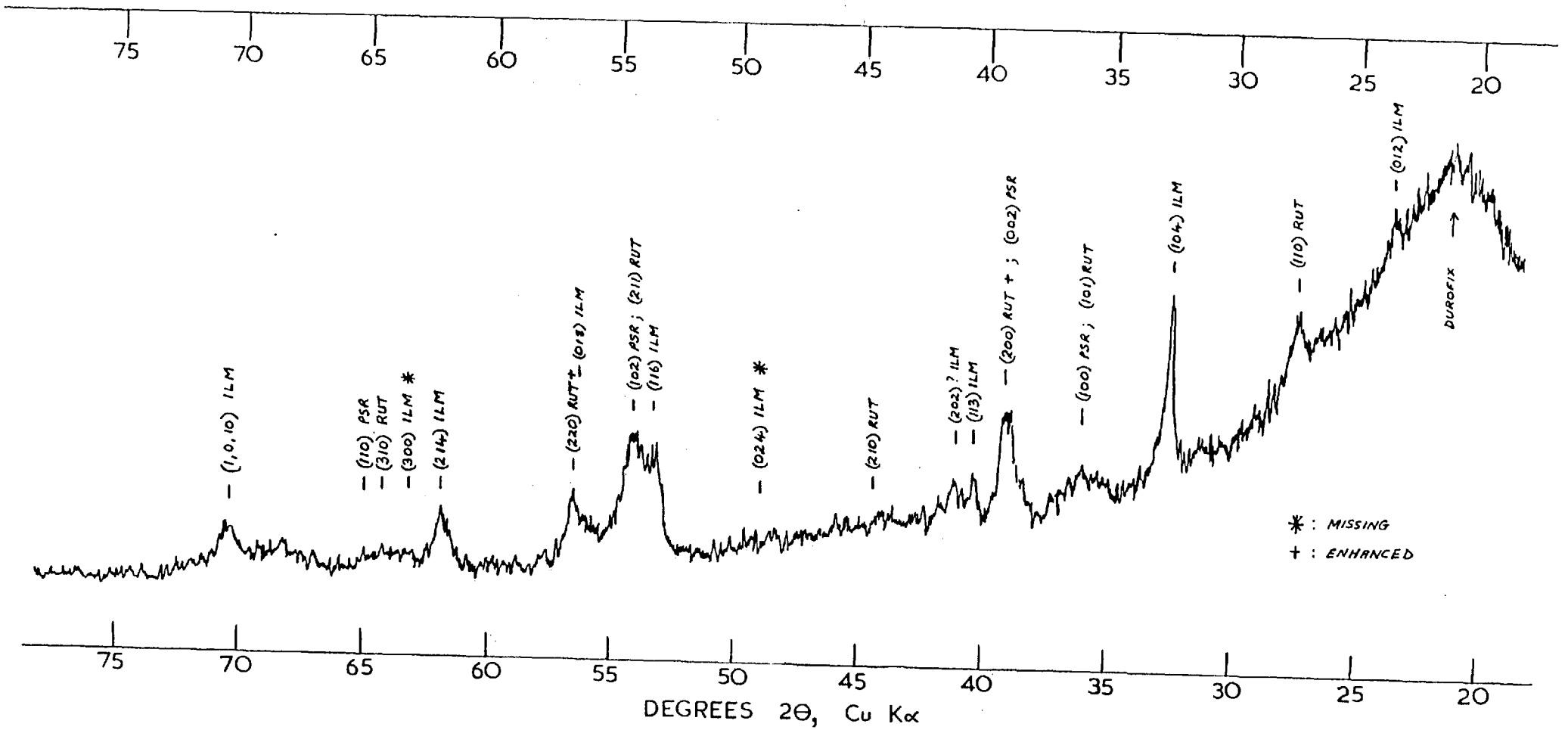

Fig. 10.8 XRD spectrum of Capel 0.05A magnetics set in Durofix with 0.2T field parallel to the mount. (Particle grain size -210 +150 um; glass-slide mount).

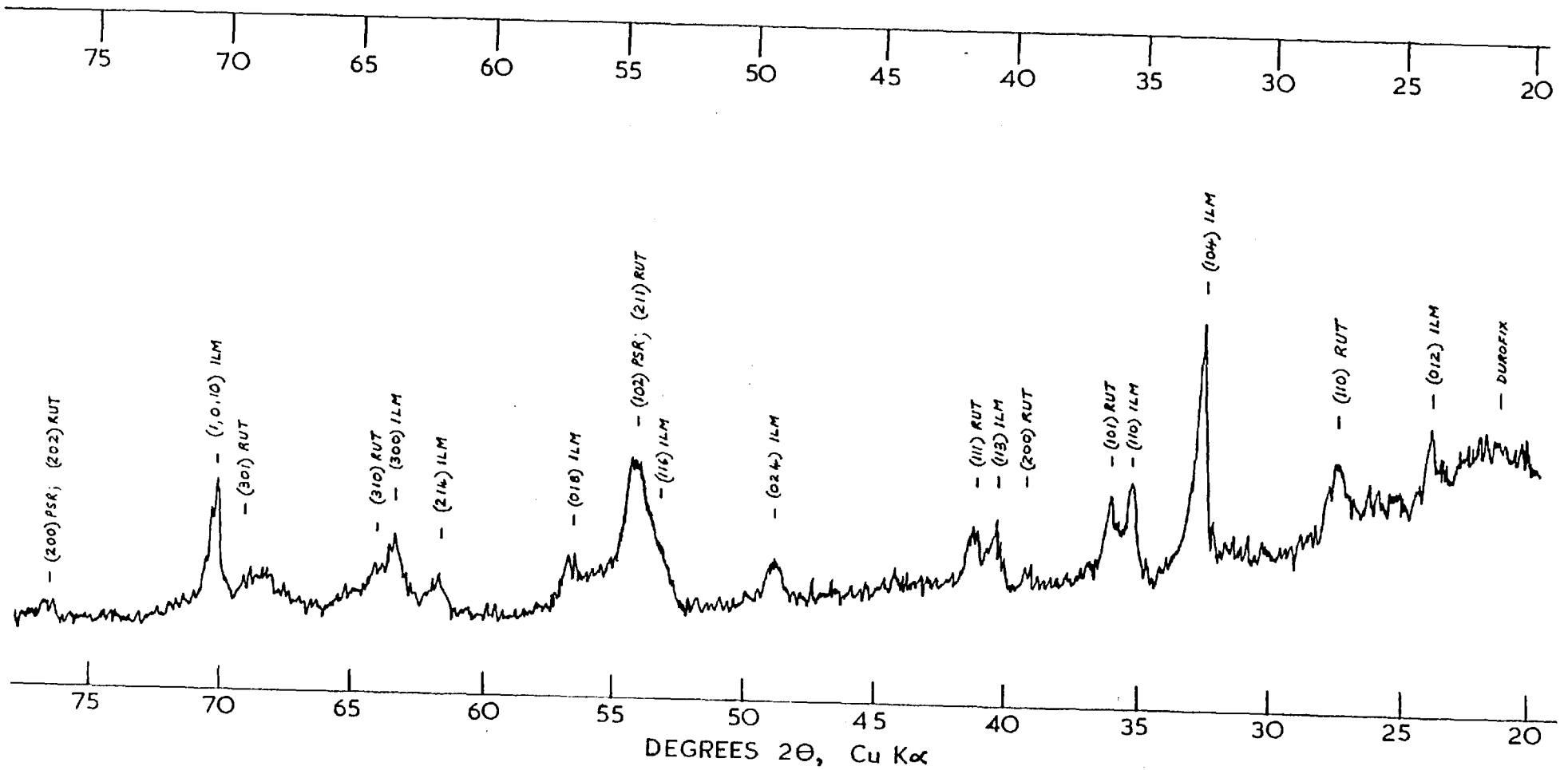

Fig. 10.9. XRD spectrum of Capel 0.05A magnetics set in Durofix with no magnetic field. (Particle grain size -210 +150 um; aluminium cavity-slide).

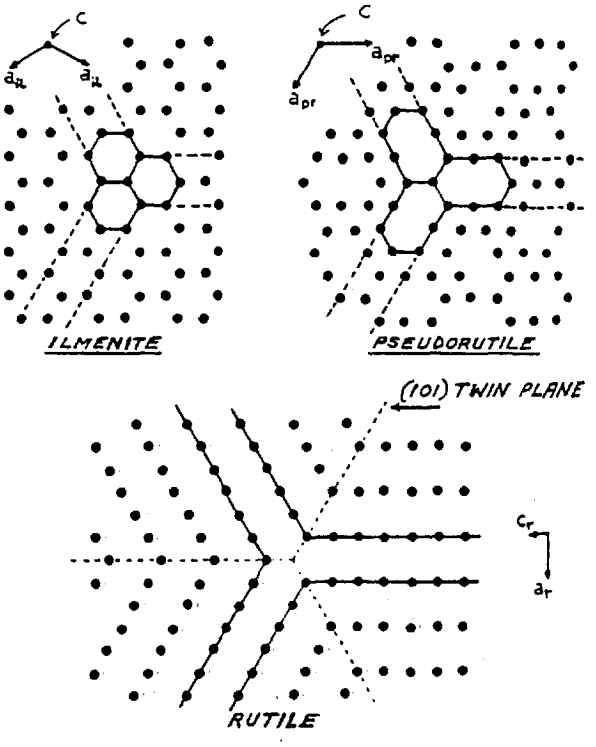

Fig. 10.10 Relative orientations of ilmenite and overlying secondary pseudorutile and rutile, determined by single-crystal XRD methods. (After Grey and Reid, 1975, p904).

10.9 Quantitative X-ray diffraction

General: Even under ideal conditions it is very difficult to obtain accurate results from quantitative XRD techniques, due chiefly to the influence of preferred particle orientation on measured intensities. The XRD data obtained in this investigation are therefore considered only to illustrate the trend of the mineralogical changes that occur.

The following peak positions and reference intensity ratios (K) were employed for the Chung "matrix flushing" technique of quantitative XRD.

	Selected Peak 2θ, CuKα	K
Ilmenite	32.68°	0.4035
Rutile	27.49°	0.5643
Pseudorutile	54.35°	0.0650
Iron (Internal Standard)	44.71°	1.0

From the observed net height of the main rutile peak at $2\theta = 27.49^{\circ}$, the expected height of the rutile peak at 54.38° was calculated. This value was then subtracted from the net height of the 54.35° peak (pseudorutile + rutile) to give a corrected peak height. In samples where a significant amount of pseudorutile was present, the net height of the main ilmenite line was also corrected for the underlying broad pseudorutile hump at 32.32°.

The corrected intensities of the selected peaks were then substituted directly in the Chung equation (Section 8.3), the approximate amount of X-ray amorphous matter being determined by the difference between 100% and the calculated sum of the three crystalline phases.

Results: The proportions of crystalline and amorphous phases determined by the above procedure are given in Table 10.11, where they are compared with the normative content of the three minerals (crystalline plus X-ray amorphous) determined by calculation from the chemical analyses. Reduced-scale reproductions of spectra used as the source for the XRD results are given in Appendix F .

Table 10.11

Comparison of apparent mineral compositions for magnetic fractions of altered Capel ilmenite, obtained by normative calculation and by quantitative X-ray diffraction

Sep'n Current A	Normative Comp'n %			Comp'n by Chung XRD method			
	ILM	PSR	RUT	ILM	PSR	RUT	AMORPH
0.05	45	52	1	31	24	4	41
0.10	49	49	1	38	30	3	29
0.15	51	49	-1	50	32	3	15
0.20	52	44	1	48	30	2	19
0.25	57	42	-1	41	29	2	28
0.30	58	37	3	61	25	2	12
0.35	42	52	4	39	42	3	16
0.40	25	57	14	16	51	4	29
0.45	14	63	23	10	66	7	16

Table 10.12

Mineral contents of low-susceptibility fractions as indicated by quantitative XRD

Cook Sep'n Current, A	Faraday $\chi \times 10^{-2} JT^{-2} kg^{-1}$	RUT	ILM	PSR	AMORPH
0.50	31.7	12	5	62	21
0.55	26.2	14	4	55	27
0.60	22.0	16	4	52	28
0.65	18.8	18	4	55	23
0.70	17.4	26	3	36	35
0.75	14.1	28	2	31	39
0.80	12.7	33	2	32	33

For the 0.05A-0.25A magnetic fractions, the normative contents of pseudorutile are probably a little too high because the mineral proportions were calculated using the whole of the Fe_2O_3 whereas a small part of the Fe_2O_3 occurs in solid solution in the ilmenite. The calculated pseudorutile figure 'consumes' a certain amount of TiO_2 and thus affects the calculated rutile figure. (The normative mineral proportions are not normalised and were calculated from chemical analyses that did not add up to exactly 100%).

Within the 0.05 - 0.25A range, the most highly magnetic fractions have the highest amorphous mineral content, suggesting that these fractions are the most altered. Both the amorphous content and the Fe_2O_3 content are at a minimum in the 0.30A fraction for which reflected-light examination has revealed the highest proportion of relatively unaltered 'pink' ilmenite, as mentioned in Section 10.5.

The 0.30A fraction gave the highest ilmenite diffraction intensities and the lowest content of Fe_2O_3 (Table 10.3) and estimates of ilmenite content obtained by the diffraction and normative calculation methods agree closely. This suggests that in this fraction virtually the whole of the ilmenite is crystalline and that most of the indicated amorphous content is attributable to pseudorutile. Because of the unknown, but probably low degree of crystallinity of the Indonesian pseudorutile that was used as a standard, both the amount of pseudorutile and the content of amorphous material are approximations only. This is because the Chung working equation only indicates amorphous content over and above any amorphous material present in the standards (Section 8.3).

Using the data in Table 10.11 and the weight distribution for the fractions given in Table 10.2, calculated weighted means were obtained for the first seven fractions (0.05 - 0.35A magnetics) which account for most of the grains in a commercial ilmenite product. Results were as follows:

Average (normative): 52% ilmenite, 45% pseudorutile, 1% rutile
" (XRD-derived): 45% ilmenite, 29% pseudorutile, 3% rutile and 23% amorphous matter.

These calculated averages differ from the proportions found by Grey and Reid (1974):

normative composition: 55.2% ilmenite, 40% pseudorutile, 1% rutile
XRD " : 50% ilmenite, 35% pseudorutile, 4% rutile

The difference in normative compositions may be ascribed to the fact that Grey and Reid were using a commercial concentrate from an earlier period, while the difference in XRD-derived composition is also due to the fact that Grey and Reid used a standard calibration-curve technique (Klug and Alexander, 1974). This technique is straightforward for mixtures of two phases, but becomes more complex when three phases are involved. The standard technique also makes no allowance for the contribution of any amorphous phases present to the mass absorption coefficient of the total specimen exposed to primary X-rays.

Low susceptibility fractions

Insufficient material was available for chemical analyses to be made of magnetic fractions collected at currents greater than 0.45A. However, fractions doped with iron as the internal standard were X-rayed using glass slide mounts, and the mineral contents determined by the Chung technique are reported in Table 10.12. The trend of the data indicates the progressive increase in rutile content and decrease in pseudorutile. Susceptibility differences between these fractions are small, and are not directly evident from the apparent mineral proportions. While the Chung data reveal the trend of the alteration, it is not considered that this technique could ever be sufficiently sensitive to reveal slight changes in susceptibility, even if there were no amorphous material present.

As mentioned in Section 10.8, small amounts of anatase and traces of possible hematite, pseudobrookite and/or brookite and goethite were evident in the XRD spectra. These were ignored in

applying the Chung technique, and therefore they contribute to the calculated "amorphous" contents in Table 10.12.

10.10 Mössbauer investigations

Two fractions were examined by Mössbauer spectroscopy (Section 9.2). Interpretation of the observed spectra is complicated by the known presence of three minerals in the samples examined - ilmenite (some with hematite in solid solution); pseudorutile; and rutile (which can carry a small amount of iron in its lattice).

The 0.05A/-15°+10° ferromagnetic fraction was examined at 293°K and 80°K and results are summarised in Table 10.13 and in Figs. 10.11, 10.12. A good fit could only be obtained at 293°K by allocating a singlet in addition to a ferrous and a ferric doublet. Theoretically a singlet represents an ion in a crystal site at which the electric field gradient is zero. It is also possible that the average electric field gradient could be zero for an amorphous, un-ordered material. The latter conditions would occur in a structure which had broken down by an alteration process i.e. in amorphous ilmenite. The dis-order would appear to be a temperature-dependent effect however, for at 80°K the spectrum was resolvable into three doublets. The ferric doublet accounts for the ferric ion in solid solution in ilmenite and for the ferric ion in pseudorutile, the latter being considered to account for the major portion of the Fe_2O_3 analysis (Table 10.6).

The 0.30A magnetics (black) were prepared by handpicking from the 0.30A magnetics all the grains with visible brown to fawn alteration coatings of secondary rutile. X-ray diffraction of this black material confirmed that it had not only less rutile but also less pseudorutile than the parent material, and was thus significantly enriched in unaltered ilmenite. The Mössbauer results are summarised in Table 10.13 and Figs. 10.13, 10.14. As with the 0.05A/-15°+10° magnetics, it was necessary to include a ferric singlet in the 293°K spectrum in order to obtain an

Table 10.13

Measured parameters in Fe^{57} Mössbauer effect spectra

Sample	Ion Type	Peak Type	Temp °K	I.S. mm/s	Q.S. mm/s	Absn. Area %
0.05A/-15°+10°Mags	Fe^{2+}	D	293	1.034(2)	0.752(3)	61.3(7)
	Fe^{3+}	D	"	0.418(4)	0.663(7)	19.9(10)
	Fe^{3+}	S	"	0.174(12)	0	18.9(12)
	Fe^{2+}	D	80	2.034(103)	0.253(81)	12.7(5.7)
	Fe^{3+}	D	"	0.323(58)	0.327(64)	45.0(7.4)
	Fe^{2+}	D	"	1.246(5)	1.021(27)	42.3(11.1)
Synthetic ilmenite	Fe^{2+}	D	293	1.068(1)	0.660(2)	100.00
0.30A Mags (black)	Fe^{2+}	D	293	1.069(2)	0.694(3)	70.7(8)
	Fe^{3+}	D	"	0.373(8)	0.436(13)	21.1(1.5)
	Fe^{3+}	S	"	0.005(14)	0	8.2(8)
	Fe^{2+}	D	80	1.243(2)	1.018(9)	59.1(2.4)
	Fe^{3+}	D	"	0.288(14)	0.355(14)	34.1(1.7)
	Fe^{2+}	D	"	2.139(45)	0.312(35)	6.75(1.52)

S = Singlet I.S. = Isomer Shift

D = Doublet Q.S. = Quadrupole Split

Figures in brackets indicate errors in the last figure quoted

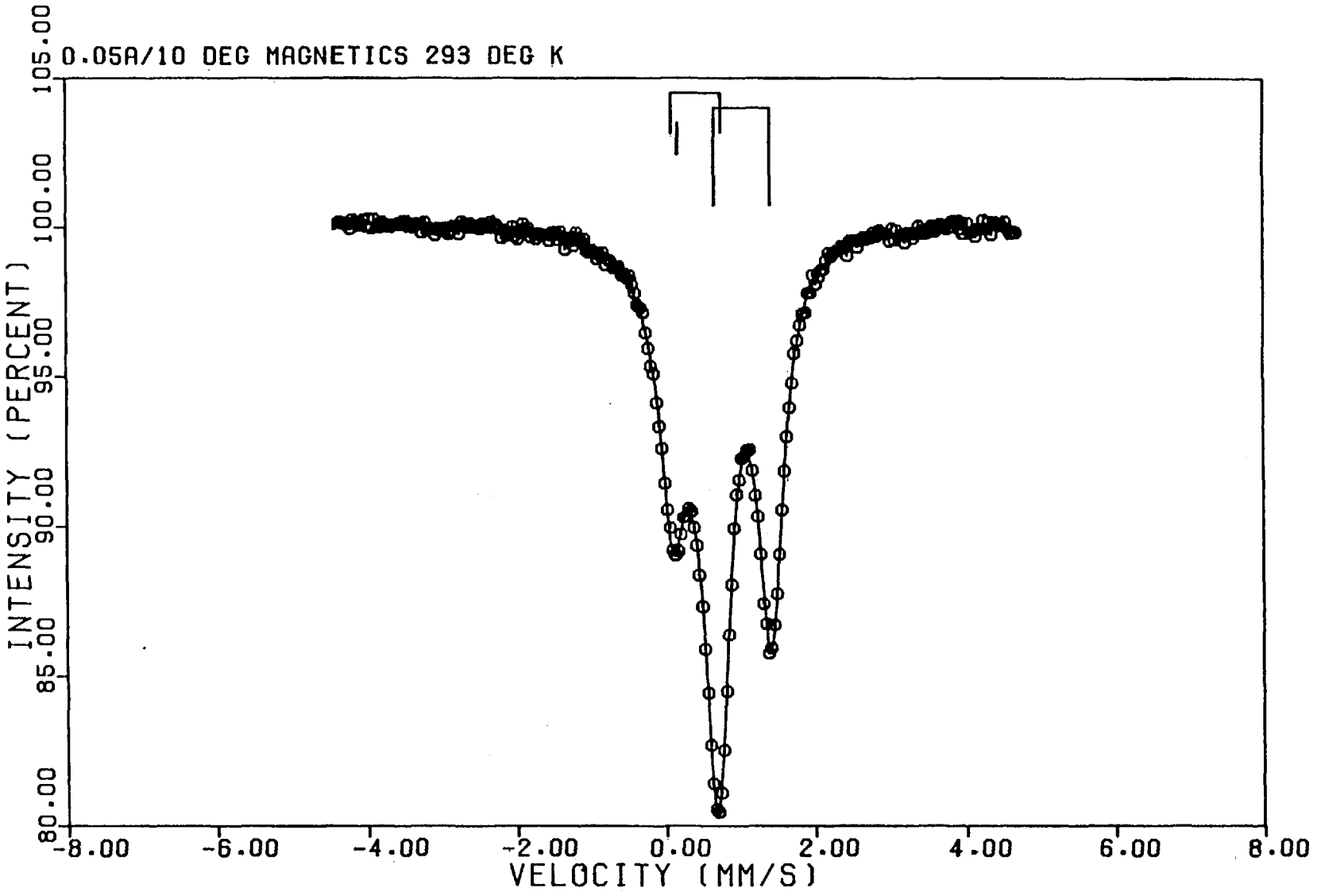

Fig. 10.11 Mössbauer spectrum of 0.05A(-)15°+10° magnetics at 293°K

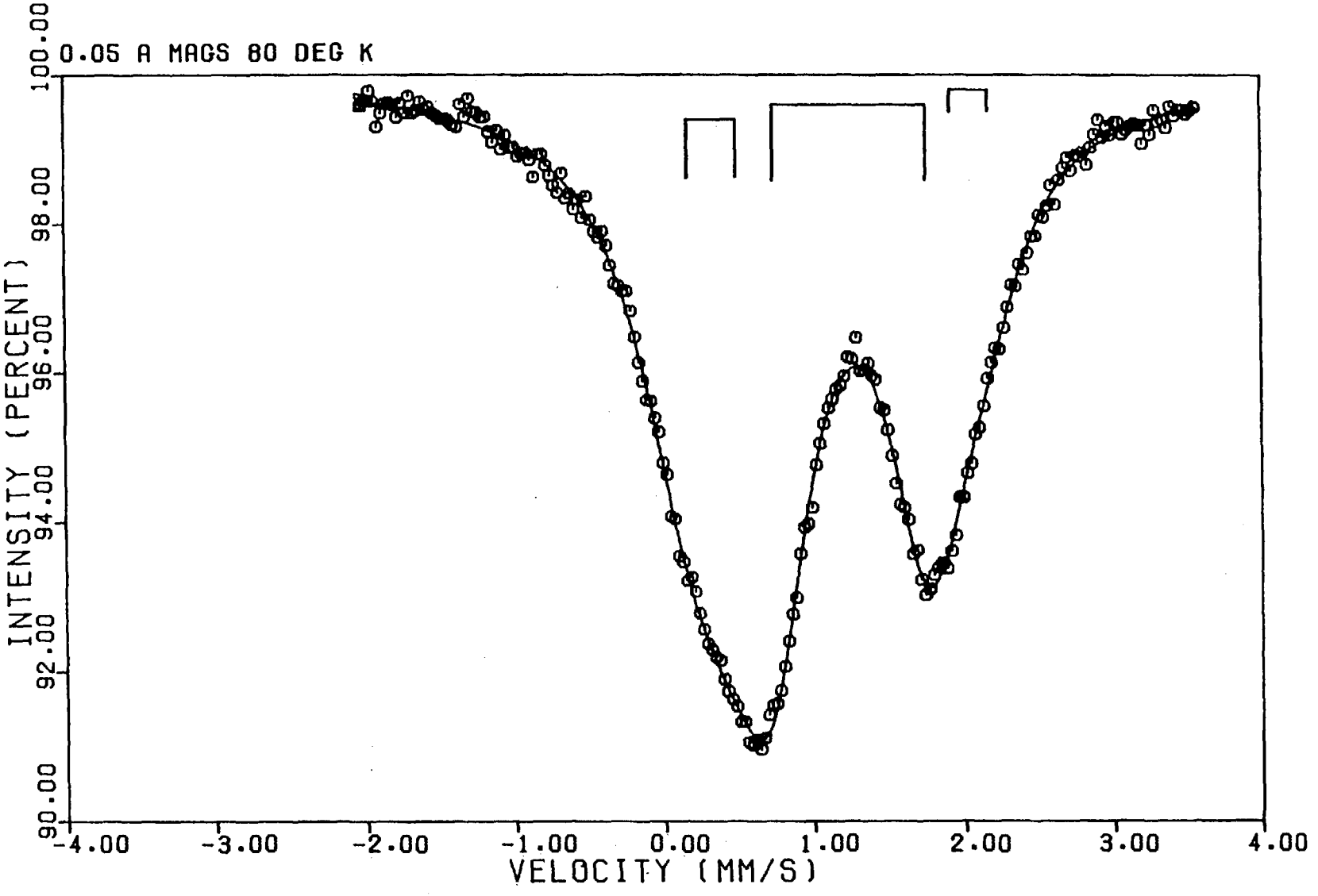

Fig. 10.12 Mössbauer spectrum of 0.05A/(-)15°+10° magnetics at 80°K

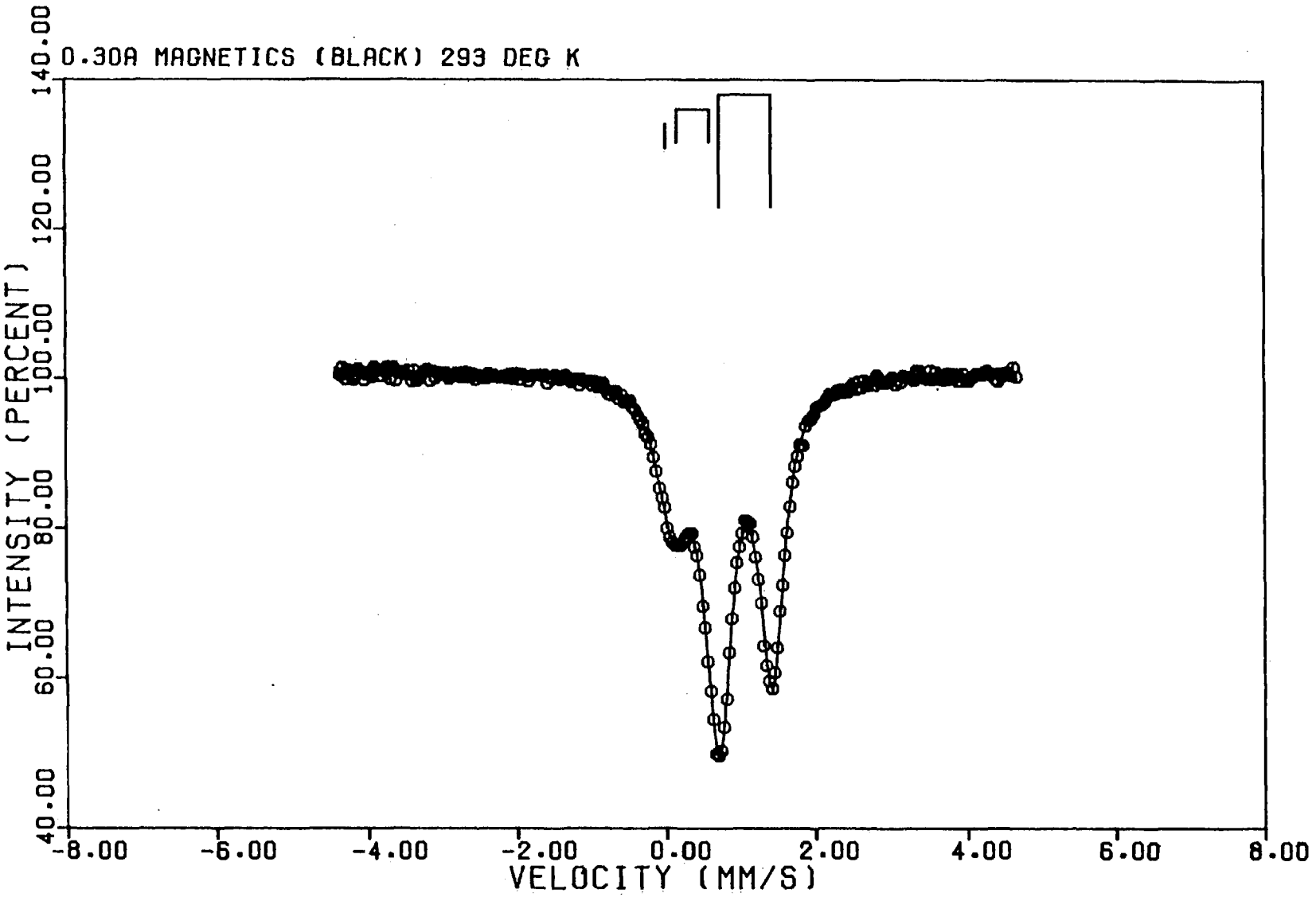

Fig. 10.13 Mössbauer spectrum of cleaned, black 0.30A magnetics at 293°K

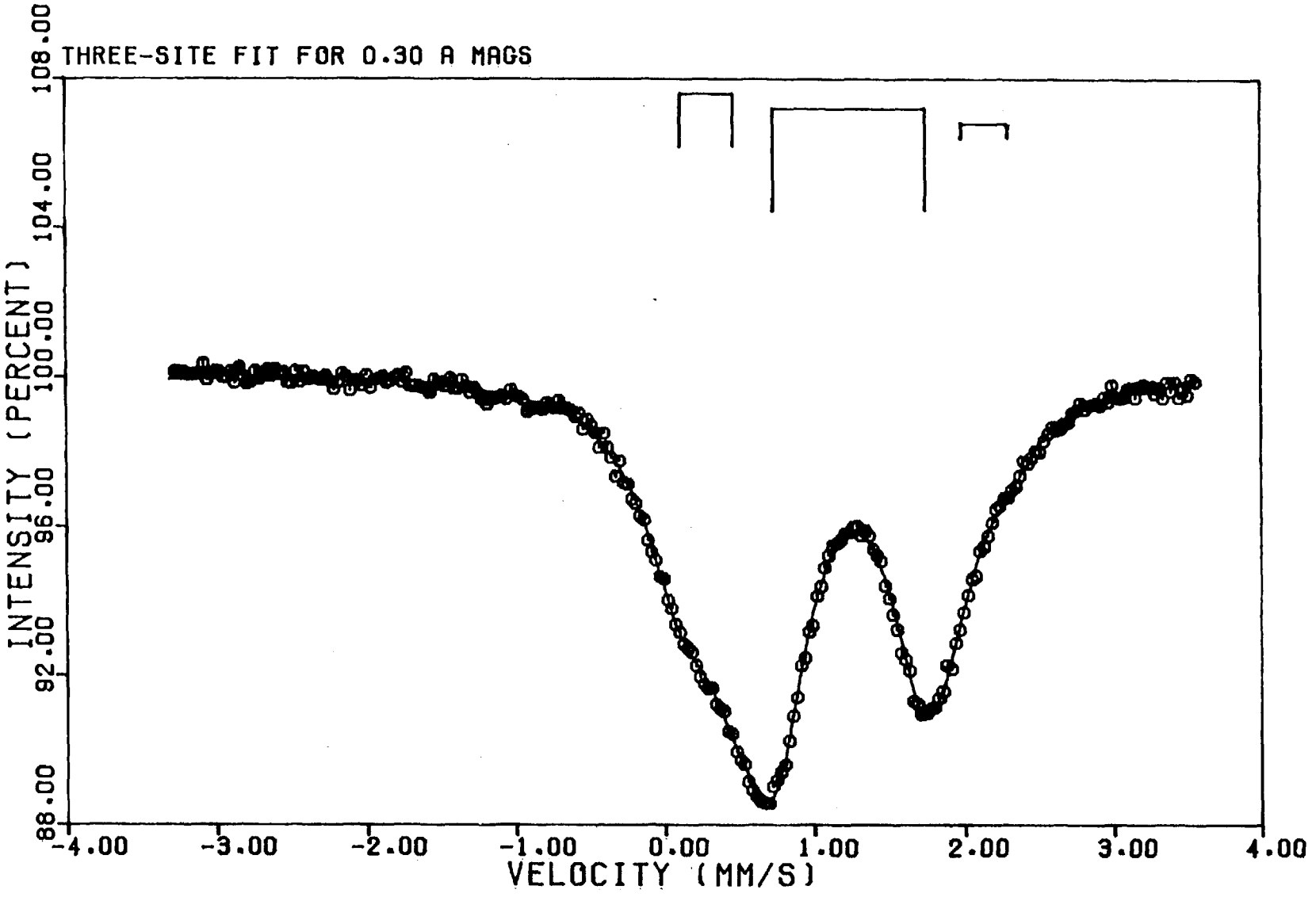

Fig. 10.14 Mössbauer spectrum of cleaned, black 0.30A magnetics at 80°K

acceptably good fit. The 80°K spectrum contains a third doublet, tentatively identified as ferrous, which like the 0.05A/-15°+10° sample has a questionable, high isomer shift (2.1 mm/s).

The relative absorption areas given in Table 10.13 for the ferrous and ferric ions differ at different temperatures for the same sample. Also, the relative concentration indicated by the absorption areas agree only qualitatively with the ferrous/ferric ion ratios indicated by the chemical analyses. These discrepancies are explained by the fact that Mössbauer absorption areas for a given ion in a given site are a function of the recoil-free fraction (f) which is itself a temperature-dependent function (Greaves, 1979).

The observation of paramagnetic spectra for both samples indicates that the magnetic ordering temperatures are below 80°K: this was expected for the 0.30A mags since for ilmenite T_N is about 55°K.

Further work on the more highly susceptible fractions 0.05A/25° and 0.05A/-25°+15° would be of value, as would lower temperature runs on the two samples considered above. However, some of the information which would thus be yielded has been obtained by magnetic measurements.

Anomalous isomer shifts (e.g. 2.1 mm/s, Table 10.13) are produced by relaxation processes that cause line broadening due either to electric field gradient fluctuations or magnetic hyperfine field fluctuations. Much further work is required before a detailed explanation of the anomalous components of the observed spectra can be provided.

10.11 Microscopic observations (reflected light)

The most highly magnetic fractions (0.05–0.25A) contain some grains with strongly altered surface zones. Most of the grains are greyish white in appearance and only a few grains show the 'pink' areas characteristic of unaltered ilmenite.

Generally the grains in these highly magnetic fractions are noticeably anisotropic when viewed with slightly uncrossed polarisers.

Ferrimagnetic grains containing hematite in solid solution are identifiable only if exsolved phases or trains of elongated pits can be seen. Such pit trains show a distinct lineation in some grains: where exsolved blebs are also present, they are in parallel alignment with the pits. This feature strongly suggests that the pits represent leached-out blebs of exsolved ferrian-ilmenite. The pits are commonly concentrated in an outer zone.

A less magnetic fraction (the 0.30A magnetics) reveals a marked concentration of relatively fresh, pink anisotropic ilmenite. In more altered, less magnetic fractions, any remaining pink areas are paler and are largely restricted to the cores of the grains. Anisotropy still persists even when the pink tint has disappeared but it is weaker than for fresh pink ilmenite. Greyish-white grains that have lost their anisotropy and become isotropic are not specifically identifiable as either "isotropic ilmenite" (Baker,1962), amorphous ilmenite, or amorphous pseudorutile. Pseudorutile has not in fact been positively identified optically, although narrow zones of possible pseudorutile have been seen. The occurrence of significant Fe_2O_3 in the chemical analysis coupled with XRD evidence are the best indications of the presence of pseudorutile.

Formation of secondary rutile (leucoxenisation) begins with development of fine veinlets and 'efflorescent' spots of bluish-grey alteration. If these spots are present in a markedly anisotropic host, the internal reflections of secondary rutile are not always readily visible when viewed in air. Internal reflections are generally more strongly developed when the secondary rutile occurs in a weakly anisotropic or isotropic (and possibly amorphous) ground mass. The blue tint seems to be a subjective colour-contrast effect, and generally is only developed in small areas. Larger areas of dull grey microporous

secondary rutile in otherwise isotropic grains generally give strong yellowish-white internal reflections. Some blue-grey streaks of alteration have been noted which give internal reflections but which extinguish uniformly - optical evidence for topotaxial formation of secondary rutile.

Magnetic fractions collected at currents greater than 0.30A show a progressive increase in the number of isotropic grains and of grains carrying internally-reflecting secondary rutile. However, each fraction shows grains having a wide variety of alteration states and textures. The average level of alteration can be judged by noting the presence or absence of pink, strongly anisotropic ilmenite; greyish-white weakly anisotropic ilmenite; isotropic grains; and the level of development of internally-reflecting rutile. Optical examination alone, however, gives at best an inaccurate estimate of the average degree of alteration and this method should be used in conjunction with XRD, magnetic susceptibility and chemical analysis.

Some photomicrographs of typical textures are given in Figures 10.15 to 10.25.

10.12 EPMA investigations

It was shown by qualitative EPMA that the fine exsolved white blebs in partly-pitted grains were titanhematite, since the blebs contained both iron and titanium but with a higher level of iron and lower level of titanium than the host ilmenite. However, the exsolved blebs were too fine grained to be analysed quantitatively.

In general, the manganese concentrations sympathetically followed the iron (Figs. 10.26, 10.27) and relatively low levels of iron or manganese were present in outer zones of internally-reflecting secondary rutile (Fig. 10.28).

It was not found possible to specifically identify any areas of pseudorutile in the Capel ilmenite, largely because areas containing solely the ferric ion cannot be delineated by the EPMA instrumentation employed (Cambridge Geoscan and Microscan 5). Point analyses (Microscan 5) made on grains of pink ilmenite in the 0.30A magnetics gave the following results after matrix correction by Link System EDS computer: 52.0% TiO_2, 1.7% MnO, 46.1% FeO.

Due to porosity effects, analyses made by Microscan 5 generally totalled only 93-95% for points in the outer secondary rutile zones: the balance is due to moisture.

Silicate inclusions, which occur in small amount only, were identified as zircon.

EPMA was also used to identify chromite, (Section 5.8), which was readily distinguishable optically on account of its low reflectivity, colour, and distinctive crack patterns (Fig. 10.29).

Most of the chromite occurs in the χ = 37-46 x 10^{-2} JT^{-2} kg^{-1} fraction, and contains in addition to major Cr and Fe, significant amounts of Al but only rare traces of Mg or Mn. A small amount of chromite also occurs in the high susceptibility fractions, and this chromite contains little or no detectable Al, and no Mg or Mn.

10.13 Alteration model

The observed miscroscopic features, including optical isotropism, and the poor crystallinity and X-ray amorphism revealed by X-ray diffraction, provide a new schematic model for the alteration of ilmenite (Fig. 10.30). The relative frequency of grains with two optically distinguishable zones (Figs. 10.16, 10.27) and the rarity of three-zoned grains, Fig. 10.17, can be explained if secondary rutile surrounds an optically amorphous core of finely intergrown relict ilmenite and secondary pseudorutile, or if the pseudorutile zone is so thin that it is not optically resolvable.

The last possibility may explain published and present observations of ilmenite apparently altering directly to secondary rutile (Hartman,1959; Baker,1962). The penetration of the external environment on myriad fronts along cracks and through microporous zones probably results (in the optically undifferentiable zones) in the formation of a sub-microscopic mozaic texture, any one block of which could show the zonal sequence given by the model in Fig. 10.30.

It is unlikely that the complex solution chemistry and cyclic fluctuations of water table and temperature that effect a buried detrital ilmenite deposit could ever be adequately reproduced in the laboratory, even if the infinitesimally slow reaction rates could somehow be speeded up to take place in a practical time interval. However, an electrochemical study of ilmenite alteration, using an electrode of synthetic ilmenite, would be a possible way of investigating the energy changes accompanying the oxidation and leaching of ilmenite.

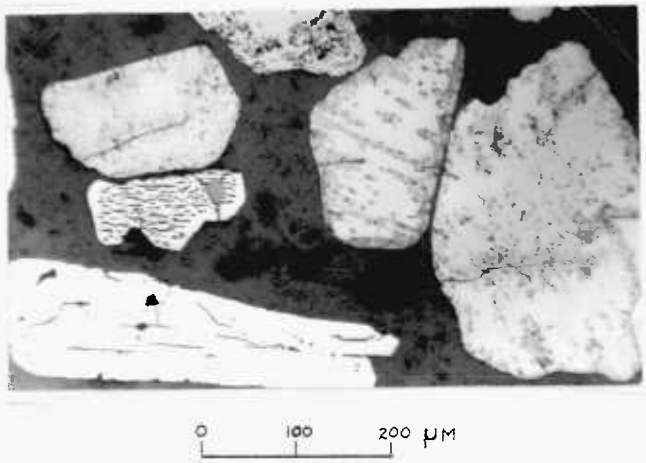

Fig. 10.15 Typical textures - 0.05A magnetics - South Capel deposit.

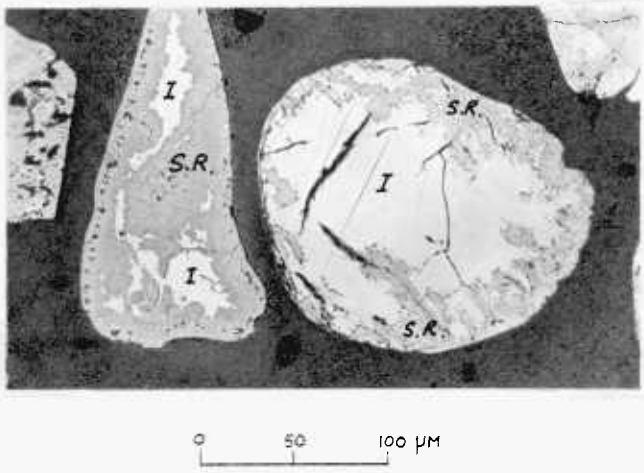

Fig. 10.16 Isotropic altered phases (I) and secondary rutile (SR) 0.05A magnetics - South Capel deposit.

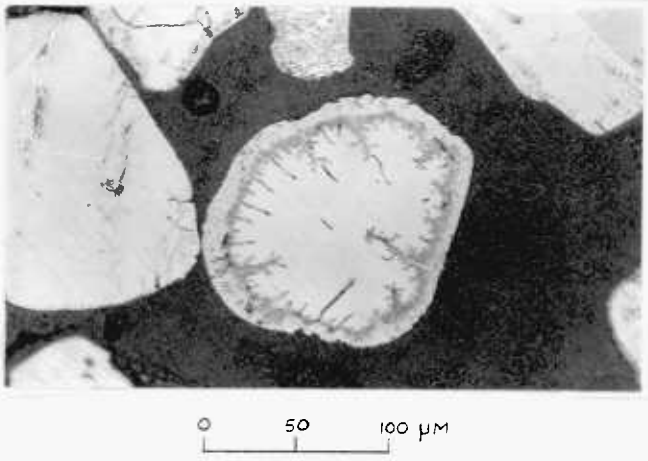

Fig. 10.17 Three-zoned grain with isotropic core; isotropic median zone (?pseudorutile) and outer zone of internally-reflecting secondary rutile. 0.05A magnetics - South Capel deposit.

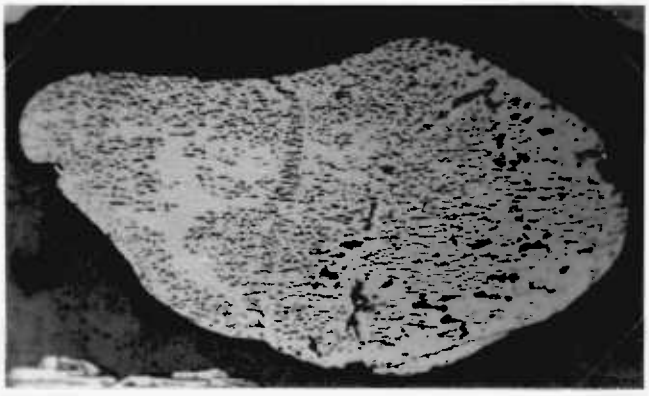

Fig. 10.18 Leached grain with pits and relict exsolved blebs of titanhematite - 0.05A magnetics - South Capel deposit.

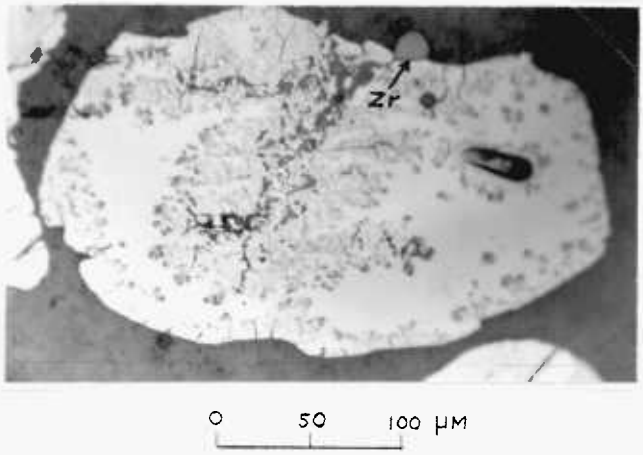

Fig. 10.19 Efflorescent alteration spots attacking the rim and spreading into the core from a crack zone. Zr = zircon 0.05A magnetics - South Capel deposit.

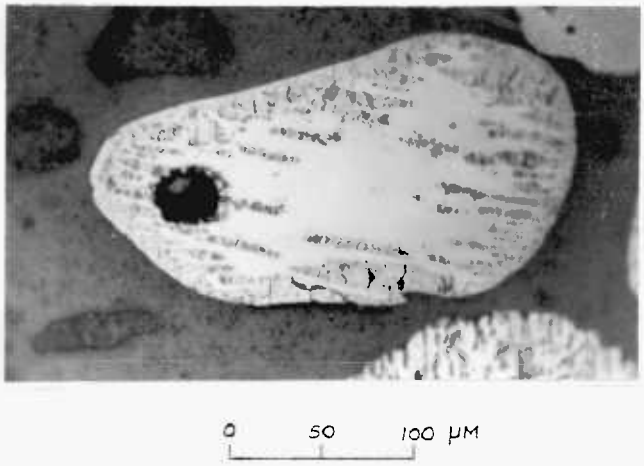

Fig. 10.20 Alteration of the rim and also selectively penetrating the core along a preferred plane. 0.05A magnetics - South Capel deposit.

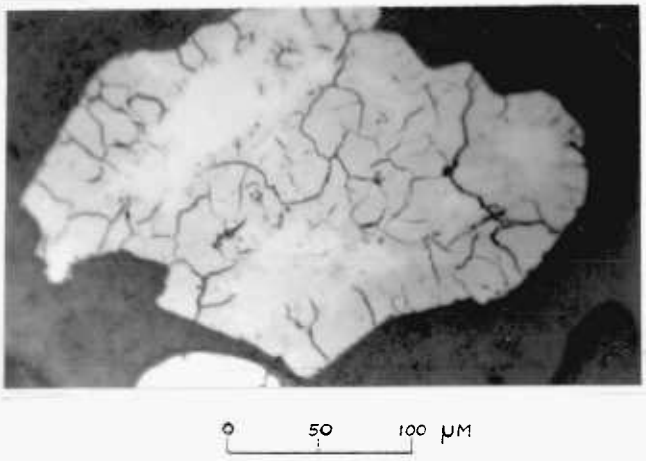

Fig. 10.21 Advanced alteration centred upon cracked areas - 0.05A magnetics - South Capel deposit.

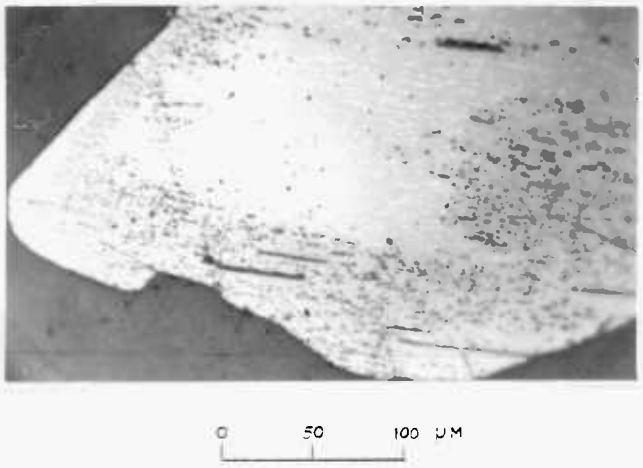

Fig. 10.22 Hemo-ilmenite with leached, pitted rim - unsized 0.35A magnetics - South Capel deposit.

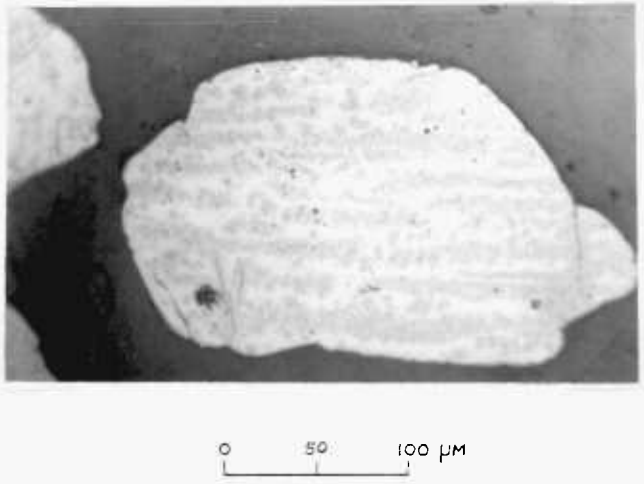

Fig. 10.23 Efflorescent spots of alteration aligned in diffuse bands - unsized 0.35A magnetics - South Capel deposit.

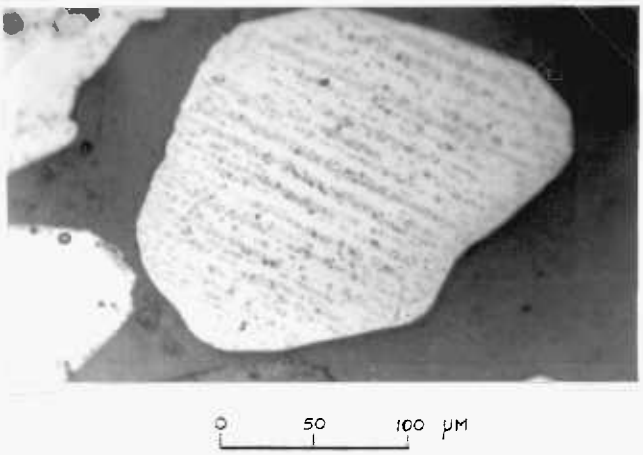

Fig. 10.24 Banded alteration - unsized 0.35A magnetics - South Capel deposit.

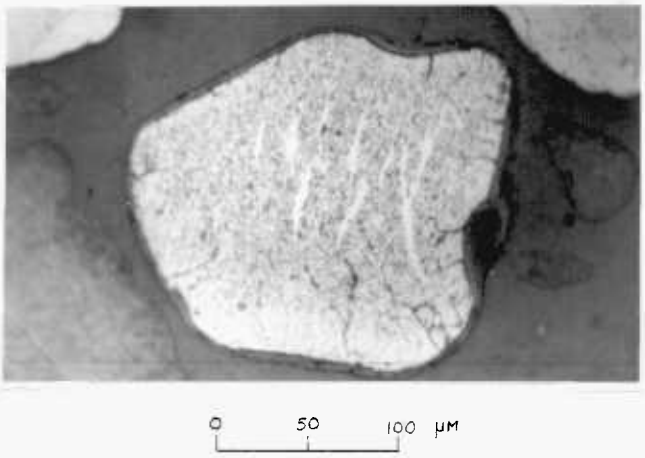

Fig. 10.25 Relict isotropic streaks in finely pitted grain with weak, barely visible internal reflections. Unsized 0.35A magnetics - South Capel deposit.

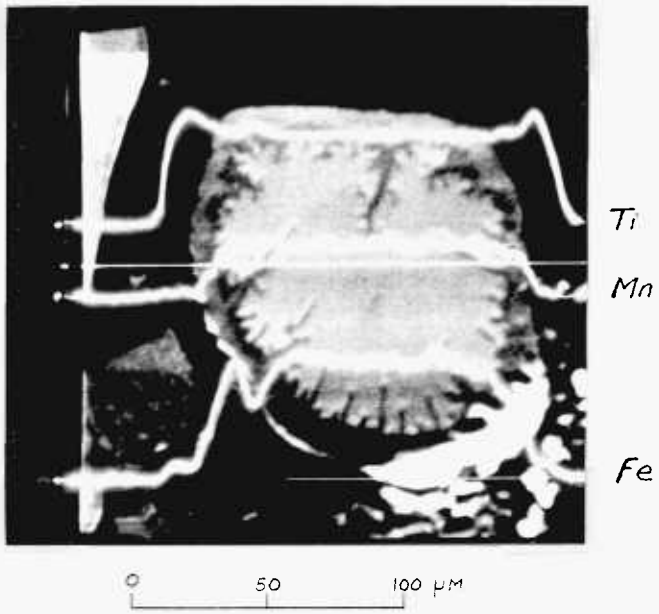

Fig. 10.26 EPMA slow scans for Ti, Mn and Fe across grain shown in Fig. 10.17. The thin intermediate zone was not detected.

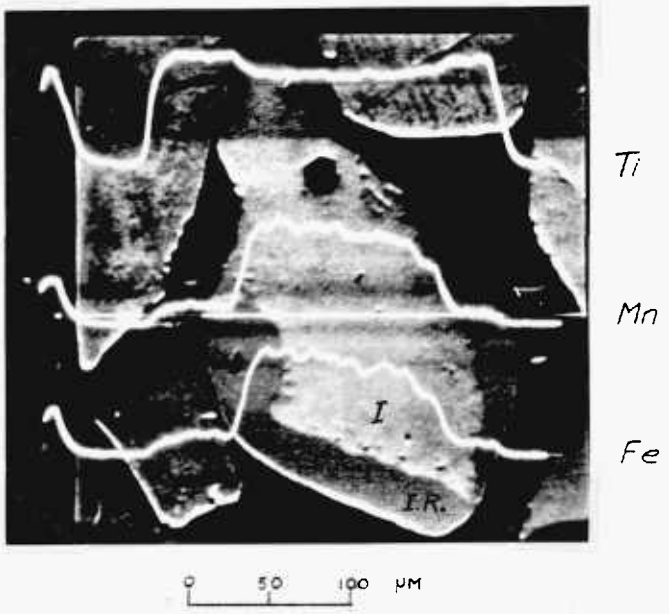

Fig. 10.27 Two-phase grain from 0.45A magnetics, South Capel deposit. The outer zone has dull grey internal reflections (I.R.) The core phase is isotropic (I).

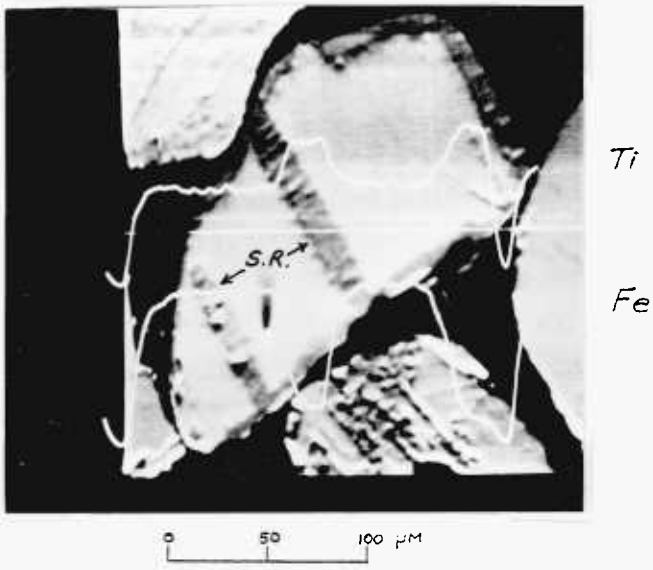

Fig. 10.28 Veins of secondary rutile (SR) cut across anisotropic greyish-white altered ilmenite core. No intermediate phase was visible even at X1600 magnification 0.30A magnetics, South Capel deposit.

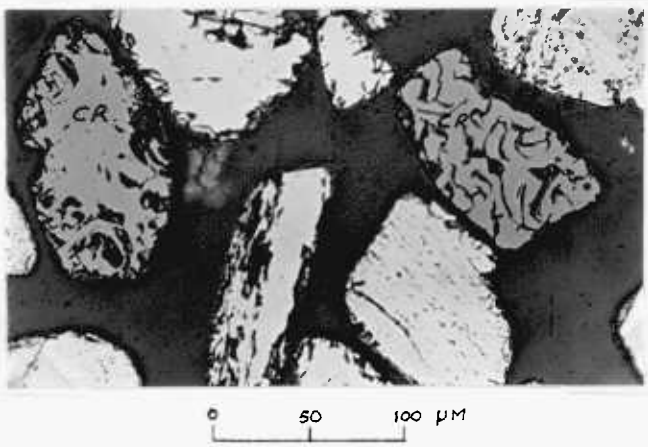

Fig. 10.29 Chromite grains in east coast ilmenite concentrate (Consolidated Rutile Ltd.)

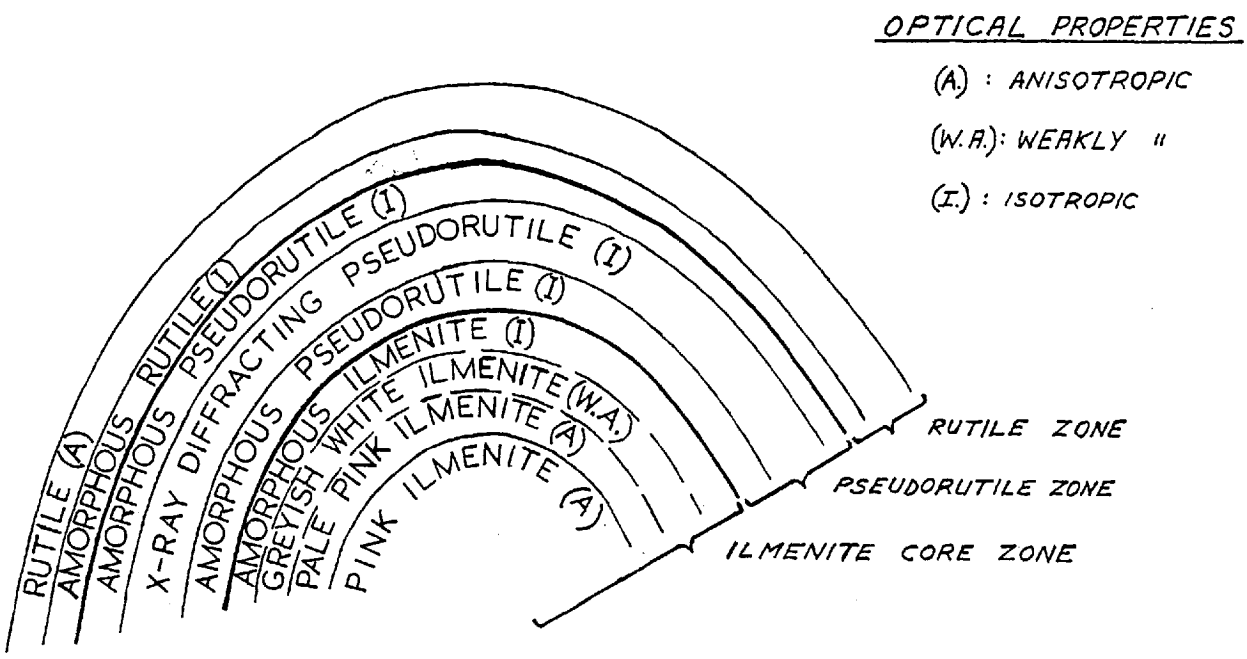

Fig. 10.30 Idealised model of ilmenite alteration.

CHAPTER 11

RESULTS FOR ENEABBA ALTERED ILMENITE

11.1 Introduction

The Eneabba heavy mineral deposit, discovered in 1970, is one of the largest in the world, and contains between 25 and 30 million tons of recoverable heavy minerals (Lissiman and Oxenford, 1975). The sample examined in this investigation came from the southern half of the Adamson deposit, which lies to the south of Eneabba (Fig. 11.1), and which is mined by Associated Minerals Consolidated Ltd.

As at Capel, the valuable minerals are 'ilmenite', zircon, rutile, secondary rutile (leucoxene) and monazite. The other heavy minerals include staurolite, garnet, hornblende, pyroxene, sillimanite, spinels, kyanite, tourmaline, brookite, limonite and laterite pebbles. The heavy minerals are concentrated in various well-defined strands, at different elevations above mean sea level. Five strands have been discovered in the Adamson deposit, and each has a distinct heavy mineral assemblage, Table 11.1 (Baxter,1977).

11.2 Material studied

An 'ilmenite' concentrate, produced as a trial product before the commencement of full-scale concentrator operations, has been the only material studied from the Eneabba deposit. A size distribution is given in Table 11.2, and the chemical analysis of a fraction from which free silicates (mainly staurolite) had been removed by handpicking is given in Table 11.3. It can be seen that this 'ilmenite' product is close to pseudorutile in composition.

The Eneabba heavy minerals are much more rounded in shape than at Capel. In addition, grains coated with yellow,

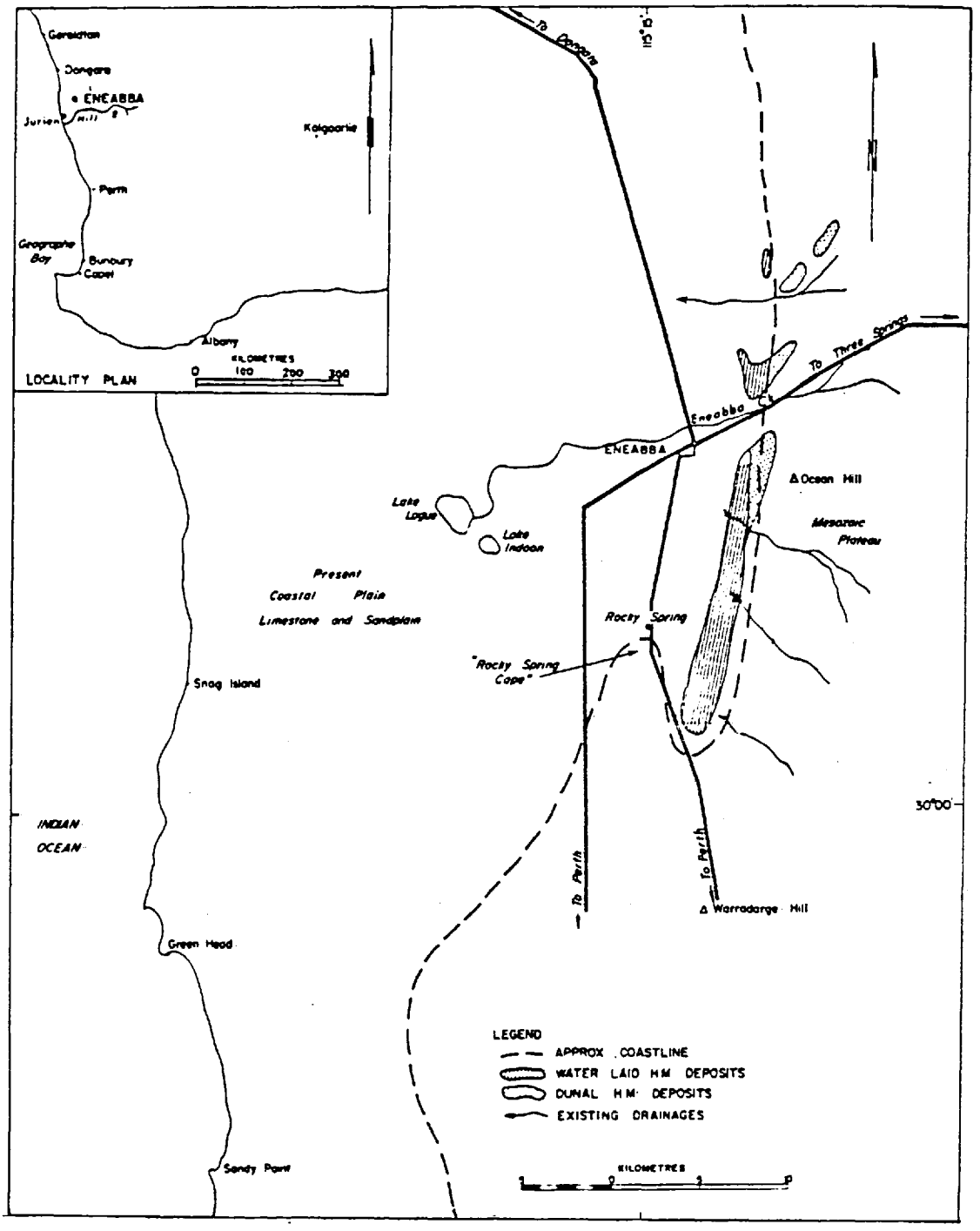

Fig. 11.1 Location of the Eneabba heavy mineral deposit (after Lissiman and Oxenford, 1975)

Table 11.1

Compositions of heavy mineral fractions from strand lines in the Adamson deposit

Mineral	Strand Line metres above m.s.l. 128 m	115 m	103 m	97 m	91 m
	Weight per cent				
Ilmenite	37.9	43.9	61.4	64.8	66.1
Leucoxene	n.d.	1.7	2.1	2.2	1.9
Rutile	7.0	8.6	9.7	10.9	8.6
Zircon	19.6	39.7	18.6	17.1	15.0
Monazite	n.d.	0.4	0.1	0.2	0.2
Kyanite	1.7	1.6	2.4	2.7	4.1
Others	32.6*	3.7	5.7	2.3	3.2

*Includes 24.2 per cent limonite. n.d. = not determined
m.s.l. = mean sea level

Taken from Baxter (1977)

Table 11.2

Size distribution of Eneabba altered ilmenite

Size µm	Wt. %	Cum. Wt.% finer
+355	0.4	99.6
+250	16.3	83.3
+180	48.8	34.5
+125	28.5	6.0
+ 90	5.8	0.2
- 90	0.2	

Table 11.3

Composition of Eneabba altered ilmenite

		Comparable Analyses		
Wt.%	A	B	C	D
TiO_2	60.0	63.3	63.2	62.2
Fe_2O_3	31.1	31.2	25.0	26.3
FeO	4.5	2.6	5.2	4.3
Cr_2O_3	0.14+	0.14	0.29	0.03
V_2O_5	0.17	n.d.	0.16	0.05
MnO	1.22	1.34	1.28	2.7
MgO	0.12	n.d.	0.17e	0.03
Al_2O_3	0.42	n.d.	n.d.	n.d.
SiO_2	0.34++	0.68	n.d.	n.d.
P_2O_5	n.d.	0.08	n.d.	n.d.
	98.01	99.34	95.30	95.61

A. Tioxide International Ltd. ++including other acid fusion insolubles

B. Lissiman and Oxenford,(1975,p1068) for another sample

C. Capel 0.45A magnetics (rich in pseudorutile) for comparison

D. Indonesian pseudorutile analysis by Tioxide International Ltd.

n.d.:not determined

e: estimated

\+ This is a higher value than for Capel ilmenite ($Cr_2O_3 \sim 0.04\%$)
Some free chromite occurs, as at Capel: at Capel the chromite is concentrated in the 0.45A magnetic fraction, (C).

reddish-brown or soft white clay, or cemented into ferruginous aggregates occur in parts of the deposit. The 'ilmenite' itself ranges from black through dark brown to brown, and ultimately to fawn grains in which the grain surface has changed to secondary rutile. The overall colour is brown, and the concentrate is visibly much more altered than the black ilmenite concentrate from Capel.

11.3 Magnetic fractionation and susceptibility determination

Because of the limited amount of sample available, magnetic fractionation by Cook isodynamic separator was conducted on an unsized split. The separator was calibrated in the manner outlined in Section 6.7. As with the heavy mineral concentrate from Capel, separation commenced using a current of 0.05A. Separation terminated after production of the twelfth fraction at 0.60A, and the results are given in Table 11.4. Results of detailed susceptibility determination by the Faraday method are presented in Table 11.5, and it can be seen that the values obtained are similar to those obtained for Capel ilmenite (Table 10.5).

When powdered, the magnetic fractions show a distinct colour change from a very dark brown (0.05A magnetics), through dark brown (0.25A magnetics) to brown (0.50A magnetics) and yellow-brown (0.60A magnetics).

11.4 Qualitative X-ray diffraction

The XRD spectra of the Eneabba altered ilmenite are dominated by pseudorutile peaks. The most ilmenite occurs in the most highly magnetic fraction, and the amount decreases in the more weakly magnetic fractions as the pseudorutile becomes more prominent.

Contrary to the findings of Lissiman and Oxenford,(1975) no XRD lines were visible for any fraction which would suggest the presence of discrete pseudobrookite or hematite.Very minor amounts

Table 11.4

Magnetic separation of Eneabba altered ilmenite

Cook Mags A	Cook calc. Lr $\chi \times 10^2$	wt %	Comments
0.05	2737	5.45	
0.10	703	4.91	
0.15	317	4.50	
0.20	180	7.86	Trace pale staurolite.
0.25	116	8.24	
0.30	81	9.43	
0.35	60	12.91	
0.40	46	11.63	Staurolite present.
0.45	37	12.02	"
0.50	30	12.23	"
0.55	25	6.60	"
0.60	21	2.50	Fair staurolite, very minor tourmaline.
N/Mags		1.72	Abundant staurolite and tourmaline; plus minor white silicates, spinels and rutile.
		100.00	

Table 11.5

Susceptibility measurements on Eneabba altered ilmenite by the Faraday method

Cook Mags A	Cook calc. Lr $\chi \times 10^2$	Faraday χ* values x $10^2 JT^{-2} kg^{-1}$ 5A	10A	15A	20A	H∞	
0.05	2737	378	273	226	208	170	F
0.10	703	174	134	119	113	100	F
0.15	317	125	102	90	87	84	F
0.20	180	108	90	82	80	78	F
0.25	116	79	72	68	67	65	F
0.30	81	62	64	61	61	-	P
0.35	60	55	52	52	52	-	P
0.40	46	43	43	43	43	-	P
0.45	37	31	37	37	37	-	P
0.50	30	32	32	32	33	-	P
0.55	25	24	28	28	29	-	P
0.60	—	— Insufficient sample			—	—	

*determined with Faraday pole pieces and a 0.12g-capacity container.

of anatase were detected in the 0.50 and 0.60A magnetics and also in the 0.60A non-magnetics. The 0.60A magnetics give a nearly pure pseudorutile spectrum with no detectable ilmenite and only a small amount of rutile - slightly more than in a purified sample of Indonesian pseudorutile (Section 12.4).

There is nothing in the XRD spectra which could explain the high susceptibility of some of the fractions. No lines of magnetite, hematite or other magnetic phases are present but a few grains of intergrown hematite and ilmenite were noted microscopically. The high frequency of grains with pitted textures (Section 11.6) suggests that many of the grains were originally hemo-ilmenite, of which the groundmass is an ilmenite containing hematite in solid solution. The high susceptibility of such a solid solution would completely swamp the contribution from pseudorutile ($\chi = 34.5 \times 10^{-2}$ $JT^{-2}kg^{-1}$).

To test this hypothesis, a portion of the 0.05A magnetics was mounted in a fluid glue and left to set with a 0.2T magnetic field acting perpendicular to the face of the mount. The mount was then subjected to XRD, and the spectrum obtained (Fig. 11.2) shows the selective enhancement of two ilmenite prism reflections by a magnetic particle-orientation effect, in exactly the same way as was found for the 0.05A magnetics of the Capel ilmenite (Section 10.8). This result confirms that ferrimagnetic ilmenite-hematite solid solutions are present and can adequately explain the observed high susceptibilities. It also ties in with the microscopic observation of small numbers of grains showing exsolved white blebs: EPMA showed that these blebs contained more iron and less titanium than the ilmenite ground mass (0.05A magnetics).

11.5 Quantitative X-ray diffraction

Using the Chung matrix-flushing technique, the mineral content of each magnetic fraction has been estimated (Table

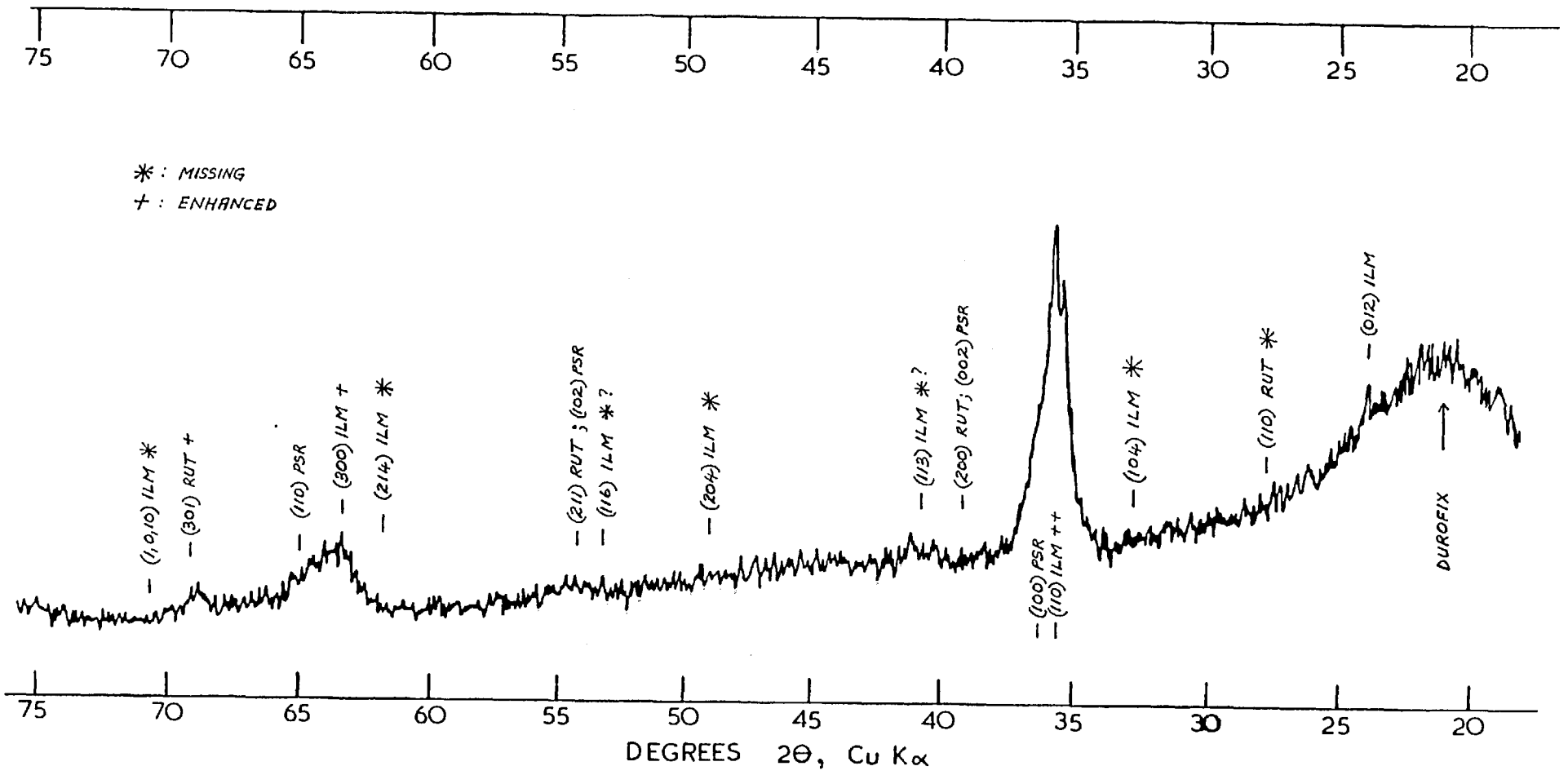

Fig. 11.2 XRD spectrum of Eneabba 0.05A magnetics set in Durofix with 0.2T field acting perpendicular to the mount.

11.6). Significant features are the progressive decrease in ilmenite content, and the high levels of pseudorutile. In the three fractions for 0.45A to 0.60A, the high pseudorutile figures correlate with low figures for amorphous content. The susceptibilities of these fractions are compatible with the high pseudorutile contents in all but the 0.60A fraction, suggesting that the apparent pseudorutile content in this fraction (and possibly for all of the 0.45A - 0.60A range) is too high. These fractions yield closely similar spectra, and the most probable reason for the discrepancy is that the pseudorutile in these fractions has a higher crystallinity than that of the hand-picked Indonesian pseudorutile used as a standard. This example highlights the interpretational problems arising in quantitative X-ray diffraction when the crystallinity of the standard does not match that of the mineral to be determined. The trend of the pseudorutile figures, indicating maximum pseudorutile in the 0.45 and 0.50A fractions, is consistent however with the known specific susceptibility of this mineral ($34.5 \times 10^{-2} JT^{-2} kg^{-1}$).

Data for Table 11.6 were obtained from the spectra given in Appendix G.

11.6 Microscopic observations (reflected light)

The Eneabba altered ilmenite grains are distinctly more rounded, and the average degree of alteration is higher, than for the ilmenite from the South Capel mine.

In agreement with the XRD evidence for the presence of ilmenite, small numbers of grains of pink ilmenite were noted in the 0.05A and 0.10A fractions. The 0.15A to 0.30A fractions contain progressively less pink ilmenite, which is generally confined to the cores of altered grains.

Table 11.6

Mineral contents of magnetic fractions of Eneabba altered ilmenite, estimated by quantitative XRD.

Cook Sep'n Current, A	Cook calc. $Lr\chi x10^2$	RUT	ILM	PSR	AMORPH
0.05	2737	3	28*	49	20
0.10					
0.15	317	2	8*	75	15
0.20					
0.25	116	3	10*	74	13
0.30					
0.35	60	3	8	79	10
0.40					
0.45	37	3	1	92	4
0.50	30	3	1	90	5
0.55					
0.60	21	11	-	86?	3?

*Containing grains with ferrimagnetic hematite-ilmenite solid solution.

In addition to the pink ilmenite, a few particles showing lamellar intergrowth of hematite and ilmenite were observed in the high-susceptibility ferrimagnetic fractions, as were rare particles of ilmenite with exsolved fine blebs of titanhematite. In partly pitted grains in which the relict areas of ilmenite contained exsolved blebs, the blebs were in linear alignment with the pits. The original presence of many grains with exsolved blebs is indicated by the high proportion of isotropic grains with linear trains of pits. No visible cracks link the pits with the particle surface, suggesting that the ground mass of the particles has a marked sub-microscopic porosity.

Of the rutile present in the 0.05A to 0.30A fractions, most occurs in incomplete surface layers, but grains showing complete encapsulation by thin secondary rutile skins, or traversed by thin veins have also been observed.

The 0.45 and 0.50A fractions are visibly richer in secondary rutile than the more highly magnetic fractions. The rutile occurs both as rims and as irregular internal patches. Some of this secondary rutile has a relatively coarse grain size up to 12 μm. This optical evidence, together with the XRD determined rutile values (Table 11.6) indicate that the values for the amorphous content (which would include X-ray amorphous rutile) are too low. These considerations support the magnetic evidence that the indicated pseudorutile contents for the 0.45, 0.50 and 0.60A fractions appear to be too high, but by what amounts cannot be precisely determined from the available evidence.

Chromite grains were observed in all fractions which have $\chi > 180 \times 10^{-2} JT^{-2} kg^{-1}$, corresponding to a maximum Cook separator collection current of 0.20A. Some chromite was also observed in the 0.45A fraction ($\chi = 37\text{-}46 \times 10^{-2} JT^{-2} kg^{-1}$). The observed distribution of chromite is in sympathy with the relatively high Cr_2O_3 content (0.14%) recorded for the head sample.

Most of the textures displayed are similar to those that can be found in the more altered fractions from the South Capel deposit including rare 3-zoned grains. Some examples are given in Figs. 11.3 to 11.7.

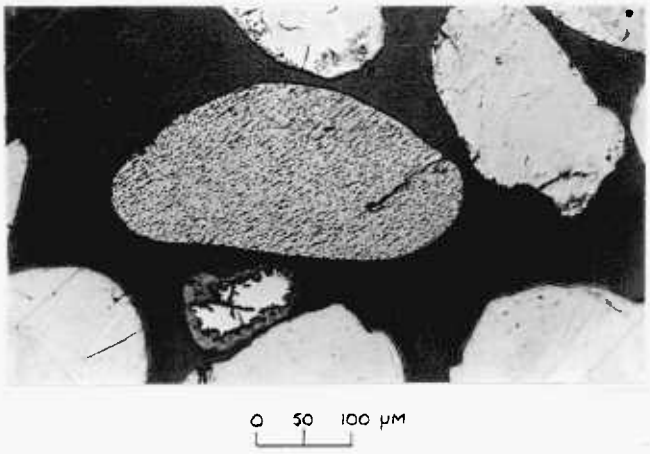

Fig. 11.3 Heavily pitted grain after original hemo-ilmenite, from Eneabba altered ilmenite concentrate.

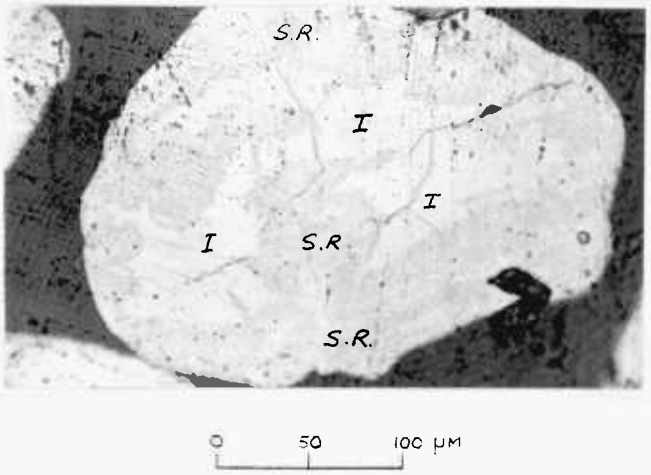

Fig. 11.4 Two-phase altered grain with isotropic (I) core and outer zone of secondary rutile (S.R.) showing dull yellow-orange internal reflections under crossed polarisers; Eneabba altered ilmenite concentrate.

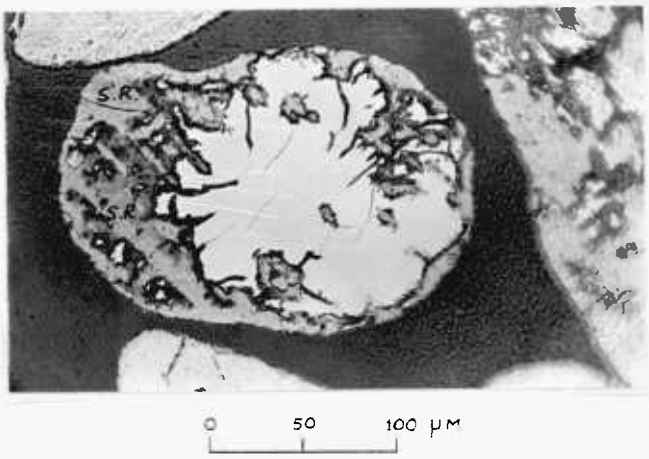

Fig. 11.5 Two-phase altered grain with weakly anisotropic core. Outer secondary rutile (S.R.) zone shows dull yellow-grey internal reflections under crossed polarisers. From Eneabba altered ilmenite concentrate.

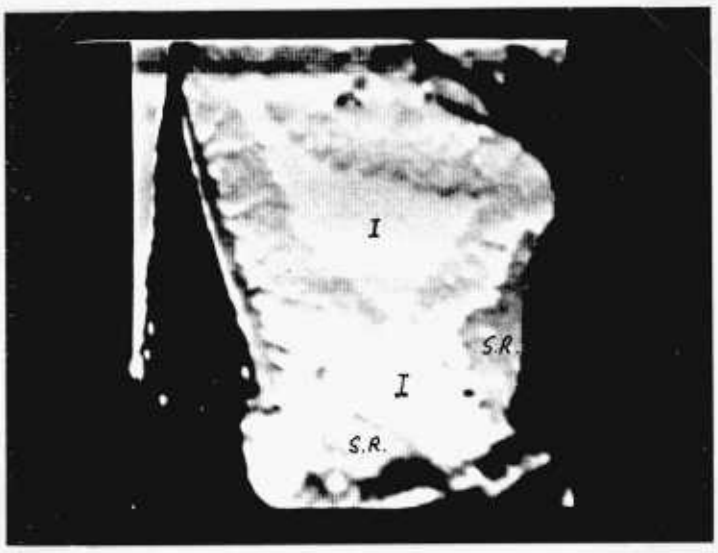

0 50 100 μM

Fig. 11.6 Three-phase grain with isotropic core and intermediate zones, and outer secondary rutile (S.R.) zone. From 0.05 Amp Magnetics, Eneabba altered ilmenite.

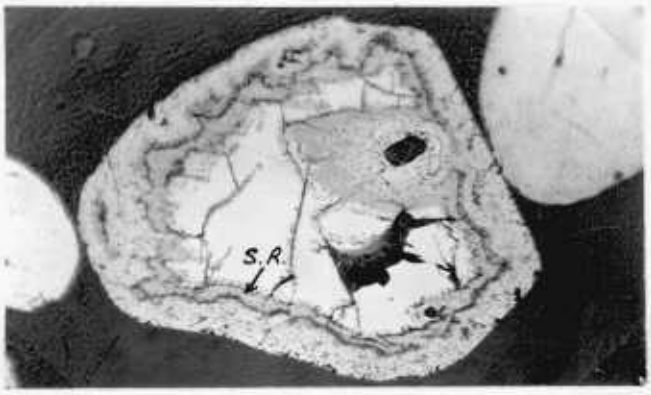

0 50 100 μM

Fig. 11.7 Three-phase grain with weakly anisotropic core and rim zones and impure secondary rutile (S.R.) in thin intermediate zone which appears to extinguish uniformly under crossed polarisers. From Eneabba altered ilmenite concentrate.

11.7 EPMA investigations

Line scans for Ti and Fe across grains from the 0.05A and 0.20A magnetics indicated that the fine white inclusions were titanhematite.

In a three-zoned grain from the 0.05A magnetics (Figs. 11.6, 11.8), Ti occurred throughout the grain but was richest in the rim, and the highest levels of Fe and Mn were in the core. The core and intermediate zones were optically isotropic. The partially developed rim zone of secondary rutile had orange internal reflections; these, together with the iron content, indicate the presence of iron oxide. Point analyses calculated from EPMA (Microscan 5) results are given in Table 11.7A. The porosity of the more altered zones results in lower analysis totals, which will correlate with the contents of absorbed moisture. The intermediate zone has a composition close to that required for stoichiometric pseudorutile (60% TiO_2, 40% Fe_2O_3), but the trivalent state necessary for the iron has not been demonstrated.

An unusual three-zoned grain (Figs. 11.7, 11.9) has an internal narrow zone of impure secondary rutile developed along the boundary of a weakly anisotropic core and a more porous but also weakly anisotropic outer zone. The secondary rutile is formed by removal of iron, suggesting that the outer zone is highly permeable. Point analyses obtained by EPMA (Microscan 5) are given in Table 11.7B.

Chromite grains in the 0.05A magnetics contained major Cr and Fe and occasional trace amounts of Al. Minor aluminium was detected in chromite from the 0.20A magnetics, while chromite from the 0.45A magnetics contained a higher level of Al and possible traces of Mg. This compositional trend is the same as that found in the South Capel ilmenite deposit and indicates that chromites containing non-magnetic ions (Al^{3+}, Mg^{2+}) have lower susceptibilities than grains closer to Fe Cr_2O_4 in composition.

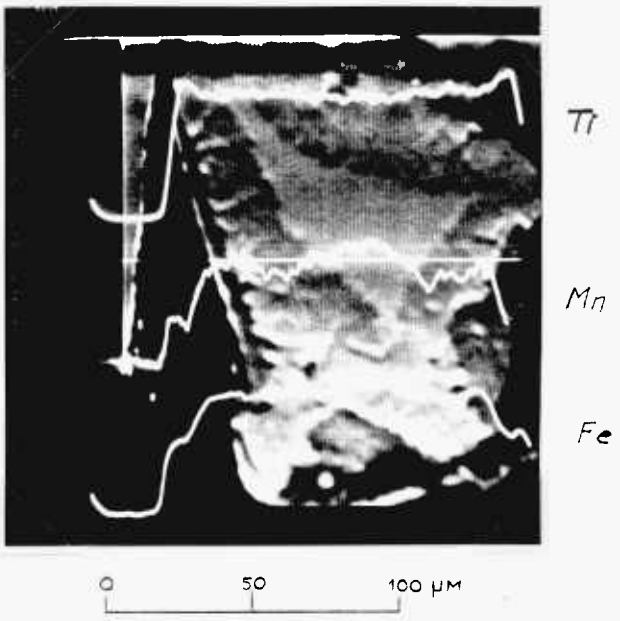

Fig. 11.8 EPMA slow scans for Ti, Mn and Fe across 3-zoned grain shown in Fig. 11.6.

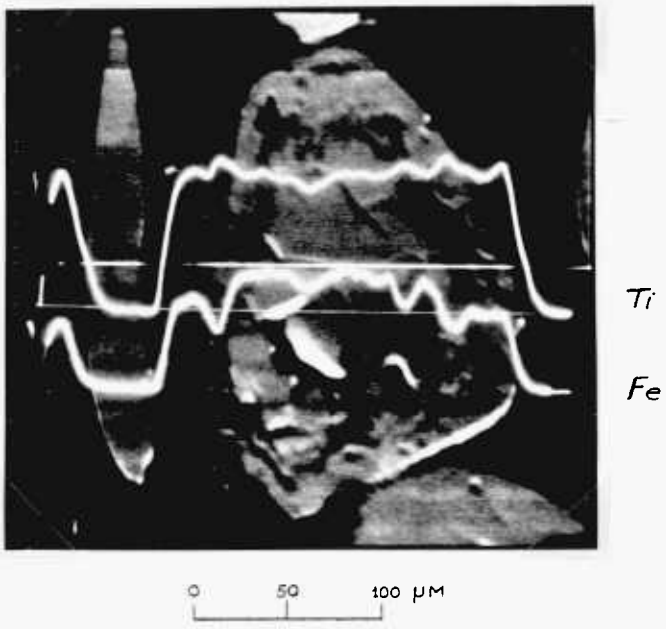

Fig. 11.9 EPMA slow scans for Ti and Fe across 3-zoned grain shown in Fig. 11.7.

Table 11.7A

EPMA results for a three-zoned grain of Eneabba Altered Ilmenite

	Calculated Analyses				Normalised Analyses		
	TiO_2%	Tot.Fe as Fe_2O_3%	MnO%	Total	TiO_2%	Tot.Fe as Fe_2O_3%	MnO%
Core	52.3	43.2	3.3	98.8	53.0	43.7	3.3
Intermediate	55.8	38.0	2.4	96.3	58.0	39.5	2.5
Rim	69.6	21.2	0.4 MnO 1.0 Al_2O_3	92.2	75.5	23.0	0.4 MnO 1.1 Al_2O_3

Table 11.7B

EPMA results for a three-zoned grain with internal zone of secondary rutile

	Calculated Analyses				Normalised Analyses		
	TiO_2%	Fe_2O_3%	MnO%	Total	TiO_2%	Fe_2O_3%	MnO%
Core	52.5	46.5	1.2	100.2	52.4	46.4	1.2
Intermediate	66.4	26.1	-	92.5	71.8	28.2	-
Rim	57.5	36.7	-	94.2	61.0	39.0	-

CHAPTER 12

RESULTS FOR PSEUDORUTILE

12.1 Introduction

Progress in understanding the mineralogy of ilmenite alteration products up to the naming of pseudorutile in 1966 has been discussed in Section 3.1.

Teufer and Temple's discovery of this new phase allows the re-interpretation of work by Lynd et al(1954). They noted that weakly magnetic fractions of altered ilmenite concentrates gave rutile-like spectra which did not show the main peak of rutile. In the present study, the broad maximum peak found by Lynd et al at d = 1.69 Å is considered to be the main peak of pseudorutile (d = 1.688 Å).

Nominally pure pseudorutile has only been reported from South Australia (Larrett and Spencer, 1971). Grey and Reid(1974) showed that pseudorutile also occurs in altered ilmenite grains from Capel, Western Australia, and in addition, in a slightly impure form containing minor ilmenite and rutile in detrital specimens from Indonesia. This study has confirmed the above findings and has shown that the mineral is developed in altered ilmenite from Eneabba, Western Australia (Lissiman and Oxenford, 1975,p1068); in ilmenite concentrates from Eastern Australia; and from Pulmoddai, Sri Lanka (Fig. 12.1). It has also been shown (Teufer and Temple, 1966) that pseudorutile occurs in Florida; in Brazil and at Quilon in Southern India. An optically isotropic alteration product is a general feature of many detrital ilmenite grains. This product includes material that gives a pseudorutile X-ray diffraction pattern. However, pseudorutile is hexagonal (Teufer and Temple,1966; Grey and Reid,1975), and should be markedly anisotropic. It is concluded that the pseudorutile crystals are so small with respect to the wavelength of light that they behave as if they were optically isotropic. This

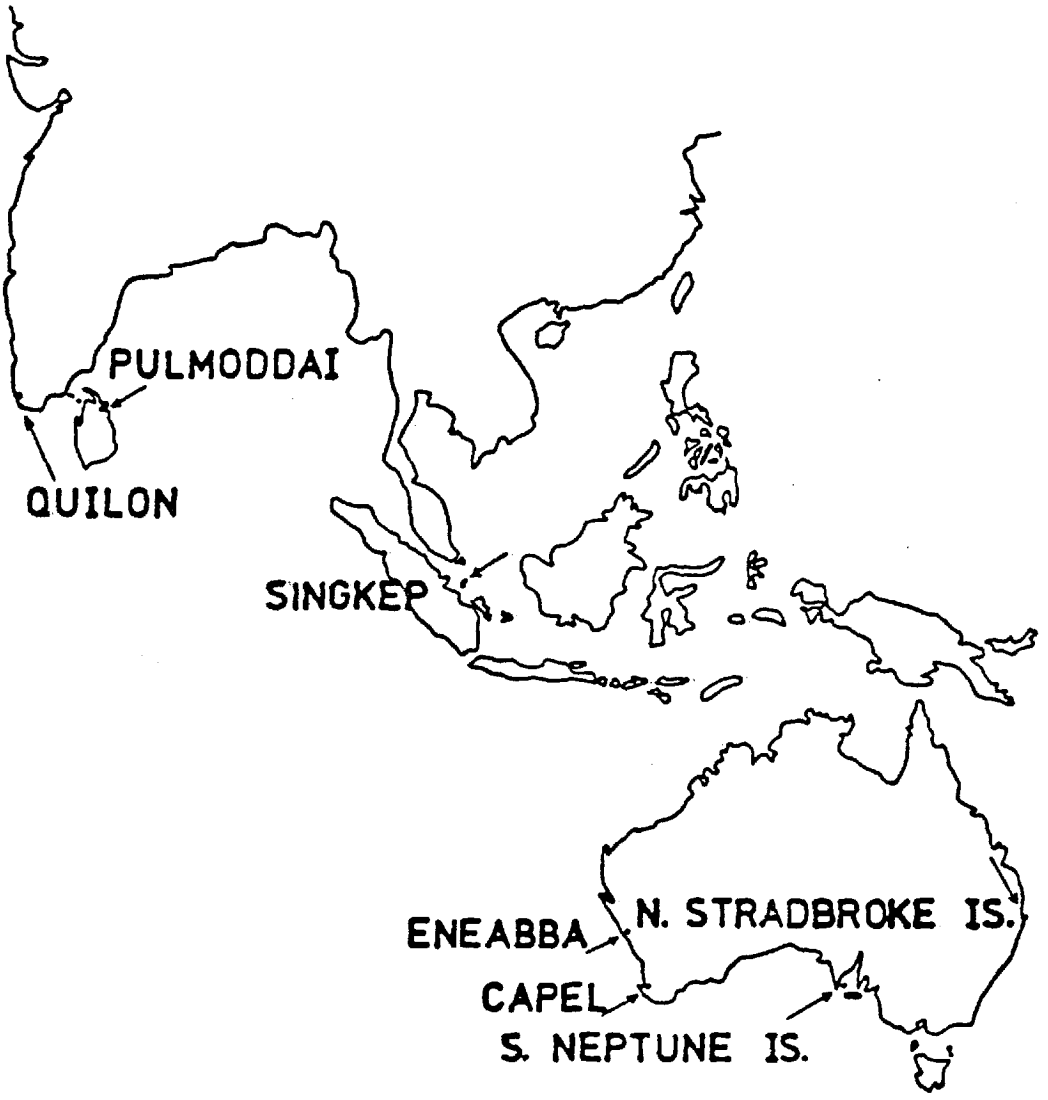

Fig. 12.1 Some occurrences of pseudorutile

conclusion is supported by the 3 nm granularity observed in specimens of pseudorutile by electron microscopy (A.K. Temple, 1966).

A feature of isotropic grains from pseudorutile-rich fractions examined in this study, both from Western Australia and Indonesia, is the presence of euhedral zircon crystals in very small quantity as inclusions within some of the grains. Both zircon and ilmenite crystallise at high temperatures in cooling igneous melts, and are among the first accessory minerals to form. The presence of such zircon inclusions is thus a pointer to the original high temperature (ilmenite) phase even when all detectable traces of ilmenite have been destroyed by alteration. No zircon inclusions have yet been reported for the South Australian pseudorutile, however.

12.2 Composition of pseudorutile

Table 12.1 compares the published chemical compositions of South Australian and Indonesian specimens with the analyses of the author's sample (5) of purified Indonesian pseudorutile.

Table 12.1

Composition of pseudorutile

Chemical Analysis Wt %	S.Aust. PSR (1)	S.Aust. PSR (2)	Ind. PSR (3)	Ind. PSR (4)	Ind. PSR (5)
TiO_2	62.05	58.84	64.01	63.02	62.2
Tot. Fe	(25.09)	(25.20)	(20.30)	(21.70)	(21.74)
Fe_2O_3	34.20	34.65	24.37	26.00	26.3
FeO	1.50	1.24	4.18	4.51	4.3
MnO	0.54	-	-	-	2.7
Mn_2O_3	-	0.60	2.36	2.87	-
MgO	-	-	-	-	0.03
Cr_2O_3	-	-	-	-	0.03
V_2O_5	-	-	-	-	0.05
Acid fusion insol.++	-	-	-	-	-
H_2O,OH^-*	-	3.24	2.56	2.08	-
Total	98.29	98.57	97.48	98.48	95.61

++ includes silica

* From wt. loss on heating to 800°C in air, corrected for oxidation of iron

(1) Larrett & Spencer, 1977. (2,3,4) Grey & Reid, 1975. (5) Tioxide International Ltd.

12.3 Stoichiometry of South Australian pseudorutile

Chemical and microprobe analyses (Larrett and Spencer, 1971) show that pseudorutile from South Neptune Island, South Australia, departs noticeably from the theoretical formula $Fe_2Ti_3O_9$. The specific gravity of this mineral is 4.2 and the specific susceptibility (χ) falls between 25 and 40 x 10^{-2} JT^{-2}kg^{-1}.

The published diffractogram for South Australian pseudorutile shows no detectable peaks for ilmenite or rutile, and the implication that these phases are absent is apparently supported by the chemical homogeneity of the grains (Larrett and Spencer, 1971). However, a mixture of 86% stoichiometric pseudorutile, 9% rutile and 5% ilmenite would yield a similar molecular formula ($Fe^{3+}_{1.71}\ Fe^{2+}_{0.13}\ Ti^{4+}_{3.15}\ O_9$) to that for the South Australian material ($Fe^{3+}_{1.74}\ Fe^{2+}_{0.09}\ Mn^{2+}_{0.03}\ Ti^{4+}_{3.16}\ O_9$). Such quantities of rutile and ilmenite would escape detection if they were X-ray amorphous.

12.4 Indonesian pseudorutile

Origin of sample: Six grams of pseudorutile from Singkep, Indonesia (Fig. 12.1) were provided by courtesy of Dr. K.J. Henley of AMDEL, Adelaide, South Australia. This pseudorutile occurs in cassiterite-bearing, water-logged (K.J.H.) alluvium and is associated with other heavy minerals including rutile, monazite and xenotime. The alluvium is processed by on-dredge jigging followed by magnetic and high-tension separation. The pseudorutile reports to the magnetic conductor fraction along with ilmenite.

The pseudorutile is believed to have been separated from the ilmenite in a Frantz isodynamic separator, and to be close in composition to a sample provided to Grey and Reid(1974) (Section 12.2).

Sample description: The grains lie chiefly in the size-range 200 - 600 μm and are mainly a dark brown colour, similar to Eneabba altered ilmenite and noticeably browner than the black, bulk ilmenite concentrate from Capel. The grains are sub-angular in shape and are less rounded than the Capel material, and a significant proportion

display a tabular, 'hexagonal' form, preserved from the original ilmenite, (Fig. 12.2). A few fawn grains with surface coatings of secondary rutile occur: other grains show only partial coatings. A very small amount of nearly black grains is also present.

Trace quantities of free silicate grains occur and, in addition, some pseudorutile grains carry surface inclusions of clear transparent or white translucent minerals. Many pseudorutile grains also carry fine to coarse globular surface encrustations of yellow sulphides (Fig. 12.3), or cusps where they have snapped off. The presence of these yellow sulphides has important genetic implications, since the reducing conditions which permitted their growth may also account for the almost complete alteration of the original ilmenite to pseudorutile, with minimal development of secondary rutile, (Fig. 12.4).

In polished section, the sulphides were identified as marcasite with minor pyrite, and the inclusions were identified as zircon and quartz. The identifications were confirmed by X-ray diffraction and EPMA.

The surfaces of the grains commonly carry cavities and indentations and a significant number of grains show a pseudo-cleavage of surficial grooves (Fig. 12.5). Ilmenite has no cleavage but can display partings on (0001) and $(01\bar{1}2)$: it is not known whether the grooves in the pseudorutile are related to these ilmenite partings.

EPMA slow scans for Ti, Mn and Fe showed that some pseudorutile grains were very uniform in composition, while others were variable. Although all grains examined were isotropic, slight inhomogeneity when examined in reflected light at high power was a common feature. These inhomogeneities may represent partially leached areas which are transforming to amorphous secondary rutile.

Point analyses calculated from EPMA (Microscan 5) results did not add up to 100% because of porosity (and probably absorbed moisture). Some analyses and their normalised equivalents are given in Table 12.2.

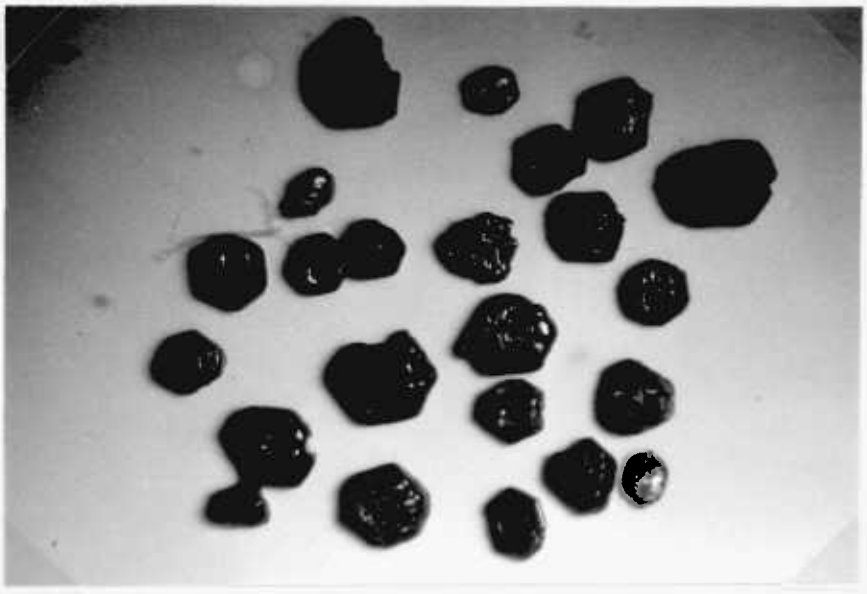

Fig. 12.2 Grains of Indonesian pseudorutile, pseudomorphous after 'hexagonal' ilmenite crystals

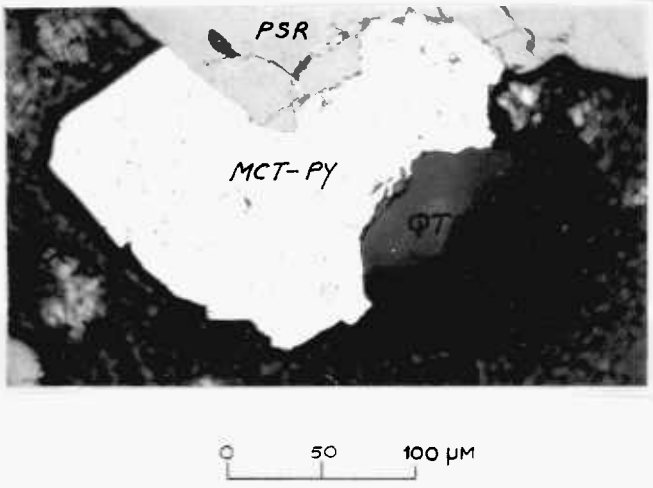

Fig. 12.3 Indonesian pseudorutile grain with overgrowth of marcasite-pyrite and cemented quartz grain



Fig. 12.4 Indonesian pseudorutile grain with streaks of relict pink ilmenite (IL) and a zircon inclusion (Zr). No secondary rutile is discernible.

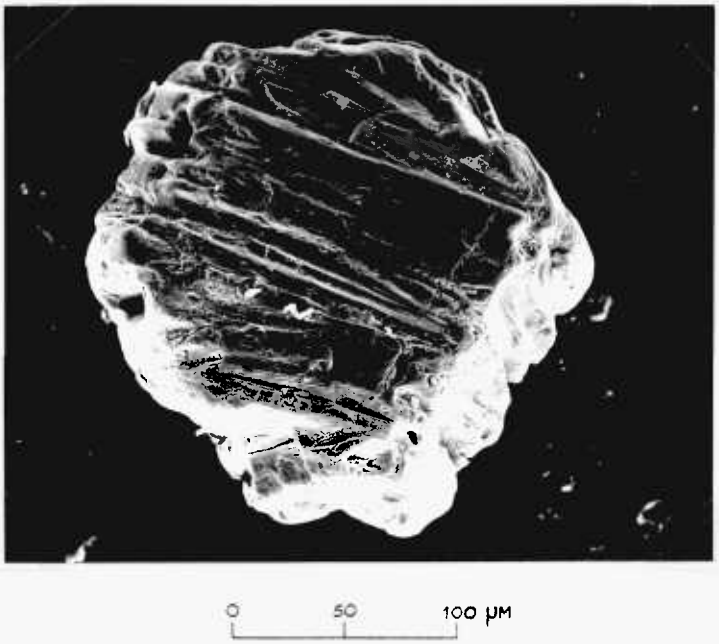

Fig. 12.5 Indonesian pseudorutile with grooved surface

Table 12.2

EPMA results for Indonesian pseudorutile

	Calculated Analyses					Normalised Analyses			
	TiO_2%	Tot.Fe as Fe_2O_3%	MnO%	Al_2O_3%	Total	TiO_2%	Tot.Fe as Fe_2O_3%	MnO%	Al_2O_3%
(1) Brown	67.5	23.8	1.9	1.2	94.4	71.5	25.2	2.0	1.3
(2) Black	68.3	26.5	1.6	0.8	97.2	70.3	27.3	1.6	0.8
(3) Black	56.3	36.2	3.6	0.2	96.3	58.5	37.6	3.7	0.2

Grains (1) and (2) are low in iron, and amorphous secondary rutile has probably started to form.

Grains carrying surficial secondary rutile were also examined by EPMA. Rim zones, and also replacement veins which traversed the grains, were shown to contain higher TiO_2 and significantly lower Fe and Mn than the core material. When examined under crossed polarisers, the secondary rutile showed the typical internal reflections.

X-ray diffraction: The XRD spectrum of a sample from which all visible sulphides, transparent minerals, and grains carrying surficial secondary rutile had been removed, is given in Fig. 12.6. Peak positions obtained from a slow scan at $\frac{1}{2}^{o}$ 2θ/min have been previously shown in Table 8.3.

The great similarity of the pseudorutile peak positions to those of rutile is brought out in Fig. 12.7, and it is easy to see how earlier investigators had difficulty detecting the presence of pseudorutile in altered samples containing ilmenite, hematite and rutile. The low crystallinity of Indonesian pseudorutile is suggested by the low intensity of the peaks; this also suggests the possible presence of a significant X-ray amorphous component.

A qualitative estimate from the purified sample, gained by inspection of the spectrum given in Fig. 12.6, is that 95% of the diffracting material consists of pseudorutile. Unfortunately insufficient sample was available to permit determination of the rutile and ilmenite content by XRD analysis of duplicate splits to which staged additions of these impurities had been made.

Measurements of the width of the main pseudorutile peak at half-height can be used to indicate the size of the X-ray diffracting particles (Cullity, 1956 p99,262). In this sample the crystallite size was estimated to be about 10 nm, a similar value to that found for pseudorutile in the Capel 0.45A magnetics.

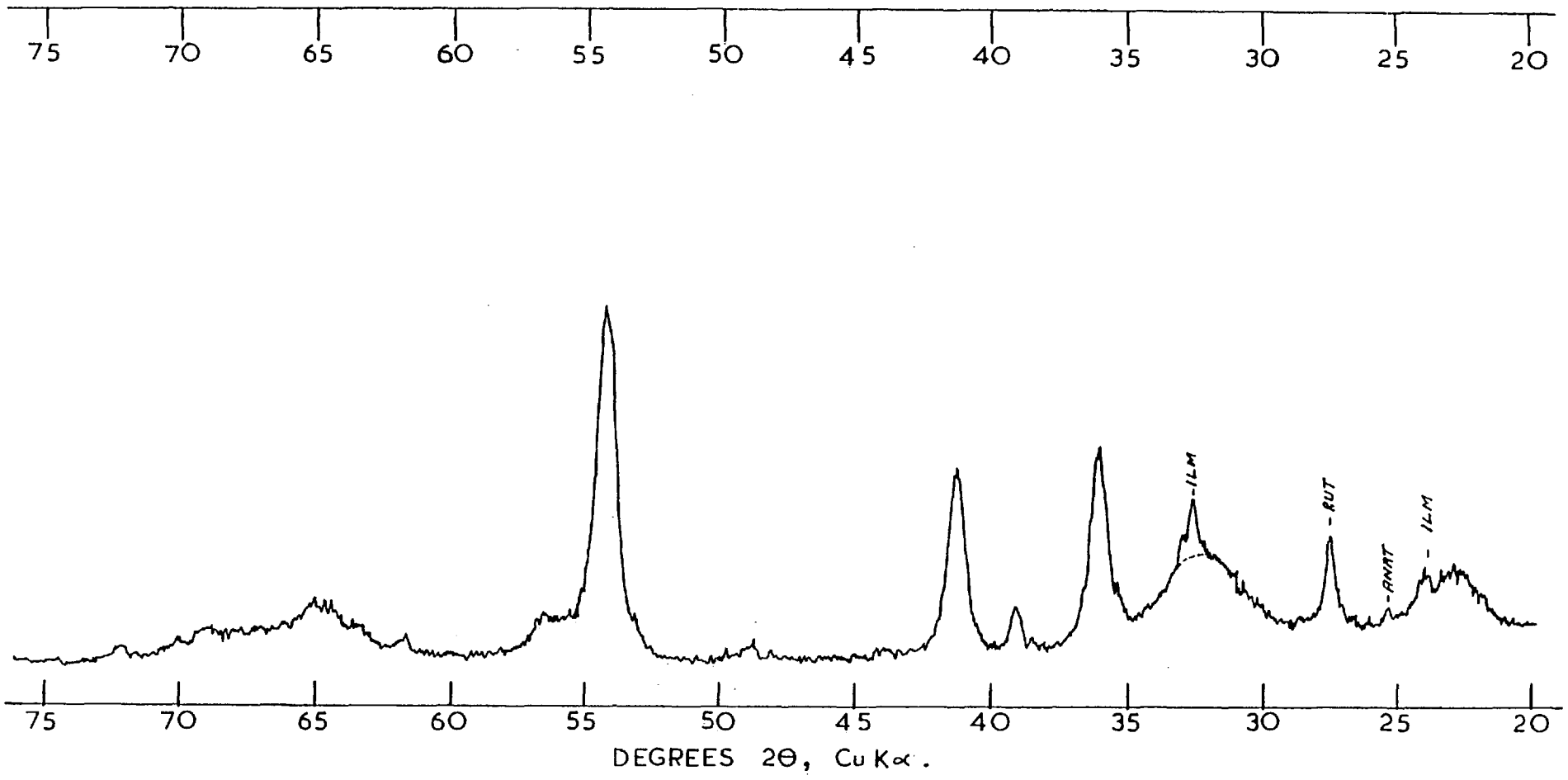

Fig. 12.6 XRD spectrum of Indonesian pseudorutile, from which grains carrying visible surficial secondary rutile have been removed.

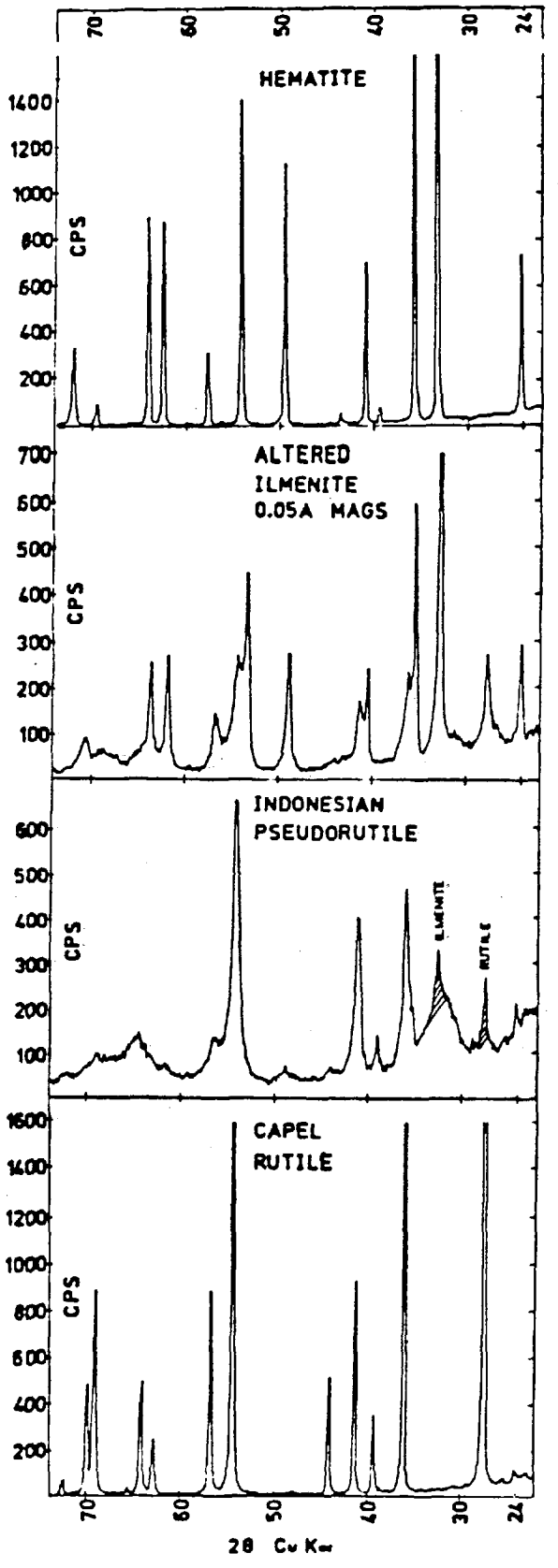

Fig. 12.7 Comparison of XRD spectra for hematite, ilmenite, pseudorutile and rutile

Stoichiometry: Pseudorutile specimens from different localities display differences in composition and in crystallinity; these features account partly for the observed differences in the chemical analyses and XRD spectra of the South Australian and the Indonesian pseudorutile. A published molecular formula $Fe^{3+}_{1.34}\ Fe^{2+}_{0.26}\ Mn^{3+}_{0.15}\ Ti^{4+}_{3.25}\ O_9 \cdot 0{\cdot}48H_2O$) for this Indonesian pseudorutile (Grey and Reid, 1975) does not include any correction for the presence of the ilmenite and rutile and consequently implies a lower degree of stoichiometry in the pseudorutile than is actually the case. The allocation of manganese (Table 12.1) to the trivalent state is also not unequivocal, since Mn has a wide range of possible valences, and it is very difficult to ascertain the oxidation state of this element in a solid phase. While Mn is known to be incorporated into the structure of many natural ilmenites, where it is divalent, much less is known about its valence once the ilmenite becomes largely altered to pseudorutile. However, it is unlikely that the Mn remains in a divalent state except in small areas of relict ilmenite. The high Mn-Fe ratio suggests that much of the Mn has in fact entered the pseudorutile structure, and no areas free of Mn could be detected by our EPMA.

Magnetic properties: The magnetic properties of pseudorutile were established by a combination of (a) magnetic susceptibility measurements, (b) neutron diffraction and (c) Mössbauer spectroscopy.

The room-temperature specific susceptibility of a cleaned sample, determined by the Gouy method (Section 6.3) at natural grain size was $34.5 \times 10^{-2} JT^{-2} kg^{-1}$, calculated using a determined density of 4.18. These results are similar to those published for South Australian pseudorutile (Section 12.3), and are supported by the observed distribution of pseudorutile in magnetic factions of Capel ilmenite (Tables 10.11, 10.12).

Susceptibility measurements (Fig. 12.8) made with an a.c. induction bridge (Section 6.5) showed an apparent magnetic ordering at $23^{\circ}K$. From the shape of the curve the mineral could be

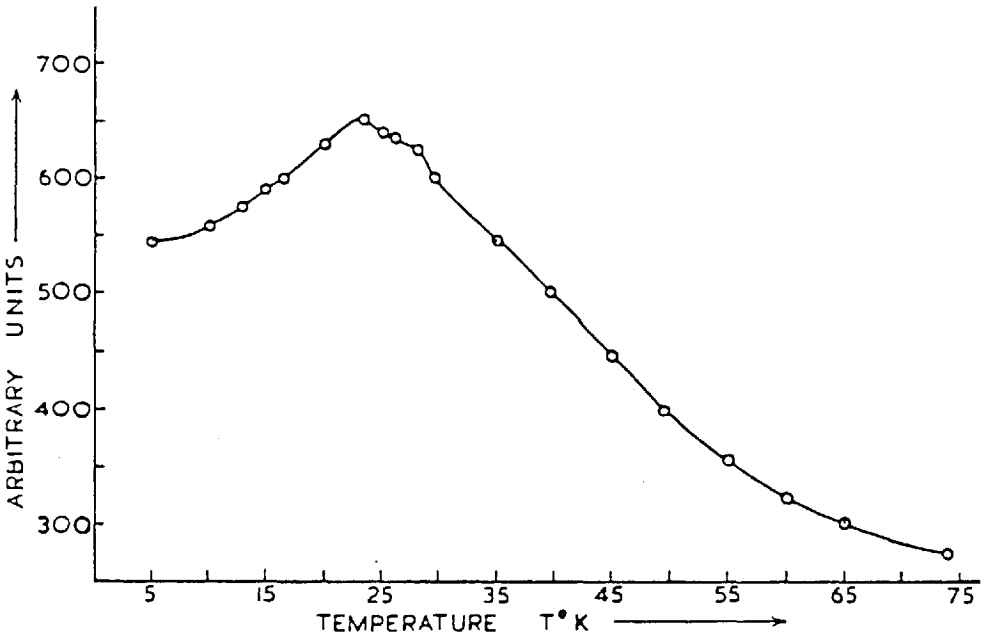

Fig. 12.8 Low-temperature susceptibility of Indonesian pseudorutile

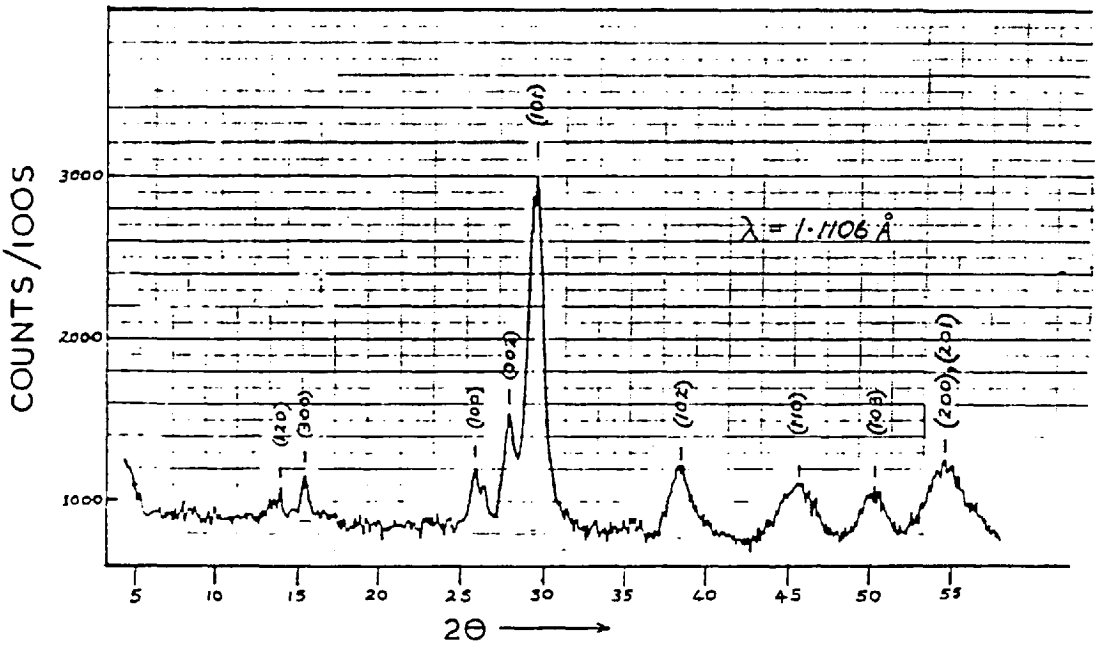

Fig. 12.9 Neutron diffraction spectrum of pseudorutile at 4°K

either antiferromagnetic, ferromagnetic or a magnetic spin-glass (Section 4.2). However, when ferromagnetic or anti-ferromagnetic materials are examined by neutron diffraction at temperatures below T_c or T_N, the spectra are visibly different from those obtained above the critical temperatures. If the magnetic cell is the same as the chemical cell, the intensity of certain peaks may be enhanced, as for magnetite (Bacon, 1955 p241). If the magnetic cell is larger than the chemical cell, then additional 'superlattice' lines of magnetic origin will appear, as in the case of ilmenite (Section 9.1). In the case of pseudorutile, the ND spectra obtained at 293°K, 80°K and 4.2°K were essentially identical (Fig. 12.9). These results indicate that the magnetic ordering which sets in at 23°K is insufficiently long range to produce coherent neutron diffraction from "superlattice" planes. This lack of long-range magnetic order is the chief characteristic of a magnetic spinglass.

Although the neutron diffraction spectrum of pseudorutile showed no increases in peak height or the appearance of magnetic superlattice lines below the magnetic ordering temperature of 23°K, two low-angle lines appear on the spectrum corresponding to crystal planes which do not contribute to the XRD spectrum.

By analogy with the two low-angle lines which similarly appear in the ND spectrum of ilmenite, even above its Néel point, the two low-angle lines are attributed to structure factor effects (Section 9.1). The ND spectrum of Fig. 12.9 is analysed in Table 12.3.

The structural space group has been shown to be $P6_322$ (Grey and Reid, 1975) but the iron and titanium atoms were not distinguished in the averaged structural model employed, and so the individual distributions of Fe and Ti for each occupied metal site in the structure are not known. This does not prevent structure factors (F), and hence relative diffraction peak intensities, from being calculated for XRD since the X-ray scattering amplitudes for Fe and Ti are close in value. For

Table 12.3

Neutron diffraction spectrum of pseudorutile

hkl	ASTM dÅ *	Calc. 2θ**	Obs. d	Obs. 2θ	Obs. I/I_1
120	-	13.57	4.55	14.0	10
300	-	15.38	4.12	15.5	13
$(111)^+$	3.85 d	16.59	-	-	-
$(140,131)^+$	2.77 d	23.13	-	-	-
100	2.489	25.78	2.48	25.9	17
002	2.297	27.97	2.30	27.9	33
101	2.187	29.42	2.18	29.5	100
102	1.688	38.41	1.688	38.4	21
$(261)^+$	1.630 d	39.84	-	-	-
$(081,123)^+$	1.470 d	44.39	-	-	-
110	1.436	45.50	1.433	45.6	17
$(181)^+$	1.380 d	47.46	-	-	-
103	1.304	50.41	1.306	50.3	16
200	1.244	53.02	1.210	54.6	25
201	1.200	55.13			

d diffuse lines
** calculated for λ = 1.1106 Å
* ASTM 19-635 PSEUDORUTILE
+ possible contributing planes

Table 12.4

Measured parameters in Fe^{57} Mössbauer effect spectra for pseudorutile

	Ion type	Peak type	Temp °K	I.S. mm/s	Q.S. mm/s	Abs'n.Area %
Pseudorutile	Fe^{2+}	S	293	1.516(16)	0	8.7(8)
	Fe^{3+}	D	"	0.379(1)	0.628(2)	91.3(8)
	Fe^{2+}	D	80	1.256(19)	1.884(33)	23.53(192)
	Fe^{3+}	D	"	0.479(2)	0.647(3)	76.47(73)
	Fe^{3+}	H	4.2	0.460(20)	0.125(38)	100 ± 21

S = singlet
D = doublet
H = 6 peaks

neutron scattering however, the scattering amplitudes are very different (b_{Fe} = 0.96 x 10^{-12}cm, b_{Ti} = -0.38 x 10^{-12}cm), and structure factors cannot be calculated unless the individual Fe and Ti positions are known.

Five medium to low-intensity, broad reflections which occur in the XRD spectrum of pseudorutile, do not appear in the ND spectrum. Grey and Reid(1975) ascribe these reflections to poor ordering of metal atoms on layers of the cell having odd values of l.

Further information on the nature of the magnetic ordering in pseudorutile could be obtained by polarised neutron diffraction, but unfortunately attempts to arrange for this within the study period were not successful.

Mössbauer spectroscopy (Section 9.2) yielded further data however, and spectra obtained at 293°K and 80°K show a simple ferric ion doublet with a very minor contribution from ferrous ions (Fig. 12.10,12.11). The 293°K spectrum was fitted with a ferrous singlet (Table 12.4) but this was resolvable into a doublet with a large quadrupole split at 80°K. At 4°K, a noisy but distinctly ordered magnetic 6-fingered spectrum (Fig. 12.12) was obtained: this supports the magnetic ordering temperature (T_F) noted at 23°K. The calculated magnetic hyperfine field of 45.2T is compared with the hyperfine fields of other iron oxide minerals in Table 12.5.

The neutron diffraction results and supporting magnetic susceptibility and Mössbauer spectroscopic data, indicate that pseudorutile is a naturally occurring example of a magnetic spinglass. Spinglasses are recognised as being a much more common class of magnetic material than previously suspected (Section 4.2).

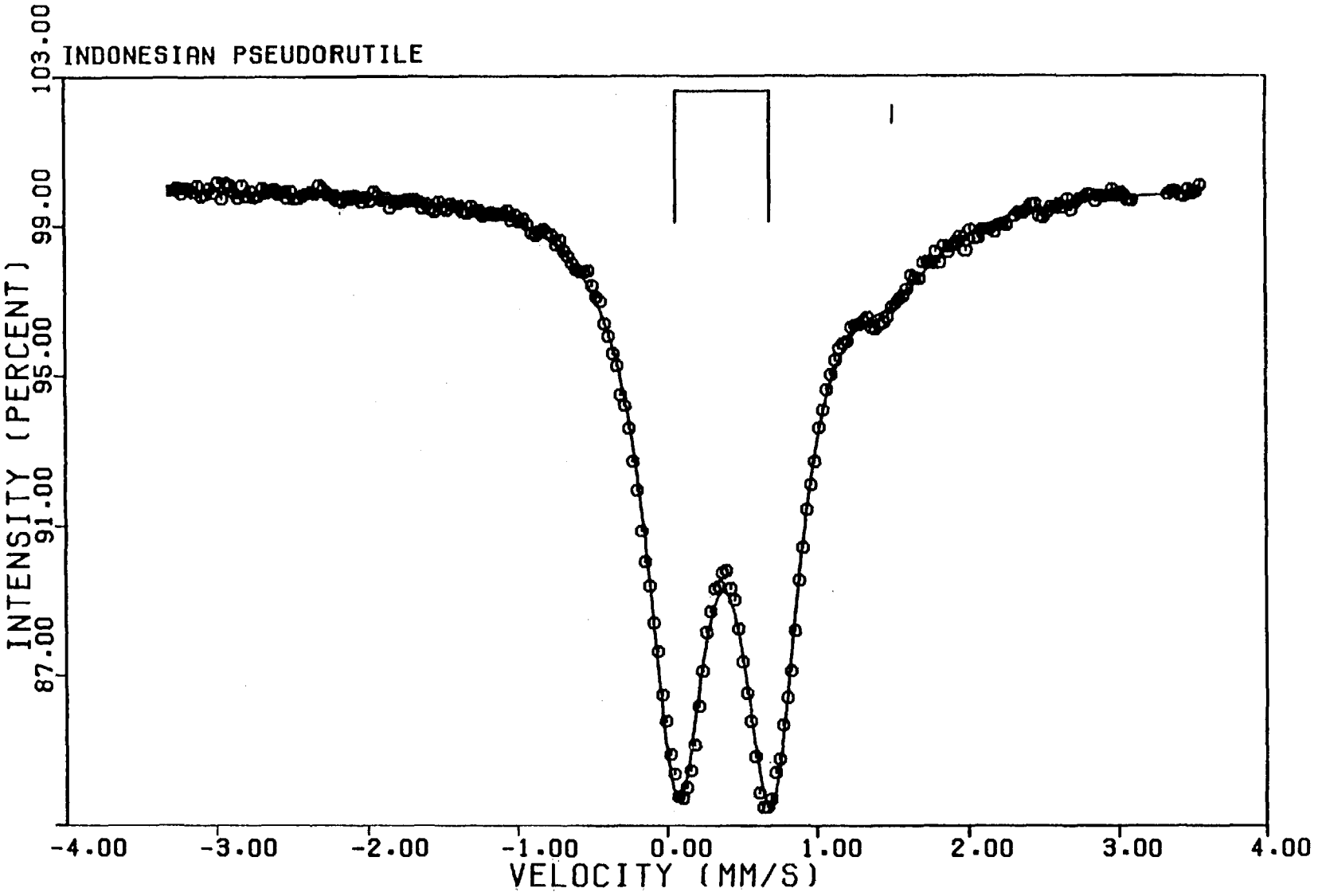

Fig. 12.10 Mössbauer spectrum of Indonesian pseudorutile at 293°K

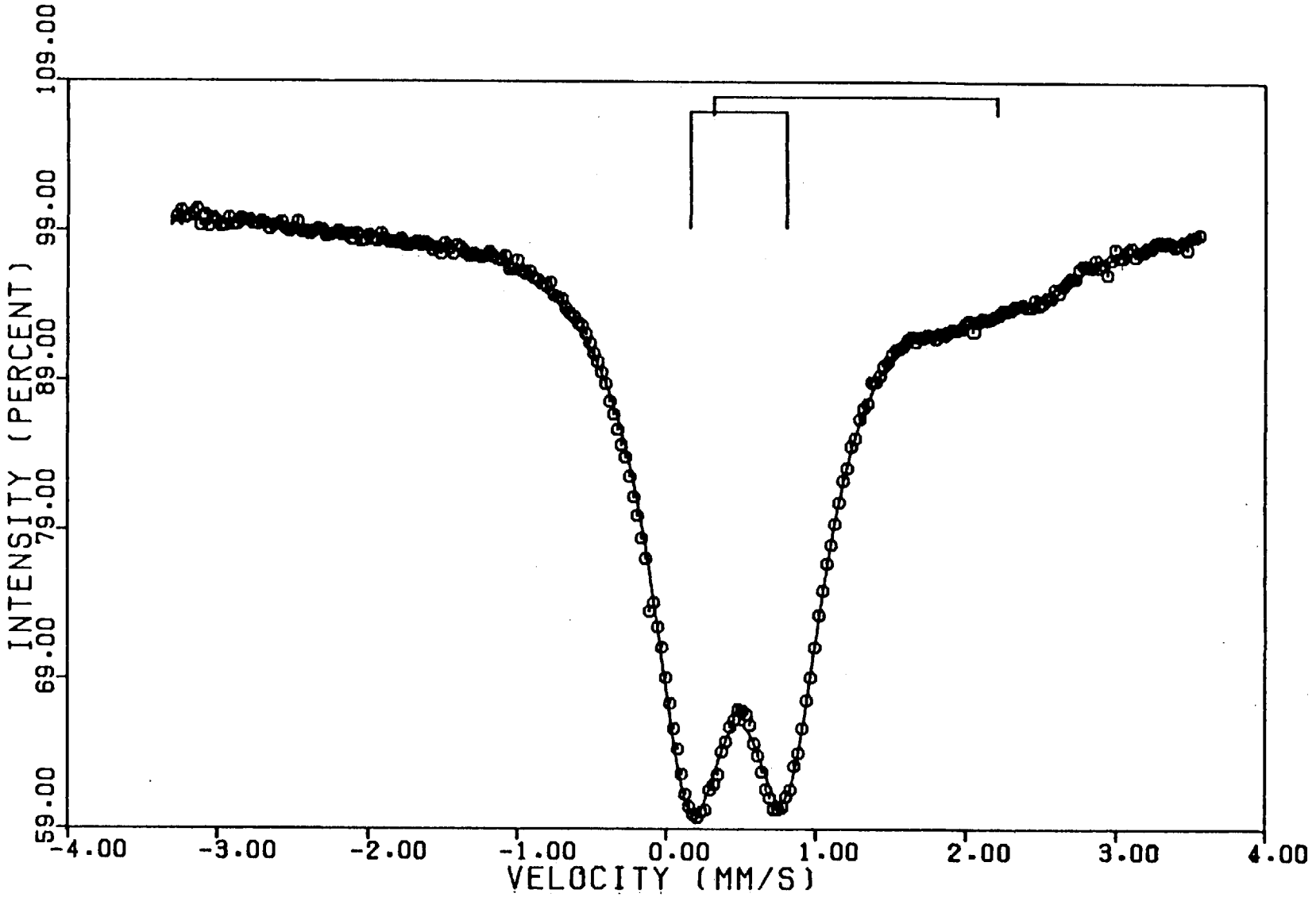

Fig. 12.11 Mössbauer spectrum of Indonesian pseudorutile at 80°K

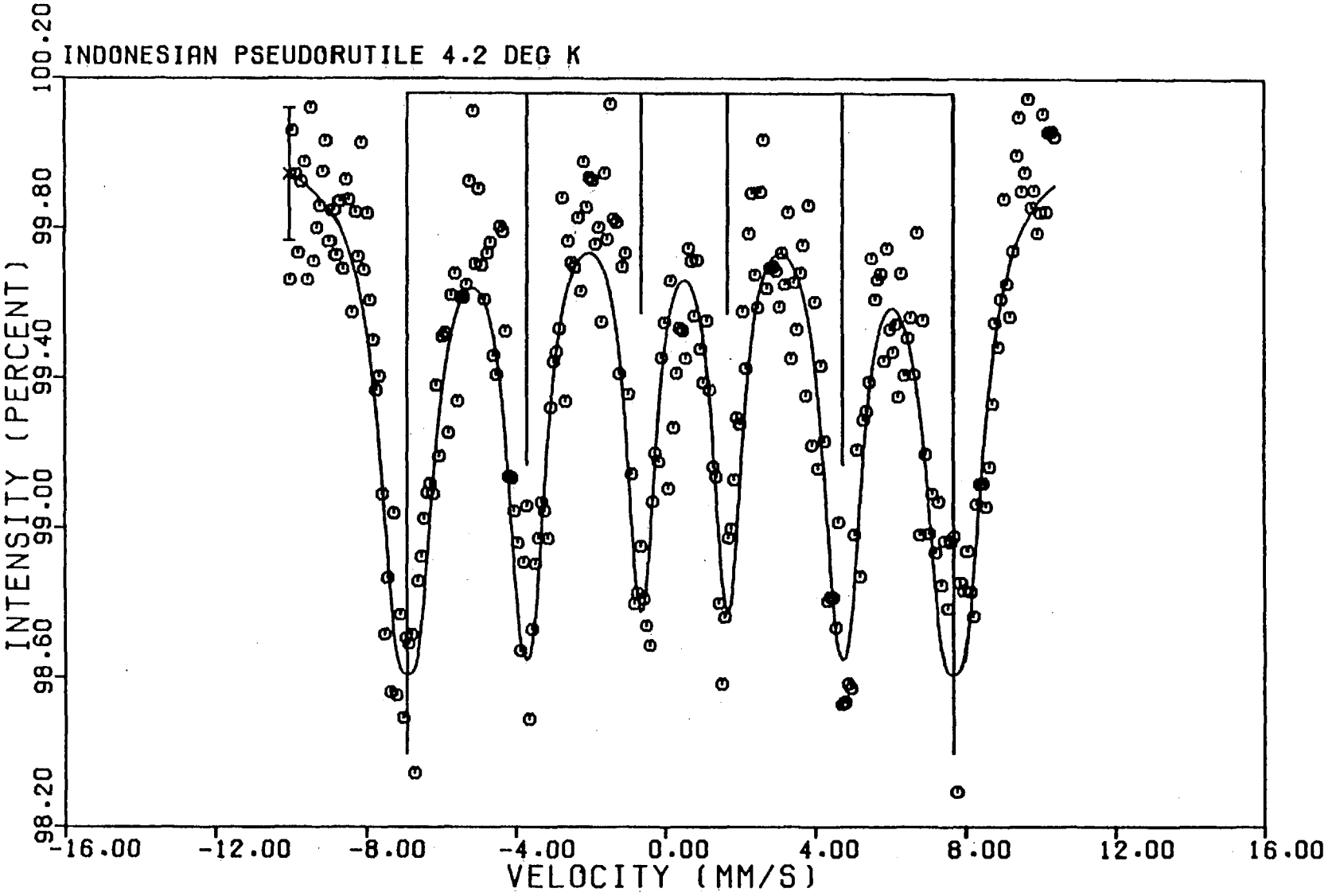

Fig. 12.12 Mössbauer spectrum of Indonesian pseudorutile at 4.2°K

Table 12.5 Magnetic hyperfine fields (H) of iron-bearing oxide minerals

Mineral	H. Tesla	Temp°K
*α-Fe_2O_3	(51.5 (54.4	298 0
*γ-Fe_2O_3	48.8-49.9	293
* Fe_3O_4	49.1 'A' site) 45.3 'B' site)	300
Fe TiO_3	(-) 43 $\pm$ 3(H_{INT}) (-) 47	5(Grant et al,1972) 4.2(Ito and Morimoto, 1973)
$Fe_2Ti_3O_9$	45.2	4.2

*Data taken from Greenwood and Gibb,(1971).

CHAPTER 13

CONCLUSIONS

In the course of this study, many of the published observations on detrital ilmenite and pseudorutile have been confirmed. The chemical composition and mineralogical content of the weathered ilmenite in heavy mineral sands from various deposits will clearly differ. These differences do not mask the underlying basic course of the ilmenite alteration process, nor significantly affect the ultimate product of the alteration which is normally secondary rutile.

Thus, the techniques employed and the results obtained in this study of material from two Western Australian detrital deposits will nevertheless be applicable to many other similar deposits.

The reported magnetic susceptibility anisotropy of ilmenite has been confirmed using a natural single crystal of known composition from Kenya. The shape and intensity of the curve for $\chi_{\perp}$ are significantly different from that given by Bizette and Tsai (1956), however. In addition, curves for both $\chi_{\parallel}$ and $\chi_{\perp}$ have been found to have an unusual shape below 10°K, and this feature remains to be explained.

A synthetic ilmenite, used as a reference for the magnetic properties and XRD spectrum of ilmenite, has been shown to have a specific susceptibility that agrees with the published value, and a (Mössbauer) Néel point within a few degrees of the published value. The XRD peak positions differ slightly and the peak intensities differ markedly from ASTM 3-0781 but are in closer agreement with data given by Brown(1961). Low-angle peaks that appear in the neutron diffraction spectrum of ilmenite but not in its XRD spectrum have been shown to be due to structure factor effects. Errors in published reflection indices have been corrected.

For ilmenite from the South Capel deposit, the fractions with highest susceptibility are more highly altered and have higher Fe_2O_3 analyses than fresher, less altered ilmenite from the same deposit. XRD peak shifts, Curie points below 70°K, magnetic orientation effects, chemical analyses and EPMA identification of minor amounts of exsolved titanhematite, have shown that the high susceptibility and qualitatively ferromagnetic behaviour are due to small amounts of hematite (Fe_2O_3) in solid solution in the ilmenite.

The magnetic orientation effects demonstrated by XRD also provide supporting evidence for previously reported topotaxial relative orientations determined by single-crystal XRD methods.

Paramagnetic fractions of the South Capel ilmenite have essentially only three phases present, permitting meaningful mineral contents to be calculated for each fraction. Average magnetic susceptibilities calculated from the normative contents agree well with measured susceptibilities.

The ilmenite concentrate from the southern part of the Adamson deposit at Eneabba is very much more altered than the ilmenite from the South Capel deposit, and consists mainly of pseudorutile. High, field-dependent susceptibilities are due to the presence of small amounts of ferrimagnetic ilmenite-hematite solid solutions (as at Capel) and the ferrimagnetism was clearly manifested by XRD on magnetically-oriented grains. As at Capel, distinctive pitted textures are ascribed to the leaching out of trains of exsolved titanhematite blebs. These pitted textures are more abundant in the Eneabba ilmenite than the Capel ilmenite.

The success in correlating magnetic behaviour with chemical and mineralogical composition, where previous studies have failed, is ascribed to the preparation of fractions of comparatively small magnetic susceptibility range by using small electromagnet current increments, particularly in the low-current (high susceptibility) region.

A qualitative geometrical model for ilmenite alteration has been outlined which accounts for features such as poor crystallinity, optical isotropy and X-ray amorphism, compatible with the published suggestion of the initial dissolution and re-precipitation of TiO_2 gel (Grey and Reid,1975) during the transformation of pseudorutile to secondary rutile.

The reason why pseudorutile has formed extensively in some deposits, with only minimal development of secondary rutile, is not known.

Pseudorutile has been shown to be a naturally-occurring example of a magnetic spinglass and was the first mineral to be specifically allocated to the spinglass group. Previously published observations of certain hematite-ilmenite solid solutions include features of the spinglass type of behaviour; more recently ferric pseudobrookite has been shown to be an anisotropic spinglass.

Indonesian pseudorutile has a density and specific susceptibility close to values published for South Australian specimens, and has a maximum susceptibility at $T_f = 23^{\circ}K$. The optical isotropism of pseudorutile is ascribed to the fine grain size, approximately 10 nm. Reinterpretation of work by Lynd et al(1954) clearly indicates that the then unknown mineral pseudorutile was contributing to the XRD spectra they obtained. Two low angle lines present in the ND spectrum but not the XRD spectrum of pseudorutile have been explained as due to structure factor effects by analogy with ilmenite. The new data support previously published work and indicate that despite earlier lack of acceptance, pseudorutile is indeed a valid mineral species.

Free chromite reports chiefly to the $\chi = -46 + 37 \times 10^{-2} JT^{-2} kg^{-1}$ specific susceptibility fraction at Capel. This explains its low level in the commercial 'primary' ilmenite containing grains mainly with $\chi > 60 \times 10^{-2} JT^{-2} kg^{-1}$. At Eneabba the chromite shows much higher values for magnetic susceptibility and this accounts for the relatively high Cr_2O_3 analysis of the concentrate examined.

The Chung matrix-flushing method of quantitative XRD has been shown to be valuable for demonstrating the trend of progressive changes in mineral content occurring in natural mineral alteration processes. Such processes tend to result in secondary products of variable and sometimes poor crystallinity, and this feature limits the precision of the Chung method when applied to such materials. The advantage of the method is that it permits estimation of the amount of amorphous material, quantification of which is a necessarily important part of a meaningful explanation of ilmenite alteration.

The effect of compositional variations on the magnetic anisotropy of natural ilmenite and on the magnetic properties of pseudorutile remain to be investigated, particularly the influence of manganese.

Although ilmenite concentrates produced from particular detrital heavy mineral deposits each have their own characteristic mineralogical and chemical properties, many of their features are shared in common. This work shows that a correlation may be established between the mineralogical, chemical and magnetic properties of the constituent mineral grains, thus opening the way for improved selectivity of the separation processes and hence for improved product quality control.

BIBLIOGRAPHY

Allen, V.J. 1956. Is leucoxene always finely crystalline rutile? Econ. Geol., 51, 830-833.

Abras, A. and Mansur, R.A. 1975. Application of the Mössbauer Effect to the Study of Brazilian Ilmenites. in Int. Conv. Mossb. Spectr., A.E.C., Poland, Cracow, 135-136.

Angus, W.R. and Hill, W.K., 1943. Magnetochemical Investigations Part I. Introduction and Experimental Technique. Trans. Faraday Soc., 39, 185-190.

Bacon, G.E. 1955. Neutron Diffraction. Oxford University Press, London.

Bailey, S.W., Cameron, E.N., Spedden, H.R., and Weege, R.J. 1956 The Alteration of Ilmenite in Beach Sands, Econ. Geol., 51, 263-279.

———— , ————. 1957. Is leucoxene always finely crystalline rutile - a reply. Ibid., 52, 716-720.

Baker, G. 1962. Detrital Heavy Minerals in Natural Accumulates. Monograph Series No. 1, Aus. I.M.M., Melbourne.

Banerjee, S.K. 1963. Magnetic Properties of Rocks and Minerals. Ph.D. Thesis, Univ. of Cambridge, 156 pp.

Barth, T.F.W. and Posnjak, E. 1934. The crystal structure of ilmenite. Zeit. für Krist., 88, 265-270.

Baxter, J.L. 1977. Heavy Mineral Sand Deposits of Western Australia. Geol. Surv. W. Australia, Min. Res. Bull. 10.

Beck, P.A. 1978. Properties of Mictomagnets (Spinglasses). Progr. in Mat. Sci., 23, 1-49.

Birss, R.R. 1964. Symmetry and Magnetism. North-Holland Publishing Co., Amsterdam.

Bizette, H. and Tsai, B. 1956. Susceptibilités magnétiques principales d'un cristal naturel d'ilménite $TiFeO_3$. Comptes Rendus. Acad. Sci. 2me Partie, 242 2124-2127.

Bloss, F.D. 1971. Crystallography and Crystal Chemistry. Holt, Rinehart and Winston, New York.

Brown, R.N., Riley, J.F. and Schultz, P.K. 1970. Contributions to Australasian Mineralogy 1. A New Zinc-Bearing Ilmenite from Broken Hill. Amdel Bull., No. 10, 48-50.

Buddington, A.F., Fahey, J. and Vlisidis, A. 1963. Degree of oxidation of Adirondack iron oxide and iron-titanium oxide minerals in relation to petrogeny. J. Petrol., 4, 138-169.

Canella, V. and Mydosh, J.A. 1972. Magnetic Ordering in Gold-Iron Alloys. Phys. Rev. B., 6, 4220-4237.

Carmichael, C.M. 1959. Remanent Magnetism of The Allard Lake Ilmenite. Nature, 183, 1239-1241.

———————, 1961. The Magnetic Properties of Ilmenite-Hematite Crystals. Proc. Roy. Soc. Lond. A263, 508-530.

Carrol, D. 1960. Ilmenite Alteration Under Reducing Conditions in Unconsolidated Sediments. Econ. Geol., 55, 618-619.

Chevallier, R. 1953. Constitution de l'ilménite paramagnétique. Bull. Soc. Chim. de France, 5, 973-974.

Chung, F.H. 1974a. Quantitative Interpretation of X-ray Diffraction Patterns of Mixtures. I.Matrix Flushing Method for Quantitative Multicomponent Analysis. J. Appl. Cryst., 7, 519-525.

———————, 1974b Idem. II Adiabatic Principle of X-ray Diffraction Analysis of Mixtures. Ibid. 526-531.

Clark, H.C. 1967. A Fused-Quartz Curie-Point Balance. in Methods in Palaeomagnetism. Nato Adv. Study Inst., Elsevier, 438-439.

Crangle, J. 1977. The Magnetic Properties of Solids. Edward Arnold, London.

Cullity, B.D. 1956. Elements of X-ray Diffraction. Addison-Wesley, London.

———————, 1972. Introduction to Magnetic Materials. Addison-Wesley, London.

Curnow, C.E., and Parry, L.G. 1954. Oxidation Changes in Natural Ilmenite. Nature, 174, 1101.

Dimanche, F. and Bartholomé, P. 1976. The Alteration of Ilmenite in Sediments. Minerals Sci. Engng., 8, 187-201.

Doell, R.R. and Cox, A. 1967. Recording Magnetic Balance. in Methods in Palaeomagnetism. Nato. Adv. Study. Inst., Elsevier, 440-444.

Edwards, S.F. and Anderson, P.W. 1975. Theory of Spin Glasses. J. Phys. F: Metal Phys., 5, 965-974.

Edwards, A.B. 1942. The chemical composition of leucoxene in Cainozoic bauxite from Boolarra, Victoria. Min. Mag., 26, 273-274.

———————, 1960. Textures of The Ore Minerals and Their Significance, Aus. I.M.M., Melbourne.

Elsdon, R. 1975. Iron-Titanium Oxide Minerals In Igneous And Metamorphic Rocks. Minerals Sci. Engng., 7, 48-70.

Fleischer, M. 1964. New Mineral Names. Am. Mineral., 49, 1774.

———————, 1967. New Mineral Names. Ibid. 52, 299-300.

Flinter, B.H. 1959. The Alteration of Malayan Ilmenite Grains and The Question of Arizonite. Econ. Geol., 54, 720-729.

———— , 1960. Malayan Ilmenite vs Arizonite. Ibid. 55, 1068-1070.

Foner, S. 1959. Versatile and Sensitive Vibrating-Sample Magnetometer. Rev. Sci. Instr. 30, 548-557.

Ford, W.E. 1966. Dana's Textbook of Mineralogy, 4th Editn. John Wiley & Sons, London.

Gibb, T.C., Greenwood, N.N. and Twist, W. 1969. The Mössbauer Spectra of Natural Ilmenites. J. inorg. nucl. chem., 31, 947-954.

Golding, H.G. 1961. Leucoxene Terminology and Genesis. Econ. Geol., 56, 1138-1149.

Goodenough, J.B. and Stickler, J.J. 1967. Theory of the Magnetic Properties of the Ilmenites M TiO_3. Phys. Rev., 164, 768-778.

Grant, R.W., Housley, R.M. and Geller, S. 1972. Hyperfine Interactions of Fe^{2+} in Ilmenite. Phys. Rev. B. 5, 1700-1703.

Greaves, E.D. 1979. Mössbauer Effect and Nuclear Resonance in Lateritic Minerals. Ph.D. Thesis, Univ. of London.

Grey, I.E. and Reid, A.F. 1972. Shear Structure Compounds $(Cr,Fe)_2 Ti_{n-2}O_{2n-1}$ derived from the α-PbO_2 Structural Type. J. Sol. State Chem., 4, 186-194.

————. 1974. Reaction sequences in the reduction of ilmenite: 3—reduction in a commercial rotary kiln; an X-ray diffraction study. Trans. Inst. Min. Metall., 83, C39-46.

———— , 1975. The Structure of Pseudorutile and Its Role in The Natural Alteration of Ilmenite. Am. Mineral. 60, 898-906.

Gruner, J.W. 1959. The Decomposition of Ilmenite. Econ. Geol. 54, 1315-1316.

Haggerty, S.E. 1976. Oxidation of Opaque Mineral Oxides in Basalts. in Oxide Minerals. Mineral. Soc. Am., Short Course Notes., 3, Ed. D. Rumble III, Hg1-100.

Hartman, J.A., 1959. The titanium mineralogy of certain bauxites and their parent minerals. Econ. Geol., 54, 1380-1405.

Hess, H.H. 1959. Notes on Operation of Frantz Isodynamic Separator. S.G. Frantz Co., Inc. New Jersey, U.S.A.

Ishikawa, Y. 1958. An Order-Disorder Transformation Phenomenon in the $FeTiO_3$-Fe_2O_3 Solid Solution Series. J. Phys. Soc. Japan, 13, 828-837.

———— and Sawada, S. 1956. The Study on Substances having the Ilmenite Structure. I. Physical Properties of Synthesised $FeTiO_3$ and $NiTiO_3$ Ceramics. Ibid. 11, 496-501.

Ishikawa, Y. and Akimoto, S. 1957. Magnetic Properties of the $FeTiO_3$-Fe_2O_3 Solid Solution Series. Ibid. 12,1083-1098.

———— , ————, 1958. Magnetic Property and Crystal Chemistry of Ilmenite ($MeTiO_3$) and Hematite (Fe_2O_3) System.I. Crystal Chemistry. Ibid., 13, 1110-1118:II.Magnetic Property. Ibid. 13, 1298-1310.

Ito, A. and Morimoto, S. 1973. Electronic Properties of Fe^{2+} in $MTiO_3$. *in* 5th Int. Conv. Mossb. Spectr., Czech. A.E.C., Bratislava. Part 1, 161-166.

Jones, D.G. 1973. Reaction sequences in the reduction of ilmenite: 2-gaseous reduction by carbon monoxide. Trans. Inst. Min. Metall., 82,C186-192.

———— , 1974. Optical microscopy and electron-probe micro-analysis study of ilmenite reduction. Ibid. 83,C1-9.

Karkhanavala, M.D. 1959. The Nature of Arizonite. Econ. Geol. 54, 1302-1308.

———— and Momin, A.C. 1959. The Alteration of Ilmenite. Ibid. 54, 1095-1102.

———— , ———— and Rege, S.G. 1959. An X-ray Study of Leucoxene from Quilon, India. Ibid. 54, 913-918.

Klug, H.P. and Alexander, L.E. 1974. X-ray diffraction procedures, 2nd Edn. Wiley, New York.

Krishnan, K.S. and Mookherji, A. 1936. The Magnetic Anisotropy of Copper Sulphate Pentahydrate $CuSO_4.5H_2O$ in Relation to its Crystal Structure Part I. Phys. Rev. 50, 860-863.

———— , ———— . 1938a. Ibid. Part II. Phys. Rev. 54, 533-539.

———— , ———— . 1938b. Ibid. Part III. Phys. Rev. 54, 841-845.

Larrett, M.J.W. and Spencer, W.G. 1971. Contributions to Australasian Mineralogy: 3. "Pseudorutile" from South Neptune Island, South Australia. Amdel Bull. No. 12.Oct. 74-80.

Larochelle, A. 1961. Design of A Curie Point Meter. Bull. 69, Geol. Surv. Can., Dept. Mines & Tech. Surveys, 18pp.

Lee, E.W. 1963. Magnetism. Penguin Books, U.K.

Lipson, H. and Steeple, H. 1970. Interpretation of X-ray powder diffraction patterns. MacMillan, London.

Lissiman, J.C. and Oxenford, R.J. 1975. Eneabba Rutile-Zircon-Ilmenite Sand Deposit, W.A. 1062-1070 in Economic Geology of Australia and Papua-New Guinea 1 Metals. Monograph 5, Aus. I.M.M., Melbourne.

Lynd, L.E. 1960a. Study of the Mechanism and Rate of Ilmenite Weathering. Trans. AIME, Soc. Mining Engrs., 217, 311-318.

———— , 1960b. Alteration of Ilmenite. in Discussions, Econ. Geol., 55. 1064-1068.

———— , Sigurdson, H., North, C.H. and Anderson, W.W. 1954. Characteristics of Titaniferous Concentrates. Trans. AIME, Mining Engng., 817-824.

Lindsley, D.H. 1976a. The Crystal Chemistry and Structure of Oxide Minerals as Exemplified by the Fe-Ti Oxides. L1-60 in Oxide Minerals, Short Course Notes 3. Mineral. Soc. Am., Ed. D. Rumble III.

———— , 1976b. Experimental Studies of Oxide Minerals. L61-88. Ibid.

McAndrew, J. 1957. Calibration of a Frantz Isodynamic Separator and its Application to Mineral Separation. Proc. Aus. I.M.M. No. 181, 59-73.

Mulay, L.N. 1963. Magnetic Susceptibility. (Reprint), Interscience (John Wiley).

Nagata, T. 1961. Rock Magnetism. Revised Edn., Maruzen Co. Ltd., Tokyo (Plenum Press, New York).

———— , and Akimoto, S. 1956. Magnetic Properties of Ferromagnetic Ilmenites. Geofisca Pura e. Applic., 34, 36-50.

———— , ———— , and Uyeda, S. (1953). Self-Reversal of Thermo-Remanent Magnetism of Igneous Rocks III. J. Geomag. Geoelect., 5, 168-184.

———— , Yukutake, T., ———— . 1957. On Magnetic Susceptibility of Olivines. J. Geomag. Geoelect., 9, 51-56.

Nairn, P.R. 1965. Comparison of Ore Dressing Methods Used by Ilmenite Producers in Western Australia. Proc. Aus. I.M.M. No. 213, 175-196.

Néel, L. and Pauthenet, R. 1952. Étude thermomagnétique d'un monocrystal de Fe_2O_3 . Comptes Rendus Acad. Sci., 234, 2172-2174.

Neumann, E.R. 1974. The Distribution of Mn^{2+} and Fe^{2+} Between Ilmenites and Magnetites in Igneous Rocks. Am. J. Science, 274, 1074-1088.

Newnham, R.E. 1974. Domains in Minerals. Am. Mineral., 59, 906-918.

Norton, A.E. 1976. An Investigation of the Magnetic Properties of a Norwegian Ilmenite. Unpub. Dissertation, Mineral Technology Dept., Royal School of Mines, London.

Overholt, J.L., Vaux, G. and Rodda, J.L. 1950. The Nature of "Arizonite". Am. Mineral., 35, 117-119.

Parasnis, D.S. 1961 Magnetism. Hutchinson, London.

Parks, G.A. and Akhtar, S. 1968. Magnetic Moment of Fe^{2+} in Paramagnetic Minerals. Am. Mineral., 53, 406-415.

Pillinger, W.L., Jastram, P.S., and Daunt, J.G. 1958. Electronic a.c. Mutual Inductance Bridge for Measuring Small Susceptibilities at Low Temperatures. Rev. Sci. Instr., 29, 159-162.

Rao, A.T. 1978. Magnetic Chromites From Kondapilli, Andhra Pradesh, India. Mineral. Mag. 42, No. 323, M38-39.

Raymond, K.N. and Wenk, H.R. 1971. Lunar Ilmenite (Refinement of the Crystal Structure). Contr. Mineral and Petrol., 30, 135-140.

Ruby, S.L. and Shirane, G. 1961. Magnetic Anomaly in $FeTiO_3$ - Fe_2O_3 System by Mössbauer Effect. Phys. Rev., 123, 1239-1240.

Rumble III, D. 1976. Oxide Minerals in Metamorphic Rocks in Oxide Minerals. Mineral. Soc. Am., Short Course Notes 3, R1-24.

Schieber, M.M. 1967. Experimental Magnetochemistry, North-Holland Publishing Co., Amsterdam.

Schwartz, E.J. 1968. A Recording Thermomagnetic Balance. Geol. Surv. Can. Dept. Energy, Mines & Resources, Paper 68-37.

Schwerer, F.C. and Gundaker, W. 1975. Magnetic Properties of Natural Chromites: Mechanical and Thermal Effects. Trans. AIME., Soc. of Min. Engrs. 258, 88-95.

Selwood, P.W. 1956. Magnetochemistry, 2nd Editn., Interscience, New York.

Senftle, F.E., Thorpe, A.N., Briggs, C., Alexander, C., Minkin, J., and Griscom, D.L. 1975. The Néel Transition and Magnetic Properties of Terrestrial, Synthetic and Lunar Ilmenites. Earth Planet. Sci. Lett., 26, 377-386.

Sherrington, D. 1975. Recent Developments in the theory of spin glasses in AIP Conference Proceedings No. 29, Magnetism and Magnetic Materials - 1975., 224-228.

Shirane, G., Pickart, S.J., Nathans, R., and Ishikawa, Y. 1959. Neutron Diffraction Study of Antiferromagnetic $FeTiO_3$ and its Solid Solutions with α-Fe_2O_3. J. Phys. Chem. Solids, 10, 35-43.

———— , Cox, D.E., Takei, W.J., and Ruby, S.L. 1962. A Study of the Magnetic Properties of the $FeTiO_3$ - α Fe_2O_3 System by Neutron Diffraction and the Mössbauer Effect. J. Phys. Soc. Japan, 17, 1598-1611.

———— , and Ruby, S.L. 1962. Mössbauer Study of $FeTiO_3$ and its Solid Solutions with α-Fe_2O_3. J. Phys. Soc. Japan, Suppl. B-1, Proc. Int. Conf. Magnetism & Crystallography 1961 Vol. 1, 133-135.

Shull, C.G., Strauser, W.A., and Wollan, E.O. 1951. Neutron diffraction by Paramagnetic and Antiferromagnetic Substances Phys. Rev. 83, 333-345.

Snetsinger, K.G. 1969. Manganoan Ilmenite from a Sierran Adamellite. Am. Mineral., 54, 431-436.

Stacey, F.D., and Banerjee, S.K. 1974. The Physical Principles of Rock Magnetism, Elsevier, London.

Stickler, J.J., Kern, S., Wold, A. and Heller, G.S. 1967. Magnetic Resonance and Susceptibility of Several Ilmenite Powders.,Phys. Rev., 164, 765-767.

Tarling, D.H. 1971. Principles And Applications of Palaeomagnetism, Chapman and Hall, London.

Temple, A.K. 1966. Alteration of Ilmenite. Econ. Geol., 61, 695-714.

Teufer, G. and Temple, A.K. 1966. Pseudorutile - A New Mineral Intermediate between Ilmenite and Rutile in the Natural Alteration of Ilmenite. Nature, 211, 179-181.

Tyler, S.A. and Marsden, R.W. 1938. The Nature of Leucoxene. J. Sed. Pet., 8,55-58.

Vernon, R.H. 1961. Magnetic Susceptibility as a Measure of Total Iron Plus Manganese in some Ferromagnesian Silicate Minerals., Am. Mineral., 46, 1141-1153.

Weigts, A.G.L.M., Poulis, J.A., and Spence, R.D. 1967. The Use of a Commercially Available Fluxgate Magnetometer in Determination of the Curie Point of Rock Samples. in Methods in Palaeomagnetism, NATO Adv. Study Inst., Elsevier. 447-449.

Welch, B.K. 1964. The Ilmenite Deposits of Geographe Bay. Proc. Aus. I.M.M., No. 211, 25-48.

Welch, B.K., Sofoulis, J., and Fitzgerald, A.C.F. 1975. Mineral Sand Deposits of the Capel Area, W.A. in Economic Geology of Australia and Papua-New Guinea, 1. Metals, Monograph 5 , Aus. I.M.M., Melbourne. 1070-1088.

Zussman, J. 1977. Physical Methods in Determinative Mineralogy. 2nd Editn. Academic Press.

ADDITIONAL REFERENCES

Andrews, D.H. and Kokes, R.J. 1965. Fundamental Chemistry, 2nd Editn. John Wiley, London.

Atzmony, U., Gurewitz, E., Melamud, M., et al 1979. Anisotropic Spin-Glass Behaviour in Fe_2TiO_5. Phys. Rev. Letters, 43, Sept., 782-785.

Flanders, P.J. 1971. Observing a C-axis Moment in α-Fe_2O_3. A.I.P. Conf. Proc. No. 5, Magnetism and Magnetic Materials, 17th Annual Conf., Am. Inst. Phys., 795.

Greenwood, N.N. and Gibb, T.C. 1971. Mössbauer Spectroscopy, Chapman and Hall, London.

Wort, M.J. and Jones, M.P. X-ray diffraction and magnetic studies of altered ilmenite and pseudorutile. Min. Mag. (in press).

APPENDIX A

Synthesis of Ilmenite

The starting material for the synthesis of ilmenite was a stoichiometric mixture prepared according to the following equation in the indicated relative proportions:

$$Fe_2O_3 + 3TiO_2 + Fe = 3FeTiO_3$$
$$159.7 \quad 239.7 \quad 55.85 \quad 3 \times 151.75$$

The individual ingredients were Hopkins & Williams calcined ferric oxide No. 4886; white TiO_2 pigment consisting mainly of rutile with a trace of anatase (Tioxide R-SM2); and 99.5% pure iron powder ex iron carbonyl (Koch Light Laboratories No. 8365W).

The powder was thoroughly mixed by lightly grinding in a mortar and pestle until the colour appeared totally homogeneous when the powder was viewed by stereo-binocular microscope at X40 magnification.

The powder was pressed into imperfect cylindrical pellets in a die constructed of EN24 high-carbon steel, using a pressure of 13800N/m^2 held for 2 minutes. The pellets were then wrapped in platinum foil and placed in a porcelain boat ready for firing.

Firing of the pellets took place in a nitriding furnace made available by Dr. B. Dalgleish of the Department of Metallurgy & Materials Science. The first run of 17 h exposure at 1300°C produced material with an XRD pattern dominated by ilmenite, but also showing small amounts of ferric pseudobrookite and rutile. Examination of a polished briquette confirmed the presence of visible impurities.

The second run at 1100°C for 16 h gave improved results but slight traces of rutile were still apparent, both in the XRD pattern and in polished section.

The third run of 24 h at 1220°C with improved temperature control gave an apparently pure XRD pattern with some unlisted very low intensity lines at moderate angles. Polished section examination revealed no traces of impurities and the material has been used as an ilmenite standard.

APPENDIX B

Magnetic field calibration for the Gouy Method

A selected Gouy sample-tube was suspended from the electronic balance so that the base of the tube was at the centre of the pole pieces (Fig. 6.2). Using the experimental procedure outlined in Section 6.3, the diamagnetic weight-loss curve was then established using 1A current increments on a rising-current loop.

The sample tube was then loaded with the chemical selected as a magnetic standard, and magnetic force readings were obtained using 1A current increments up to a maximum of 20A (10A per magnet coil). Using corrected force readings and the equation $F = \frac{1}{2}(k_s - k_a)A(Bo_m^2 - Bo_L^2)$ Bo_m^2 was calculated for each current employed using $k_a = 0.029 \times 10^{-2} JT^{-2}m^{-3}$. Measurement showed that $Bo_L < 0.001T$, and could therefore be ignored. (The calculation of the effective cross sectional area A is covered in Appendix C). The volume susceptibility of the standard k_s was initially assumed to be a published value and the approximate shape of the curve for field (ordinate) v current (abscissa) was determined by calculating the field at 5, 10, 15 and 20A. An electronic gaussmeter which had been carefully calibrated against a standard magnetic field was then used to check the calculated fields. The k_s value was then slightly adjusted so that the measured field at a given current (say 1.180T at 20A) agreed with the calculated field. This adjusted k_s value was then used to recalculate the fields at all other currents. The experiment was then repeated as a check.

The advantage of combining the use of a nominally high-purity chemical standard with a magnetic gaussmeter accurately calibrated for a particular field is that the non-linearity of the gaussmeter is eliminated as a source of error and any impurities or other problems with the chemical standard (e.g. dehydration) become apparent.

The magnet has to be recalibrated whenever it has been temporarily dismantled.

An example of readings obtained during such a recalibration, using $MnSO_4.4H_2O$ ($\chi = 65.41 \times 10^{-2}\ JT^{-2}kg^{-1}$) as the standard, is given in Table B1.

Table B1 Calibration of Magnetic Field (for Gouy method).

Current A	Magnetic Force kgx10^3	Corrected* Force kgx10^3	Calculated B_o^2(T)	Calculated B_o(T)
5	.059	.060	.1243	.353
10	.224	.227	.4710	.686
15	.458	.464	.9614	.981
20	.663	.672	1.392	1.180

Note 1T ≡ 10,000 Oe

APPENDIX C

Calculation of specific susceptibility for the Gouy method

Using the procedure in Section 6.3, magnetic force data are obtained and tabulated e.g. for 5, 10, 15 and 20A. The equation for the Gouy method may be expressed as follows, using CGS units for convenience and later converting the determined value of k_s to S.I. units.

$$k_s = \frac{1962}{A} \cdot \frac{F}{H_{max}^2} + k_{air}$$

where A = effective cross-sectional area of the cylindrical powdered sample; $k_{air} = 0.029 \times 10^{-6}$ erg Oe^{-2} cm^{-3}; and F (magnetic force) is expressed in grams.

If the weight of mineral packed into the sample tube is m grams, then the volume of the mineral is $m/\rho = v$ cm^3. Using the measured height of the powder column h cm, the effective cross-sectional area is given by $A = v/h$ cm^2. With this calculated value of A, the factor 1962/A is determined and used as a constant.

Thus, for F = 0.065g, H = 11,850 Oe, m = 0.777g, ρ = 3.95 and h = 14.28 cm, the calculated volume susceptibility $k_s = 65.96 \times 10^{-6}$ erg Oe^{-2} cm^{-3}. The specific susceptibility $\chi = k_s/\rho = 16.70 \times 10^{-6}$ erg Oe^{-2} g^{-1} (CGS) = 16.70×10^{-2} $JT^{-2}kg^{-1}$(S.I.).

The calculated values of apparent χ at each current are inspected. A fairly constant value of χ indicates paramagnetic behaviour at the temperature of the experiment. Relatively high χ values at a low field, which progressively decrease as the field increases, indicate that a ferro- or ferrimagnetic component is present in the sample.

APPENDIX D

Calculation of specific susceptibility for the Faraday method.

The equation $F = \chi m B_o \cdot \frac{dB_o}{d_x}$ requires a knowledge of the value of $B_o \frac{dB_o}{d_x}$ for χ to be calculated. This requirement is avoided by use of a magnetic standard which is measured under identical conditions to the unknown sample, (Section 6.4),

since $\chi_1 = \frac{F_1}{F_s} \cdot \left(\frac{m_s \chi_s}{m_1}\right)$

where F_1, χ_1 and m_1 refer to the sample under investigation and F_s, χ_s and m_s refer to the standard substance.

As an example, when $F_1 = .061g$; $F_s = .037g$; $m_1 = .121g$; $m_s = .058g$, and $\chi_s = 65.4 \times 10^{-2} JT^{-2} kg^{-1}$, the calculated value of $\chi_1 = 51.7 \times 10^{-2} JT^{-2} kg^{-1}$.

Using a standard substance, values can be calculated for $B_o \frac{dB_o}{d_x}$ when required.

APPENDIX E

Calculation of calibration constants for the Cook magnetic separator

With reference to Fig. 6.8, the readings corresponding to $\theta = 10^{\circ}$ and $\theta = 30^{\circ}$ for ferrous ammonium sulphate were used to calculate the values of k and n in the equation $\sin \theta/\chi = ki^{n}$.

Taking $\chi = 31.08 \times 10^{-2} JT^{-2} kg^{-1}$ and rewriting the equation as $\log(\sin \theta/\chi) = n \log i + \log k$ the following equations were obtained

For $\theta = 30^{\circ}$, $i = 0.84A$

$$0.206488 = n \times (-) 0.075721 + \log k \quad \ldots\ldots(1)$$

For $\theta = 10^{\circ}$, $i = 0.49A$

$$-0.252813 = n \times (-) 0.309804 + \log k \quad \ldots\ldots(2)$$

$$\therefore \quad 0.459301 = 0.234083\ n \quad \ldots\ldots(3)$$

$$\therefore \quad n = 1.9621288 = \tan^{-1} 62.99^{\circ} \quad \ldots\ldots(4)$$

Substituting n = 1.9621288 in equation (1)

$$1.9621288 \times (-) 0.075721 + \log k = 0.206488 \quad \ldots\ldots(5)$$

$$\therefore \log k = 0.3550623 \quad \ldots\ldots(6)$$

$$\therefore k = 2.26497 \quad \ldots\ldots(7)$$

For calculation of χ at each separator current, the calibration equation thus becomes

$$\sin \theta/\chi = 2.265 \times i^{1.96213}$$

APPENDIX F

Quantitative XRD spectra for magnetic fractions from the South Capel deposit

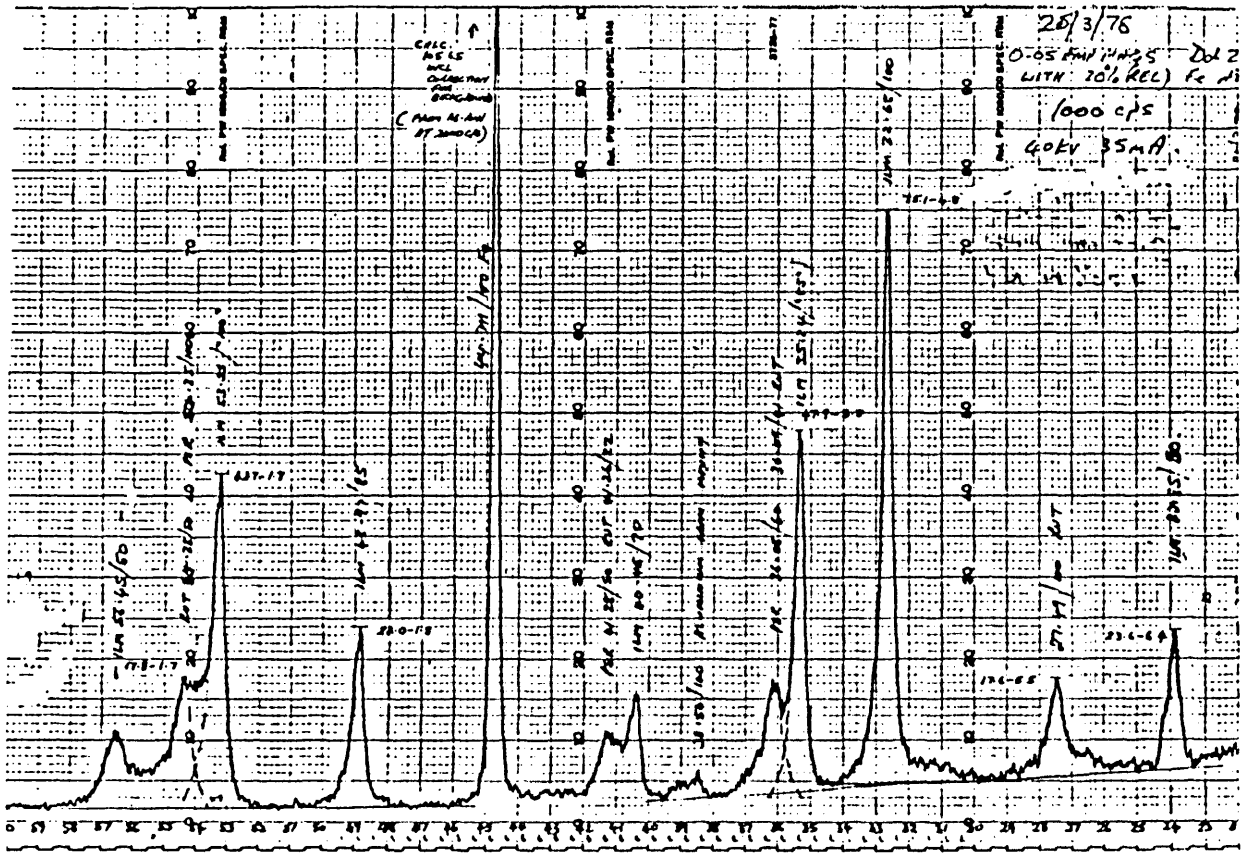

Fig. F1 XRD spectrum of 0.05A magnetics plus 20% Fe - South Capel deposit

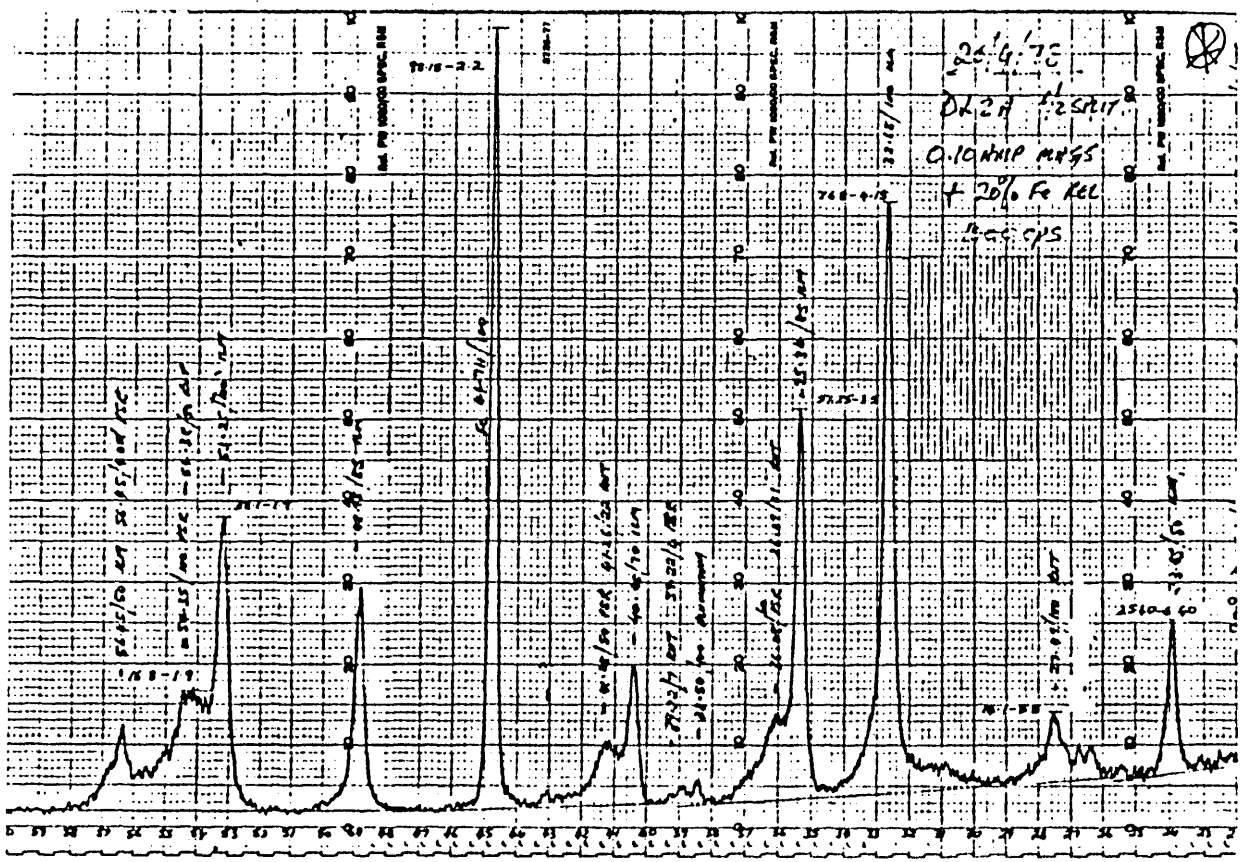

Fig. F2 XRD spectrum of 0.10A magnetics plus 20% Fe - South Capel deposit

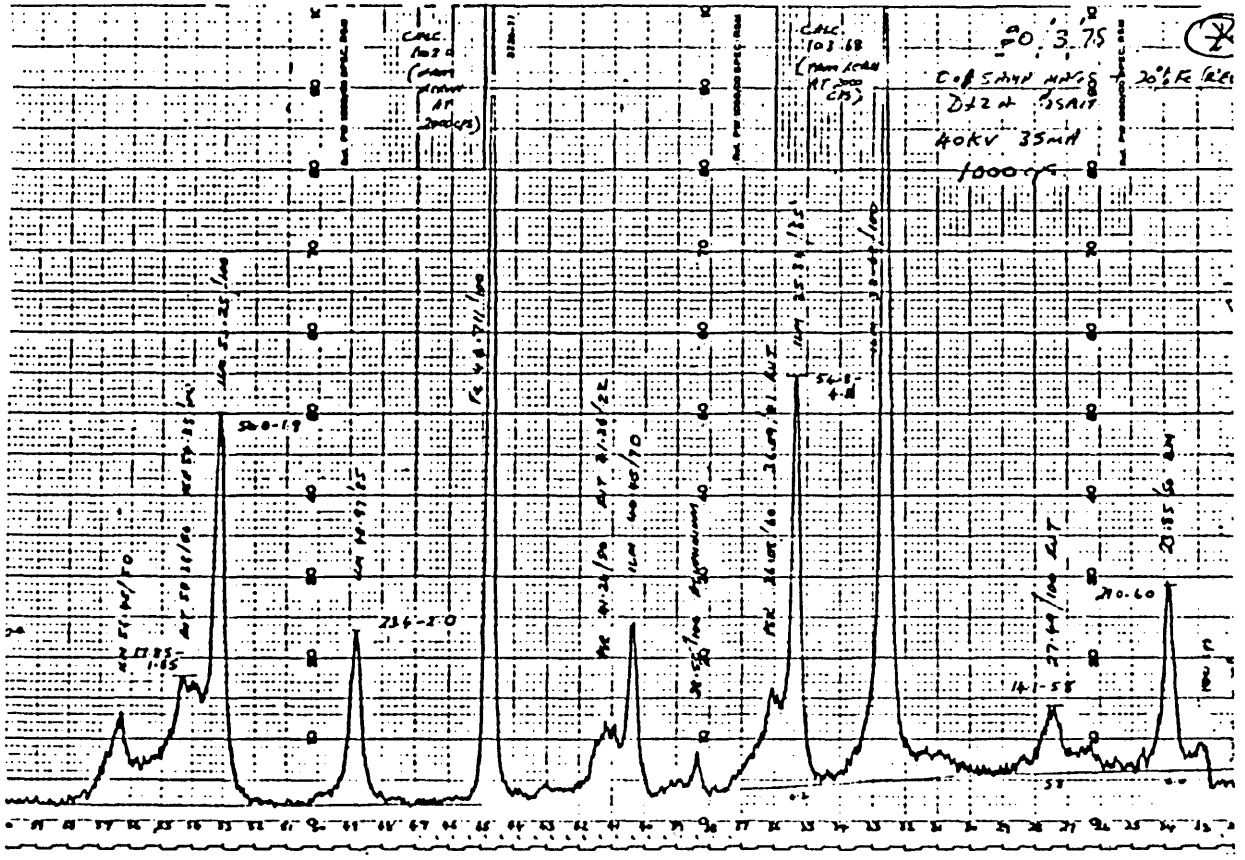

Fig. F3 XRD spectrum of 0.15A magnetics plus 20% Fe – South Capel deposit.

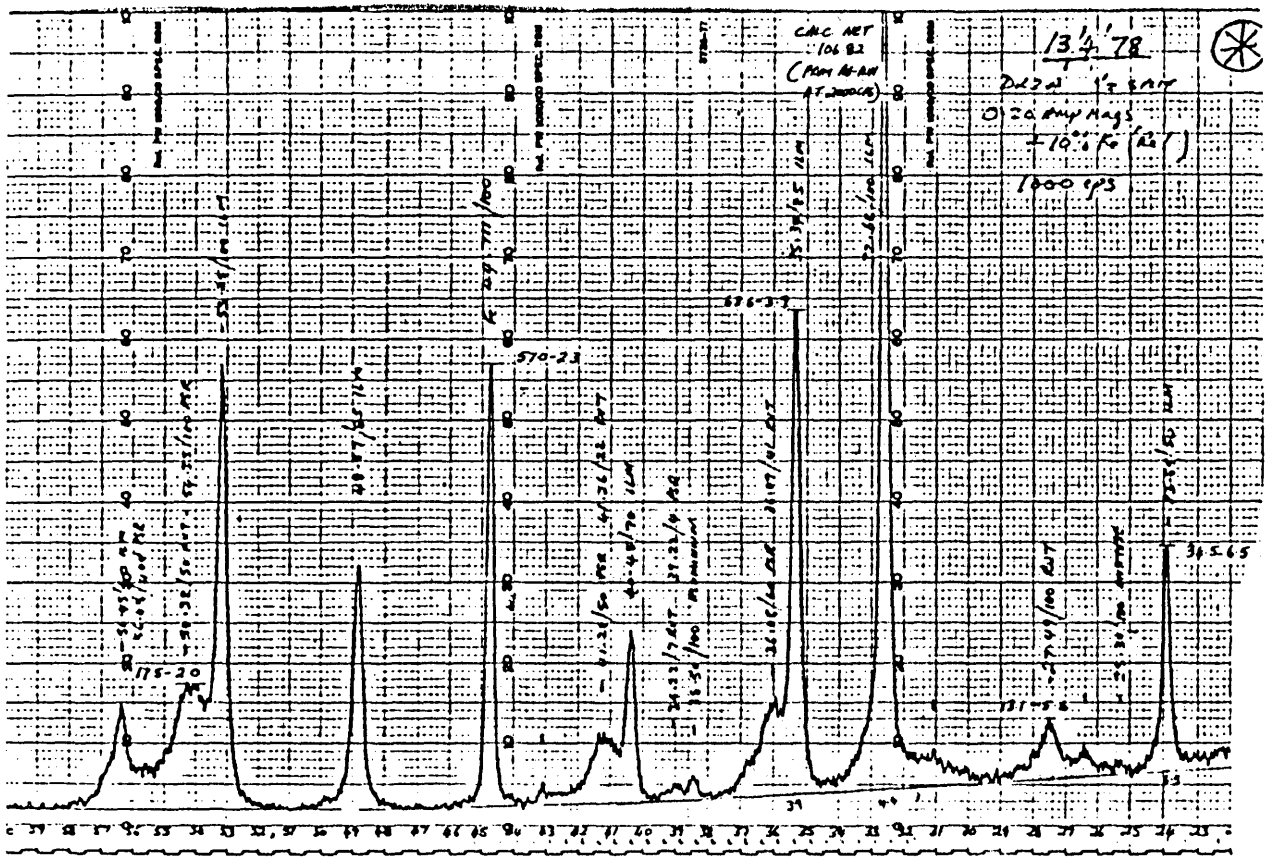

Fig. F4 XRD spectrum of 0.20A magnetic plus 10% Fe - South Capel deposit

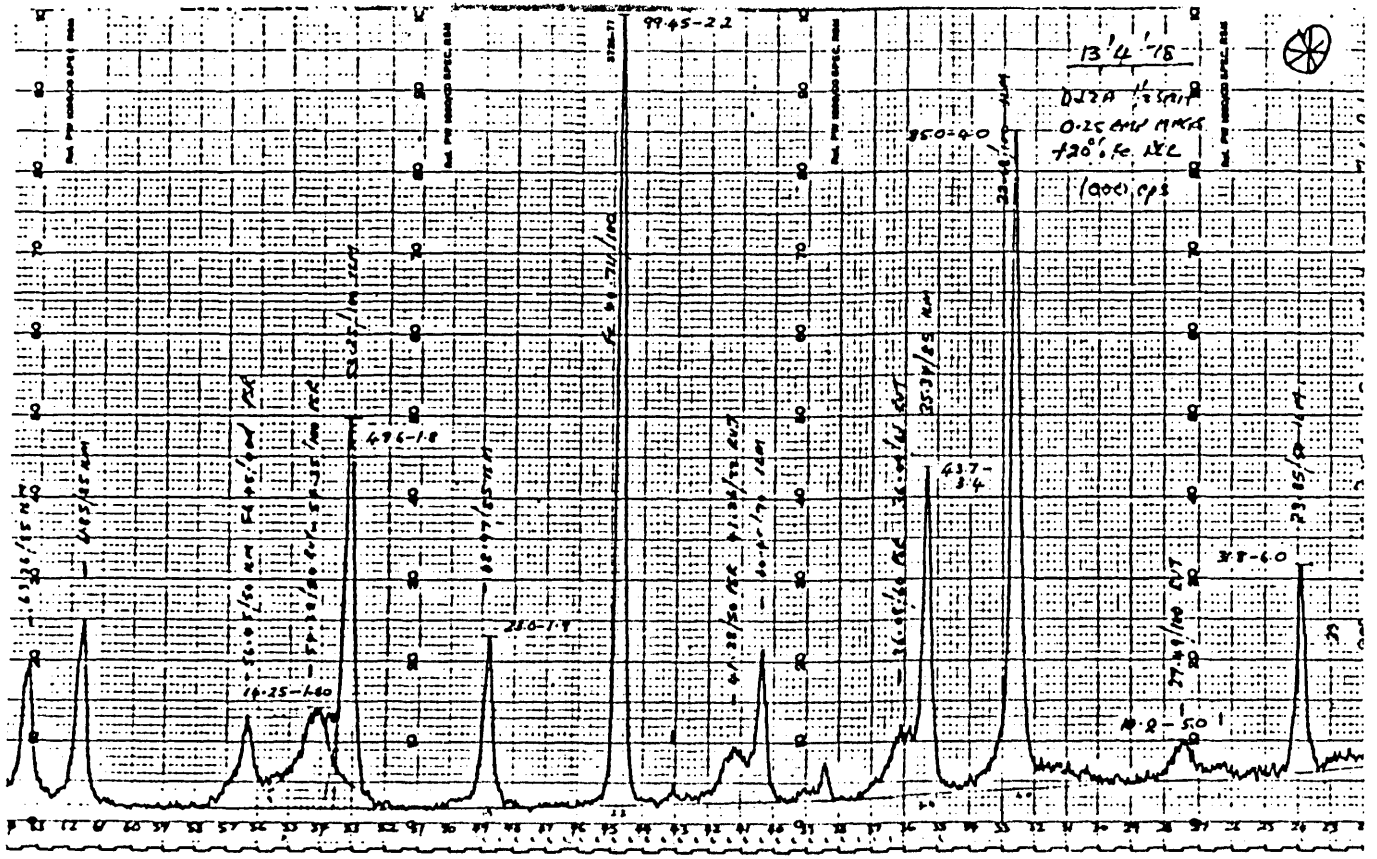

Fig. F5 XRD spectrum of 0.25A magnetics plus 20% Fe - South Capel deposit

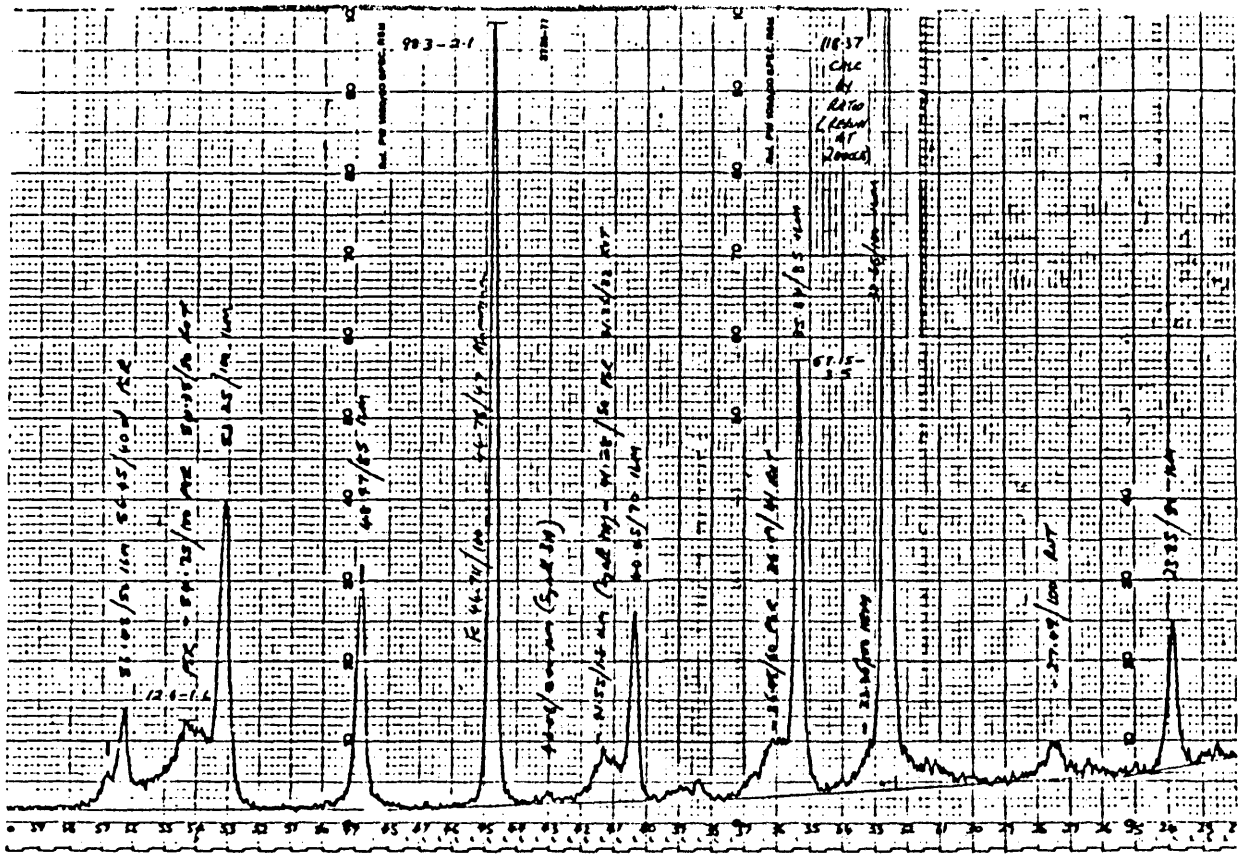

Fig. F6 XRD spectrum of 0.30A magnetics plus 20% Fe - South Capel deposit

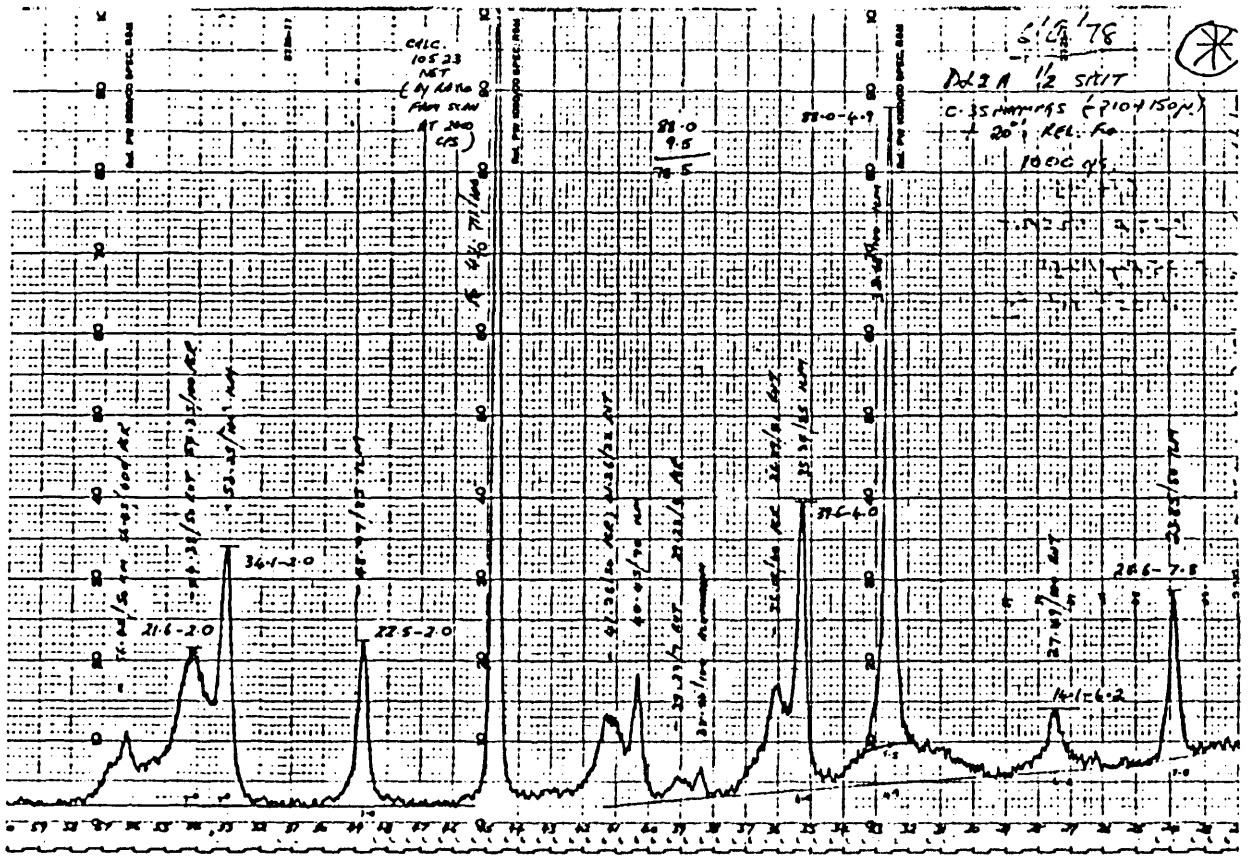

Fig. F7 XRD spectrum of 0.35A magnetics plus 20% Fe - South Capel deposit

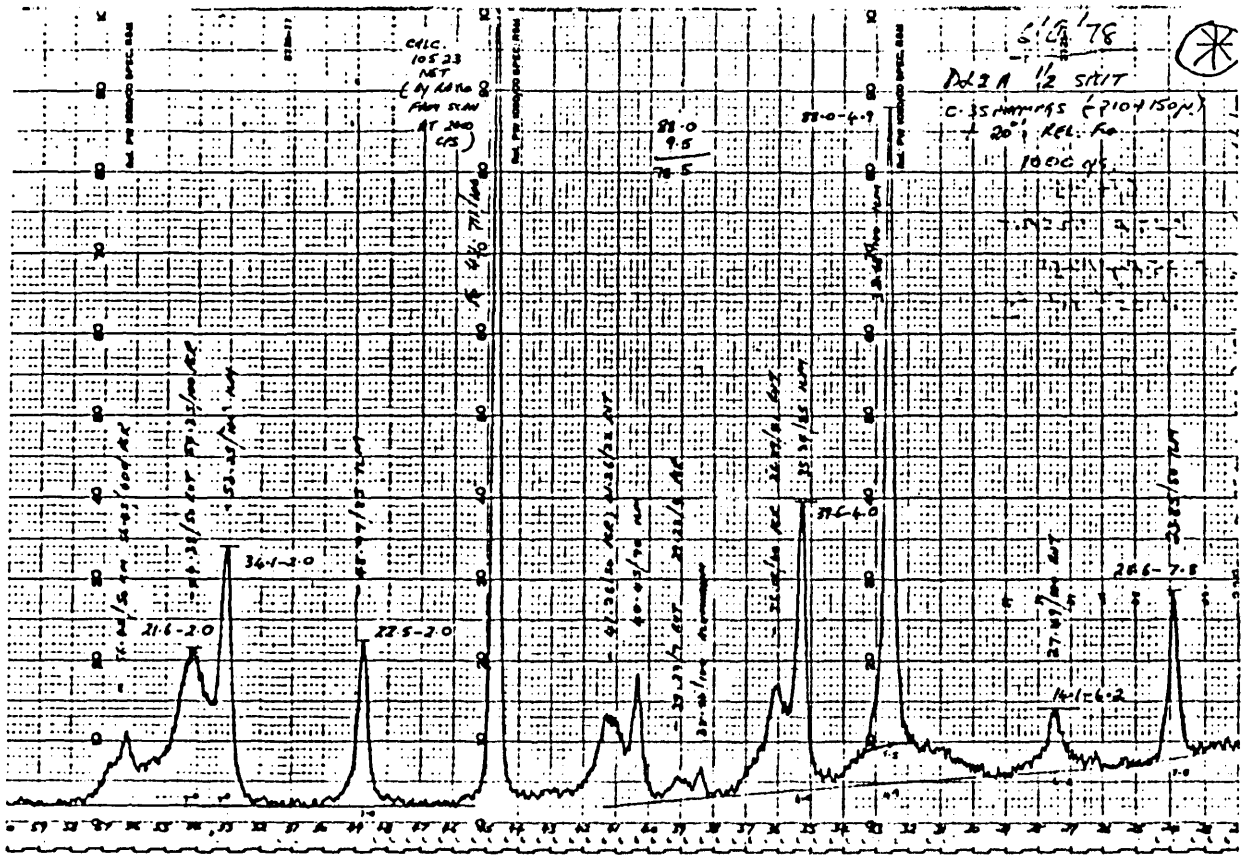

Fig. F7 XRD spectrum of 0.35A magnetics plus 20% Fe - South Capel deposit

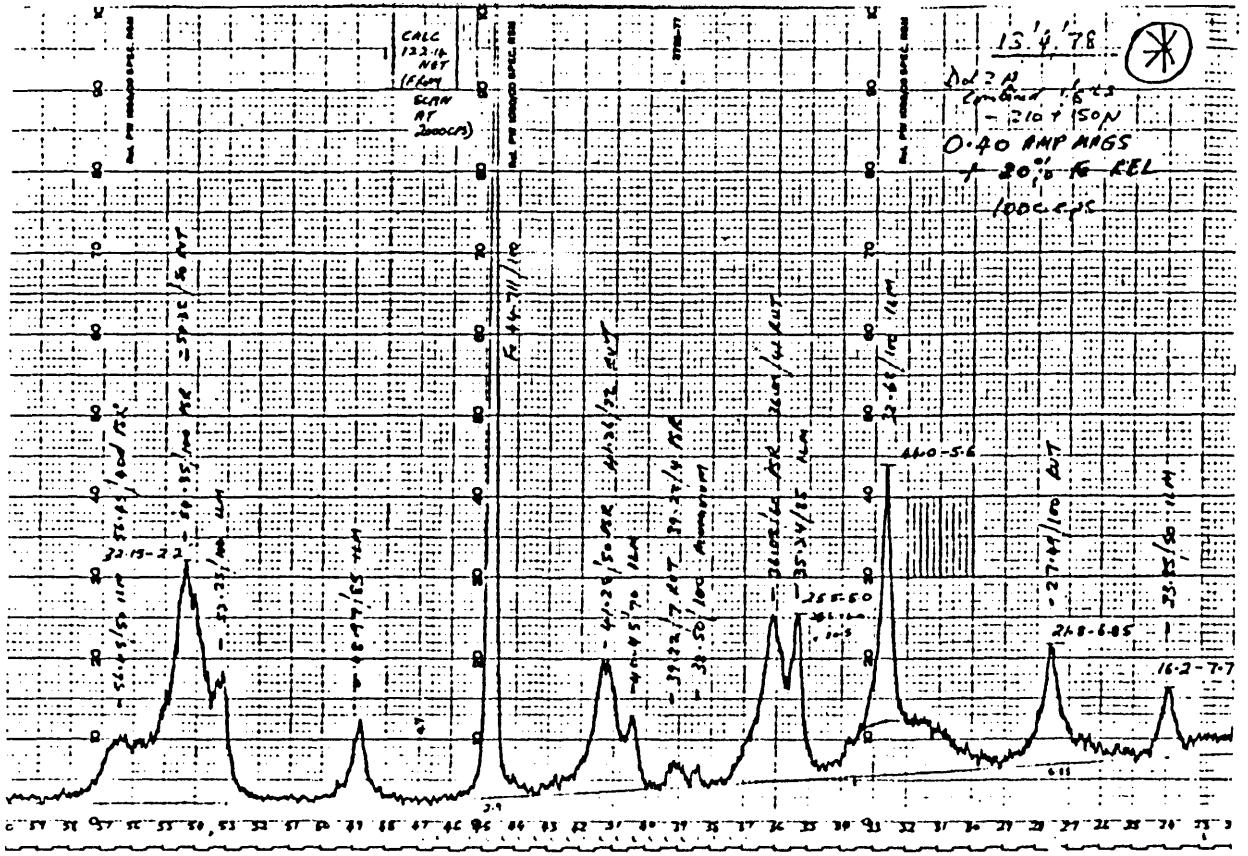

Fig. F8 Spectrum of 0.40A magnetics plus 20% Fe - South Capel deposit

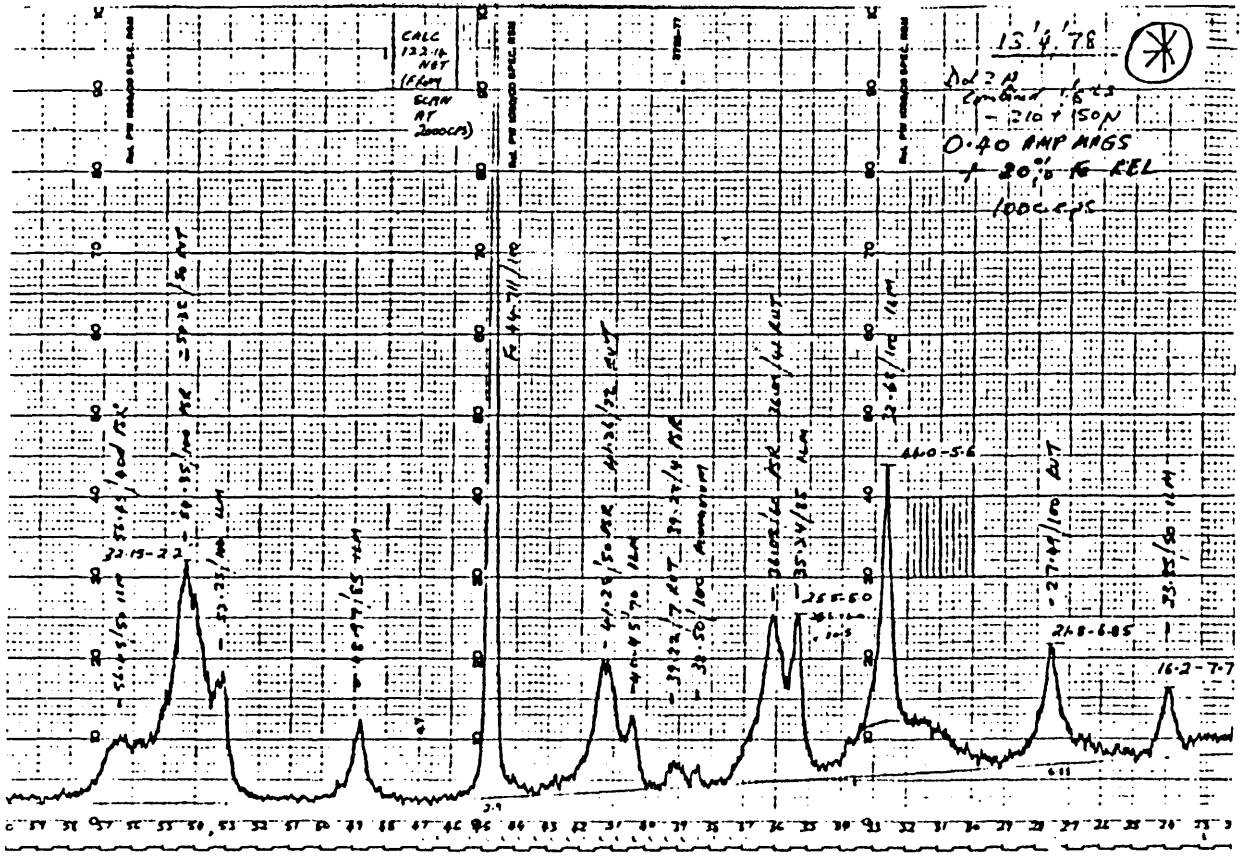

Fig. F8 Spectrum of 0.40A magnetics plus 20% Fe - South Capel deposit

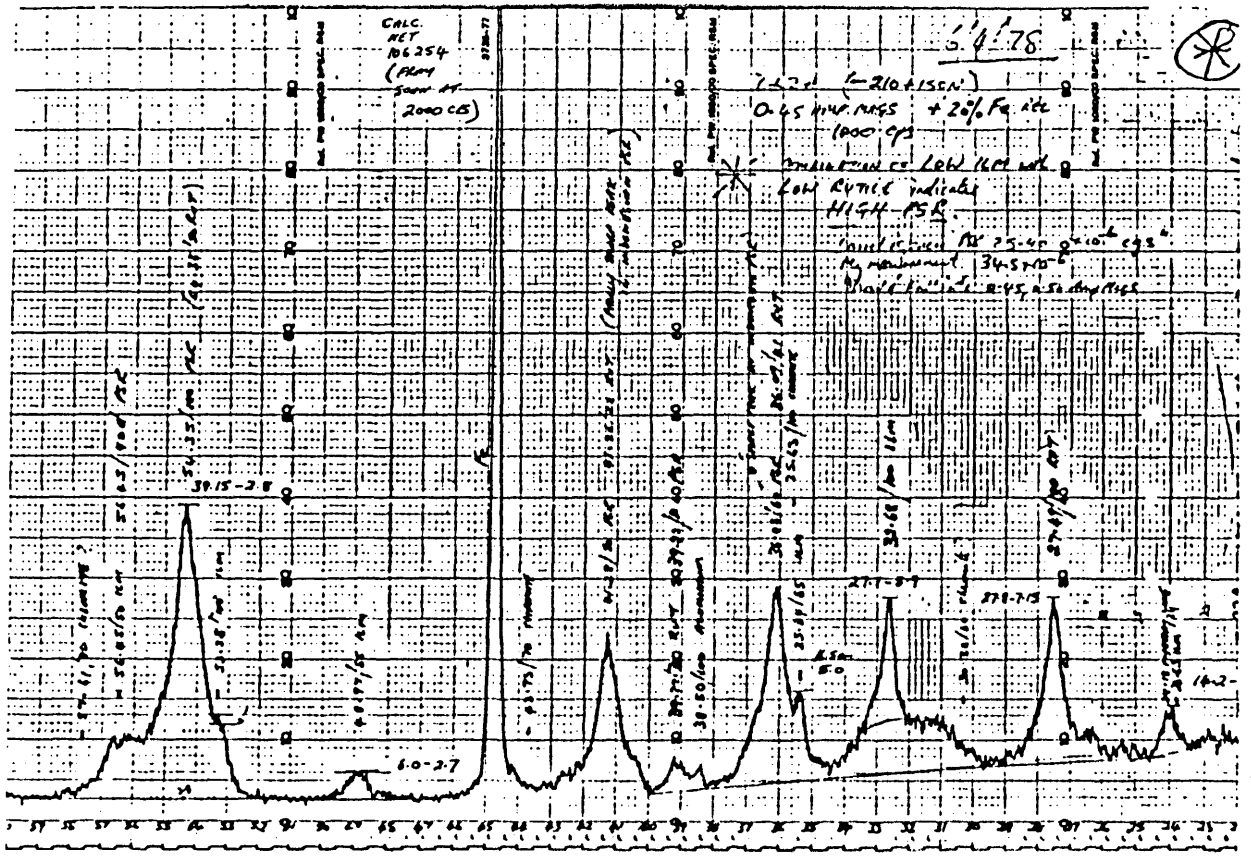

Fig. F9 XRD spectrum of 0.45A magnetics plus 20% Fe - South Capel deposit

APPENDIX G

Quantitative XRD spectra for magnetic fractions of Eneabba altered ilmenite

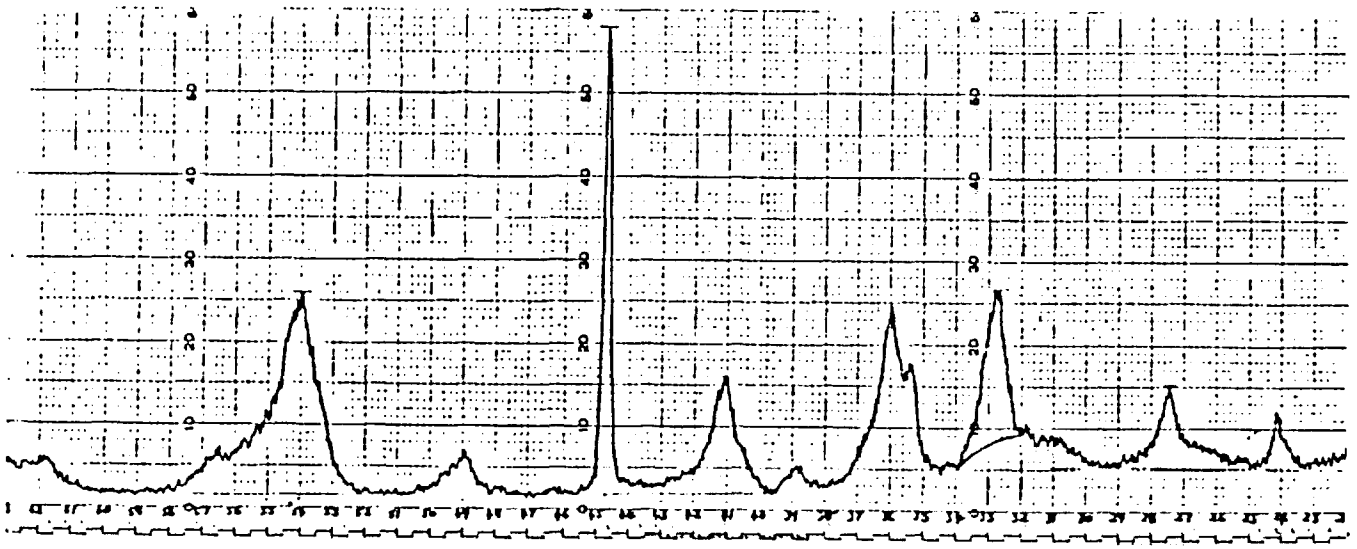

Fig. G1. Eneabba Altered Ilmenite
0.05A magnetics +10% Fe

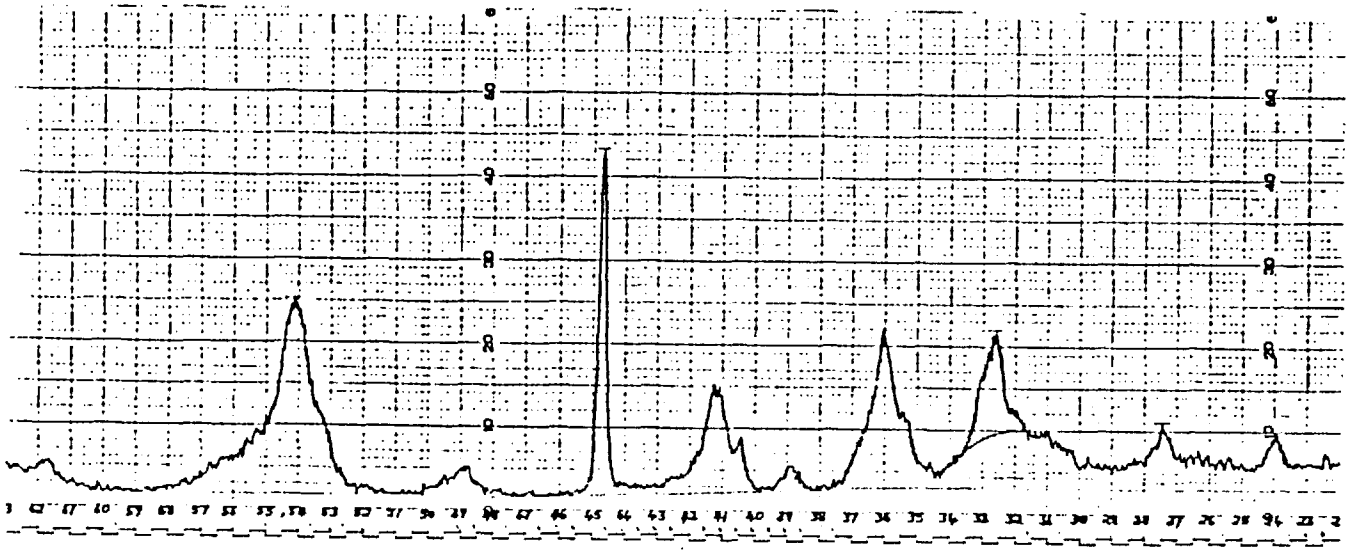

Fig. G2. Eneabba Altered Ilmenite
0.15A magnetics +10% Fe

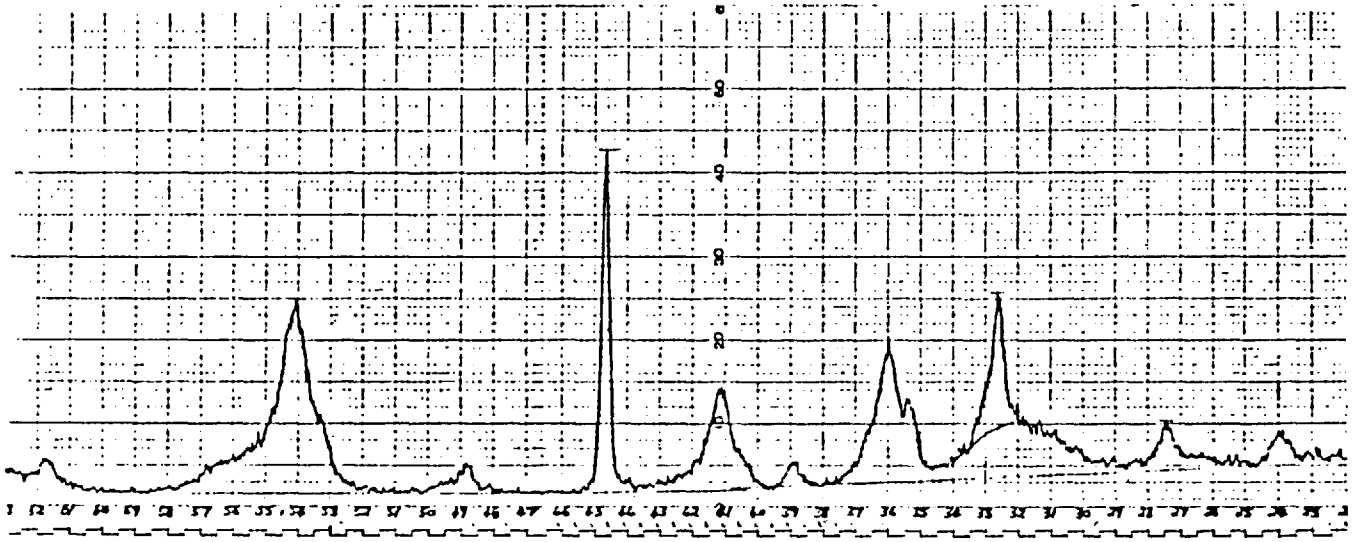

Fig. G3. Eneabba Altered Ilmenite
0.25A magnetics +10% Fe

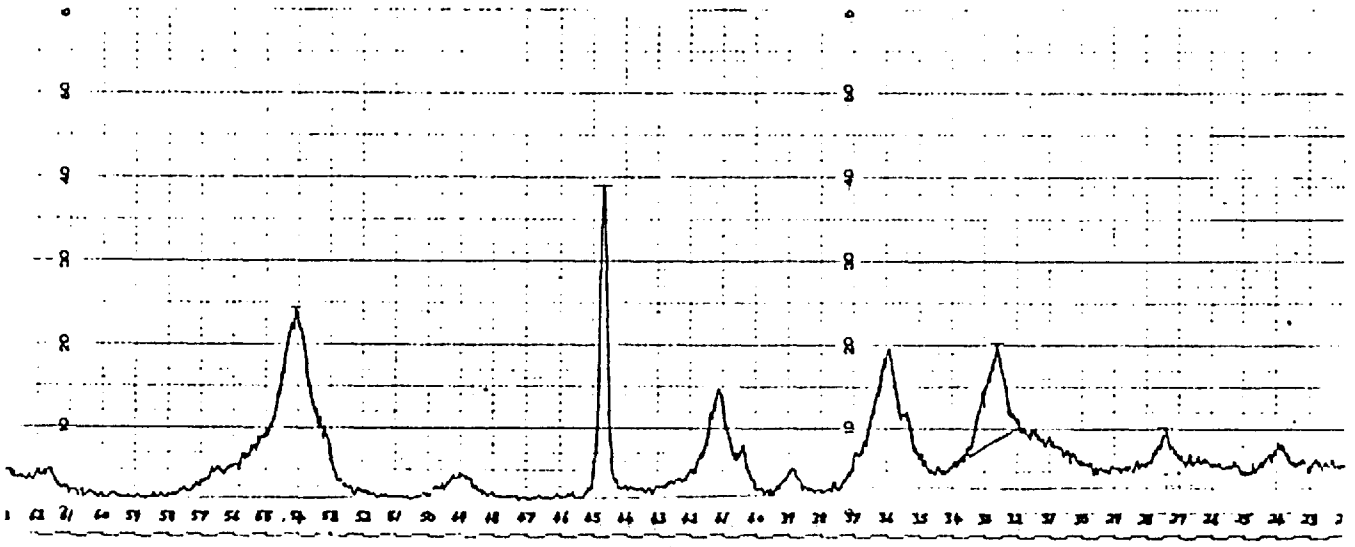

Fig. G4. Eneabba Altered Ilmenite
0.35A magnetics +10% Fe

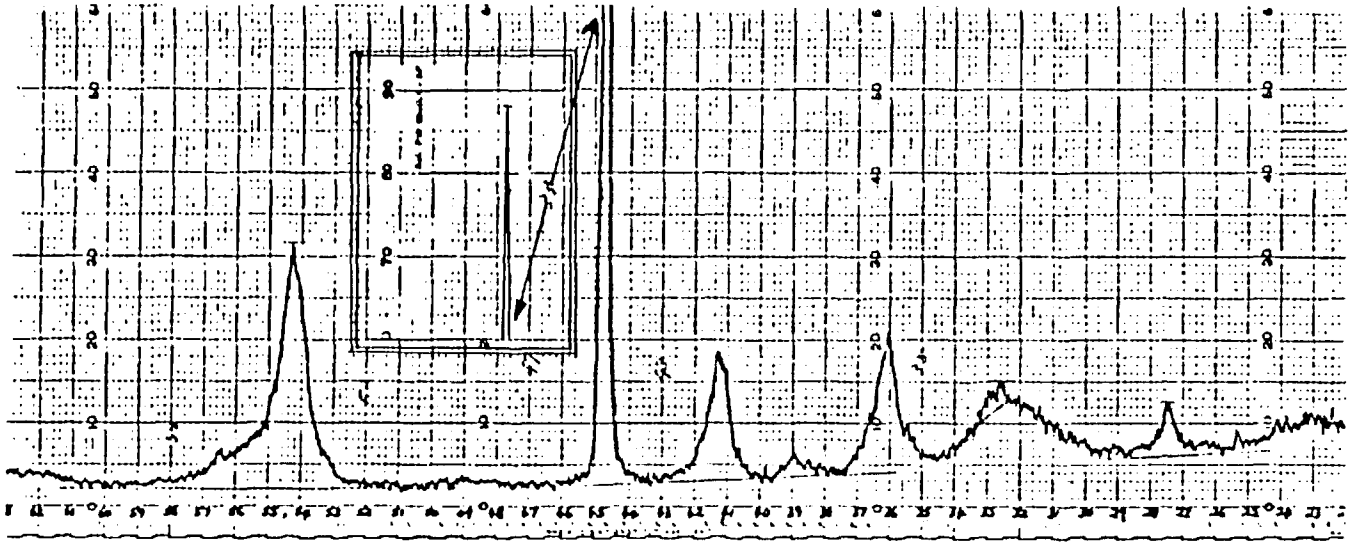

Fig. G5. Eneabba Altered Ilmenite
0.45A magnetics +20% Fe

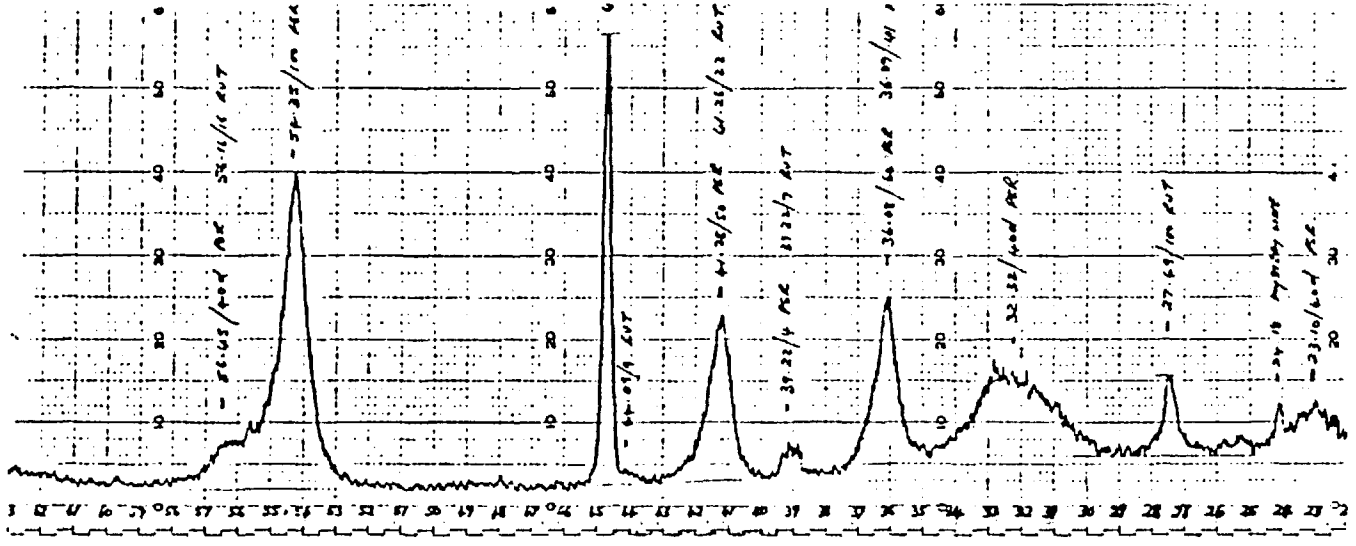

Fig. G6. Eneabba Altered Ilmenite
0.50A magnetics +10% Fe

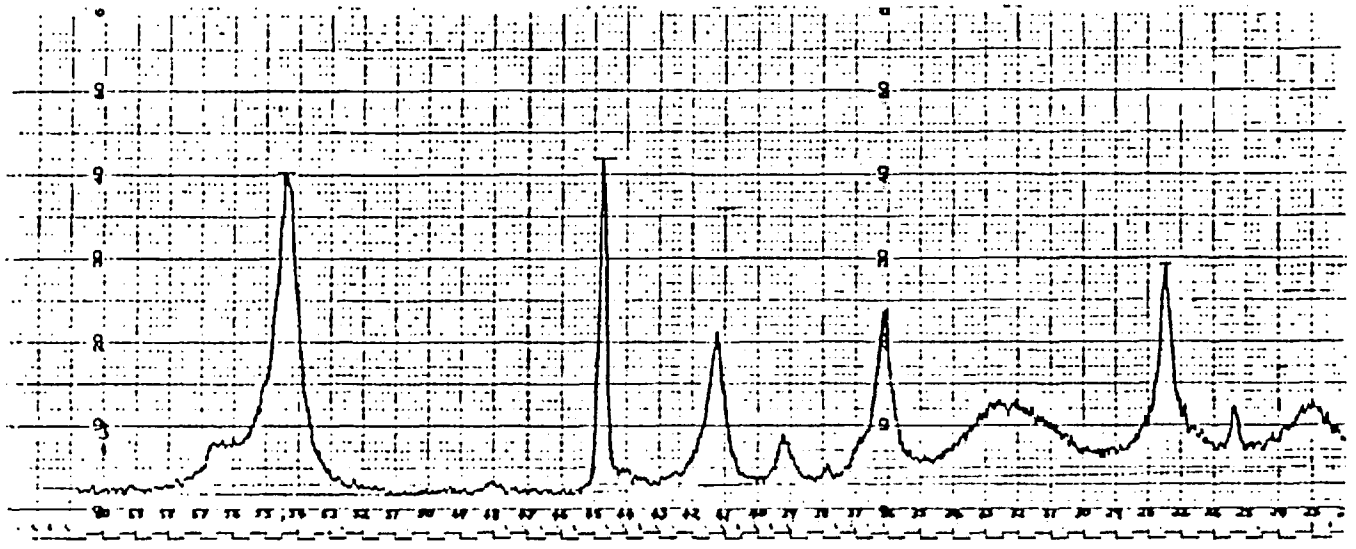

Fig. G7. Eneabba Altered Ilmenite
0.60A magnetics +10% Fe

APPENDIX H

List of Symbols - (chiefly for Chapter 4)

μ_B	Bohr magneton
χ	specific susceptibility (magnetic susceptibility per gram)
$\chi_{\parallel}$	" " parallel to the spin-axis
$\chi_{\perp}$	" " perpendicular to the spin-axis
θ	a constant with the dimensions of temperature
C	the Curie constant
T	temperature ^{o}K
σ_s	spontaneous magnetisation
σ_{s_A}	magnetisation for the 'A' sub-lattice
σ_{s_B}	" " " 'B' sub-lattice
I_s	spontaneous magnetisation for a ferromagnetic
D_s	upper size-limit for a single domain
D_p	" " " superparamagnetism
T_N	Néel point
T_C	Curie point
T_F	'freezing' temperature for a spinglass
M	magnetisation
H	magnetic field
B_o	free - space magnetic induction
μ_o	permeability of free space
k	magnetic volume susceptibility
ρ	density
Oe	CGS unit of magnetic field strength (Oersted).